Localized failure for coupled thermo-mechanics problems : applications to steel, concrete and reinforced concrete

van Minh Ngo

ENSC-(n° d'ordre)

THESE DE DOCTORAT

DE L'ECOLE NORMALE SUPERIEURE DE CACHAN

Présentée par

Monsieur NGO Van Minh

pour obtenir le grade de

DOCTEUR DE L'ECOLE NORMALE SUPERIEURE DE CACHAN

Domaine :

MECANIQUE- GENIE MECANIQUE – GENIE CIVIL

Sujet de la thèse :

Localized Failure for Coupled Thermo-Mechanics Problems: Applications to Steel, Concrete and Reinforced Concrete

Thèse présentée et soutenue à Cachan le 06/12/2013 devant le jury composé de :

Georges CAILLETAUD	Professeur, École des Mines, Président du Jury
Luc DAVENNE	Maîtres de Conférences, Université Paris Ouest, Rapporteur
Karam SAB	Professeur, École des Ponts-ParisTech, Rapporteur
Delphine BRANCHERIE	Maîtres de Conférences, UTC, Examineur
Pierre VILLON	Professeur , UTC, Examineur
Christophe KASSIOTIS	Docteur, ASN, Invité
Amor BOULKERTOUS	Docteur, AREVA, Invité
Adnan IBRAHIMBEGOVIC	Professeur, ENS Cachan, Directeur de thèse

LMT-Cachan, ENS CACHAN
61, avenue du Président Wilson, 94235 CACHAN CEDEX (France)

La rupture localisée pour les problèmes couplés thermomécaniques, applications en béton, acier et béton armé

Remerciements

Ce travail de thèse s'est déroulé au sein de la groupe 'Construction sous conditions extrêmes' du Secteur Génie Civil, Laboratoire de Mécanique et Technologie (LMT-Cachan), Ecole Normale Superieure de Cachan. Ces quelques lignes sont dédiées à tous les personnes qui ont contribué de près ou loin d'aboutissement de cette thèse, en m'excusant d'avance auprès de ceux ou celles que je n'aurais pas eu la délicatesse de mentionner.

Mes premiers remerciment vont à Monsieur Adnan Ibrahimbegovic et Madamme Delphine Brancherie, qui ont initié et encadré mes travaux de thèse. Je leur suis reconnaissant de m'avoir accordé leur confiance et d'avoir su partager leur dynamisme et leur excellence scientifique avec une grande attention, faisant de nos rencontres des événements toujours stimulants.

Je tiens à remercier Monsieur Georges Cailletaud d'avoir bien voulu, dans une période chargée, participer à mon jury de thèse et de m'avoir fait l'honneur d'en assurer la présidence. Tous mes remerciements et un respect profond vont également à ceux qui ont accepté la lourde et fastidieuse tâche de rapporter ce travail :Monsieur Luc Davenne et Monsieur Karam Sab. Enfin, je remercie très sincèrement les examinateurs : Monsieur Pierre Villon, Monsieur Christophe Kassiotis et Monsieur Amor Boulkertous d'avoir accepté de participer à l'examen de ce travail.

Je voudrais également remercier Monsieur Pierre Jehel, qui a été encadré mes travaux de master avec patience et sympathie.

Je remercie Professeur Tran Duc Nhiem, Professeur Duong Thi Minh Thu, qui m'ont démontré la signification d'être un enseignant et un ingénieur civil.

Je remercie Madamme Nitta Ibrahimbegovic pour les bons dinners et les bons sentiments.

Je remercie mes amis: A. Hung, Hieu, Tien, Son, Pierre, Bahar, Nghia, Miha, Edouard, Mijo, Emina, Zvonamir, Bobo, He, Cécile, A.Diep, C. Bich, A. Thanh, C.Ngan, A. Cuong, C. Lan, A. Trang, A. Kien, C.Hoa, C. Thai, Le, A. Hung, C.Hop, Tuan, Lan, Trang, Hung, Thu, Cuong, Huong,… et beaucoup d'autres. Je me souviendrai du beau temps avec eux à l'ENS Cachan.

Enfin, à ma famille et à Sue je decide cette thèse.

Lời cảm ơn đến gia đình

Con cảm ơn bố mẹ đã nuôi nấng, dạy bảo, yêu thương, tin tưởng, động viên, chăm sóc con, vợ chồng con và các cháu trong suốt những năm qua. Cảm ơn bố mẹ đã lo lắng mọi mặt để con có thể yên tâm bước trên con đường của mình. Kết quả nhỏ này con xin gửi tặng bố mẹ.

Con cảm ơn những tình cảm của bố Quyền, mẹ Hạnh và em Trung; cảm ơn bố mẹ và em Trung đã luôn ở bên, thông cảm và giúp đỡ con, Quỳnh và các cháu Bin, Sue trong suốt thời gian con vắng nhà.

Cảm ơn anh chị Nam, Trang và các cháu Bống, Bon đã luôn hỗ trợ, động viên vợ chồng em và cháu Bin. Không có các bác và các chị, Bin chắc đã buồn hơn rất nhiều khi bố vắng nhà.

Anh cảm ơn sự hi sinh và tình yêu của Quỳnh. Cho tất cả những gì đã xảy ra, anh xin lỗi vì đã không ở bên em quá lâu và cảm ơn em đã chăm sóc bố mẹ, chăm sóc các con. Cảm ơn em đã đọc và sửa từng dòng trong quyển luận văn này. Cảm ơn em đã theo dõi từng bước đi, đã vui khi anh có một vài kết quả nhỏ, đã buồn khi anh gặp khó khăn và đã tha thứ mỗi khi anh làm em buồn. Cảm ơn em đã đem Bin và Sue đến trong cuộc sống của chúng ta.

Luận văn này hoàn thành là lúc ba có thể về chơi ô tô với anh Bin và đón chào sự ra đời của em Sue như ba đã hứa. Ba mẹ và anh Bin tặng luận văn này cho em Sue, thành viên mới trong một gia đình nhỏ mà từ nay sẽ luôn ở gần bên nhau. Ba hứa với các con là chúng ta sẽ ở bên nhau, chắc chắn là như vậy.

Abstract

During the last decades, the localized failure of massive structures under thermo-mechanical loads becomes the main interest in civil engineering due to a number of construction damaged and collapsed due to fire accident. Two central questions were carried out concerning the theoretical aspect and the solution aspect of the problem.

In the theoretical aspect, the central problem is to introduce a thermo-mechanical model capable of modeling the interaction between these two physical effects, especially in localized failure. Particularly, we have to find the answer to the question: how mechanical loading affect the temperature of the material and inversely, how thermal loading result in the mechanical response of the structure. This question becomes more difficult when considering the localized failure zone, where the classical continuum mechanics theory can not be applied due to the discontinuity in the displacement field and, as will be proved in this thesis, in the heat flow.

In terms of solution aspect, as this multi-physical problem is mathematical represented by a differential system, it can not be solved by an 'exact' analytical solution and therefore, numerical approximation solution should be carried out.

This thesis contributes to both of these two aspects. Particularly, thermomechanical models for both steel and concrete (the two most important materials in civil engineering), which capable of controling the hardening behavior due to plasticity and/or damage and also the softening behavior due to the localized failure, are carried out and discussed. Then, the thermomechanical problems are solved by 'adiabatic' operator split procedure, which 'separates' the multi-physical process into the 'mechanical' part and the 'thermal' part. Each part is solved individually by another operator split procedure in the frame-work of embbed-discontinuity finite element method. In which, the 'local' discontinuities of the displacement field and the heat flow is solved in the element level, for each element where localized failure is detected. Then, these discontinuities are brought into the 'static condensation' form of the overall equilibrium equation, which is used to solved the displacement field and the temperature field of the structure at the global level.

The thesis also contributes to determine the ultimate response of a reinforced concrete frame submitted to fire loading. In which, we take into account not only the degradation of material properties due to temperature but also the thermal effect in identifying the total response of the

structure. Moreover, in the proposed method, the shear failure is also considered along with the bending failure in forming the overal failure of the reinforced structure.

The thesis can also be extended and completed to solve the behavior of reinforced concrete in 2D or 3D case considering the behavior bond interface or to take into account other type of failures in material such as fatigue or buckling. The proposed models can also be improved to determine the dynamic response of the structure when subjected to earthquake and/or impact.

Résumé

Ces dernières années, l'étude de la rupture localisée des structures massives sous chargement thermomécanique est devenue un enjeu important en Génie Civil du fait de l'augmentation du nombre de constructions endommagées ou totalement effondrées après un feu. Deux questions centrales ont émergé: la modélisation mathématique des phénomènes mis en jeu lors d'un feu d'une part et la simulation numérique de ces problèmes d'autre part.

Concernant la modélisation mathématique, la principale difficulté est la mise en place de modèles thermomécaniques capables de modéliser le couplage existant entre les effets thermiques et mécaniques, en particulier dans une zone de rupture localisée. Comment le chargement mécanique affecte la distribution de température dans le matériau et inversement, comment le chargement thermique influence la réponse mécanique? Sont des questions qui doivent être abordées. Ces questions sont d'autant plus difficiles à aborder que l'on considère une zone de rupture où la mécanique des milieux continus classiques ne peut pas être appliquée du fait de la présence de discontinuités du champ de déplacement et, comme cela est démontré dans ce travail, du flux thermique.

Pour ce qui concerne la simulation numérique, la complexité du problème multi-physique posé en termes de système d'équations aux dérivées partielles impose le développement de méthodes de résolution approchées adaptées, efficaces et robustes, la solution analytique n'étant en général pas disponible.

Cette thèse contribue sur tous les deux aspects précédents. En particulier, des modèles thermomécaniques pour le béton et l'acier (les deux principaux matériaux utilisés en Génie Civil) capables de contrôler simultanément les phases d'écrouissage accompagnées de plasticité et/ou d'endommagement diffus, ainsi que la phase adoucissante due au développement de macro-fissures, sont proposés. Le problème thermomécanique est ensuite résolu par une méthode dite «adiabatic operator split» qui consiste à séparer le problème multiphysique en une partie mécanique et une partie thermique. Chaque partie est résolue séparément en utilisant une fois de plus une méthode «d'operator split» dans le cadre des méthodes à discontinuités fortes. Dans ces dernières, une discontinuité du champ de déplacement ou du flux thermique est introduite et gérée au niveau élémentaire du code de calcul Éléments Finis. Une procédure de condensation statique élémentaire permet de prendre en compte ces discontinuités sans modification de

l'architecture globale du code de calcul Éléments Finis fournissant les champs de déplacement et de température.

Dans cette thèse est également abordée la question de l'évaluation de la réponse jusqu'à rupture de structures en béton armé de type poteaux/poutres soumises à un feu. L'originalité de la formulation proposée est de tenir compte de la dégradation des propriétés mécaniques du matériau due au chargement thermique pour la détermination de la résistance limite et résiduelle des structures, mais également de prendre en compte deux types de rupture caractéristiques des structures poteaux/poutres à savoir les ruptures en flexion et les ruptures en cisaillement.

Les travaux présentés dans cette thèse pourront être étendus pour décrire la rupture de structures en béton armé dans des cas bi ou tridimensionnels en tenant compte en particulier du comportement de l'interface acier/béton et/ou d'autres types de rupture comme la rupture par fatigue ou le flambage. Une extension possible est également la prise en compte des effets dynamiques mis en jeu lorsque la structure est sollicitée mécaniquement par un tremblement de terre ou un impact en plus de la sollicitation thermique.

Table of Contents

Table of Figures

List of Tables

List of Publications

Journals

[1] V.M. Ngo, A. Ibrahimbegovic, and D. Brancherie, "Model for localized failure with thermo-plastic coupling. Theoretical formulation and ED-FEM implementation," *Computers and Structures*, vol. 127, pp. 2-18, 2013.

[2] M. Ngo, A. Ibrahimbegovic, and D. Brancherie, "Continuum damage model for thermo-mechanical coupling in quasi-brittle materials," *Engineering Structure*, vol. 50, pp. 170-178, 2013.

[3] M. Ngo, A. Ibrahimbegovic, and D. Brancherie, "Softening behavior of quasi-brittle material under full thermo-mechanical coupling condition: Theoretical formulation and finite element implementation**,"** *Computer Methods in Applied Mechanics and Engineering*, Accepted.

[4] N.N Bui, M. Ngo, D. Brancherie, and A. Ibrahimbegovic, "Enriched Timoshenko beam finite element for modelling bending and shear failure of reinforced concrete frames," *Computer and Structures*, Submitted.

[5] M. Ngo, A. Ibrahimbegovic, and D. Brancherie, "Thermomechanics Failure of Reinforced Concrete Composites: Computational Approach with Enhanced Beam Model**,"** *Computer and Concretes,* Submitted.

[6] M.Ngo, A. Ibrahimbegovic and E. Hajdo, "Localized failure for large deformation of thermo-plasticity problem," *Nonlinear Coupled Mechanic System*, Submitted.

Conferences and Workshops

1. V.M. Ngo, P. Jehel, A. Ibrahimbegovic "Numerical modelling of monotonic and cyclic response of anchorage steel bar," *Workshop on Construction under Exceptional Conditions (CEC 2010)*, Hanoi,October, 2010.

2. M. Ngo, A. Ibrahimbegovic, and D. Brancherie *, "*A thermo-damage coupling model for concrete structure," *7th International Conference on Computational Mechanics for Spatial Structures. IASS-IACM 2012*, Sarajevo, April 2-4, 2012.

3. M. Ngo, A. Ibrahimbegovic, and D. Brancherie "Continuum damage model for thermo-mechanical coupling in quasi-brittle materials,*" The first AVSE Annual Doctoral Workshop. ENS Cachan*, Cachan, September 13-14, 2012.

1 Introduction

1.1 Problem statement and its importance

The characterization of the failure in steel, concrete and reinforced concrete structures under thermo-mechanical loading is not only the main theoretical importance but also the major interest for its practical application. In recent years, the number of massive constructions collapsed and/or damaged due to fire loading is increasing. A list of several major building fire accidents from 1970 onwards (given in Table 1-1) has indicated the progress of them in term of number and severity. Among these accidents, perhaps the most well-known is the collapse of the World Trade Centre in New York in September, 2001, where the thermal response and the degradation of material properties due to fire were considerably contributed into the final breakdown of the tower in addition to the mechanical response due to the airplane impact (see [1], [2], [3]). More recently, the burning occurred in the 32-storey Windsor tower in Madrid, Spain in February, 2005 (see Figure 1-1) is also a typical example of construction failure due to fire loading. In this accident, the fire started on the 21st floor then quickly spread throughout the entire building. After 24 hours exposure to fire, the steel components of the tower were destroyed while the reinforced concrete components were also partially damaged. Although not being completely destroyed in the fire, the remaining reinforced concrete structures had also lost its working capacity and had to be demolished later. These structural failures, from the civil engineering point of view, happened due to the lack of structure resistance, or more particularly, the degradation of structure resistance when exposed to extreme thermal loads. This issue is still not clearly understood presently. Therefore, it is necessary to go into deeper studies of the behavior of structure subjected to thermal loading and mechanical loading simultaneously. Of special interest is the problem of localized failure of the structure at extreme conditions that can produce the localized heavily damaged zones leading to structure softening response. In this thesis, the localized failure of structures built of standard construction materials, such as steel, concrete and reinforced concrete will be discussed. The main target, as will be explained in more detail in the following, is to provide a more robustness simulation of the ‘ultimate’ response of reinforced concrete structure, which will further lead to a better and safer design of the construction.

Table 1-1. *Several building fire accidents from 1970 to present* ***(see*** [4]***)***

No.	Names of the buildings	Description	Time
1	One New York Plaza, New York, USA	50-storey office building 2 persons died	August 15, 1970
2	MGM Grand Hotel and Casino, Paradise, Nevada, USA	21-storey hotel and casino building 85 persons died	November 21, 1980
3	First Interstate Bank – Los Angeles, California, USA	62-storey building One person died	May 4, 1988
4	One Meridian Plaza, Philadelphia, Pennylvania, USA	38-storey office building 3 persons died	February 23, 1991
5	World Trade Centrer North and South Tower (Building 1&2), New York, USA	Airpcarft impacted and then Fire happened Nearly 3000 persons died	September 11, 2001
6	World Trade Center Building 7, New York, USA	Fires burned for nearly 7 hours before collapsing	September 11, 2001
8	Cook County Administration Building, Chicago, Illinois , USA	6 persons died	October 17, 2003
9	Caracas Tower , Caracas, Venezuela	56-storey, 220 m high tower. Tower was burned for more than 17 hours before collapsing	October 17, 2004
10	Windsor Tower, Madrid, Spain	32-storey RC building, 106 m high 7 persons injured	February 12, 2005
11	Tohid Town Residential, Tehran, Iran	10-storey apartement building 116 to 128 persond died	December 6, 2005
12	The Beijing Mandarin Oriental Hotel,	160 m tall skyscraper	February 9, 2009

Figure 1-1. *Windsor Tower (Madrid) before, in and after fire disater*

1.2 Literature review

There are two types of structural analysis that can be used in determining the behavior of steel, concrete and reinforced concrete structures, which are the (one-dimensional) stress-resultant model and the multi-dimensional continuum mechanics model. In dealing with these problems in the most efficient manner, we are led to develop different both the continuum-mechanics-based models and the stress resultant models.

The stress resultant model considers the structure as a system of one-dimensional elements: beams, frames, columns, trusses. (see Figure 1-2). These elements, due to their special configurations with one dimension being much greater than the two others, are assumed to satisfy traditional hypotheses of the structural analysis such as the Saint-Venant hypothesis: '*…the difference between the effects of two different but statically equivalent loads becomes very small at sufficiently large distances from load*' (see [5]) and the beam theory assumptions: '*beam is initial straight and has a constant cross-section', 'the plane cross-section remains plane before and afterloading*'. Due to the simplicity and the low-cost of computation, this type of approach is widely used in practical design of reinfored concrete as well as steel structures submitted to combined action of fire and mechanical loading. Such is still the basic method introduced in the design code of Europe and America nowadays (see [6],[7], [8], [9], [10], [11]). However, despite the forementioned avantages, the stress-resultant model can not be applied for the 'local' regions (or the 'D' regions [12], [9]) of the structure where the Saint-Venant and

beam hypotheses are no longer valid. Examples of this kind are the beam-column joint or the footing region (see Figure 1-2).

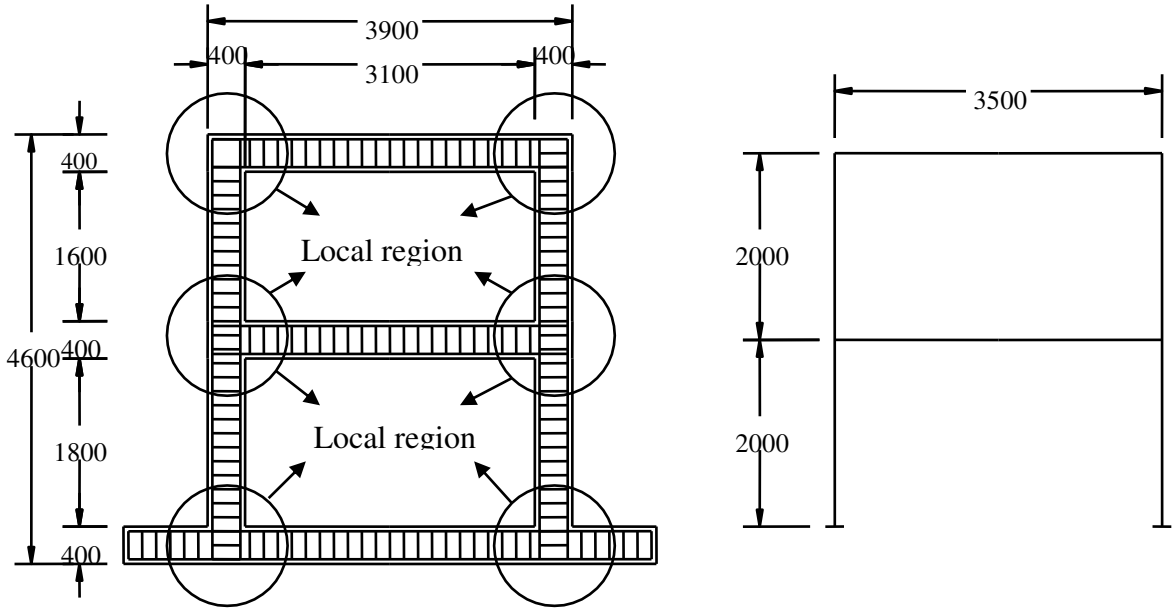

Figure 1-2. *Stress-resultant model of a reinforced concrete structure*

The latter approach, which is now developing very fast due to the development of computers, is to treat the structure as a multi-dimensional media subjected to external thermo-mechanical. This type of computation further leads to the needs of: 1) a thermo-mechanical model which is capable of modeling the response of steel and concrete material under the combining effect of thermal and mechanical loading; 2) a robust numerical solution procedure to solve such a multi-physical problem. Although this type of approach leads to a much higher calculation cost in comparison to the stress-resultant approach, it will certainly provide better results, especially when modeling the local region of the structure.

1.2.1 Previous works on stress-resultant model

The analysis combining thermo-mechanical response of reinforced concrete frame structure based on the stress-resultant model were entirely studied by many researchers and many interesting results were introduced. Among them, one can refer to the work of Kodur and Dwaikat (see [13], [14]), Hsu and Lin ([15]) or Capua and Mari ([16]). However, most of these studies considered only the bending failure and ignored the shear failure, which is also a typical damage model of the reinforced concrete structure. Moreover, practically none of the works available in the literatures considers the effect of shear force and axial force on the bending

resistance of reinforced concrete element, although the stress-strain relation of the cross-section where shear force and axial force exist are much different from the stress/strain condition of the pure bending cross-section. Another deficiency of previously proposed methods is that only the degradation of the mechanical resistance due to material strength reduction at high temperature is taken into account, while the 'thermal' response of the frame is usually neglected while at high temperature, thermal behavior might significantly contribute to the total behavior of the section. The last important model feature to be improved with respect to the previous works is to cast the stress-resultant model that can represent such a thermomechanical behavior of a reinforced concrete elements (either beam or column), which can provide an efficient computational basis in identifying the overall response of the frame structure. Therefore, a method to overcome the mentioned shortcomings of the present stress-resultant based model will be introduced in this thesis.

1.2.2 Previous works on multi-dimensional thermodynamics model

As already declared, the multi-dimensional analysis of 'local' regions should be based on a thermo-mechanical model of steel and concrete material. In the following, some main contributions on the modeling of softening behavior of construction material due to mechanical effect only and due to thermo-mechanical coupling effect are summarized.

The 'ultimate' resistance of structures under mechanical loading was previously studied by many research groups, by using a number of different approaches. The research group entitled 'Structure under Extreme Conditions' of Professor Ibrahimbegovic at LMT Cachan contributed to this topic by considering the softening behavior of material in the frame-work of Embedded-Discontinuity Finite Element Method (see [17]). Here, the localized failure of the solid is represented as a 'discontinuity' (or a 'jump') in displacement field and is modeled by an additional interpolation function using the incompatible mode in finite element method [18]. Based on this method, this research group contributed in determining the softening behavior of the structure due to both the stress-resultant model approach and the multi-dimensional analysis approach. For the stress-resultant model approach, one can refer to the study on the bending failure frame (see [19],[20]) and/or the bending failure accompanied with shear failure (see [21]) of reinforced concrete frame. In terms of the multi-dimensional analysis approach, the thermomechanical softening model of some fundamental construction materials were introduced:

elasto-plastic steel material structure (see [22],[23]), quasi-brittle material (concrete, masonry) (see [24], [25]) and reinforced concrete structures (see [26]). Other (and earlier) significant contributions to the topic that should be recalled are the work of Ortiz el al. on weak discontinuity (see [27]) and of Simo et al., Armero et al. and Oliver et al. on strong discontinuity of material (see [28], [29], [30], [31], [32]). These methods are based on a modification of classical continuum models and provide an adequate measure of the dissipation with respect to the chosen finite element discretization. However, they only consider the combination of the discontinuity with an elastic behavior of the material without taking into account the continuum inelastic behavior of the material. Therefore, these models are not actually suitable to be used in modeling the working of steel and concrete structures, since the plastic behavior and damage behavior play an important role in the total behavior of these materials.

The behavior of material under thermal loading only, or in other words, the heat transfer problem was a classical topic and was thoroughly studied. However, the coupling effect of mechanical loading and thermal loading on material was not much studied, both in terms of theoretical formulation and numerical solution. In terms of theoretical aspect, we can recall several important works of Armero and Simo (see [33]) on nonlinear coupled plasticity for small deformation, of Ibrahimbegovic et al. (see [34], [35]) on thermo-plastic coupling with large deformation, of Baker and de Borst (see [36]) on anisotropic thermomechanical damage model for concrete and of Tran and Sab (see [37]) on steel-concrete bonding interface. These works are limited to the behavior of material in classical continuum mechanical framework and thus are not able to model the behavior of solid at localized failure where ‘discontinuity’ appears in the displacement field.

We also note that in the framework of continuum mechanics, there is not much research considering the numerical solution for the problem of computing the localized failure and associated softening response due to coupled thermomechanical loads. The latter especially applies to quasi-brittle material models, which are generally the most popular for representing the mechanical behavior of construction materials employed in civil engineering nowadays.

The softening behavior of material under the fully thermo-mechanical coupling effects was analyzed by very few previous research works, and also for only special cases. For example, in 1999, Runesson and coworkers (see [38]) studied the theoretical aspect of the localization in

thermo-elastoplastic solids subjected to adiabatic condition, which is a really 'ideal' case of loading. This work has more a theoretical meaning than a practical application and need to be extended. In 2002, a one-dimensional analysis of strain localization in a shear layer under thermally coupled dynamic conditions was introduced by Armero and Park (see [39]). In that work, an analytical solution for the localization of a one-dimensional shear layer was discussed in detail. However, due to the limitation of analytical approach, this method cannot be extended to higher-dimensional problems. We can also mention the work of Wiliam *et al*. in 2004 (see [40]) who studied the interface damage model for thermomechanical degradation of heterogeneous materials. However, this work does not include a clear numerical solution for the model and thus, its application is limited to fairly simple problems.

1.3 Aims, scope and method

The first target of this thesis is to improve the present stress-resultant model in determining the overall behavior of the reinforced concrete structure. In order to do so, two central problems should be considered: 1) how to take into account the shear failure (along with the bending failure) into the overall failure of the reinforced concrete frame; 2) how to evaluate and account for the cumulative effect of thermal loading on the total response of the structure. In this thesis, the answers to these questions are found by the following procedure. First, we use the Modified Compression Theory (see [41]) to construct the stress-strain conditions of the considered beam element under different mechanical and temperature loadings. Based on the chosen stress-strain relations of the beam ingredients, we plot its bending-curvature and shear force-shear strain curve at a given temperature loading. These curves are then treated as input parameters of a beam stress-resultant model, which can finally be solved by the embedded-discontinuity finite element analysis.

The second (and also the main) goal of the thesis is to provide a thermodynamic model capable of considering the ultimate load behavior accompanied by softening phenomena not only due to mechanical loading but also to fully coupled thermomechanical condition. Both plasticity and damage models of this kind are developed in this thesis. Regarding the numerical implementation, two important tasks are examined in detail. The first one is the numerical solution of the problem. As explained in the following, the mathematical representation of thermo-mechanical problem is a system of differential equations with unknowns pertaining to

mechanical fields (displacement, strain, stress) and thermal fields (temperature, heat flux). Such a system normally does not have an 'exact' analytical solution except for some of the simplest one-dimensional cases. In general, an approximate numerical solution for the problem should be introduced. We propose and discuss, in particular, the operator split solution procedure, which is adapted to both initial hardening behavior and subsequent softening behavior of the thermoplastic or thermo-damage solid mechanics models. The latter is one of the most complex tasks when considering the aspects of numerical implementation in the thesis. The second objective is to examine the softening behavior of the solids under fully coupled thermomechanical extreme conditions. To that end, the first challenge is pick the right thermo-mechanical model for either quasi-brittle or ductile failure phenomena and validate the choice. Two models describing the corresponding inelastic behavior of solids are chosen: the thermo-plasticity and thermo-damage. These two correspond to typical choices made for the construction materials like steel and concrete. These models are carefully assembled within a complex model corresponding to the reinforced concrete composite. We also develop a more efficient structural-type model for reinforced concrete in terms of the Timoshenko beam formulation. The final challenge we address concerns the appropriate choice of the enhanced kinematics to be introduced at the point of localized failure. This has been done in a systematic manner for different models developed in this thesis.

1.4 Outline

The outline of the thesis is as follows. In the next chapter, we present the general theoretical formulation for the problem in solid mechanics subjected to thermo-mechanical actions and the approximation numerical solution. This general method is applied in detail to model the localization on elasto-plastic material such as steel in Chapter 2. One-dimensional case will be considered in this chapter in order to show a clear overview of the method. The third chapter considers the continuum damage and also the degradation of quasi-brittle material like concrete or masonry in multi-dimensional problem. This chapter removes two deficiencies of the existing documents on thermomechanical coupling reaction of quasi-brittle material, which are the numerical solution for continuum damage threshold and the model for the softening behavior of this material. Theoretical model and a numerical solution of the 'ultimate' response of reinforced concrete structure subjected to thermal loading and mechanical loading applying

simultaneously based on Timoshenko beam formulation is carried out in the fourth chapter. Finally, the conclusion summarizes all the main findings of the thesis and suggests the perspective of the study on this topic in the future.

2 Thermo-plastic coupling behavior of steel: one-dimensional simulation

2.1 Introduction

How to determine the inelastic behavior of a structure subjected to mechanical and thermal loads jointly applied is an important task in civil engineering, especially for the case of accidental loading scenarios and/or fire resistance. Studies of thermo-mechanical resistance have been performed for a number of different structures and typical construction materials. In particular, one finds the previous works pertaining to steel (see [35], [34],[42]), to masonry (see [43], [44]), as well as to concrete and reinforced concrete structures (see [45],[36],[37]). The issue of computational procedure for the thermo-mechanical coupling has also been thoroughly studied (see[33], [46], [47]) and quite considerable level of robustness has been achieved. However, these continuum models were limited to model the inelastic behavior of the material with hardening before the localized failure occurs.

None of these existing models can be applied to estimate the ultimate thermo-mechanical state of a complex structure, with the for a localized failure number of components. In such a case, it is necessary to provide a model capable of representing the thermomechanical behavior of the material in localization zone. Even for purely mechanical loading, where the material propertiesare considered to be independent of temperature, one already needs a special model formulation to capture localized failure with adding either strong displacement discontinuity for brittle failure (see [32], [29], [31]) or fracture process zone with hardening and displacement discontinuity with softening for ductile failure ([23], [25]). The new issue for coupled thermomechanics problem concerns the heat transfers and temperature changes in the localized failure zone. Only a couple of recent works tried to answer this question, resulting from opposing views. More precisely, Armero and Park ([39]) consider an elastic rectangular shear layer subjected to a propagation of stress wave from its two ends, leading to a strong displacement discontinuity in the middle, accompanied with a jump in the heat flux through the localization zone. In contrast with this hypothesis, Runesson et al. ([38]) considered the adiabatic condition with the material properties (i.e. heat capacity) at failure zone assumed to remain similar to the non-failure zone, leading to a jump in temperature field in the localized failure zone to accompany the displacement discontinuity. Neither fracture process zone, nor the temperature dependent material properties is considered in these works.

Thus, the first main target of this chapter is to provide the theoretical formulation for a coupled thermo-mechanical failure problem that can take into account both the fracture process zone and softening behavior at localized failure zone. We provide perhaps 'the best choice' compromise for describing the localized thermo-mechanical failure, introducing the displacement and deformation discontinuity for the mechanical part along with the discontinuity in temperature gradient for the thermal part. The proper justification for this choice based upon the adiabatic split is also provided. Another main aim of this chapter is to provide a very careful consideration of finite element approximation in the presence of thermo-mechanical coupling and localized failure which allows us to use the structured mesh. Here, we choose enhancement of strain field to accompany displacement discontinuity, which is needed to accommodate the temperature dependent material properties in the fracture process zone in the presence of non-homogeneous temperature field induced by localized failure. For clarity, in this chaper, the development is presented in detail for a one-dimensional bar subjected to static mechanical loading coupled with temperature transfer from one end to the other.

The efficiency of our numerical implementation is ensured by using the structured finite element mesh, which is constructed by employing the finite element methods with embedded discontinuities (ED-FEM). As explained by Ibrahimbegovic and Melnyk in [22], the proposed ED-FEM is proved to be a very successful alternative to the extended finite element method or X-FEM (see[48]), providing higher computational robustness with the discontinuities in displacement and in heat flux defined at the element level. The same helps to better separate the roles of strain versus displacement discontinuities, and considerably simplifies the numerical implementation within the standard computer code architecture.

The outline of this chapter is as follows. In Section 2.2, we provide the theoretical formulation of thermo-plastic model for localized failure in the one-dimensional framework. The embedded-discontinuity finite element method (ED-FEM) implementation for the problem is presented in Section 2.3. Several numerical simulations and illustrative results for 1D problem are given in Section 2.4. Conclusions and discussions are stated in Section 2.5.

2.2 Theoretical formulation of localized thermo-mechanical coupling problem

2.2.1 Continuum thermo-plastic model and its balance equation

The free energy of the continuum thermo-plastic consists of three components: mechanical energy, thermal energy and thermo-mechanical energy:

$$\psi\left(\varepsilon,\varepsilon^{p},\xi,\vartheta\right)=\frac{1}{2}E\left(\varepsilon-\varepsilon^{p}\right)^{2}-q\xi+\rho c\left[\left(\vartheta-\vartheta_{0}\right)-\vartheta\ln\left(\frac{\vartheta}{\vartheta_{0}}\right)\right]-\beta\left(\vartheta-\vartheta_{0}\right)\left(\varepsilon-\varepsilon^{p}\right) \tag{2-1}$$

Where E is the Young modulus, ε is the total strain, ε^{p} is the plastic strain, q is the stress-like variable associated to hardening, ξ is the hardening variable, ρ is the mass density, ϑ is the temperature, ϑ_0 is the reference temperature, c is the density heat capacity and β is the coefficient that gives the relation between stress and temperature. In this work, we consider that the mechanical properties are temperature dependent.

The state equations are given by

$$\sigma \coloneqq \frac{d\psi}{d\varepsilon} = E(\varepsilon-\varepsilon^{p})-\beta(\vartheta-\vartheta_{0}) \tag{2-2}$$

$$\eta^{e} \coloneqq -\frac{d\psi}{d\theta} = \beta(\varepsilon-\varepsilon^{p})+\rho c ln\left(\frac{\vartheta}{\vartheta_{0}}\right) \tag{2-3}$$

where σ is the stress and η^{e} is the reversible part of the entropy or "elastic" entropy (see [17])

The coefficient β can also be expressed in terms of the thermal expansion coefficient α: $\beta = E\alpha$

By taking the last result into account, (2-2) can be rewritten in an alternative form:

$$\sigma \coloneqq \frac{d\psi}{d\varepsilon} = E\left[(\varepsilon-\varepsilon^{p})-\underbrace{\alpha(\vartheta-\vartheta_{0})}_{\varepsilon_{th}}\right]=\sigma_{m}+\sigma_{th} \tag{2-4}$$

where ε_{th} denotes the thermal deformation, while σ_m denotes the mechanical part and σ_{th} the thermal part of stress.

Denoting withη^{p} the irreversible or "plastic" part of the "total" entropy η (with the additive split of entropy, $\eta = \eta^{e} + \eta^{p}$ - see ([17], [33]), the local form of internal dissipation rate can be expressed as follows:

$$0 \leq D_{int} \coloneqq \vartheta\dot{\eta} + \sigma\dot{\varepsilon} - \frac{de}{dt} = \vartheta\dot{\eta} + \sigma\dot{\varepsilon} - \frac{d(\psi+\eta^e\vartheta)}{dt} \tag{2-5}$$

where $e = \psi + \eta^e\vartheta$ is the internal energy. We can thus obtain the additive split of dissipation rate into mechanical and thermal part:

$$0 \leq D_{int} = \vartheta\left(\dot{\eta^e} + \dot{\eta^p}\right) + \sigma\dot{\varepsilon} - \underbrace{\frac{\partial\psi}{\partial\vartheta}}_{-\eta^e}\dot{\vartheta} - \underbrace{\frac{\partial\psi}{\partial\varepsilon}}_{\sigma}\dot{\varepsilon} - \underbrace{\frac{\partial\psi}{\partial\varepsilon^p}}_{-\sigma}\dot{\varepsilon^p} - \underbrace{\frac{\partial\psi}{\partial\xi}}_{-q}\dot{\xi} - \vartheta\dot{\eta^e} - \eta^e\dot{\vartheta} \tag{2-6}$$

$$0 \leq D_{int} = \underbrace{\vartheta\dot{\eta^p}}_{D_{ther}} + \underbrace{\sigma\dot{\varepsilon^p} + q\dot{\xi}}_{D_{mec\,h}} \tag{2-7}$$

The temperature dependent yield criterion for the material in the fracture process zone is defined as

$$\phi(\sigma, q, \vartheta) \coloneqq |\sigma| - (\sigma_y(\vartheta) - q(\vartheta)) \leq 0 \tag{2-8}$$

Where $\sigma_y(\theta)$ is the initial yield stress of the material at temperature ϑ and $q(\vartheta)$ is the stress-like hardening variable controlling the evolution of the yield threshold.

The form of the temperature dependence of these two variables is expressed in the following equations:

$$\sigma_y(\vartheta) = \sigma_y[1 - \omega(\vartheta - \vartheta_0)] \tag{2-9}$$

$$q = -K(\vartheta)\xi \;\; ; \;\; K(\vartheta) = K[1 - \omega(\vartheta - \vartheta_0)] \tag{2-10}$$

where σ_y and K are the values at the reference temperature ϑ_0.

The evolution laws of the state variables are established by the second law of thermodynamics, in which the internal dissipation reaches the maximum value. In particular, the Kuhn – Tucker condition is used to find the maximum of internal dissipation D_{int} among the admissible stress values with $\phi(\sigma, q, \vartheta) \leq 0$. This can be defined as the corresponding constrained minimization:

$$\underbrace{\max D_{int}(\sigma, q, \vartheta)}_{\phi(\sigma,q,\theta)\leq 0} \Leftrightarrow min\, max\, L(\sigma, q, \vartheta, \dot{\gamma}) \;;$$

$$L(\sigma, q, \vartheta, \dot{\gamma}) = -D_{int}(\sigma, q, \vartheta) + \dot{\gamma}\phi(\sigma, q, \vartheta) \tag{2-11}$$

The corresponding optimality conditions can be written as follows:

$$0 = \frac{\partial L}{\partial\sigma} \rightarrow \dot{\varepsilon^p} = \dot{\gamma}\frac{\partial\phi}{\partial\sigma} = \dot{\gamma}sign(\sigma) \tag{2-12}$$

$$0 = \frac{\partial L}{\partial q} \rightarrow \dot{\xi} = \dot{\gamma}\frac{\partial\phi}{\partial q} = \dot{\gamma} \tag{2-13}$$

$$0 = \frac{\partial L}{\partial \vartheta} \rightarrow \dot{\eta^p} = \dot{\gamma}\frac{\partial \phi}{d\vartheta} = \dot{\gamma}\left(\sigma_y + K\xi\right)\omega \tag{2-14}$$

where $\dot{\gamma}$ is the Lagrange multiplier.

The balance equations for the problem are obtained by using the force equilibrium equation and the first principle of thermodynamics. The force equilibrium equation can be written as:

$$-\rho\frac{d^2u}{dt^2} + \frac{d\sigma}{dx} + b = 0 \tag{2-15}$$

where ρ is the mass density, u is the displacement, σ is the stress and b is the distributed load. The energy balance is then established by using the first principle:

$$\frac{d}{dt}\left[e + \frac{1}{2}\rho\left(\frac{du}{dt}\right)^2\right] = b\frac{du}{dt} + \frac{d}{dx}\left(\sigma\frac{du}{dt}\right) + R - \frac{dQ}{dx} \tag{2-16}$$

where$e$ is the internal energy density, R is the distributed heat supply and Q is the heat flux. The last equation can be rewritten explicitly as:

$$\frac{de}{dt} + \rho\frac{du}{dt}\left(\frac{d^2u}{dt^2}\right) = b\frac{du}{dt} + \frac{d\sigma}{dx}\frac{du}{dt} + \sigma\frac{\partial^2 u}{\partial x \partial t} + R - \frac{dQ}{dx} \tag{2-17}$$

By combining this result with the force equilibrium equation, we get the reduced form of the first principle:

$$\frac{de}{dt} = \sigma\frac{d\varepsilon}{dt} + R - \frac{dQ}{dx} \tag{2-18}$$

By exploiting the Legrendre transformation, $e = \psi + \theta\eta^e$, we can further introduce the free energy potential ψ

$$\frac{de}{dt} = \frac{d\psi}{dt} + \dot{\vartheta}\eta^e + \vartheta\dot{\eta^e} \rightarrow \frac{de}{dt} = \underbrace{\frac{\partial \psi}{\partial \vartheta}}_{-\eta^e}\dot{\vartheta} + \underbrace{\frac{\partial \psi}{\partial \varepsilon}}_{\sigma}\dot{\varepsilon} + \underbrace{\frac{\partial \psi}{\partial \varepsilon^p}}_{-\sigma}\dot{\varepsilon^p} + \underbrace{\frac{\partial \psi}{\partial \xi}}_{-q}\dot{\xi} + \dot{\vartheta}\eta^e + \vartheta\dot{\eta^e} \tag{2-19}$$

Replacing this expression into (2-18), we get the final form of the balance equations:

$$\vartheta\dot{\eta^e} = -\frac{dQ}{dx} + \underbrace{\sigma\dot{\varepsilon^p} + q\dot{\xi}}_{D_{mec\,h}} + R \tag{2-20}$$

$$\rightarrow \vartheta\dot{\eta} = -\frac{dQ}{dx} + D_{int} + R \tag{2-21}$$

We note that the definition of thermal dissipation in (2-7), has allowed us to obtain the final result in (2-21). By considering further only quasi-static loading applications, we can recast (2-15) and (2-21) as the final form of the balance equations:

$$\begin{cases} 0 = \frac{d\sigma}{dx} + b \\ \vartheta\dot{\eta} = -\frac{dQ}{dx} + D_{int} + R \end{cases} \tag{2-22}$$

2.2.2 Thermodynamics model for localized failure and modified balance equation.

2.2.2.1 Thermodynamics model

When the localized failure happens, the free energy is decomposed into a regular part in the fracture process zone and the irregular part of free energy at the localized failure point:

$$\psi(\varepsilon, \varepsilon^p, \xi, \vartheta) = \bar{\psi}\left(\bar{\varepsilon}, \bar{\varepsilon}^p, \vartheta, \bar{\xi}\right) + \delta_{\bar{x}}\bar{\bar{\psi}}(\bar{\bar{\xi}}, \vartheta_l) \tag{2-23}$$

where $\bar{*}$ denotes the regular part and $\bar{\bar{*}}$ represents the singular part of the potential, ϑ denotes the temperature in any position and ϑ_l denotes the temperature at the localizedfailure point $\bar{x}$. In (2-23) above, the irregular part of energy is limited to the localized failure point by using $\delta_{\bar{x}}$, the Dirac delta function:

$$\delta_{\bar{x}}(x) = \begin{cases} \infty; & x = \bar{x} \\ 0; & otherwise \end{cases} \tag{2-24}$$

The regular part of the free energy pertains to the fracture process zone, and it keeps the same form as written in (2-1). The localized free energy is assumed to be equal to:

$$\bar{\bar{\psi}}(\bar{\bar{\xi}}, \vartheta_l) = \frac{1}{2}\bar{\bar{K}}(\vartheta_l)\bar{\bar{\xi}}^2 \tag{2-25}$$

where $\bar{\bar{\xi}}$ is theinternal variable quantifying the softening behavior due to localized failure. The chosen quadratic form of softening potential in (2-25) further allows us to obtain the corresponding stress-like internal variable

$$\bar{\bar{q}}\left(\vartheta, \bar{\bar{\xi}}\right) := -\frac{d\bar{\bar{\psi}}\left(\bar{\bar{\xi}}\right)}{d\bar{\bar{\xi}}} = -\bar{\bar{K}}(\vartheta_l)\bar{\bar{\xi}} \tag{2-26}$$

This variable drives the current ultimate stress value to zero, when the failure process is activated, as confirmed by the corresponding yield criterion:

$$\bar{\bar{\phi}}(t_{\bar{x}}, \bar{\bar{q}}) := |t_{\bar{x}}| - \left(\sigma_u(\vartheta_l) - \bar{\bar{q}}\left(\vartheta_l, \bar{\bar{\xi}}\right)\right) \leq 0 \tag{2-27}$$

where $|t_{\bar{x}}|$ is the traction at the localized failure point $\bar{x}$, $\sigma_u(\vartheta_l)$ is the initial value of ultimate stress.

The mechanical properties at localized failure are assumed to have the same dependence on temperature as the bulk part; hence, we can write:

$$\sigma_u(\vartheta_l) = \sigma_u[1 - \omega(\vartheta_l - \vartheta_0)] \tag{2-28}$$

$$\bar{\bar{K}}(\vartheta_l) = \bar{\bar{K}}[1 - \omega(\vartheta_l - \vartheta_0)] \tag{2-29}$$

where σ_u and $\bar{\bar{K}}$ are, respectively, the ultimate stress and softening modulus at reference temperature ϑ_0.

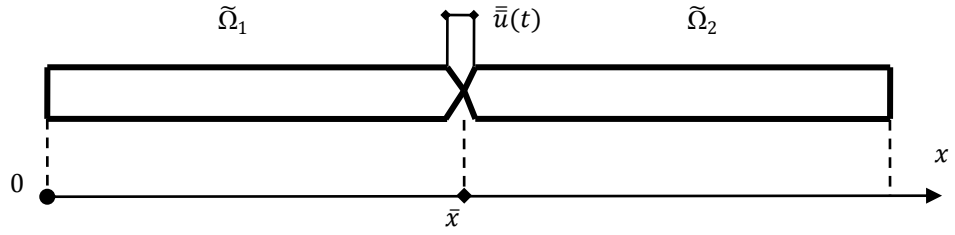

Figure 2-1.*Displacement discontinuity at localized failure for the mechanical load*

Once the localized failure occurs, the crack opening (further denoted as $\bar{\bar{u}}\,(t)$, seeFigure 2-1) contributes to a "jump" or irregular part in the displacement field. The total displacement field is thus sum of regular (smooth) part and irregular part:

$$u(x,t) = \hat{u}(x,t) + \bar{\bar{u}}(t)\{H_{\bar{x}}(x) - \varphi(x)\} \tag{2-30}$$

where$H_{\bar{x}}$ is the Heaviside function introducing the displacement jump

$$H_{\bar{x}} = \begin{cases} 0, x \le \bar{x} \\ 1, x > \bar{x} \end{cases} \tag{2-31}$$

In (2-30) above, $\varphi(x)$ is a (smooth) function, introduced to limit the influence of the displacement jump within the "failure" domain. Usual choice for $\varphi(x)$ in the finite element implementation pertains to the shape functions of selected interpolation. For example, for a 1D truss bar with 2 nodes and element length l_e, we can choose:

$$\varphi(x) = N_2(x) = \frac{x}{l_e} \tag{2-32}$$

The corresponding illustrations for $H_{\bar{x}}(x)$ and $\varphi(x)$ for a two-node truss-bar element are given inFigure 2-2

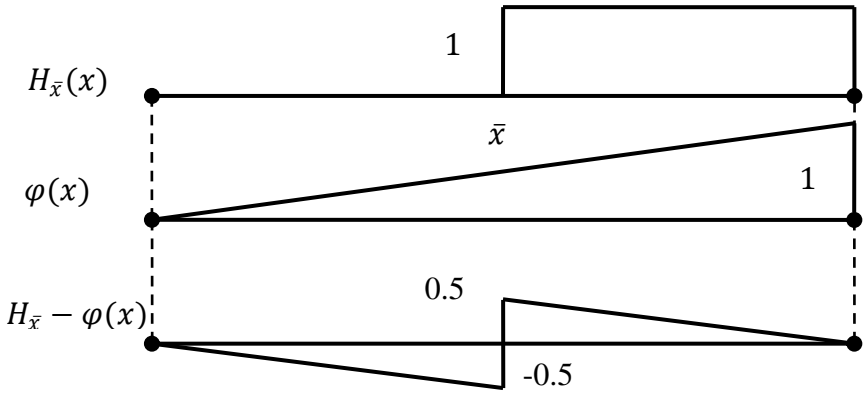

Figure 2-2.*Displacement discontinuity for 2-node bar element: Heaviside function* $\boldsymbol{H_{\bar{x}}}$ *and φ(x)*

Denoting with $\bar{u}(x,t) = \hat{u}(x,t) - \bar{\bar{u}}(t)\varphi(x)$ the continuous part of the displacement field, and with $\bar{\bar{u}}(t)$the "jump" in displacement, we can further write additive decomposition of displacement field:

$$u(x,t) = \bar{u}(x,t) + \bar{\bar{u}}(t)H_{\bar{x}}(x) \tag{2-33}$$

The corresponding strain field can then be obtained by exploiting the kinematic relation:

$$\varepsilon(x,t) := \frac{du}{dx} = \frac{\partial}{\partial x}[\bar{u}(x,t) + \bar{\bar{u}}(t)H_{\bar{x}}(x)] = \bar{\varepsilon} + \delta_{\bar{x}}(x)\bar{\bar{u}}(t) \tag{2-34}$$

The rate of internal dissipation can then be written as:

$$0 \le D_{int} = \vartheta\dot{\eta} + \sigma\dot{\epsilon} - \frac{d}{dt}e\left(\bar{\varepsilon}^e, \bar{\xi}, \bar{\bar{\xi}}, \vartheta\right) = \vartheta\dot{\eta} + \sigma\dot{\epsilon} - \frac{d}{dt}\left[\psi\left(\bar{\varepsilon}^e, \bar{\xi}, \bar{\bar{\xi}}, \vartheta\right) + \eta^e\vartheta\right]$$

$$D_{int} = \vartheta\dot{\eta}^p + \dot{\bar{\varepsilon}}^e\left[\sigma - \frac{\partial}{\partial\epsilon}\bar{\psi}\left(\bar{\varepsilon}^e, \bar{\xi}, \vartheta\right)\right] + \sigma\dot{\bar{\varepsilon}}^p - \frac{\partial\psi}{\partial\bar{\xi}}\dot{\bar{\xi}} - \delta_{\bar{x}}\frac{\partial\bar{\bar{\psi}}\left(\bar{\bar{\xi}}, \vartheta_l\right)}{\partial\bar{\bar{\xi}}}\dot{\bar{\bar{\xi}}} + \delta_{\bar{x}}\sigma_{\bar{x}}\dot{\bar{\bar{u}}}(t) + \frac{d\varphi(x)}{dx}\dot{\bar{\bar{u}}}(t) \tag{2-35}$$

For the elastic loading case where the rate of internal variables and the internal dissipation are equal to zero, we can obtain the stress constitutive equation:

$$\sigma := \frac{d}{d\epsilon}\bar{\psi}\left(\bar{\varepsilon}^e, \bar{\xi}, \vartheta\right) = E\left(\bar{\varepsilon} - \bar{\varepsilon}^p\right) - \beta(\vartheta - \vartheta_0) \tag{2-36}$$

For the bulk material, this equation remains the same as presented in (2-2). With this result in hand, we can obtain the final expression for internal dissipation for plastic loading case, where the correct interpretation ought to be given in terms of distribution (e.g. see [49]):

$$D_{int}^{\Omega} = \int_{\Omega^e} D_{int}\, dx = \int_{\Omega^e} (\vartheta\dot{\eta}^p + \sigma\dot{\varepsilon}^p + \bar{q}\dot{\bar{\xi}})\, dx + \left(\bar{\bar{q}}\dot{\bar{\bar{\xi}}}\right)|_{\bar{x}} \quad (2\text{-}37)$$

The evolution laws for localized variables are established in the same way as for the classical continuum model. In particular, the evolution equation for internal variable controlling softening can be written as:

$$0 = \frac{d\bar{\bar{L}}^{\Omega}}{d\bar{\bar{q}}} \rightarrow \dot{\bar{\bar{\xi}}}\delta_{\bar{x}} = \dot{\bar{\bar{\gamma}}}\delta_{\bar{x}} \frac{\partial\bar{\bar{\phi}}}{\partial\bar{\bar{q}}} = \dot{\bar{\bar{\gamma}}}\delta_{\bar{x}} \quad (2\text{-}38)$$

where $\dot{\bar{\bar{\gamma}}}$ is the plastic multiplier at the point of localized failure.

2.2.2.2 Thermo-mechanical balance equation

The set of force equilibrium equations consists of two equations:

(1) the local force equilibrium (established for all the bulk domain)

$$0 = \frac{d\sigma}{dx} + b \quad (2\text{-}39)$$

the stress orthogonality condition to define the traction at localized failure point

$$0 = t_{\bar{x}} + \int_{\Omega^e} \frac{d\varphi(x)}{dx}\sigma_{\bar{x}}\, dx \quad (2\text{-}40)$$

(2) Local balance of energy at the localized failure point

For the regular part, the local energy balance is still described by continuum thermodynamic model (2-21): $\vartheta\dot{\eta} = -\frac{dQ}{dx} + D_{int} + R$

The corresponding state equation (2-3) reads:

$$\eta^e = -\frac{d\psi}{d\vartheta} = \beta(\varepsilon - \varepsilon^p) + \rho c ln\left(\frac{\vartheta}{\vartheta_0}\right) \rightarrow \vartheta\dot{\eta}^e = \vartheta\beta\left(\dot{\varepsilon} - \dot{\varepsilon^p}\right) + \rho c\dot{\vartheta} \quad (2\text{-}41)$$

By considering that $\eta = \eta^e + \eta^p$, $D_{int} = D_{mec\,h} + D_{ther}$ and $D_{ther} = \vartheta\dot{\eta}^p$, the local energy balance can finally be rewritten in the format equivalent to the heat transfer equation:

$$\rho c\dot{\vartheta} = -\frac{dQ}{dx} + D_{mec\,h} - \vartheta\beta\left(\dot{\varepsilon} - \dot{\varepsilon^p}\right) + R \quad (2\text{-}42)$$

where the mechanical dissipation $D_{mec\,h}$ and the structural heating $(-\vartheta\beta\left(\dot{\varepsilon} - \dot{\varepsilon^p}\right))$ act as an additional heat source. This equation holds at any point of the material in the bulk.

We further consider that at the localized failure point, the material has no more ability to store heat, which implies setting the heat capacity to zero ($\rho c = 0$). We also take into account that at localized failure point there is no heat source ($R = 0$) nor thermal stress ($\beta = 0$). Therefore, the

mechanical dissipation at localized failure can be balanced only against the change of heat flux. Moreover, the local energy balance equation at the localized failure point ought to be interpreted in the distribution sense, resulting with the corresponding jump in the heat flux:

$$0 = -\left[\frac{dQ}{dx}\right]_{\bar{x}} + \int_{\Omega} \delta_{\bar{x}} \bar{\bar{D}}_{mec\,h} \rightarrow [\![Q]\!] = \left(\bar{\bar{D}}_{mec\,h}\right)|_{\bar{x}} \tag{2-43}$$

where the mechanical dissipation $\bar{\bar{D}}_{mec\,h}$ acts as the heat source at the failure point. As indicated in (2-21) to (2-43) above, this results in the corresponding "jump" of the heat flux through the localized failure section. We note in passing that the jump in the heat flux leads to a change of the temperature gradient at the localized point. In the finite element implementation, one needs additional shape functions for describing not only displacement but also temperature field, as described in the following.

2.3 Embedded-Discontinuity Finite Element Method (ED-FEM) implementation

2.3.1 Domain definition

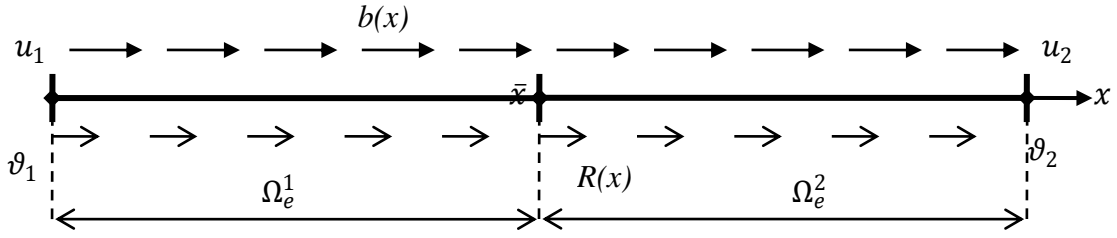

Figure 2-3. *Heterogeneous two-phase material for a truss bar, with phase-interface placed at* $\bar{x}$

We consider a 1D heterogeneous truss-bar subjected simultaneously to mechanical loading (including distributed load b(x) and prescribed displacements at both ends) and heat transfer along the bar (Figure 2-3). The material heterogeneity is the direct result of temperature dependent material parameters under heterogeneous temperature field. In particular, we consider that the bar is built of an elasto-plastic material, occupying two different sub-domains separated by localized failure point at $\bar{x}$:

$\Omega_e = \Omega_e^1 \cap \Omega_e^2$; $\Omega_e = [0, l_e]; \Omega_e^1 = [0, \bar{x}[$; $\Omega_e^2 =]\bar{x}, l_e]$

The mechanical localized failure is assumed to happen at the interface$\bar{x}$ (seeFigure 2-4)

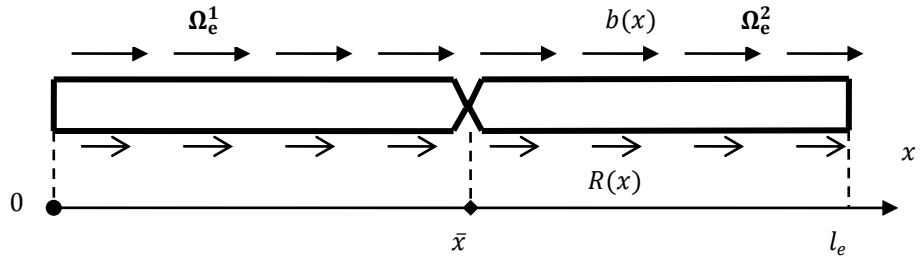

Figure 2-4.*Two sub-domain* $\boldsymbol{\Omega_e^1}$ *and* $\boldsymbol{\Omega_e^2}$ *separated by localized failure point at* $\bar{\boldsymbol{x}}$

In the following, the indices "1" is used for all the thermodynamics variables relate to sub-domain Ω_e^1, and the indices "2" to the second sub-domain Ω_e^2.

2.3.2 'Adiabatic' operator splitting solution procedure

Due to the positive experience of Kassiotis et al. (see [50]), we choose the operator split method based upon adiabatic split to solve this problem. In the most general case with active localized failure, the coupled thermomechanical problem is described by a set of mechanical balance equations defined in (2-39) and (2-40), accompanied by the energy balance equations in (2-42) and (2-43). Solving all of these equations simultaneously is certainly not the most efficient option. In order to increase the solution efficiency, we can choose between two possible operator split implementations: isothermal and adiabatic (see [17]). We note in passing that the isothermal operator split is not capable of providing the stability of the computation (see [50]). Therefore, we focus only upon the *adiabatic operator split method*. In this method, the problem is divided into two phases, with each one contribution to change of temperature:

Phase 1 - Mechanical part with "adiabatic"condition	**Phase 2- Thermal part**
$\begin{cases} 0 = \dfrac{d\sigma}{dx} + b \\ \dot{\eta} = 0 \rightarrow \rho c\dot{\theta} = D_{mec\,h} - \theta\beta\left(\dot{\varepsilon} - \dot{\varepsilon^p}\right) \end{cases}$	$\rho c\dot{\theta} = -\dfrac{dQ}{dx} + R$
(at localized failure point): $\sigma_{1\|\bar{x}} = \sigma_{2\|\bar{x}} = t_{\bar{x}}$	$[\![Q]\!] = \left(\bar{\bar{D}}_{mec\,h}\right)\|_{\bar{x}}$

The computations of the mechanical and thermal states remain coupled through the adiabatic condition.

2.3.3 Embedded discontinuity finite element implementation for the mechanical part

The basis of the numerical implementation is the weak form of the balance equations. For the mechanical part, we can write (e.g. see [17]):

$$\int_{\Omega^e} wbdx - \int_{\Omega^e} \frac{dw}{dx}\sigma dx + wb(l_e) - wb(0) = 0 \quad (2\text{-}44)$$

where *w* is the virtual displacement field. In the numerical implementation, we choose the simplest 2-node truss-bar element with linear shape functions:

$$N_1(x) = 1 - \frac{x}{l_e} \quad (2\text{-}45)$$

$$N_2(x) = \frac{x}{l_e} \quad (2\text{-}46)$$

where l_e is the element length. When the localized failure occurs, a displacement discontinuity at the failure point is introduced, with parameter $\alpha_1^m(t)$ representing the crack opening displacement. The latter is multiplied by shape function $M_1(x)$ (seeFigure 2-5), in order to limit the influence of crack opening to that particular element. Due to temperature dependence of material properties we might have potentially different values of Young's modulus in the two parts of the element. Considering that the stress remains continuous inside the element, as shown in [22], we must introduce the corresponding strain discontinuity at the localized failure point. This is carried out by using the shape function $M_2(x)$ shown inFigure 2-6 with the corresponding parameter $\alpha_2^m(t)$. We note that both $M_1(x)$ and $M_2(x)$ are chosen with respect to the localized failure that occurs in the middle of the element, so that $\bar{x} = \frac{l_e}{2}$. Thus, the displacement field interpolation can be written as:

$$u(x,t) = \sum_{a=1}^{2} N_a(x)d_a(t) + M_1(x)\alpha_1^m(t) + M_2(x)\alpha_2^m(t) \quad (2\text{-}47)$$

with

$$M_1(x) = H_{\bar{x}} - N_2(x) = \begin{cases} -\frac{x}{l_e} if x \in [0, \frac{l_e}{2}[\\ 1 - \frac{x}{l_e} if x \in]\frac{l_e}{2}, l_e] \end{cases} \quad (2\text{-}48)$$

$$M_2(x) = \begin{cases} -\frac{x}{l_e} if x \in [0, \frac{l_e}{2}[\\ \frac{x}{l_e} - 1 \quad if x \in]\frac{l_e}{2}, l_e] \end{cases} \quad (2\text{-}49)$$

The corresponding strain interpolation can then be written as:

$$\varepsilon(x,t) = \frac{du(x,t)}{dx} = \sum_{a=1}^{2} B_a(x) d_a(t) + G_1(x)\alpha_1^m(t) + G_2(x)\alpha_2^m(t) \tag{2-50}$$

$$G_1(x) = \frac{dM_1(x)}{dx} = \begin{cases} -\frac{1}{l^e} & if\ x \in [0, \frac{l_e}{2}[\cup]\frac{l_e}{2}, l_e] \\ -\frac{1}{l^e} + \delta_{\bar{x}}\ if & x = \bar{x} = \frac{l_e}{2} \end{cases} = \widetilde{G_1} + \delta_{\bar{x}_{(\bar{x}=\frac{l_e}{2})}}\ ;\ \widetilde{G_1} = -\frac{1}{l^e} \tag{2-51}$$

$$G_2(x) = \frac{dM_2(x)}{dx} = \begin{cases} -\frac{1}{l_e} if x \in [0, \frac{l_e}{2}[\\ \frac{1}{l_e} if x \in]\frac{l_e}{2}, l_e] \end{cases} \tag{2-52}$$

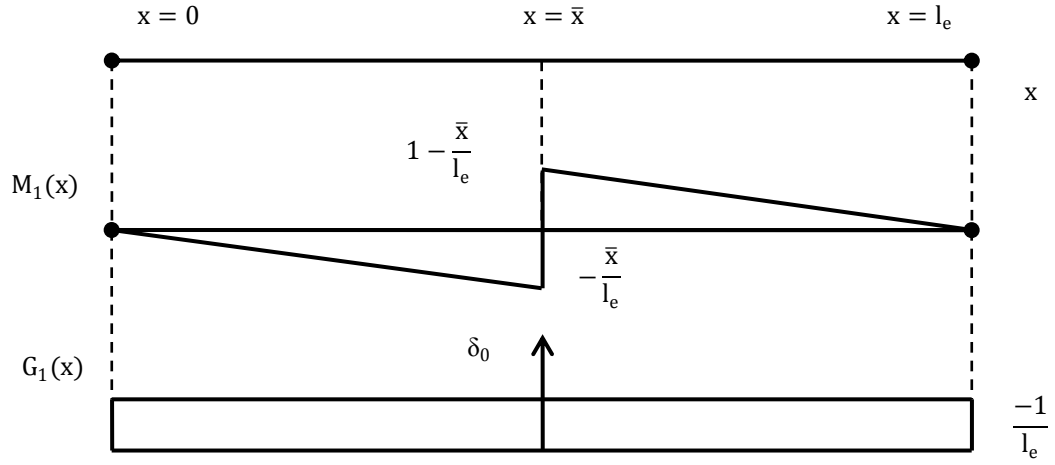

Figure 2-5*Displacement discontinuity shape function $M_1(x)$ and its derivative*.

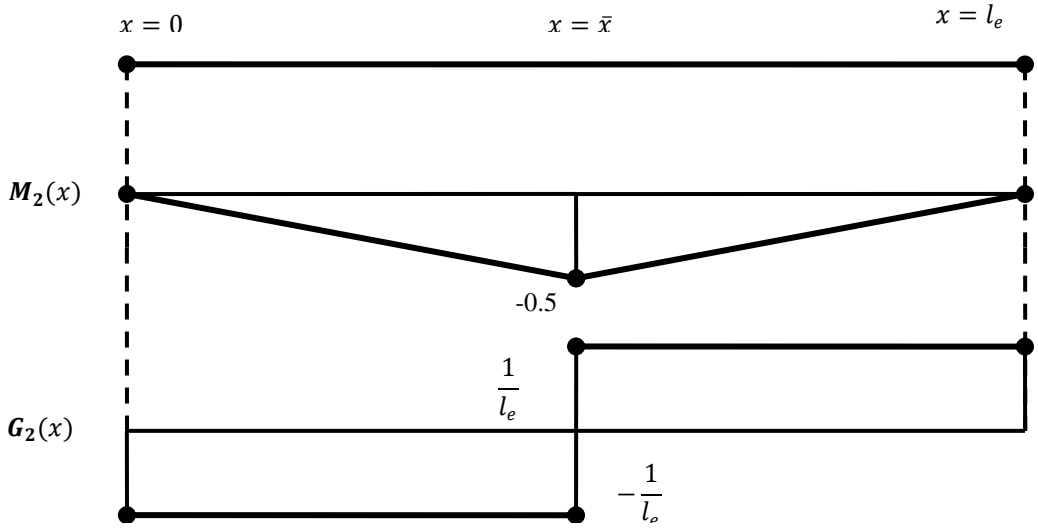

Figure 2-6. *Strain discontinuity shape function M2 and its derivative*

The corresponding discrete approximation of the virtual displacement and strain can be written in an equivalent form:

$$w(x) = N_a(x)w_a + M_1(x)\beta_1^m + M_2(x)\beta_2^m \tag{2-53}$$

$$\frac{dw(x)}{dx} = B_a(x)w_a + \widetilde{G_1}(x)\ \beta_1^m + G_2(x)\beta_2^m \tag{2-54}$$

where β_1^m and β_2^m are the variations corresponding to $\alpha_1^m(t)$ and $\alpha_2^m(t)$, respectively.With these interpolations in hand, the weak form of the equilibrium equation can be recast in incompatible mode format (see [18]) as the set of equations:

$$\begin{cases} A_{e=1}^{nel}(f^{int,e} - f^{ext,e}) = 0;\ f^{int,e} = \int_{\Omega_i^e} B_a^e \sigma_i(d_a, \alpha_1^m, \alpha_2^m, \theta_i)dx \\ h_1^e = 0;\ h_1^e = \sum \int_{\Omega_i^e} \tilde{G}_1^e \sigma_i(d_a, \alpha_1^m, \alpha_2^m, \theta_i)dx + t_{\bar{x}}(\alpha_1^m, \alpha_2^m) \\ h_2^e = 0; h_2^e = \sum \int_{\Omega_i^e} G_2^e \sigma_i(d_a, \alpha_1^m, \alpha_2^m, \theta_i)dx \end{cases} \tag{2-55}$$

Given highly nonlinear material behavior, this set of equations ought to be solved by an iterative scheme. If Newton's method is used, we make systematic use of the consistent linearization (see [17]), where the corresponding incremental stress-strain relation has to be obtained. We note that the chosen isoparametric elements provide continuum consistent interpolation, and furthermore that the continuum and discrete tangent modulus remain the same in one-dimensional setting (see [17]). Thus, we start with the consistent linearization of the continuum problem to obtain the stress rate constitutive equation, one in each sub-domain '*i*':

$$\dot{\sigma}_i = E_i\left(\dot{\varepsilon}_i - \dot{\varepsilon}_i^p\right) - \beta_i\dot{\theta}_i \tag{2-56}$$

The time derivative of temperature can be computed by imposing the adiabatic step:

$$\theta_i\dot{\eta}_i^e = \theta_i\beta_i\left(\dot{\varepsilon}_i - \dot{\varepsilon}_i^p\right) + \rho_i c_i\dot{\theta}_i = 0 \rightarrow \dot{\theta}_i = -\frac{\beta_i\theta_i}{\rho_i c_i}\left(\dot{\varepsilon}_i - \dot{\varepsilon}_i^p\right) \tag{2-57}$$

Combining the last two results, we finally obtain

$$\dot{\sigma}_i = C_i^{e,ad}\left(\dot{\varepsilon}_i - \dot{\varepsilon}_i^p\right);\ C_i^{e,ad} = E_i + \frac{\beta_i^2\theta_i}{\rho_i c_i} \tag{2-58}$$

Where $C_i^{e,ad}$ denotes the adiabatic tangent modulus. For sub-domain *i*, undergoing elastic loading, with $\dot{\varepsilon}_i^p = 0$, the constitutive equation can be simplified as:

$$\dot{\sigma}_i = C_i^{e,ad}\dot{\varepsilon}_i \tag{2-59}$$

On the other hand, if sub-domain *i* undergoes plastic loading, the consistency condition requires:

$$\dot{\bar{\phi}}_i(\sigma_i, q_i, \theta_i) = \frac{d\phi_i}{d\sigma_i}\dot{\sigma}_i + \frac{d\phi_i}{d\xi_i}\dot{\bar{\xi}}_i + \frac{d\phi_i}{d\theta_i}\dot{\theta}_i = 0 \tag{2-60}$$

With the expression for $\bar{\phi}_i$ chosen herein, (2-60) can further be simplified to:

$$sign(\sigma_i)\dot{\sigma}_i - K_i\dot{\bar{\xi}}_i + \left(\sigma_y^i + K_i\bar{\xi}_i\right)\omega_i\dot{\theta}_i = 0 \tag{2-61}$$

By using equation (2-57), we get the constitutive equation in rate form:

$$\dot{\sigma}_i = sign(\sigma_i)\left(\sigma_y^i + K_i\bar{\xi}_i\right)\omega_i\frac{\beta_i\theta_i}{\rho_i c_i}\dot{\bar{\varepsilon}}_i + \left[K_i - sign(\sigma_i)\left(\sigma_y^i + K_i\bar{\xi}_i\right)\omega_i\frac{\beta_i\theta_i}{\rho_i c_i}\right]\dot{\bar{\varepsilon}}_i^p \tag{2-62}$$

From equation (2-58), we have

$$\dot{\bar{\varepsilon}}_i^p = \dot{\bar{\varepsilon}}_i - \frac{\dot{\sigma}_i}{C_i^{e,ad}} \tag{2-63}$$

Combining equations(2-62) and (2-63) we can establish the constitutive equation for a plastic domain "*i*":

$$\dot{\sigma}_i = sign(\sigma)\left(\sigma_y^i + K_i\xi_i\right)\omega_i\frac{\beta_i\theta_i}{\rho_i c_i}\dot{\bar{\varepsilon}}_i + \left[K_i - sign(\sigma)\left(\sigma_y^i + K_i\xi_i\right)\omega_i\frac{\beta_i\theta_i}{\rho_i c_i}\right](\dot{\bar{\varepsilon}}_i - \frac{\dot{\sigma}_i}{C_i^{e,ad}})$$

$$\dot{\sigma}_i = \underbrace{\frac{K_i C_i^{e,ad}}{C_i^{e,ad} + K_i - sign(\sigma)\left(\sigma_y^i + K_i\xi_i\right)\omega_i\frac{\beta_i\theta_i}{\rho_i c_i}}}_{C_i^{p,ad}}\dot{\bar{\varepsilon}}_i \tag{2-64}$$

In conclusion, the following constitutive equation can be employed:

$$\dot{\sigma}_i = C_i^{ad}\dot{\bar{\varepsilon}}_i \;;\quad C_i^{ad} = \begin{cases} C_i^{e,ad} & ;\ if\,\bar{\phi}_i < 0 \quad elastic\ case \\ C_i^{p,ad} & ;\ if\,\bar{\phi}_i = 0 \quad plastic\ case \end{cases} \tag{2-65}$$

where $C_i^{e,ad}$ and $C_i^{p,ad}$ are defined in (2-59) and (2-64), respectively.

To solve the problem, two operator split are employed (e.g. see[17]) with 'local' and 'global' phases of computation. The former provides the internal variables, while the latter gives the nodal values of displacement. We briefly describe those two algorithm phases:

i) Local computation:

Given: $d_{a,n+1}, \bar{\varepsilon}_{i,n}^p, \bar{\xi}_{i,n},\ \alpha_{1,n}^m, \bar{\bar{\xi}}_n, \alpha_{2,n}^m$

Find: $\varepsilon_{i,n+1}^p, \bar{\xi}_{i,n+1}, \alpha_{i,n+1}^m, \bar{\bar{\xi}}_{n+1}, \alpha_{2,n+1}^m$

which should obey the following conditions:

$$\begin{cases} \bar{\phi}_i\left(\sigma_{i,n+1}, \bar{q}_{i,n+1}\right) \le 0;\ \bar{\gamma}_{i,n+1} \ge 0 \\ \quad \bar{\gamma}_{i,n+1}\bar{\phi}_{i,n+1} = 0; i = 1,2 \end{cases} \tag{2-66}$$

$$\begin{cases} \bar{\bar{\phi}}(t_{n+1}, \bar{\bar{q}}_{n+1}) \le 0;\ \bar{\bar{\gamma}}_{n+1} \ge 0 \\ \quad \bar{\bar{\gamma}}_{n+1}\bar{\bar{\phi}}_{n+1} = 0 \end{cases} \tag{2-67}$$

and

$$\int_{\Omega_1} G_2(x)\sigma_1(d_{a,n+1}, \alpha_1, \alpha_2)dx + \int_{\Omega_2} G_2(x)\sigma_2\left(d_{a,n+1}, \alpha_1, \alpha_2\right)dx = 0 \tag{2-68}$$

We note that (2-66) is used to compute plastic internal variables of two sub-domains at the step *(n+1)* from the previous step *(n)* by the so-called 'return-mapping' algorithm (see [51]). Conditions (2-67) and (2-68) are used to compute $\alpha_{1,n+1}$ and $\alpha_{2,n+1}$ by using the following algorithm:

i) Assume $\alpha_{1,n+1} \coloneqq \alpha_{1,n}$, $\alpha_{2,n+1} = 0$

ii) Compute trial stress at the two sub-domains with $\alpha_{1,n+1}$ and $\alpha_{2,n+1}$

$$\varepsilon_{n+1}^{test}(x,t) = \frac{du(x,t)}{dx} = B_a(x)d_a(t) + \tilde{G}_1(x)\alpha_{1,n}^{test,m}(t) + G_2(x)\alpha_{2,n+1}^{test,m}(t)$$

$$\sigma_{i,n+1}^{trial}\left(d_{a,n+1}, \alpha_{1,n+1}, \alpha_{2,n+1}\right) = C_i^{ead}\left(\varepsilon_{n+1}^{test} - \bar{\varepsilon}_p^i\right)$$

iii) Compute trial value of tension force at localized failure point

$$t_{n+1}^{trial} = -\sum \int_{\tilde{\Omega}_i} \tilde{G}_1\sigma_i^{trial}\left(d_{a,n+1}, \alpha_{1,n+1}^m, \alpha_{2,n+1}^m\right)dx \tag{2-69}$$

IF $\bar{\bar{\phi}}\left(t_{n+1}^{trial}, \bar{\bar{q}}_{n+1}\right) \le 0$ THEN $\alpha_{1,n+1}^m \coloneqq \alpha_{1,n}^m$ and go to step (vi)

iv) IF $\bar{\bar{\phi}}\left(t_{n+1}^{trial}, \bar{\bar{q}}_{n+1}\right) > 0$ THEN

$$\bar{\bar{\gamma}}_{n+1} = \frac{\bar{\bar{\phi}}\left(t_{n+1}^{trial}, \bar{\bar{q}}_{n+1}\right)}{\frac{C_1^{ead} + C_2^{ead}}{2l_e} + \bar{\bar{K}}} \tag{2-70}$$

(l_e is the length of the element)

$$\bar{\bar{\xi}}_{n+1} = \bar{\bar{\xi}}_n + \bar{\bar{\gamma}}_{n+1} \tag{2-71}$$

$$\alpha_{1,n+1}^m = \alpha_{1,n}^m + \bar{\bar{\gamma}}_{n+1} sign(t_{n+1}) \tag{2-72}$$

Return to step (ii) with the updated value of $\alpha_{1,n+1}$ and $\bar{\bar{\xi}}_{n+1}$

v) Compute updated value of $\alpha_{2,n+1}^m$ from condition (1-69)

$$\alpha_{2,n+1}^{m} \coloneqq \frac{(\sigma_1^{trial} - \sigma_2^{trial})l_e}{C_1^{ead} + C_2^{ead}} \tag{2-73}$$

With the updated value of $\alpha_{2,n+1}$ check

IF $\sum \int_{\Omega_i} G_2(x)\sigma_i(d_{a,n+1}, \alpha_1^m, \alpha_2^m)dx = 0$ THEN

EXIT

ELSE

Return to step (ii)

ii) Global computation

In global computation phase, the system (2-55) is rewritten in linearized form:

$$\begin{cases} Lin\left[\underset{e=1}{\overset{nel}{A}}\left(\mathbf{f}^{\text{int},e} - \mathbf{f}^{ext,e}\right)\right] = 0 \\ Lin\left[\mathbf{h}_1^e\right] = 0 \\ Lin\left[\mathbf{h}_2^e\right] = 0 \end{cases} \tag{2-74}$$

The corresponding result of consistent linearization can be recast in matrix notation:

$$\begin{bmatrix} \mathbf{K_{1e}} & \mathbf{F_{1e}} & \mathbf{F_{2e}} \\ \mathbf{F_{1e}^T} & \mathbf{H_{1e}} + \frac{\partial t(\alpha_1^m)}{\partial \alpha_1^m} & \mathbf{H_{2e}} \\ \mathbf{F_{2e}^T} & \mathbf{H_{2e}^T} & \mathbf{P_e} \end{bmatrix} \begin{Bmatrix} \mathbf{\Delta d_a} \\ \Delta\alpha_1 \\ \Delta\alpha_2 \end{Bmatrix} = \begin{Bmatrix} f_{n+1}^{int,e} - f_{n+1}^{ext,e} \\ 0 \\ 0 \end{Bmatrix} \tag{2-75}$$

where we have:

$$K_{1e} = \sum \int_{\Omega_i} B_a^T(x) C_i^{ad} B_a(x) dx \; ; \quad K_{1e} = \frac{C_1^{ad} + C_2^{ad}}{2l_e} \begin{bmatrix} 1 & -1 \\ -1 & 1 \end{bmatrix} \tag{2-76}$$

$$F_{1e} = \sum \int_{\Omega_i} B_a^T(x) C_i^{ad} \tilde{G}_1(x) dx \; ; \quad F_{1e} = \frac{C_1^{ad} + C_2^{ad}}{2l_e} \begin{Bmatrix} 1 \\ -1 \end{Bmatrix} \tag{2-77}$$

$$F_{2e} = \sum \int_{\Omega_i} B_a^T(x) C_i^{ad} G_2(x) dx \; ; \quad F_{2e} = \frac{C_1^{ad} - C_2^{ad}}{2l_e} \begin{Bmatrix} 1 \\ -1 \end{Bmatrix} \tag{2-78}$$

$$H_{1e} = \sum \int_{\Omega_i} \tilde{G}_1(x) C_i^{ad} \tilde{G}_1(x) dx \; ; \quad H_{1e} = \frac{C_1^{ad} + C_2^{ad}}{2l_e} \tag{2-79}$$

$$H_{2e} = \sum \int_{\tilde{\Omega}_i} \tilde{G}_1(x) C_i^{ad} G_2(x) dx \; ; \quad H_{2e} = \frac{C_1^{ad} - C_2^{ad}}{2l_e} \tag{2-80}$$

$$P_e = \sum \int_{\Omega_i} G_2(x) C_i^{ad} G_2(x) dx \; ; \quad P_e = \frac{C_1^{ad} + C_2^{ad}}{2l_e} \tag{2-81}$$

$$\frac{\partial t(\alpha_1^m)}{\partial \alpha_1^m} = \bar{\bar{K}} \, \mathrm{sign}(t_{\bar{x}}) \tag{2-82}$$

By using static condensation at the converged value of incompatible mode parameters, $\mathbf{\Delta d_a}$ is obtained as the solution of:

$$\mathbf{\hat{K} \Delta d_a} = f_{n+1}^{int,e} - f_{n+1}^{ext,e} \tag{2-83}$$

where $\hat{K}$ takes the standard form for the stiffness matrix:

$$\hat{K} = \left[\frac{C_1^{ad} + C_2^{ad}}{2l_e} - \frac{\frac{(C_1^{ad} + C_2^{ad}) C_1^{ad} C_2^{ad}}{2le^3} + \bar{\bar{K}} sign(t) \frac{\left(C_1^{ad} - C_2^{ad}\right)^2}{4l_e^2}}{\frac{C_1^{ad} C_2^{ad}}{l_e^2} + \frac{\bar{\bar{K}} sign(t) \left(C_1^{ad} + C_2^{ad}\right)}{2l_e}} \right] \begin{bmatrix} 1 & -1 \\ -1 & 1 \end{bmatrix} \tag{2-84}$$

Once $\Delta \mathbf{d_a}$ is obtained from (1-83), the nodal displacement can be updated: $\mathbf{d_{a,n+1} = d_{a,n} + \Delta d_a}$.

2.3.4 Embedded discontinuity finite element implementation for the thermal part

In thermal part, the heat transfer equation is written for two sub-domains as the following:

$$\rho_i c_i \dot{\vartheta}_i = -\frac{dQ_i}{dx} + R_i \tag{2-85}$$

And at the localized failure zone, the heat propagation happens with a jump in heat flux:

$$[\![\boldsymbol{Q}]\!] = \left(\bar{\bar{\boldsymbol{D}}}_{\boldsymbol{mech}}\right)|_{\bar{\boldsymbol{x}}} \tag{2-86}$$

In each of two sub-domains, the heat transfer obeys the Fourier heat conduction law:

$$Q_i = -k_i \frac{d\vartheta_i}{dx} \tag{2-87}$$

The local energy balance can be rewritten in the equivalent form to the heat equation:

$$\rho c\dot{\vartheta}_i = k_i \frac{d^2\vartheta_i}{dx^2} + R_i \tag{2-88}$$

The strong form (2-85) is further transferred into weak form by introducing an arbitrary temperature field, denoted as $\mathfrak{V}$, and by applying the virtual work laws:

$$\int_0^l \vartheta_i \left(\rho_i c_i \dot{\vartheta}_i - \frac{k_i d^2\vartheta_i}{dx^2} - R_i\right) dx = 0 \tag{2-89}$$

After integration by part, we can finally obtain the following weak form:

$$\int_0^l \vartheta_i \rho_i c_i \dot{\vartheta}_i dx + \int_0^l \frac{d\vartheta_i}{dx} k_i \frac{d\vartheta_i}{dx} dx = \int_0^l \vartheta_i R_i dx \tag{2-90}$$

We consider a 2-node truss-bar element. The nodal values of temperature and the weighting temperature at node i are denoted as $d_{\vartheta i}$ and $w_{\vartheta i}$, respectively. $\mathbf{d}_{\boldsymbol{\vartheta}}$and $\mathbf{w}_{\boldsymbol{\vartheta}}$ denote the real and the arbitrary nodal temperature vector, respectively. For a 2-node element, we have:

$$\mathbf{d}_{\boldsymbol{\theta}} = \begin{Bmatrix} d_{\vartheta_1} \\ d_{\vartheta_2} \end{Bmatrix}; \mathbf{w}_{\boldsymbol{\vartheta}} = \begin{Bmatrix} w_{\vartheta_1} \\ w_{\vartheta_2} \end{Bmatrix},$$

The real and weighting temperature fields along the element are constructed with interpolation shape functions. Furthermore, the jump of temperature gradient at the localized failure point, is represented by an additional shape function:

$$\vartheta_i(x) = \sum_{a=1}^{2} N_a(x) d_\vartheta^a(t) + M_2(x)\alpha_2^t(t) \tag{2-91}$$

where $N_a(x)$ and $M_2(x)$ are defined in (2-49) and illustrated in Figure 2-6 for a two-node truss-bar element, whereas $\alpha_2^t(t)$ is the variable controlling the 'jump' in temperature gradient. We note that $\theta_l(t) = \frac{1}{2}\left(d_\theta^1(t) + d_\theta^2(t)\right) + \alpha_2(t)$, where θ_l is the temperature at the interface (at the middle of the element).

Apply the Fourier laws to the localized point, we have:

$$\|Q\|\delta_{\bar{x}} = -k_{\bar{x}}\left(\frac{d^2\vartheta}{dx^2}\right)_{\bar{x}} = -k_{\bar{x}}\left[\frac{d^2N_a(x)}{dx^2} d_\vartheta^a(t) + \underbrace{\frac{d^2M_2(x)}{dx^2}}_{\delta_{\bar{x}}}\alpha_2^t(t)\right] = -k_{\bar{x}}\alpha_2^t(t)\delta_{\bar{x}}$$

$$\rightarrow \|Q\| = -k_{\bar{x}}\alpha_2^t(t) \tag{2-92}$$

where $k_{\bar{x}}$ denotes the heat conductivity coefficient at the localized failure. By combining equation (2-92) with equation (2-86), we can infer the equation for $\alpha_2^t(t)$:

$$\|Q\| = -k_{\bar{x}}\alpha_2^t(t) = \bar{\bar{D}}_{mec\,h} \rightarrow \alpha_2^t(t) = \frac{\bar{\bar{D}}_{mec\,h}}{k_{\bar{x}}} \tag{2-93}$$

The iso-parametric interpolation functions are used for the weighting temperature field:

$$w_\vartheta(x) = N_a(x)w_\vartheta^a \tag{2-94}$$

By taking into account the interpolation of real and weight temperature fields, the weak form (2-90) is finally reduced to:

$$\int_{\Omega_i^e}\left[N_a(x)\rho_i c_i N_a(x)\dot{d}_\vartheta^a + N_a(x)\rho_i c_i M_2(x)\dot{\alpha}_2(t) + B_a(x)k_i B_a(x)d_\vartheta^a + B_a(x)k_i G_2(x)\alpha_2(t)\right]dx = Q_\vartheta^a \tag{2-95}$$

Finally, the finite element equations to be solved for the "thermal" phase are given by:

$$A_{e=1}^{N_{el}}\left(\mathbf{M^e}\dot{\mathbf{d}}_\vartheta^\mathbf{e} + \mathbf{P^e}\dot{\alpha}_2^e + \mathbf{K^e}\mathbf{d}_\vartheta^\mathbf{e} + \mathbf{F^e}\alpha_2^e\right) = A_{e=1}^{N_{el}}\left(\mathbf{Q_\theta^1}\right) \tag{2-96}$$

where

$$\mathbf{M}_{2x2}^e = \sum\int_{\Omega_i^e} N_a(x)\rho_i c_i N_a\ (x)\,dx\ ;\ \mathbf{M}_{2x2}^e = \frac{l_e}{24}\begin{bmatrix} 7\rho_1 c_1 + \rho_2 c_2 & 2(\rho_1 c_1 + \rho_2 c_2) \\ 2(\rho_1 c_1 + \rho_2 c_2) & \rho_1 c_1 + 7\rho_2 c_2 \end{bmatrix} \tag{2-97}$$

$$\mathbf{P}_{1x2}^e = \sum\int_{\Omega_i^e} N_a(x)\rho_i c_i M_2(x)\,dx\ ;\ \mathbf{P}_{1x2}^e = -\frac{l_e}{24}\begin{Bmatrix} 2\rho_1 c_1 + \rho_2 c_2 \\ \rho_1 c_1 + 2\rho_2 c_2 \end{Bmatrix} \tag{2-98}$$

$$\mathbf{K}_{2x2}^e = \sum\int_{\Omega_i^e} B_a(x)k_i B_a(x)\ dx;\mathbf{K}_{2x2}^e = \frac{(k_1+k_2)}{2l_e}\begin{bmatrix} 1 & -1 \\ -1 & 1 \end{bmatrix} \tag{2-99}$$

$$\mathbf{F}_{1x2}^e = \sum\int_{\Omega_i^e} B_a(x)k_i G_2(x)\ dx;\mathbf{F}_{1x2}^e = \frac{k_1-k_2}{2l_e}\begin{Bmatrix} 1 \\ -1 \end{Bmatrix} \tag{2-100}$$

$$\mathbf{Q}_{\vartheta\,1x2}^1 = Q_\vartheta^a;\mathbf{Q}_{\vartheta\,1x2}^1 = \frac{l_e}{8}\begin{Bmatrix} 3R_1 + R_2 \\ R_1 + 3R_2 \end{Bmatrix} \tag{2-101}$$

There are many methods capable of solving the time-dependent equation (2-96) (see [17]). In this paper, the Newmark integration scheme is chosen. Assuming that the heat transfer problem lasts for a duration $[0,T]$, this duration can be divided into n increments: $[t_0=0,\ t_1..,\ t_k,\ ..t_{n-1},\ t_n=T]$ with the time step $h = t_{k+1} - t_k$.

By considering the equation of Newmark: $\Delta\dot{\boldsymbol{d}}_\vartheta = \Delta\boldsymbol{v} = \frac{\gamma}{\beta h}\Delta\boldsymbol{d}_\vartheta$ (where γ and β are the Newmark coefficients) and by linearization, equation (2-96) becomes:

$$A_{e=1}^{N_{el}}\left(\left(\frac{\gamma}{\beta\Delta t}\mathbf{M}^{e}+\mathbf{K}^{e}\right)\Delta\mathbf{d}_{\vartheta}\right)=A_{e=1}^{N_{el}}\left(\mathbf{R}^{k}\right) \tag{2-102}$$

where the residuals are computed by the following equation

$$\mathbf{R}^{k}=\mathbf{Q}_{\vartheta}^{1}-\mathbf{M}^{e}\dot{\mathbf{d}}_{\vartheta}^{k}-\mathbf{P}^{e}\dot{\alpha}_{2}^{k}-\mathbf{K}^{e}\mathbf{d}_{\vartheta}^{k}-\mathbf{F}^{e}\alpha_{2}^{k} \tag{2-103}$$

Once $\boldsymbol{\Delta d}_{\vartheta}$ is known, the nodal temperature at the next time step can be updated by the formula:

$$\mathbf{d}_{\vartheta}^{k+1}=\mathbf{d}_{\vartheta}^{k}+\boldsymbol{\Delta}\mathbf{d}_{\vartheta} \tag{2-104}$$

We note that the nodal temperature received in equation (2-104) should also be added the increment of temperature due to structural heating (adiabatic condition) which was explained in equation (2-57).

2.4 Numerical simulations

2.4.1 Simple tension imposed temperature example with fixed mesh

In this section we consider several numerical examples in order to illustrate the satisfying performance of the proposed model. We consider a steel bar 5 mm long. The bar is built-in at left end and subjected to an imposed displacement at right end. The imposed displacement increases 1.6×10^{-4} mm in each step. Simultaneously, right end of the bar is heated and its temperature is raised from 0^0C to 1000^0C, with 10^0C increase in each step. The temperature at left end is kept equal to 0^oC. The loading increases until localized failure of the bar. The problem geometric data and loading program are described in Figure 2-7and Figure 2-8, respectively.

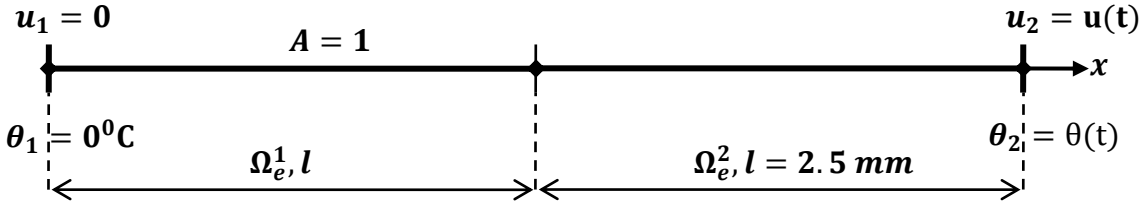

Figure 2-7. *Bar subjected to imposed displacement and temperature applied simultaneously*

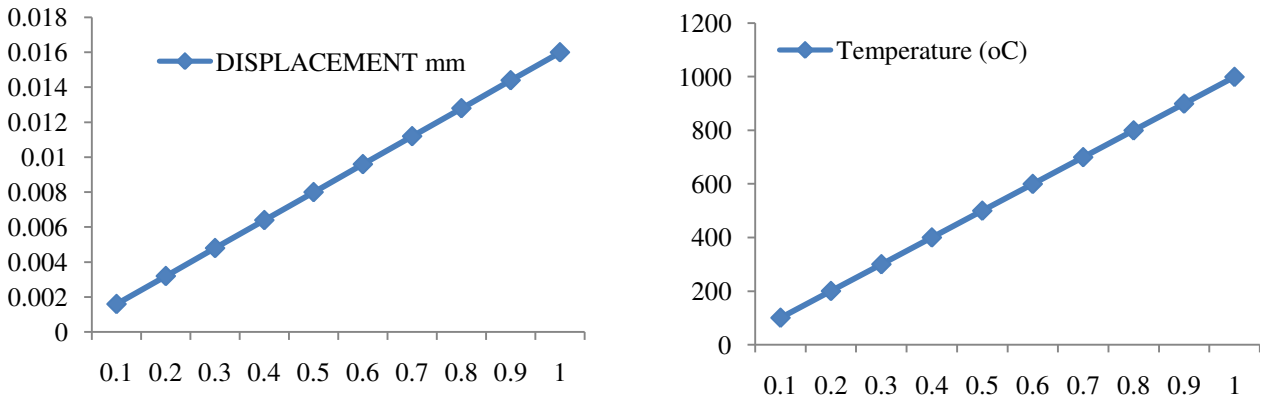

Figure 2-8. *Time variation of imposed displacement and temperature*

The problem is subsequently considered for three different variations of material properties: (i) the material properties are independent of temperature, (ii) the material properties are linearly dependent on temperature and (iii) the material properties are non-linearlydependent on temperature (following suggestion given by regulation of Eurocode [6])

2.4.1.1 Material properties independent on temperature

In this case, the material properties of the bar are assumed to be constant with respect to any change in temperature. The chosen values for material parameters are given in Table 2-1.

Table 2-1. *Material properties of steel bar*

Material Properties	**Value**	**Dimension**
Young modulus (E)	205000	MPa
Initial yield stress (σ_y)	250	MPa
Ultimate stress (σ_u)	300	MPa
Plastic hardening modulus (K_p)	20000	MPa
Localized softening modulus ($\bar{\bar{K}}$)	-30000	$MPam^{-1}$
Mass Density (ρ)	$7.865\ 10^{-9}$	Ns^2mm^{-4}
Thermal conductivity (k)	45	$N\ s^{-1}K^{-1}$
Heat specific (c)	$0.46\ 10^{9}$	$mm^2s^{-2}K^{-1}$
Thermal elongation (α)	0.00001	

The computed results for stress-strain curves in two sub-domains are presented in Figure 2-9, while the force-displacement curve of the bar is given in Figure 2-10. In Table 2-2 and Figure 2-11, we show the resulting time evolution of temperature and its distribution along the bar. For this case with material properties independent on temperature, we can conclude that there is no difference in the strain values between two sub-domains. The 'jump' in temperature gradient (α^{th}), which appears at localized failure point, also remains very small. The computed dissipation due to plasticity in fracture process zone is 36.63Nmm, while the dissipation due to localized failure is 29.44Nmm. In summary, the total mechanical dissipation in the bar is equal to 66.07Nmm.

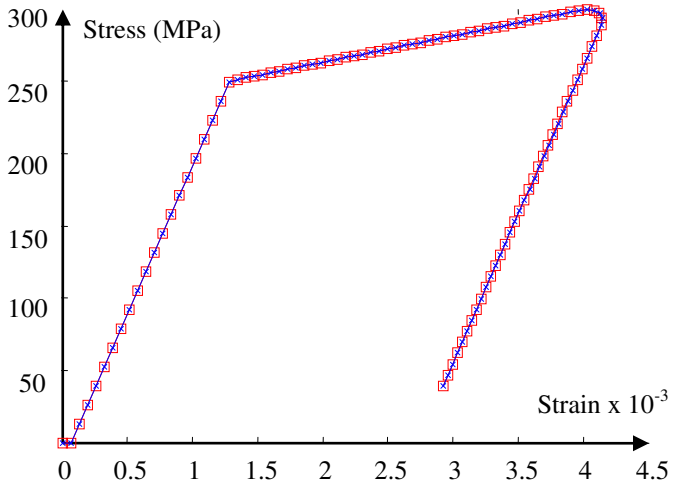

Figure 2-9. *Stress– strain curves in two sub-domains*

(blue line for the 1st sub-domain, red square for the 2nd sub-domain)

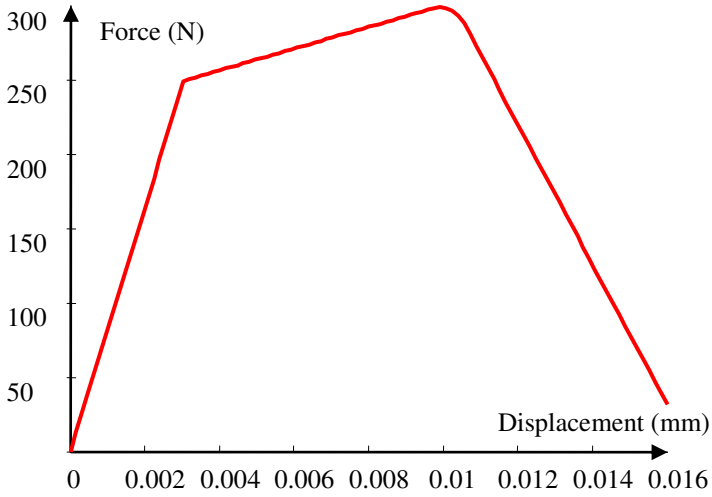

Figure 2-10. *Force – displacement curve of the bar*

Table 2-2.*Time Evolution of Temperature along the Bar*

Time	ϑ at x =0	ϑ at x=0.25le	ϑ at x = 0.5le	ϑ at x=0.75le	ϑ at x = le	$\Delta\vartheta$
0	0.0000	0.0000	0.0000	0.0000	0.0000	0.0000
0.1	0.0000	25.0000	50.0000	75.0000	100.0000	0.0000
0.2	0.0000	50.0000	100.0000	150.0000	200.0000	0.0000
0.3	0.0000	75.0000	150.0000	225.0000	300.0000	0.0000
0.4	0.0000	100.0000	200.0000	300.0000	400.0000	0.0000
0.5	0.0000	125.0000	250.0000	375.0000	500.0000	0.0000
0.6	0.0000	150.0000	300.0000	450.0000	600.0000	0.0000
0.7	0.0000	175.0005	350.0010	525.0005	700.0000	0.0010
0.8	0.0000	200.0007	400.0014	600.0007	800.0000	0.0014
0.9	0.0000	225.0008	450.0015	675.0008	900.0000	0.0015
1	0.0000	250.0008	500.0016	750.0008	1000.000	0.0016

where $\Delta\vartheta = \vartheta_{x=0.5l_e} - 0.5(\vartheta_{x=0} + \vartheta_{x=l_e})$

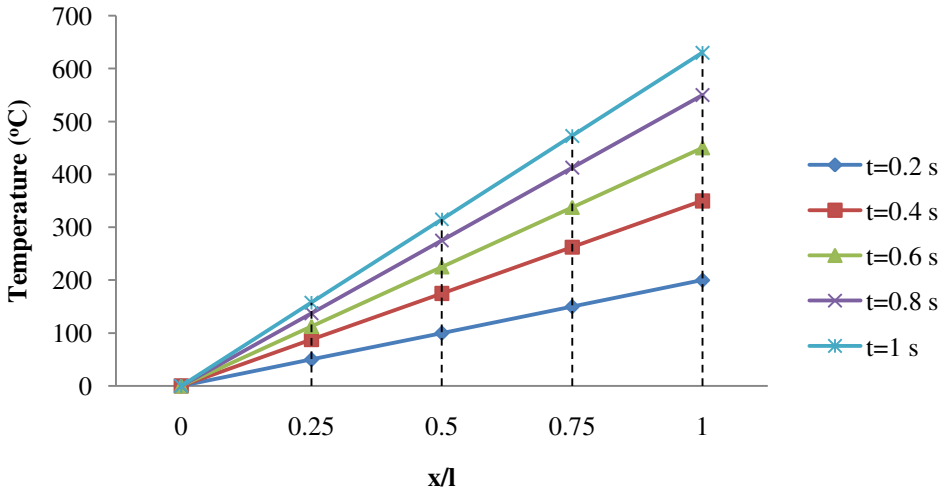

Figure 2-11. *Distribution of temperature (^oC) along the bar at chosen values of time*

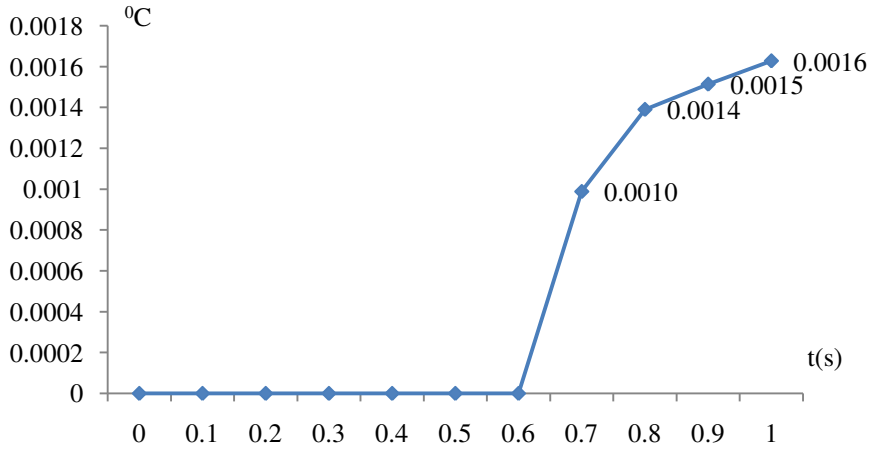

Figure 2-12. *Evolution of $\Delta\,\vartheta$ versus time (in ^0C)*

2.4.1.2 Material properties are linearly dependent on temperature

In this example, the mechanical material properties of the steel bar chosen in the first example (see Table 2-1) are assumed to hold only at reference temperature (equal to 0^0C). For other temperature values, they vary linearly according to the following expression:

initial yield stress: $\sigma_y(\theta) = 250(1 - 0.001\theta)$ MPa

ultimate strength: $\sigma_u(\theta) = 300(1 - 0.0015\theta)\ MPa$

Young's modulus: $E(\theta) = 2.05 \times 10^5(1 - 0.0008\theta)\ MPa$

plastic hardening modulus: $K_p(\theta) = 2 \times 10^4(1 - 0.0008\theta)\ MPa$

localized softening modulus: $\bar{\bar{K}}(\theta) = -3 \times 10^4(1 - 0.0008\theta)\ MP$a

The thermal material properties are independent on temperature and equal to those in the first example. The resulting stress-strain curves in two sub-domains and resulting force-displacement diagram are presented in Figure 2-13 and Figure 2-14, respectively.

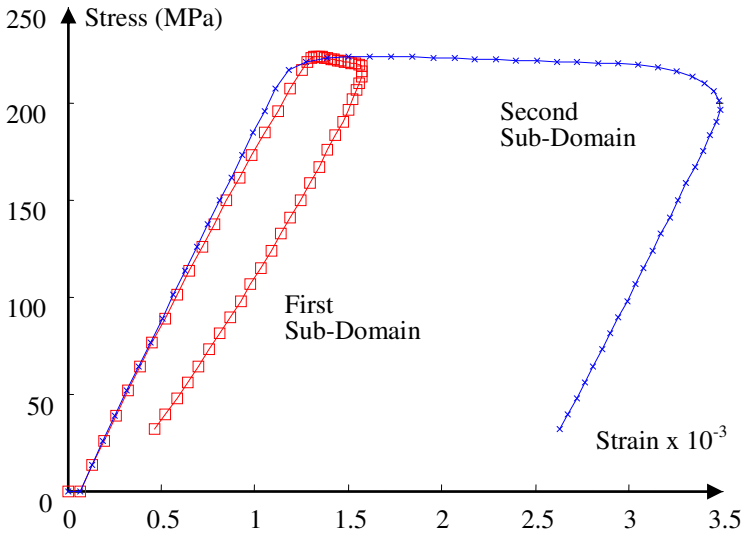

Figure 2-13. *Stress-strain curves in two sub-domains*

(blue line for the 1st sub-domain, red square for the 2nd sub-domain)

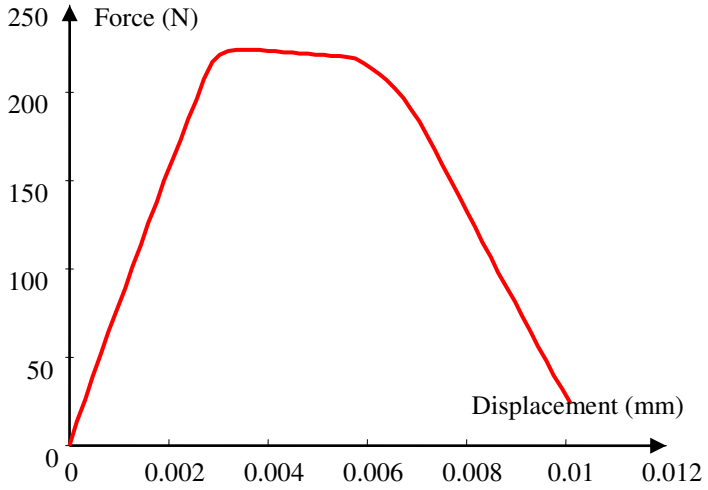

Figure 2-14. *Force displacement curve*

In this example, the total plastic dissipation and the total localized dissipation are 14.08Nmm and 13.82Nmm, respectively. Thus, the total mechanical dissipation is equal to 27.90Nmm.

Table 2-3.*Time evolution of temperature along the bar*

Time	ϑ at x =0	ϑ at x=0.25le	ϑ at x = 0.5le	ϑ at x=0.75le	ϑ at x = le	$\Delta\vartheta$
0.0000	0.0000	0.0000	0.0000	0.0000	0.0000	0.0000
0.1000	0.0000	25.0000	50.0000	75.0000	100.0000	0.0000
0.2000	0.0000	50.0000	100.0000	150.0000	200.0000	0.0000
0.3000	0.0000	75.0000	150.0000	225.0000	300.0000	0.0000
0.3500	0.0000	87.5000	175.0000	262.5000	350.0000	0.0000
0.4000	0.0000	100.0000	199.9999	300.0000	400.0000	-0.0001
0.4500	0.0000	112.5002	225.0005	337.5002	450.0000	0.0005
0.5000	0.0000	125.0004	250.0007	375.0004	500.0000	0.0007
0.5500	0.0000	137.5004	275.0008	412.5004	550.0000	0.0008
0.6000	0.0000	150.0004	300.0008	450.0004	600.0000	0.0008
0.6300	0.0000	157.5004	315.0008	472.5004	630.0000	0.0008

where $\Delta\vartheta = \vartheta_{x=0.5l_e} - 0.5(\vartheta_{x=0} + \vartheta_{x=l_e})$

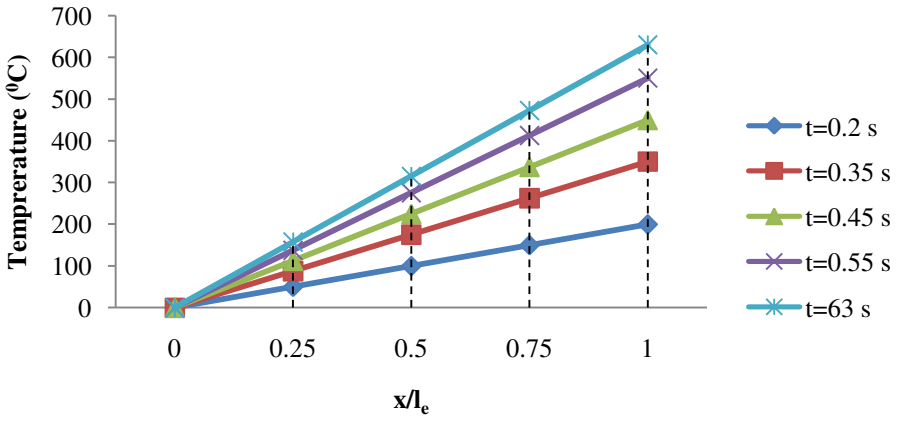

Figure 2-15. *Evolution of temperature (^oC) along the bar in time*

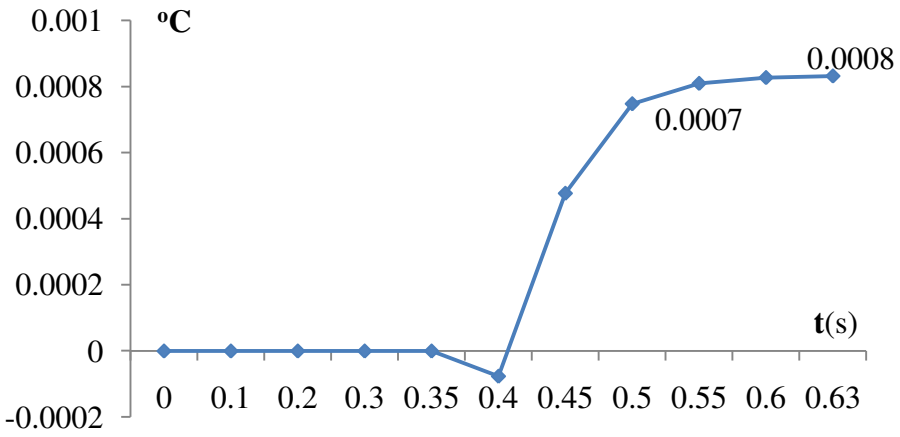

Figure 2-16. *Evolution of $\Delta\vartheta$ versus time (in ^0C)*

From the results presented in the figures above, we can conclude that the temperature variations deeply influence the behavior of the bar. In particular, the displacement at the end of the bar when failure occurs reduces from 0.016mm to 0.011mm, the initial yield stress falls down to approximately 225MPa from 250MPa and so the ultimate strength reduces from 300MPa to about 220MPa. The total dissipation in this example is also reduced, from 66.07Nmm to 27.90Nmm. Figure 2-13indicates that the variation of temperature field leads to a significant difference in the material behavior and computed stress-strain curves in two parts of the bar. The "jump" in temperature gradient accompanying localized failure remains relatively small.

2.4.1.3 Material properties non-linearly dependent on temperature (Eurocode 1993-1-2 [6])

In Eurocode1993-1-2 (see[6]), the material properties of steel bar subjected to thermal loading are not constant but dependent on temperature as multi-linear functions. Based on those regulations, evolution of mechanical properties as functions of temperature can be established as follows:

initial yield stress: $\sigma_y(\vartheta) = 250\left(1 - \omega_{\sigma_y}(\vartheta - 20)\right)$ MPa

ultimate strength: $\sigma_u(\vartheta) = 300\left(1 - \omega_{\sigma_u}(\vartheta - 20)\right)$ MPa

Young's modulus: $E(\vartheta) = 2.05 \times 10^5\left(1 - \omega_E(\vartheta - 20)\right)$MPa

plastic hardening modulus: $K_p(\vartheta) = 2 \times 10^4\left(1 - \omega_{K_p}(\vartheta - 20)\right)$ MPa

localized softening modulus: $\bar{\bar{K}}(\vartheta) = -3 \times 10^4\left(1 - \omega_{\bar{\bar{K}}}(\vartheta - 20)\right)$ MPa

where ω_* are the temperature dependent coefficients. The values of the temperature dependent coefficientsfor yield stress, ultimate strength and Young's modulus are taken from Eurocode 1993-1-2 (see[6]). The corresponding values of coefficients for plastic hardening modulus and localized softening modulus are taken the same as the one for Young's modulus. All the values used for these coefficients are presented inTable 2-4.

Table 2-4. *Temperature dependent coefficients*

$\vartheta(^0\mathrm{C})$	ω_{σ_u}	ω_{σ_y}	ω_E	ω_{K_p}	$\omega_{\overline{K}}$
0	0.00000	0.00000	0.00000	0.00000	0.00000
20	0.00000	0.00000	0.00000	0.00000	0.00000
100	0.00000	0.00000	0.00000	0.00000	0.00000
200	0.00000	0.00107	0.00056	0.00056	0.00056
300	0.00000	0.00138	0.00071	0.00071	0.00071
400	0.00000	0.00153	0.00079	0.00079	0.00079
500	0.00046	0.00133	0.00083	0.00083	0.00083
600	0.00091	0.00141	0.00119	0.00119	0.00119
700	0.00113	0.00136	0.00128	0.00128	0.00128
800	0.00114	0.00122	0.00117	0.00117	0.00117
900	0.00107	0.00109	0.00106	0.00106	0.00106
1000	0.00098	0.00099	0.00097	0.00097	0.00097
1100	0.00091	0.00091	0.00091	0.00091	0.00091
1200	0.00085	0.00085	0.00085	0.00085	0.00085

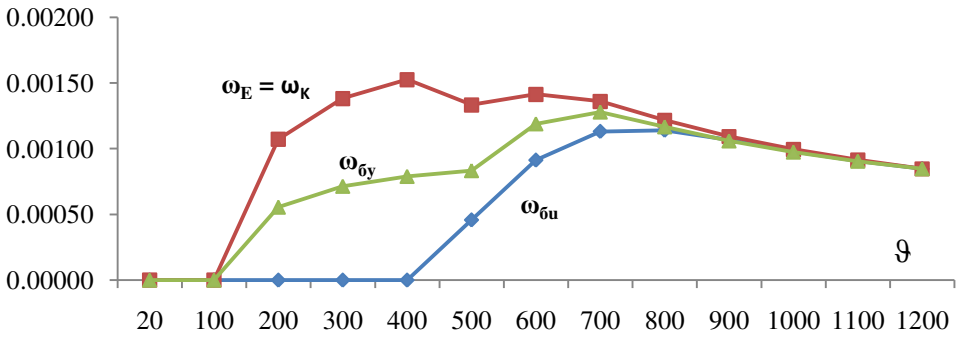

Figure 2-17.*Temperature dependent coefficients (according to* **[6]***)*

The evolution of thermal properties is also taken from Eurocode1993-1-2.

Thermal elongation

$$\alpha = \begin{cases} 1.2 \times 10^{-5}\vartheta_a + 0.4 \times 10^{-8}\vartheta_a^2 - 2.416 \times 10^{-4}, if 20^0C \le \vartheta_a < 750^0C \\ 1.1 \times 10^{-2}, if 750^0C \le \vartheta_a < 860^0C \\ 2 \times 10^{-5}\vartheta_a - 6.2 \times 10^{-3}, if 860^0C \le \vartheta_a < 1200^0C \end{cases}$$

Specific heat

$$c = \begin{cases} 425 + 7.73 \times 10^{-1}\vartheta_a - 1.69 \times 10^{-3}\vartheta_a^2 + 2.22 \times 10^{-6}\vartheta_a^3 \dfrac{J}{kgK} & if 20^0C \le \vartheta_a < 600^0C \\ 666 + \dfrac{13002}{738 - \vartheta_a}\dfrac{J}{kgK} & if 600^0C \le \vartheta_a < 735^0C \\ 545 + \dfrac{17820}{\vartheta_a - 731}\dfrac{J}{kgK} & if 735^0C \le \vartheta_a < 900^0C \\ 650\dfrac{J}{kgK} & if \vartheta_a \ge 900^0C \end{cases}$$

Thermal conductivity

$$k = \begin{cases} 54 - 3.33 \times 10^{-2}\vartheta_a \dfrac{W}{mK}, if\ 20^0C \le \vartheta_a < 800^0C \\ 27.3\dfrac{W}{mK}, if\ 800^0C \le \vartheta_a \le 1200^0C \end{cases}$$

The main results obtained considering those evolutions are described subsequently in terms of the stress-strain curves, force-displacement diagram and corresponding temperature variations.

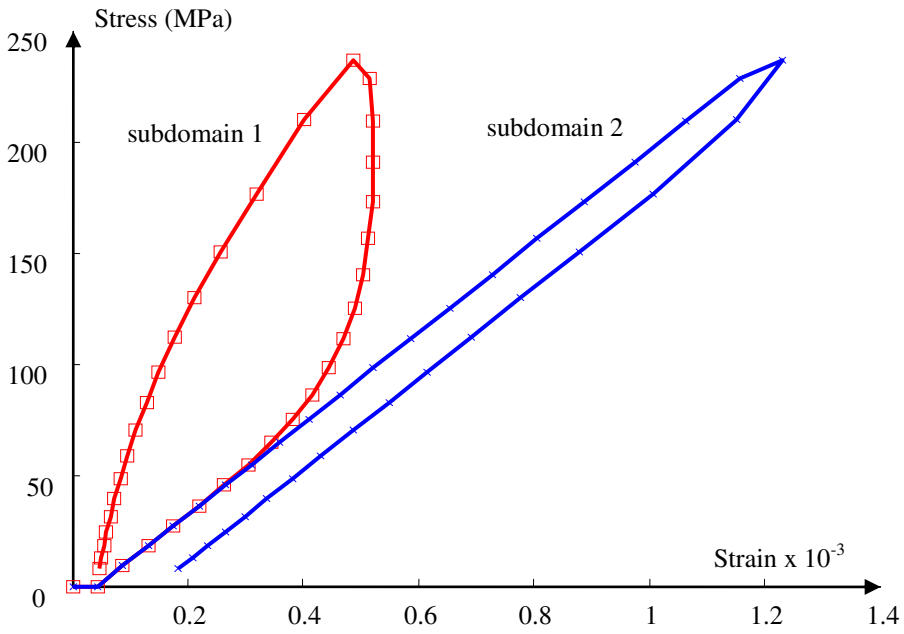

Figure 2-18. *Stress-strain curvesfor two sub-domains*

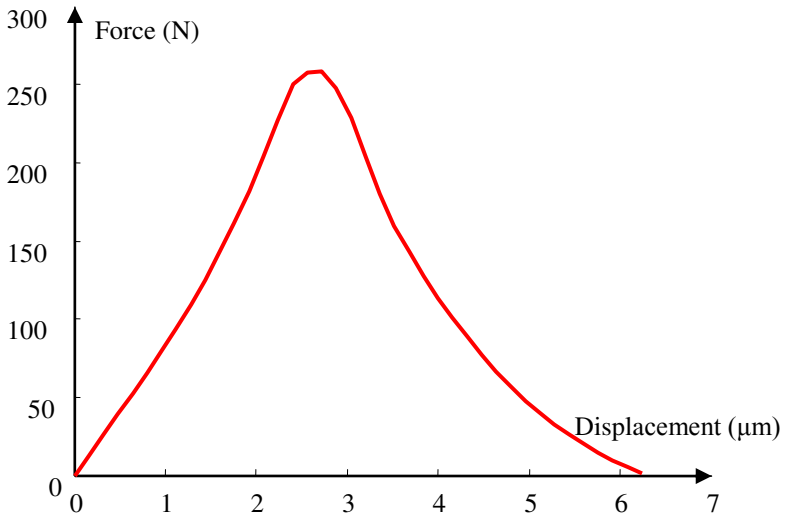

Figure 2-19. *Force-displacement diagram for the bar*

Table 2-5. *Distribution of temperature along the bar*

Time	ϑ at x =0	ϑ at x=0.25le	ϑat x = 0.5le	ϑ at x=0.75le	ϑat x = le	$\Delta\vartheta$
0.0000	0.0000	0.0000	0.0000	0.0000	0.0000	0.0000
0.0500	0.0000	12.5000	25.0000	37.5000	50.0000	0.0000
0.1000	0.0000	25.0000	50.0000	75.0000	100.0000	0.0000
0.1500	0.0000	37.5000	75.0000	112.5000	150.0000	0.0000
0.2000	0.0000	49.9998	99.9996	149.9998	200.0000	-0.0004
0.2500	0.0000	62.5020	125.0041	187.5020	250.0000	0.0041
0.3000	0.0000	75.0053	150.0106	225.0053	300.0000	0.0106
0.3500	0.0000	87.5094	175.0188	262.5094	350.0000	0.0188
0.3900	0.0000	97.5133	195.0265	292.5133	390.0000	0.0265

where $\Delta\vartheta = \vartheta_{x=0.5l_e} - 0.5(\vartheta_{x=0} + \vartheta_{x=l_e})$

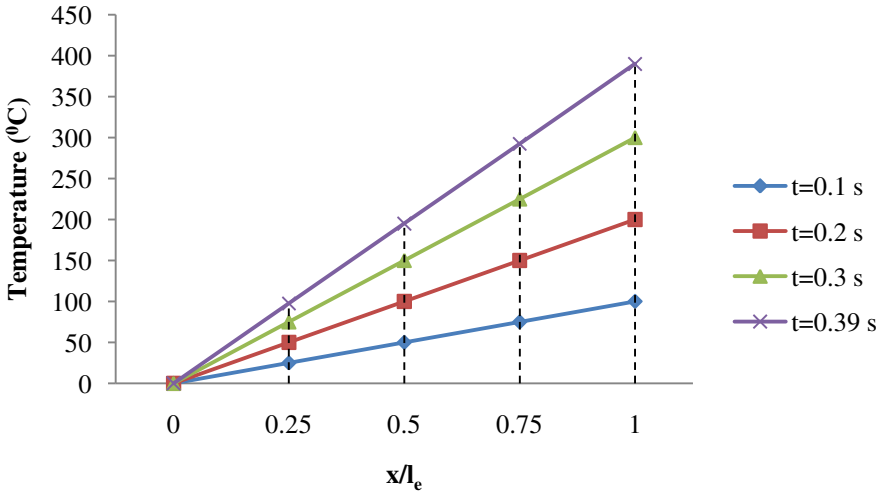

Figure 2-20. *Distribution of temperature (^0C) along the bar due to time*

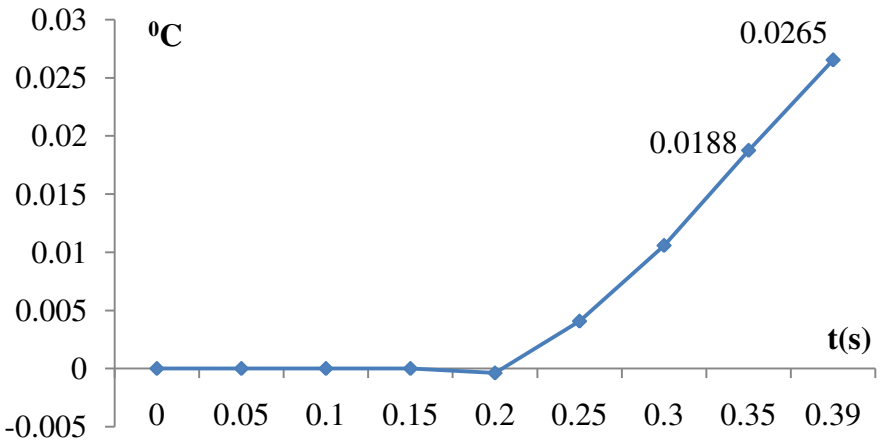

Figure 2-21. *Evolution of $\Delta\vartheta$ vs time*

where $\Delta\vartheta = \vartheta_{x=0.5l_e} - 0.5(\vartheta_{x=0} + \vartheta_{x=l_e})$

Figure 2-18 clearly shows the large difference in strain between the two sub-domains, both before and after the initiation of localized failure. Mathematically, this difference is due to different values of α_1^m and α_2^m (see (2-51)). Before the initiation of localized failure, the difference in temperature will lead to a difference in tangent modulus between two sub-domains, which results in the appearence of α_2^m which represents the difference in strain between the two sub-domains. After localized failure occurs, α_1^m increases and contributes to the different behaviors in the two parts of the bar.

From Table 2-5 and Figure 2-20, we can see that the temperature distribution is nonlinear. Its gradient changes at the middle of the bar. This change can be computed through α_2 (see equation (2-92)). It is noted that the magnitude of α_2 increases and then decreases with time (see Table 2-5and Figure 2-20). However, Figure 2-20also shows that the change in temperature gradient is relatively small in comparison with the temperature at the localized failure point (the maximum ratio of $\frac{\Delta\vartheta}{\vartheta_l}$ (ϑ_l is the temperature of the localized point) is approximately 0.0136%.), and therefore does not significantly contribute to the final results.

In this example, once again, we observe a reduction in the strength of the bar: the maximum displacement that can be applied to the bar now reduces to roughly 0.006 mm from 0.010 mm and 0.016 mm in the second and the first example, respectively.

The total mechanical dissipation along the bar is significantly smaller than the second and the first example (15.01Nmm in comparison to 27.90Nmm and 66.07Nmm). The major contribution

comes from the localized dissipation: 10.55 Nm in comparison with the total plastic dissipation: 4.47Nm.

2.4.2 Mesh refinement, convergence and mesh objectivity

In this example, we study the influence of the chosen number of elements upon the computed final results. The geometry description is given in Figure 2-22.

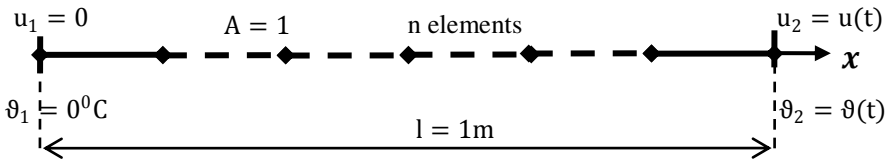

Figure 2-22.*Bar subjected to imposed loading and imposed temperature*

We consider a steel bar built-in at left end and subjected to an imposed displacement at right end (increasing linearly to 2mm). Simultaneously, right end of the bar is heated and its temperature is raised from 0^0C to 100^0C. The temperature of left end is kept constant and equal to 0^oC. The material properties of the bar are considered as temperature independent and shown in Table 2-6.

Table 2-6. *Material properties*

Material Properties	**Value**	**Dimension**
Young modulus (E)	205000	MPa
Initial yield stress (σ_y)	250	MPa
Ultimate stress (σ_u)	300	MPa
Plastic hardening modulus (K_p)	20000	MPa
Localized softening modulus ($\bar{\bar{K}}$)	-45	$MPam^{-1}$
Mass Density (ρ)	$7.865\ 10^{-9}$	Ns^2mm^{-4}
Thermal conductivity (k)	45	$N\ s^{-1}K^{-1}$
Heat specific (c)	$0.46\ 10^9$	$mm^2s^{-2}K^{-1}$
Thermal elongation(α)	0.00001	

The results are again illustrated by using several figures. In particular, Figure 2-23shows the load – displacement diagram of the bar computed by using 3, 5, 7 and 9 elements. It is noted that the computed curve after localized failure is not dependent on the chosen mesh (see Figure 2-23).This result proves the convergence of the numerical solution with respect to mesh refinement (see[17]).

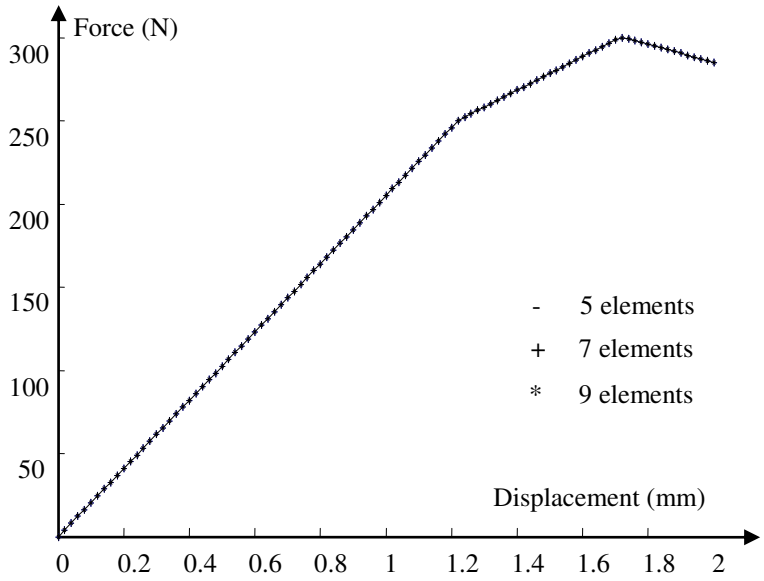

Figure 2-23. *Load-displacement diagram with different number of elements*

2.4.3 Heating effect of mechanical loading

In this example, we would like to illustrate the heating effect produced by mechanical dissipation in a bar when localized failure occurs. Consider a steel bar of 10mm long, fixed at left end and subjected to an increasing displacement (0.045mm/s) at right end until collapse. The initial temperature is constant along the bar and equal to 0^0C. Material properties of the bar are given inTable 2-1. Due to a problem in manufacturing, the ultimate stress at the middle point reduces to 299MPa instead of 300MPa in other part (see Figure 2-24).

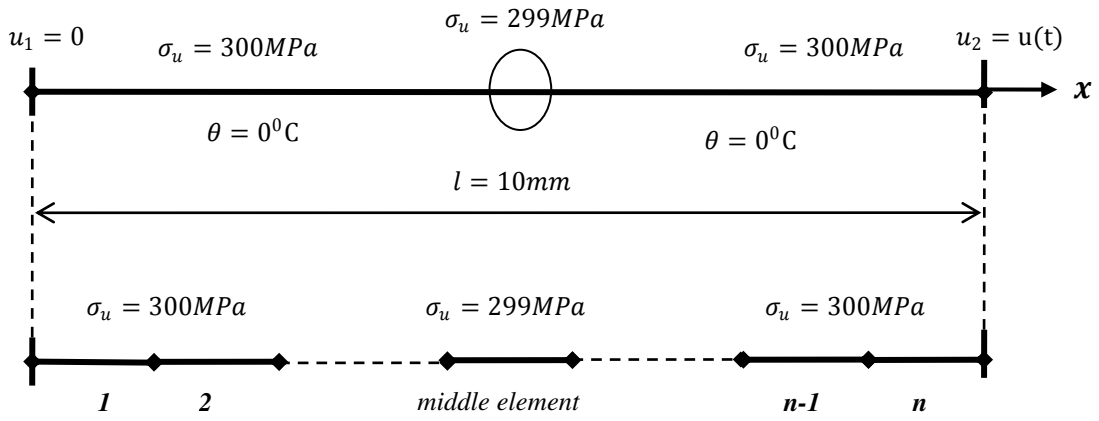

Figure 2-24. *Description of the third example and its mesh*

The problem is solved with two different meshes: 5 elements and 9 elements. In these two meshes, the middle element represents the zone with smaller ultimate stress ($\sigma_u = 299MPa$). The localized failure will therefore occur in this element. The computed load-displacement diagram of the bar is given in FigureFigure 2-25, while the evolution of temperature in the bar is shown inFigure 2-26 and Figure 2-27.

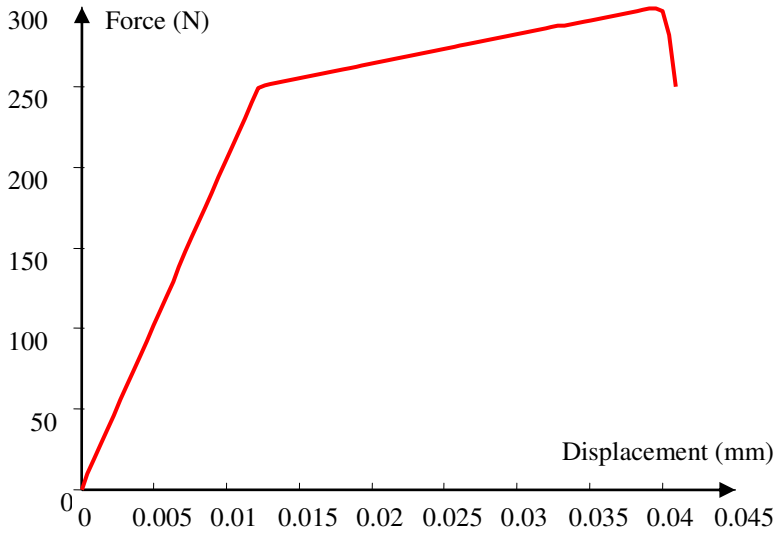

Figure 2-25. *Load-displacement curve*

The computed results clearly show the heating effect produced by the mechanical dissipation. Namely, the plastic dissipation equals heat supply leading to temperature increase. Initially, the dissipation in FPZ is equally distributed along the bar so that the temperature at every part of the bar remains the same. However, with the start of localized failure, additional dissipation at

failure point acts as a concentrated heat supply. This further leads to a heat transfer process in the bar and results in the evolution of temperature, as shown inFigure 2-26 and Figure 2-27.

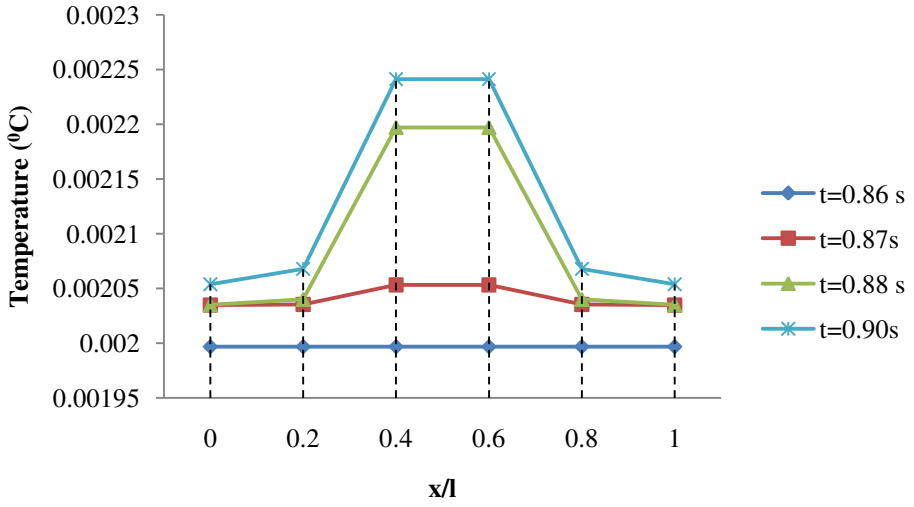

Figure 2-26. *Temperature evolution along the bar before and after the localized failure occurs (computed with 5 elements mesh)*

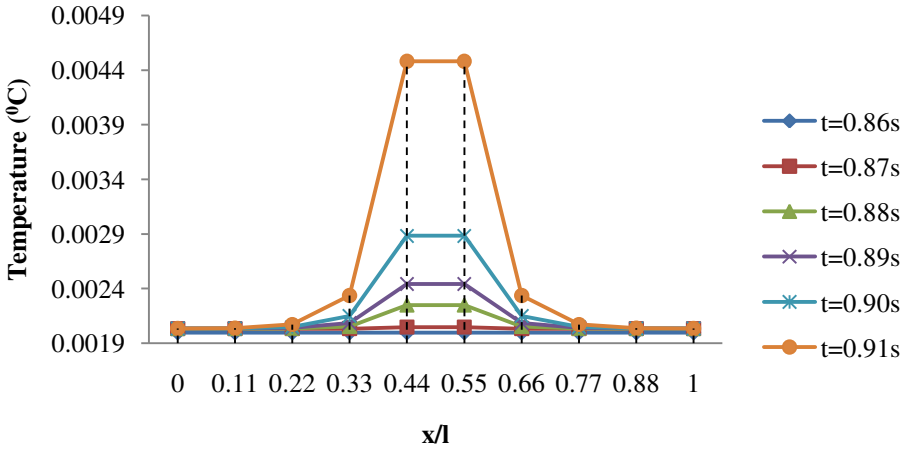

\

Figure 2-27. *Temperature evolution along the bar before and after the localized failure occurs (computed with 9 elements mesh)*

2.5 Conclusions

In this chapter, a novel localized failure model with thermoplastic coupling for heterogeneous material is introduced. The model is capable of modeling the behavior of material subjected to mechanical and thermal loading applied simultaneously. We have shown that very careful

considerations of both theoretical formulation and finite element implementation are needed in order to make such a development successful. The first main novelty of the proposed model with respect to number of previous works is its capability to represent the mechanical behavior of the material brought to localized failure and to account appropriately for the temperature induced changes in material properties as well as for the heat conduction due to mechanical dissipation at the localized failure surface.

The second important novelty concerns the optimal choice of finite element approximation capable of accommodating the localized failure modes for coupled thermoplastic model. The latter requires a careful combination of the displacement discontinuity to handle the localized failure mode, the strain discontinuity to handle the material heterogeneities induced by the heterogeneous temperature field along with the temperature dependence of material properties, and the temperature gradient jump at the localized failure surface to account for the corresponding discontinuity of heat flux. The finite element interpolations of this kind have been elaborated for 1D case of 2-node truss-bar element.

The solution procedure for this class of problems exploits the adiabatic operator split. This implies that the problem is first solved formechanics part (with adiabatic condition), and then for heat transfer part. The former delivers the values of nodal displacementsand internal variables, whereas the latter delivers the update of temperature field and the corresponding value of the jump in the heat flux at the localized failure surface.It was shown that such a split provides the most convenient implementation, and computational efficiency due to symmetry of tangent operators.

The numerical examples shave shown that the temperature dependence of material properties greatly influence the behavior of the bar. The most detailed study of this kind is performed in the first example, showing that the bar properties linearly dependent on temperature can significantly reduce the resistance of the truss-bar due to temperature increase. The same applies for non-linear variation of properties with respect to temperature, as advocated in Eurocode1993. The first example also shows that the temperature dependent properties can lead to large difference in strain(even for the same stress value) in two sub-domains of a single truss-bar element separated by the localized failure point.

3 Behavior of concrete under fully thermo-mechanical coupling conditions

3.1 Introduction

In the previous chapter, we have studied on the thermo-elastoplastic with softening behavior of steel, which was presented in one-dimensionalcase to clarify the theoretical model, as well as the numerical solution for the problem. That model can be applied to model the behavior of the rebarin reinforced concrete structure. To modeling the behavior of general reinforced concrete structure, one have also to study on the thermo-mechanical behavior of the concrete material. Previous works on the topic were carried out, for example see Galerkin et al.[45], Baker and de Borst [36]. However, these works only consider the continuum damagebehavior and do not consider the "ultimate" response. Futhermore, they do not provide a clear numerical solution for the problem.

In this chapter, their two remaining deficiencies of problem will be removed. We first introduce a new thermo-damage model, which is capable of modeling not only the continuum damagebut also the softening behavior of concrete under thermo-mechanical coupling effect. By that way, a united model can be applied to the hole concrete structure without "pre-chosing" a localized failure region for the modeling structure ([40], [38]). The second novelty presented in this chapter is a numerical solution for the problem, which is based on the "adiabatic" splitting procedure and the embedded-discontinuity finite element method.

The outline of this chapter is as follows. In the next two sections, we introduce the theoretical developments of the problem, which concentrate on the propagation of thermal effects through the localized failure (the marco cracks). The discrete approximation of the problem and its numerical solution using finite element method for the problem are presented in section 3.4. Several illustrative examples are presented in section 3.5, followed by a conclusion in section 3.6.

3.2 General framework

3.2.1 General continuum thermodynamic model

Several authors contributed to the thermo-damage coupling model, we can cite among others Baker and de Borst [36], or Ngo *et al.* [44].

The starting point is the local form of the first principle of thermodynamics for the case of thermo-mechanical inelastic response [17]:

$$r - \nabla \mathbf{q} = -\boldsymbol{\sigma} \cdot \dot{\boldsymbol{\varepsilon}} + \dot{e}(\boldsymbol{\varepsilon}, \eta^e) \tag{3-1}$$

Where r is the internal heat supply, $\mathbf{q}$ is the heat flux, $\boldsymbol{\sigma}$ is the stress field, $\boldsymbol{\varepsilon}$ is the strain field, e is the internal stored energy and η^e is the reversible part of entropy ($\dot{\bullet}$ denotes the time rate of the variable $\bullet$).

By following ([33], [42], [36]), the entropy is considered as the composition of the reversible part (or "elastic" entropy) and irreversible part (or "inelastic" entropy):

$$\eta = \eta^e + \eta^d \tag{3-2}$$

By the Legrendre transformation, the internal stored energy can be expressed in terms of the free energy ψ :

$$e = \psi + \eta^e \vartheta \tag{3-3}$$

where ϑ denotes the absolute temperature of the media.

In thermo-damage framework, we can assume as the most generally accepted ([36], [44]) that $\psi(\boldsymbol{\varepsilon}, \vartheta, \mathbf{D}, \xi)$ is the function of the state variables: the total strain $\boldsymbol{\varepsilon}$, the temperature ϑ, the compliance tensor $\mathbf{D}$ and the hardening variable ξ.

The Clausius-Duhem inequality for the model is written as:

$$0 \le D_{\text{int}} = \boldsymbol{\sigma} \cdot \dot{\boldsymbol{\varepsilon}} + \vartheta \dot{\eta} - \dot{e} = \boldsymbol{\sigma} \cdot \dot{\boldsymbol{\varepsilon}} + \vartheta \dot{\eta} - \dot{\psi} - \dot{\eta}^e \vartheta - \eta^e \dot{\vartheta} \tag{3-4}$$

$$0 \le D_{\text{int}} = \left(\boldsymbol{\sigma} - \frac{\partial \psi}{\partial \boldsymbol{\varepsilon}} \right) \cdot \dot{\boldsymbol{\varepsilon}} - \left(\eta^e + \frac{\partial \psi}{\partial \vartheta} \right) \dot{\vartheta} + \left(\vartheta \dot{\eta}^e - \vartheta \dot{\eta}^e \right) + \vartheta \dot{\eta}^d - \frac{\partial \psi}{\partial \mathbf{D}} \dot{\mathbf{D}} - \frac{\partial \psi}{\partial \xi} \dot{\xi} \tag{3-5}$$

In the case of "elastic" process, where $\dot{\mathbf{D}} = 0$ and $\dot{\xi} = 0$, the Clausius-Duhem inequality becomes equal and therefore, the constitutive equations for the stress and the "elastic" entropy can be established:

$$\boldsymbol{\sigma} = \frac{\partial \psi}{\partial \boldsymbol{\varepsilon}} \tag{3-6}$$

$$\eta^e = -\frac{\partial \psi}{\partial \vartheta} \tag{3-7}$$

and the dissipation equation can also be written:

$$D_{\text{int}} = -\frac{\partial \psi}{\partial \mathbf{D}} \dot{\mathbf{D}} - \frac{\partial \psi}{\partial \xi} \dot{\xi} + \vartheta \dot{\eta}^d \tag{3-8}$$

Also, by applying equation (3-3) and the constitutive equations (3-6), (3-7), the first principle of thermodynamics can be rewritten:

$$r - \nabla \mathbf{q} = -\boldsymbol{\sigma} \cdot \dot{\boldsymbol{\varepsilon}} + \dot{\psi} + \dot{\eta}^e \vartheta + \eta^e \dot{\vartheta}$$

$$r - \nabla \mathbf{q} = (\frac{\partial \psi}{\partial \boldsymbol{\varepsilon}} - \boldsymbol{\sigma}) \cdot \dot{\boldsymbol{\varepsilon}} + \left(\frac{\partial \psi}{\partial \vartheta} + \eta^e \right) \dot{\vartheta} + \frac{\partial \psi}{\partial \mathbf{D}} \cdot \dot{\mathbf{D}} + \frac{\partial \psi}{\partial \xi} \dot{\xi} + \dot{\eta}^e \vartheta$$

$$r - \nabla \mathbf{q} = \frac{\partial \psi}{\partial \mathbf{D}} \cdot \dot{\mathbf{D}} + \frac{\partial \psi}{\partial \xi} \dot{\xi} + \vartheta \dot{\eta}^e \tag{3-9}$$

We also define of the second order tensor $\boldsymbol{\beta}$ which represents the relation between stress and temperature, the heat capacity coefficient ρc and the tangent modulus $\mathbf{C}$ (see [44]):

$$\boldsymbol{\beta} := \frac{\partial \boldsymbol{\sigma}}{\partial \vartheta} = \frac{\partial \eta^e}{\partial \boldsymbol{\varepsilon}} = -\frac{\partial^2 \psi}{\partial \vartheta \partial \boldsymbol{\varepsilon}} \tag{3-10}$$

$$\rho c := \frac{\partial e}{\partial \vartheta} = \frac{\partial \psi}{\partial \vartheta} + \frac{\partial \eta^e}{\partial \vartheta} \vartheta + \eta^e = -\vartheta \frac{\partial^2 \psi}{\partial \vartheta^2} \tag{3-11}$$

$$\mathbf{C} := \frac{\partial \boldsymbol{\sigma}}{\partial \boldsymbol{\varepsilon}} = \frac{\partial^2 \psi}{\partial \boldsymbol{\varepsilon} \partial \boldsymbol{\varepsilon}} = \mathbf{D}^{-1} \tag{3-12}$$

Note that the tangent stiffness tensor $\mathbf{C}$ is the inverse of the compliance damage tensor $\mathbf{D}$. From equation (3-10) and equation (3-12), we have

$$\boldsymbol{\beta} = \frac{\partial \sigma}{\partial \vartheta} = \frac{\partial \boldsymbol{\sigma}}{\partial \boldsymbol{\varepsilon}} \frac{\partial \boldsymbol{\varepsilon}}{\partial \vartheta} = \mathbf{D}^{-1} \boldsymbol{\alpha} \tag{3-13}$$

Where $\boldsymbol{\alpha} := \frac{\partial \boldsymbol{\varepsilon}}{\partial \vartheta}$ is the thermal expansion.

Note that in thermo-mechanical problem, the strain field is the composition of the mechanical strain ($\boldsymbol{\varepsilon}_m$) and the thermal strain ($\boldsymbol{\varepsilon}_\vartheta$):

$$\boldsymbol{\varepsilon} = \boldsymbol{\varepsilon}_m + \boldsymbol{\varepsilon}_\vartheta \tag{3-14}$$

where the thermal strain is computed from the temperature and the thermal expansion:

$$\boldsymbol{\varepsilon}_{\vartheta} = \boldsymbol{\alpha}\left(\vartheta - \vartheta_0\right) \tag{3-15}$$

The free energy potential is chosen as the composition of mechanical energy (ψ_m) and the thermal energy (ψ_t):

$$\psi = \underbrace{\frac{1}{2}\boldsymbol{\varepsilon}_m \cdot \mathbf{D}^{-1} \cdot \boldsymbol{\varepsilon}_m + \Xi(\xi)}_{\psi_m} + \underbrace{\rho c\left[\left(\vartheta - \vartheta_0\right) - \vartheta \ln \frac{\vartheta}{\vartheta_0}\right]}_{\psi_t} \tag{3-16}$$

$$\psi = \underbrace{\frac{1}{2}[\boldsymbol{\varepsilon} - \boldsymbol{\alpha}(\vartheta - \vartheta_0)] \cdot \mathbf{D}^{-1} \cdot [\boldsymbol{\varepsilon} - \boldsymbol{\alpha}(\vartheta - \vartheta_0)] + \Xi(\xi)}_{\psi_m} + \underbrace{\rho c\left[\left(\vartheta - \vartheta_0\right) - \vartheta \ln \frac{\vartheta}{\vartheta_0}\right]}_{\psi_t} \tag{3-17}$$

Where ϑ_0 is the reference temperature and $\Xi(\xi)$ is the hardening energy.

With this definition of the free potential, the constitutive equation for stress and entropy can be re-written:

$$\boldsymbol{\sigma} = \frac{\partial \psi}{\partial \boldsymbol{\varepsilon}} = \mathbf{D}^{-1} \cdot \left[\boldsymbol{\varepsilon} - \boldsymbol{\alpha}\left(\vartheta - \vartheta_0\right)\right] \tag{3-18}$$

$$\eta^e = -\frac{\partial \psi}{\partial \vartheta} = (\mathbf{D}^{-1} \cdot \boldsymbol{\alpha}) \cdot \left[\boldsymbol{\varepsilon} - \boldsymbol{\alpha}(\vartheta - \vartheta_0)\right] + \rho c \ln\left(\frac{\vartheta}{\vartheta_0}\right) \tag{3-19}$$

The stress-like variable q associated to the hardening variable ξ and $\mathbf{Y}$ to the compliance damage tensor $\mathbf{D}$ are defined as:

$$q := -\frac{\partial \psi}{\partial \xi} = -\frac{\partial \Xi(\xi)}{\partial \xi} \tag{3-20}$$

$$\mathbf{Y} := -\frac{\partial \psi}{\partial \mathbf{D}} = \frac{1}{2}\left(\mathbf{D}^{-1} \cdot \left[\boldsymbol{\varepsilon} - \boldsymbol{\alpha}(\vartheta - \vartheta_0)\right]\right) \otimes \left(\mathbf{D}^{-1} \cdot \left[\boldsymbol{\varepsilon} - \boldsymbol{\alpha}(\vartheta - \vartheta_0)\right]\right) = \frac{1}{2}\boldsymbol{\sigma} \otimes \boldsymbol{\sigma} \tag{3-21}$$

The internal dissipation of the media leads to the final result:

$$D_{\text{int}} = \mathbf{Y} \cdot \dot{\mathbf{D}} + q\dot{\xi} + \vartheta \dot{\eta}^d \tag{3-22}$$

$$D_{\text{int}} = \underbrace{\frac{1}{2}\boldsymbol{\sigma} \cdot \dot{\mathbf{D}} \cdot \boldsymbol{\sigma} + q\dot{\xi}}_{D_{mech}} + \underbrace{\vartheta \dot{\eta}^d}_{D_{ther}} \tag{3-23}$$

where D_{mech} and D_{ther} denote the mechanical and the thermal part of dissipation, respectively.

The damage threshold defining the elastic domain is chosen (see [25]) as:

$$0 \geq \Phi(\boldsymbol{\sigma}, q, \vartheta) = \sqrt{\boldsymbol{\sigma} \cdot \mathbf{D}^e \cdot \boldsymbol{\sigma}} - \frac{1}{\sqrt{E}}\left(\sigma_f - q\right) \tag{3-24}$$

Where $\mathbf{D}^e$ denotes the "thermo-mechanical" undamaged elastic compliance, σ_f denotes the

damage limit stress and $q = -\dfrac{d\Xi}{d\xi}$ denotes the stress-like variable associated to ξ (as introduced above)

Considering the second principle of thermodynamics and the principle of maximum inelastic dissipation we obtain the following evolution equations for internal variables:

$$\gamma \frac{\partial \Phi}{\partial q} = \frac{\partial D_{\text{int}}}{\partial q} \rightarrow \dot{\xi} = \frac{\gamma}{\sqrt{E}} \tag{3-25}$$

$$\gamma \frac{\partial \Phi}{\partial \boldsymbol{\sigma}} = \frac{\partial D_{\text{int}}}{\partial \boldsymbol{\sigma}} \rightarrow \dot{\mathbf{D}} \cdot \boldsymbol{\sigma} = \gamma \frac{\mathbf{D}^e \cdot \boldsymbol{\sigma}}{\sqrt{\boldsymbol{\sigma} \cdot \mathbf{D}^e \cdot \boldsymbol{\sigma}}} \rightarrow \dot{\mathbf{D}} = \gamma \frac{\mathbf{D}^e}{\sqrt{\boldsymbol{\sigma} \cdot \mathbf{D}^e \cdot \boldsymbol{\sigma}}} \tag{3-26}$$

$$\gamma \frac{\partial \Phi}{\partial \vartheta} = \frac{\partial D_{\text{int}}}{\partial \vartheta} \rightarrow \dot{\eta}^d = \gamma \frac{\partial \Phi}{\partial \vartheta} \tag{3-27}$$

Where, γ is the Lagrange multiplier.

Considering equations (3-1) and (3-9) the system of local balance equation finally consists of the force balance equation and the energy conservation equation (see [42], [36]).

$$\begin{cases} 0 = \nabla \cdot \boldsymbol{\sigma} + \mathbf{b} \\ \vartheta \dot{\eta} = -\nabla \cdot \mathbf{q} + D_{\text{int}} + r \end{cases} \tag{3-28}$$

From the state equation (20), we can compute the "elastic" entropy evolution:

$$\eta^e = -\frac{\partial \psi}{\partial \vartheta} = (\mathbf{D}^{-1} \cdot \boldsymbol{\alpha}) \cdot [\boldsymbol{\varepsilon} - \boldsymbol{\alpha}(\vartheta - \vartheta_0)] + \rho c \ln\left(\frac{\vartheta}{\vartheta_0}\right)$$

$$\rightarrow \vartheta \dot{\eta}^e = \vartheta(\mathbf{D}^{-1} \cdot \boldsymbol{\alpha}) \cdot \left(\dot{\boldsymbol{\varepsilon}} - \boldsymbol{\alpha}\dot{\vartheta}\right) - \vartheta((\mathbf{D}^{-1} \cdot \dot{\mathbf{D}} \cdot \mathbf{D}^{-1}) \cdot \boldsymbol{\alpha})\left[\boldsymbol{\varepsilon} - \boldsymbol{\alpha}\left(\vartheta - \vartheta_0\right)\right] + \rho c \dot{\vartheta} \tag{3-29}$$

This equation, combined with equation (2), gives the following balance equations:

$$\begin{cases} 0 = \nabla \cdot \boldsymbol{\sigma} + \mathbf{b} \\ \underbrace{\left(\rho c - \vartheta(\mathbf{D}^{-1} \cdot \boldsymbol{\alpha})\boldsymbol{\alpha}\right)}_{\widetilde{\rho c}} \dot{\vartheta} = -\nabla \cdot \mathbf{q} + D_{mech} \underbrace{- \vartheta(\mathbf{D}^{-1} \cdot \boldsymbol{\alpha}) \cdot \dot{\boldsymbol{\varepsilon}} + \vartheta((\mathbf{D}^{-1} \cdot \dot{\mathbf{D}} \cdot \mathbf{D}^{-1}) \cdot \boldsymbol{\alpha})\left[\boldsymbol{\varepsilon} - \boldsymbol{\alpha}\left(\vartheta - \vartheta_0\right)\right]}_{F(\boldsymbol{\varepsilon}, \mathbf{D}, \vartheta)} + r \end{cases} \tag{3-30}$$

where

$$F(\boldsymbol{\varepsilon}, \mathbf{D}, \vartheta) := -\vartheta(\mathbf{D}^{-1} \cdot \boldsymbol{\alpha}) \cdot \dot{\boldsymbol{\varepsilon}} + \vartheta((\mathbf{D}^{-1} \cdot \dot{\mathbf{D}} \cdot \mathbf{D}^{-1}) \cdot \boldsymbol{\alpha})\left[\boldsymbol{\varepsilon} - \boldsymbol{\alpha}\left(\vartheta - \vartheta_0\right)\right] \tag{3-31}$$

is the structural heating (see[42], [36]), and

$$\widetilde{\rho c} := \rho c - \vartheta(\mathbf{D}^{-1} \cdot \boldsymbol{\alpha})\boldsymbol{\alpha} \tag{3-32}$$

is the 'modified' heat conduction of the material.

3.2.2 Localized failure in damage model

3.2.2.1 Discontinuity of displacement field

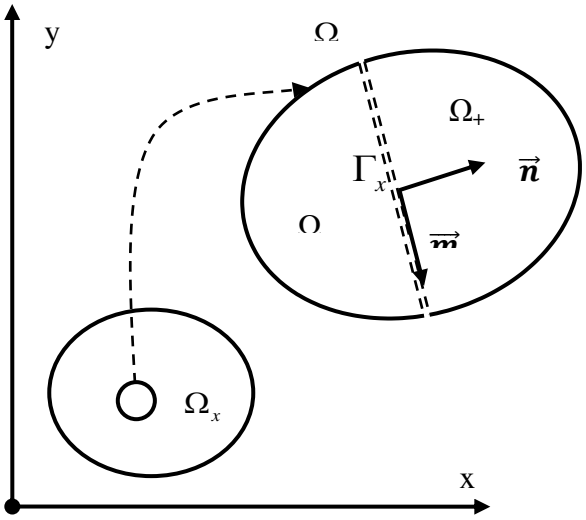

Figure 3-1. *Localized failure happens at crack surface and the "local" zone*

In quasi-brittle materials, micro-cracks appear in the fracture process zone and will further coalesce to generate macro crack. We assume in the following that such a failure happens in a "local" zone $\Omega_{\mathbf{x}}$ (see Figure 3-1). The failure can be represented by a strong discontinuity in the displacement field across the surface $\Gamma_{\mathbf{x}}$ passing through point **x** (see [29], [52], [25], [24]), which finally allows us to write the displacement field in the "local" zone $\Omega_{\mathbf{x}}$ as follows:

$$\mathbf{u}(\mathbf{x},t) = \hat{\mathbf{u}}(\mathbf{x},t) + \overline{\overline{\mathbf{u}}}(t)[\mathrm{H}_{\Gamma_x}(\mathbf{x}) - \varphi(\mathbf{x})] \tag{3-33}$$

where $\overline{\overline{\mathbf{u}}}(t)$ is the "jump" of displacement across the crack surface $\Gamma_{\mathbf{x}}$ (considered as constant in Ω_x), $\mathrm{H}_{\Gamma_x}(\mathbf{x})$ denotes the Heaviside function and $\varphi(\mathbf{x})$ is a smooth function being 0 on $\partial\Omega_x^-$ and 1 on $\partial\Omega_x^+$ (where $\partial\Omega_x^-$ and $\partial\Omega_x^+$ are the boundary of two domains of the element separated by the crack).

$$\mathrm{H}_{\Gamma_x}(x) = \begin{cases} 1 & for \quad x \in \Omega^+ \\ 0 & for \quad x \in \Omega^- \end{cases} \tag{3-34}$$

The infinitesimal strain which corresponds to this displacement is given by:

$$\boldsymbol{\varepsilon}(\mathbf{x},t) = \nabla^s \hat{\mathbf{u}}(\mathbf{x},t) - \left[\overline{\overline{\mathbf{u}}}(t) \otimes \nabla\varphi(\mathbf{x})\right]^s + \left[\overline{\overline{\mathbf{u}}}(t) \nabla \mathrm{H}_{\Gamma_x}(\mathbf{x})\right]^s \tag{3-35}$$

where $[\bullet]^s$ is the symmetric part of $[\bullet]$.

We also note that $\left[\bullet \nabla \mathrm{H}_{\Gamma_{\mathbf{x}}}(\mathbf{x})\right]^s = (\bullet \otimes \mathbf{n})^s \delta_{\Gamma_{\mathbf{x}}}$, where δ_{Γ_x} is the Dirac function on Γ_x and **n** is the

unit normal vector, then:

$$\boldsymbol{\varepsilon}(\mathbf{x},t) = \nabla^s \hat{\mathbf{u}}(\mathbf{x},t) - \left[\overline{\overline{\mathbf{u}}}(t) \otimes \nabla\varphi(\mathbf{x})\right]^s - \nabla^s \overline{\overline{\mathbf{u}}}(t) \mathrm{H}_{\Gamma_x}(\mathbf{x}) + (\overline{\overline{\mathbf{u}}}(t) \otimes \mathbf{n})^s \delta_{\Gamma_\mathbf{x}} \tag{3-36}$$

The infinitesimal strain at the "local" zone can then be divided into a regular part and a singular part as:

$$\boldsymbol{\varepsilon}(\mathbf{x},t) = \bar{\boldsymbol{\varepsilon}}(\mathbf{x},t) + \bar{\bar{\boldsymbol{\varepsilon}}}(t)\delta_{\Gamma_\mathbf{x}} \tag{3-37}$$

where:

$$\bar{\boldsymbol{\varepsilon}}(\mathbf{x},t) = \nabla^s \hat{\mathbf{u}}(\mathbf{x},t) - \left(\bar{\bar{\mathbf{u}}}(t) \otimes \nabla\varphi(\mathbf{x})\right)^s \tag{3-38}$$

and

$$\bar{\bar{\boldsymbol{\varepsilon}}}(t) = (\bar{\bar{\mathbf{u}}}(t) \otimes \mathbf{n})^s \tag{3-39}$$

3.2.2.2 Localized Free Energy

From the state equation (3-16) we can obtain the strain field in terms of the stress field as:

$$\boldsymbol{\sigma} = \mathbf{D}^{-1} \cdot \boldsymbol{\varepsilon}(\mathbf{x},t) - \mathbf{D}^{-1} \cdot \boldsymbol{\alpha}(\vartheta - \vartheta_0) \rightarrow \boldsymbol{\varepsilon}(\mathbf{x},t) - \boldsymbol{\alpha}(\vartheta - \vartheta_0) = \mathbf{D} \cdot \boldsymbol{\sigma}$$

$$\rightarrow \bar{\boldsymbol{\varepsilon}}(\mathbf{x},t) + \bar{\bar{\boldsymbol{\varepsilon}}}(t)\delta_{\Gamma_\mathbf{x}} - \boldsymbol{\alpha}(\vartheta - \vartheta_0) = \mathbf{D} \cdot \boldsymbol{\sigma} \tag{3-40}$$

By taking into account that the stress field must be bounded and assuming that there is no thermal dilatation on the discontinuity Γ_x, the damage compliance tensor should be decomposed into a singular part and a regular part (see [24], [25]):

$$\mathbf{D} = \overline{\mathbf{D}} + \overline{\overline{\mathbf{D}}}\delta_{\Gamma_\mathbf{x}} \tag{3-41}$$

so that:

$$\bar{\boldsymbol{\varepsilon}}(x,t) - \boldsymbol{\alpha}(\vartheta - \vartheta_0) = \overline{\mathbf{D}} \cdot \boldsymbol{\sigma} \qquad \text{on } \Omega_x \setminus \Gamma_x$$

and

$$\bar{\bar{\boldsymbol{\varepsilon}}}(t) = \left(\overline{\overline{\mathbf{u}}}(t) \otimes \mathbf{n}\right)^s = \overline{\overline{\mathbf{D}}} \cdot \boldsymbol{\sigma} \qquad \text{on } \Gamma_x$$

The appearance of a "singular" part of the damage compliance tensor $\overline{\overline{\mathbf{D}}}$ leads to the introduction of "singular" part of hardening variable $\bar{\bar{\xi}}$, which controls the damage condition of the material at the localization zone. Therefore, the hardening variable ξ should also be split into two parts:

$$\xi = \bar{\xi} + \bar{\bar{\xi}}\delta_{\Gamma_x} \tag{3-42}$$

The decomposition of these state and internal variables allows us to write the decomposition of the free energy into a regular part $\bar{\psi}$ associated to the bulk and a singular part $\bar{\bar{\psi}}$ associated to

the discontinuity Γ_x:

$$\psi = \underbrace{\frac{1}{2}\left(\boldsymbol{\varepsilon}-\boldsymbol{\alpha}\left(\vartheta-\vartheta_0\right)\right)\cdot\mathbf{D}^{-1}\cdot\left(\boldsymbol{\varepsilon}-\boldsymbol{\alpha}\left(\vartheta-\vartheta_0\right)\right)+\Xi\left(\xi\right)}_{\psi_m}+\underbrace{\rho c\left[\left(\vartheta-\vartheta_0\right)-\vartheta\ln\frac{\vartheta}{\vartheta_0}\right]}_{\psi_t}\rightarrow$$

$$\psi = \underbrace{\frac{1}{2}\left(\bar{\boldsymbol{\varepsilon}}-\boldsymbol{\alpha}\left(\vartheta-\vartheta_0\right)\right)\cdot\bar{\mathbf{D}}^{-1}\cdot\left(\bar{\boldsymbol{\varepsilon}}-\boldsymbol{\alpha}\left(\vartheta-\vartheta_0\right)\right)+\Xi\left(\bar{\xi}\right)+\rho c\left[\left(\vartheta-\vartheta_0\right)-\vartheta\ln\frac{\vartheta}{\vartheta_0}\right]}_{\bar{\psi}} \tag{3-43}$$

$$+\left[\underbrace{\frac{1}{2}\left(\left(\bar{\bar{\mathbf{u}}}(t)\otimes\mathbf{n}\right)^s\cdot\bar{\bar{\mathbf{D}}}^{-1}\cdot\left(\bar{\bar{\mathbf{u}}}(t)\otimes\mathbf{n}\right)^s\right)+\Xi\left(\bar{\bar{\xi}}\right)}_{\bar{\bar{\psi}}}\right]\delta_{\Gamma_x}$$

By denoting $\bar{\bar{\mathbf{Q}}}=\left(\mathbf{n}\cdot\bar{\bar{\mathbf{D}}}^{-1}\cdot\mathbf{n}\right)^{-1}$ the internal variable for describing the damage response at the discontinuity (see [25]), we have the form of the singular part of free energy:

$$\bar{\bar{\psi}}\left(\bar{\bar{\mathbf{u}}},\bar{\bar{\mathbf{Q}}},\bar{\bar{\xi}}\right)=\bar{\bar{\psi}}_m=\frac{1}{2}\bar{\bar{\mathbf{u}}}(t)\cdot\bar{\bar{\mathbf{Q}}}^{-1}\cdot\bar{\bar{\mathbf{u}}}(t)+\Xi\left(\bar{\bar{\xi}}\right) \tag{3-44}$$

We note here that the 'thermal' energy does not appear in the singular part of the free energy (see equation (3-44)), it is due to the assumption that there is no material (and therefore no heat conductor) in the crack.

3.2.2.3 The dissipation and the evolution laws of internal variables

The dissipation of the material is computed by the equation

$$D_{\text{int}}=\vartheta\dot{\eta}+\boldsymbol{\sigma}\cdot\dot{\boldsymbol{\varepsilon}}-\dot{e}=\vartheta\dot{\eta}^e+\vartheta\dot{\eta}^d+\boldsymbol{\sigma}\cdot\dot{\boldsymbol{\varepsilon}}-\vartheta\dot{\eta}^e-\eta^e\dot{\vartheta}-\dot{\psi}$$

$$D_{\text{int}}=\boldsymbol{\sigma}\cdot\dot{\boldsymbol{\varepsilon}}-\eta^e\dot{\vartheta}-\dot{\psi}+\vartheta\dot{\eta}^d \tag{3-45}$$

Note that the decomposition of the free energy and the strain lead to the decomposition of entropy, so that equation (43) can be rewritten:

$$D_{\text{int}}=\underbrace{\boldsymbol{\sigma}\cdot\dot{\bar{\boldsymbol{\varepsilon}}}-\bar{\eta}^e\dot{\vartheta}-\dot{\bar{\psi}}+\vartheta\dot{\bar{\eta}}^d}_{\bar{D}_{\text{int}}}+\delta_{\Gamma_x}\underbrace{\left(\underbrace{\left(\boldsymbol{\sigma}\cdot\mathbf{n}\right)}_{\mathbf{t}}\cdot\dot{\bar{\bar{\mathbf{u}}}}(t)-\bar{\bar{\eta}}^e\dot{\vartheta}_{\bar{\bar{x}}}-\dot{\bar{\bar{\psi}}}+\vartheta_{\bar{\bar{x}}}\dot{\bar{\bar{\eta}}}^d\right)}_{\bar{\bar{D}}_{\text{int}}} \tag{3-46}$$

The singular part of dissipation is:

$$\overline{\overline{D}}_{\text{int}} = \mathbf{t}\cdot\dot{\overline{\overline{\mathbf{u}}}}(t) - \overline{\overline{\eta}}^{e}\dot{\vartheta}_{\Gamma_x} - \dot{\overline{\overline{\psi}}} + \vartheta_{\Gamma_x}\dot{\overline{\overline{\eta}}}^{d}$$

$$\rightarrow \overline{\overline{D}}_{\text{int}} = \left(\underbrace{\mathbf{t} - \frac{\partial\overline{\overline{\psi}}}{\partial\overline{\overline{\mathbf{u}}}}}_{0}\right)\cdot\dot{\overline{\overline{\mathbf{u}}}}(t) - \frac{\partial\overline{\overline{\psi}}}{\partial\overline{\overline{\mathbf{Q}}}}\cdot\dot{\overline{\overline{\mathbf{Q}}}} - \frac{\partial\overline{\overline{\psi}}}{\partial\overline{\overline{\xi}}}\dot{\overline{\overline{\xi}}} - \left(\underbrace{\overline{\overline{\eta}}^{e} + \frac{\partial\overline{\overline{\psi}}}{\partial\vartheta_{\Gamma_x}}}_{0}\right)\dot{\vartheta}_{\Gamma_x} + \vartheta_{\Gamma_x}\dot{\overline{\overline{\eta}}}^{d}$$

$$\overline{\overline{D}}_{\text{int}} = -\frac{\partial\overline{\overline{\psi}}}{\partial\overline{\overline{\mathbf{Q}}}}\cdot\dot{\overline{\overline{\mathbf{Q}}}} - \frac{\partial\overline{\overline{\psi}}}{\partial\overline{\overline{\xi}}}\dot{\overline{\overline{\xi}}} + \vartheta_{\Gamma_x}\dot{\overline{\overline{\eta}}}^{d} \tag{3-47}$$

where ϑ_{Γ_x} denotes the temperature at the localized failure zone.

The formulation of singular part of internal dissipation allows us to find out the constitutive equation for the singular part of state variables:

$$\mathbf{t} = \frac{\partial\overline{\overline{\psi}}}{\partial\overline{\overline{\mathbf{u}}}} = \overline{\overline{\mathbf{Q}}}^{-1}\cdot\overline{\overline{\mathbf{u}}} \tag{3-48}$$

$$\overline{\overline{\eta}}^{e} = -\frac{\partial\overline{\overline{\psi}}}{\partial\vartheta_{\Gamma_x}} \tag{3-49}$$

Singular parts of internal variables can also be computed:

$$\overline{\overline{q}} = -\frac{\partial\overline{\overline{\psi}}}{\partial\overline{\overline{\xi}}} = -\overline{\overline{K}}\,\overline{\overline{\xi}} \quad \text{where } \overline{\overline{K}} = \frac{\partial^2\Xi\left(\overline{\overline{\xi}}\right)}{\partial\overline{\overline{\xi}}^{2}} \tag{3-50}$$

$$\overline{\overline{\mathbf{Y}}} = -\frac{\partial\overline{\overline{\psi}}}{\partial\overline{\overline{\mathbf{Q}}}} = \frac{1}{2}\overline{\overline{\mathbf{u}}}\cdot(\overline{\overline{\mathbf{Q}}}^{-1}\overline{\overline{\mathbf{Q}}}^{-1})\cdot\overline{\overline{\mathbf{u}}} \rightarrow \overline{\overline{\mathbf{Y}}} = \frac{1}{2}\mathbf{t}\otimes\mathbf{t} \tag{3-51}$$

These state equations allow us to write the singular part of the internal dissipation in a similar manner:

$$\overline{\overline{D}}_{\text{int}} = \underbrace{\frac{1}{2}\mathbf{t}\cdot\dot{\overline{\overline{\mathbf{Q}}}}\cdot\mathbf{t} + \overline{\overline{q}}\,\dot{\overline{\overline{\xi}}}}_{\overline{\overline{D}}_{mech}} + \underbrace{\vartheta\dot{\overline{\overline{\eta}}}^{d}}_{\overline{\overline{D}}_{ther}} \tag{3-52}$$

Where $\overline{\overline{D}}_{mech}$ and $\overline{\overline{D}}_{ther}$ denote the mechanical part and the thermal part of the singular part of internal dissipation.

Next step is to choose a failure criterion for the discontinuity, for that purpose, we base our work on the multi-surface criterion proposed in (see [25]):

$$\begin{cases} \overline{\overline{\Phi}}_1(\mathbf{t},\overline{\overline{q}}) = \mathbf{t}\cdot\mathbf{n} - \left[\overline{\overline{\sigma}}_f - \overline{\overline{q}}\right] \le 0 \\ \overline{\overline{\Phi}}_2(\mathbf{t},\overline{\overline{q}}) = \left|\mathbf{t}\cdot\mathbf{m}\right| - \left[\overline{\overline{\sigma}}_s - \frac{\overline{\overline{\sigma}}_s}{\overline{\overline{\sigma}}_f}\overline{\overline{q}}\right] \le 0 \end{cases} \tag{3-53}$$

where $\overline{\overline{\sigma}}_f$ is the given fracture stress, $\overline{\overline{\sigma}}_s$ is the limit value of shear stress on the discontinuity and

$\overline{\overline{q}}$ is the stress-like variable describing strain softening. Note that the two failure functions are coupled through the stress-like variable $\overline{\overline{q}}$. We note that equation $(3\text{-}53)_1$ controls the crack criteria due to the normal stress (mode I) and equation $(3\text{-}53)_2$ controls the failure happen due to shear stress (mode II).

The principle of maximum dissipation has to be enforced under the two constraints: $\overline{\overline{\Phi}}_1 \le 0$ and $\overline{\overline{\Phi}}_2 \le 0$, by introducing two Lagrange multipliers $\overline{\overline{\gamma}}_1$ and $\overline{\overline{\gamma}}_2$ and applying the Kuhn Tucker optimality condition. With such a process, the evolutions of the singular parts of the internal variables are computed as:

$$\underbrace{\max \overline{\overline{D}}_{\text{int}}}_{\overline{\overline{\Phi}}_1 \le 0, \overline{\overline{\Phi}}_1 \le 0} \Leftrightarrow \underbrace{\min \overline{\overline{L}}(\mathbf{t}, \overline{\overline{q}}, \vartheta)}_{\overline{\overline{\gamma}}_1 \ge 0, \overline{\overline{\gamma}}_2 \ge 0}; \; \overline{\overline{L}}(\mathbf{t}, \overline{\overline{q}}, \vartheta) = -\overline{\overline{D}}_{\text{int}} + \overline{\overline{\gamma}}_1 \overline{\overline{\Phi}}_1 + \overline{\overline{\gamma}}_2 \overline{\overline{\Phi}}_2$$

$$\frac{\partial \overline{\overline{L}}}{\partial \mathbf{t}_m} = -\dot{\overline{\overline{\mathbf{Q}}}} \cdot \mathbf{t} + \overline{\overline{\gamma}}_1 \frac{\partial \overline{\overline{\Phi}}_1}{\partial \mathbf{t}} + \overline{\overline{\gamma}}_2 \frac{\partial \overline{\overline{\Phi}}_2}{\partial \mathbf{t}} = 0 \rightarrow \dot{\overline{\overline{\mathbf{Q}}}} = \overline{\overline{\gamma}}_1 \frac{1}{\mathbf{t} \cdot \mathbf{n}} \mathbf{n} \otimes \mathbf{n} + \overline{\overline{\gamma}}_2 \frac{1}{|\mathbf{t} \cdot \mathbf{m}|} \mathbf{m} \otimes \mathbf{m} \tag{3-54}$$

$$\frac{\partial \overline{\overline{L}}}{\partial \overline{\overline{q}}} = -\dot{\overline{\overline{\xi}}} + \overline{\overline{\gamma}}_1 \frac{\partial \overline{\overline{\Phi}}_1}{\partial \overline{\overline{q}}} + \overline{\overline{\gamma}}_2 \frac{\partial \overline{\overline{\Phi}}_2}{\partial \overline{\overline{q}}} = 0 \rightarrow \dot{\overline{\overline{\xi}}} = \overline{\overline{\gamma}}_1 + \overline{\overline{\gamma}}_2 \frac{\overline{\overline{\sigma}}_s}{\overline{\overline{\sigma}}_f} \tag{3-55}$$

$$\frac{\partial \overline{\overline{L}}}{\partial \vartheta_{\overline{\overline{x}}}} = -\frac{\partial \overline{\overline{D}}_{\text{int}}}{\partial \vartheta_{\overline{\overline{x}}}} + \overline{\overline{\gamma}}_1 \frac{\partial \overline{\overline{\Phi}}_1}{\partial \vartheta_{\overline{\overline{x}}}} + \overline{\overline{\gamma}}_2 \frac{\partial \overline{\overline{\Phi}}_2}{\partial \vartheta_{\overline{\overline{x}}}} = 0 \rightarrow \dot{\overline{\overline{\eta}}}^d = \overline{\overline{\gamma}}_1 \frac{\partial \overline{\overline{\Phi}}_1}{\partial \vartheta_{\overline{\overline{x}}}} + \overline{\overline{\gamma}}_2 \frac{\partial \overline{\overline{\Phi}}_2}{\partial \vartheta_{\overline{\overline{x}}}} \tag{3-56}$$

3.2.3 Discontinuity in the heat flow

The previous section 3.2.2.3 describes the thermodynamical ingredients of the model associated to the displacement discontinuity. This leads to a damage model linking, on the 'crack' surface, the traction $\mathbf{t}$ to the displacement jump $\overline{\overline{\mathbf{u}}}$. Therefore, the crack surface is not a traction free surface but a cohesive crack.

In that sense, the temperature at the crack surface Γ_x can be considered as continuous whereas the heat flux is considered as discontinuity.

$$\mathbf{q} = \overline{\mathbf{q}} + \left\| \mathbf{q} \right\|_{\Gamma_x} H_{\Gamma_x} \tag{3-57}$$

where $\left\| \mathbf{q} \right\|_{\Gamma_x}$ denotes the jump in heat flux through the crack interface.

With such an assumption, we obtain:

$$\nabla \mathbf{q} = \nabla \overline{\mathbf{q}} + \left(\left\| \mathbf{q} \right\|_{\Gamma_x} \cdot \mathbf{n} \right) \delta_{\Gamma_x} \tag{3-58}$$

The local balance equation given in $(3\text{-}28)_b$ then decomposed into two main equation concerning the heat transfer equation in the bulk and in the localized failure zone:

In the bulk:

$$\left(\rho c - \vartheta(\overline{\mathbf{D}}^{-1}\cdot\boldsymbol{\alpha})\boldsymbol{\alpha}\right)\dot{\vartheta} + \nabla\overline{\mathbf{q}} = \overline{D}_{mech} - \vartheta(\overline{\mathbf{D}}^{-1}\cdot\boldsymbol{\alpha})\cdot\dot{\bar{\boldsymbol{\varepsilon}}} + \vartheta((\overline{\mathbf{D}}^{-1}\cdot\dot{\overline{\mathbf{D}}}\cdot\overline{\mathbf{D}}^{-1})\cdot\boldsymbol{\alpha})\left[\bar{\boldsymbol{\varepsilon}} - \boldsymbol{\alpha}\left(\vartheta - \vartheta_0\right)\right] + r \qquad (3\text{-}59)$$

In the localized failure zone:

$$\left\|\mathbf{q}\right\|_{\Gamma_x}\cdot\mathbf{n} = \overline{\overline{D}}_{mech} \qquad (3\text{-}60)$$

Equation (3-60) allows us to conclude: there is a "jump" in heat flux at the mechanical localized failure zone. This conclusion is similar to the conclusion of Armero and Park for plastic shear layer (see [39]) and Ngo et al. for general plasticity problem ([53]).

3.2.4 System of local balance equation

The system of balance equations has the similar form as for the continuum model:

$$\begin{cases} 0 = \nabla\cdot\boldsymbol{\sigma} + \mathbf{b} \\ \vartheta\dot{\eta} = -\nabla\cdot\mathbf{q} + D_{\text{int}} + r \end{cases}$$

which consists of the force equilibrium equation and the energy balance equation. However, we note that at localized failure zone, the balance equations are represented in the following form:

Force equilibrium equation (Cauchy condition):

$$\left(\boldsymbol{\sigma}\cdot\mathbf{n}\right)\big|_{\Gamma_x} = \mathbf{t}\big|_{\Gamma_x} \qquad (3\text{-}61)$$

Energy balance equation (see equation 3-60):

$$\left\|\mathbf{q}\right\|_{\Gamma_x}\cdot\mathbf{n} = \overline{\overline{D}}_{mech}$$

These equations allow us to write the local system equation fulfilled by the fully coupled localized problem:

$$\begin{cases} \begin{cases} 0 = \nabla\cdot\boldsymbol{\sigma} + \mathbf{b} & for \quad \mathbf{x}\in\Omega_{\mathbf{x}}/\Gamma_{\mathbf{x}} \\ \left(\boldsymbol{\sigma}\cdot\mathbf{n}\right)\big|_{\Gamma_x} = \mathbf{t}\big|_{\Gamma_x} & for \quad \mathbf{x}\in\Gamma_{\mathbf{x}} \end{cases} \\ \begin{cases} \tilde{\rho}\tilde{c}\,\dot{\vartheta} = -\nabla\overline{\mathbf{q}} + \overline{D}_{mech} + \overline{F}\left(\vartheta,\bar{\varepsilon}\right) + r & for \quad \mathbf{x}\in\Omega_{\mathbf{x}}/\Gamma_{\mathbf{x}} \\ \left\|\mathbf{q}\right\|_{\Gamma_{\mathbf{x}}}\cdot\mathbf{n} = \overline{\overline{D}}_{mech} & for \quad \mathbf{x}\in\Gamma_{\mathbf{x}} \end{cases} \end{cases} \qquad (3\text{-}62)$$

Where $\overline{F}\left(\vartheta,\boldsymbol{\varepsilon}\right) = -\vartheta(\overline{\mathbf{D}}^{-1}\cdot\boldsymbol{\alpha})\cdot\dot{\bar{\boldsymbol{\varepsilon}}} + \vartheta((\overline{\mathbf{D}}^{-1}\cdot\dot{\overline{\mathbf{D}}}\cdot\overline{\mathbf{D}}^{-1})\cdot\boldsymbol{\alpha})\left[\bar{\boldsymbol{\varepsilon}} - \boldsymbol{\alpha}\left(\vartheta - \vartheta_0\right)\right]$ is the structural heating due to the continuum damage and $\tilde{\rho}\tilde{c}$ is the modified heat conduction as already introduced.

3.3 Finite element approximation of the problem

3.3.1 Finite element approximation for displacement field

We present the finite element interpolations corresponding to a triangular three-node element (CST) for which the displacement "jump" is considered as constant. The displacement

discontinuity is taken into account by introducing an additional shape function $\mathbf{M_1(x)}$, then the following approximation is considered for the displacement field:

$$\mathbf{d}(\mathbf{x}) = \sum_{a=1}^{N_{nodes}} \mathbf{N}_a(\mathbf{x})\mathbf{d}_a + M_1(\mathbf{x})\overline{\overline{\mathbf{u}}}(t) \tag{3-63}$$

where $\mathbf{N}_a(\mathbf{x})$ is the vector of isoparametric shape function for CST element, $\mathbf{d}_a$ is the vector of displacement at node a, $\overline{\overline{\mathbf{u}}}$ is the vector of displacement "jump" and $M_1(\mathbf{x})$ is the additional shape function with unit "jump" on Γ_x, represented in Figure 3-2.

The strain field interpolation therefore becomes:

$$\boldsymbol{\varepsilon}(\mathbf{x},t) = \sum_{a=1}^{N_{nodes}} \mathbf{B}_a(\mathbf{x})\mathbf{d}_a + \mathbf{G_{1r}}(\mathbf{x})\overline{\overline{\mathbf{u}}} \tag{3-64}$$

where $\mathbf{B}_a(\mathbf{x}) = \mathbf{L}\mathbf{N}_a(\mathbf{x})$ and $\mathbf{G_{1r}}(\mathbf{x}) = \mathbf{L}M_1(\mathbf{x})$, $\mathbf{L}$ denotes the matrix form of the strain-displacement operator ∇^s. Due to the form of $M_1(\mathbf{x})$, $\mathbf{G_{1r}}(\mathbf{x})$ is decomposed into a regular part and a singular part as:

$$\mathbf{G_{1r}}(\mathbf{x}) = \overline{\mathbf{G}}_{\mathbf{1r}}(\mathbf{x}) + \overline{\overline{\mathbf{G}}}_{\mathbf{1r}}(\mathbf{x})\delta_{\Gamma_x} \tag{3-65}$$

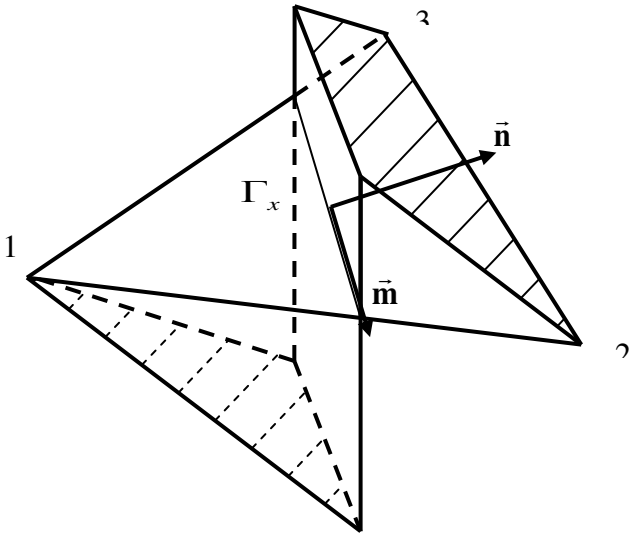

(Γ_x denotes the discontinuity surface, $\vec{\mathbf{n}}$ and $\vec{\mathbf{m}}$ the unit normal and tangential vectors to Γ_x)

Figure 3-2. *Additional shape function M_1(x) for displacement discontinuity*

3.3.2 Finite element interpolation function for temperature

Equation (3-60) shows that there is a "jump" in heat flux through the cracking surface due to the localized mechanical dissipation and also indicates a different evolution of temperature on each

side of the discontinuity surface due to thermo-mechanical dissipation. This evolution should be taken into account in the interpolation function for temperature (see Figure 3-3).

$$\vartheta(\mathbf{x}) = \sum_{a=1}^{N_{nodes}} N_a^{\vartheta}(\mathbf{x}) d_a^{\vartheta} + M_2^{\vartheta}(\mathbf{x})\lambda = \mathbf{N}^{\vartheta}(\mathbf{x})\mathbf{d}^{\vartheta} + M_2^{\vartheta}(\mathbf{x})\lambda \tag{3-66}$$

Where d_a^{ϑ} denotes the temperature at node a, $N_a^{\vartheta}(\mathbf{x})$ is the iso-parametric shape function, λ is the evolution of temperature at the localized failure point related to the heat flux "jump" on Γ_x, $M_2^{\vartheta}(\mathbf{x})$ is an additional shape function (see Figure 3-3) ; the latter allows to take into account the different evolution of temperature on each side of the discontinuity due to the modification in heat conduction produced by the discontinuity Γ_x and the localized mechanical dissipation taking place on Γ_x.

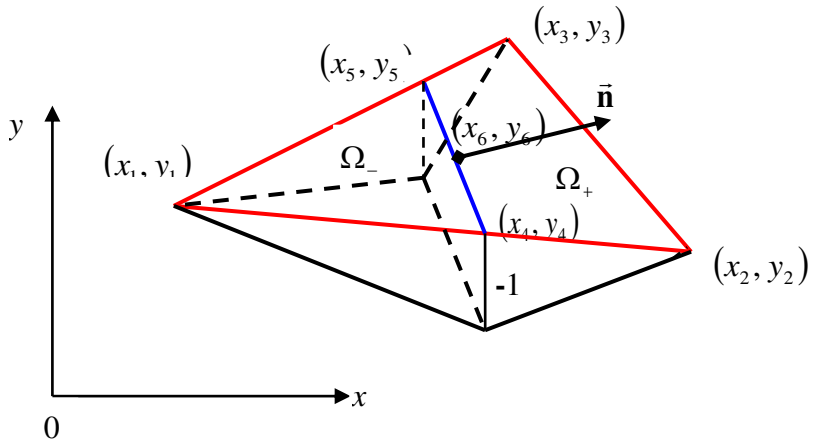

Figure 3-3. *Additional shape function*

If we assume that the crack line is passing through the gravity point (x_6,y_6) of the triangular three-node element then $M_2^{\vartheta}(\mathbf{x})$ has the following form:

$$M_2^{\vartheta}(\mathbf{x}) = \begin{cases} \dfrac{(y-y_1)[(x_4-x_1)+(x_6-x_1)z_4]-(x-x_1)[(y_6-y_1)z_4-(y_4-y_1)]}{3[(x_6-x_1)(y_4-y_1)-(x_4-x_1)(y_6-y_1)]} & \mathbf{x}\in\Omega_- \\ \dfrac{(y_3-y_2)(x-x_2)-(y-y_2)(x_3-x_2)}{(x_6-x_2)(y_3-y_2)-(x_3-x_2)(y_6-y_2)}, & \mathbf{x}\in\Omega_+ \end{cases} \tag{3-67}$$

$$\mathbf{G}_2^{\vartheta}(\mathbf{x}) = \nabla M_2^{\vartheta}(\mathbf{x}) = \begin{cases} \dfrac{\partial M_2^{\vartheta}(\mathbf{x})}{\partial x} = \begin{cases} -\dfrac{(y_6 - y_1)z_4 - (y_4 - y_1)}{3\left[(x_6 - x_1)(y_4 - y_1) - (x_4 - x_1)(y_6 - y_1)\right]} & if\ \mathbf{x} \in \Omega_- \\ \dfrac{y_3 - y_2}{(x_6 - x_2)(y_3 - y_2) - (x_3 - x_2)(y_6 - y_2)} & if\ \mathbf{x} \in \Omega_+ \end{cases} \\ \dfrac{\partial M_2^{\vartheta}(\mathbf{x})}{\partial y} = \begin{cases} \dfrac{(x_6 - x_1)z_4 + (x_4 - x_1)}{3\left[(x_6 - x_1)(y_4 - y_1) - (x_4 - x_1)(y_6 - y_1)\right]} & if\ \mathbf{x} \in \Omega_- \\ -\dfrac{x_3 - x_2}{(x_6 - x_2)(y_3 - y_2) - (x_3 - x_2)(y_6 - y_2)} & if\ \mathbf{x} \in \Omega_+ \end{cases} \end{cases} \tag{3-68}$$

where (x_1,y_1); (x_2,y_2) and (x_3,y_3) are the coordinates of the three nodes, (x_4,y_4), (x_5,y_5) are the coordinate of the point at the intersection of the crack line and the element edges and z_4 is defined as:

$$z_4 = \frac{(y_4 - y_2)(x_3 - x_2) - (y_3 - y_2)(x_4 - x_2)}{(x_6 - x_2)(y_3 - y_2) - (x_3 - x_2)(y_6 - y_2)} \tag{3-69}$$

3.3.3 Finite element equation for the problem

We start from the strong form of equilibrium equation for the thermomechanical problem (equation (3-62))

$$\begin{cases} \begin{cases} 0 = \nabla \cdot \boldsymbol{\sigma} + \mathbf{b} & for \quad \mathbf{x} \in \Omega_{\mathbf{x}} / \Gamma_{\mathbf{x}} \\ (\boldsymbol{\sigma} \cdot \mathbf{n})\big|_{\Gamma_x} = \mathbf{t}\big|_{\Gamma_x} & for \quad \mathbf{x} \in \Gamma_{\mathbf{x}} \end{cases} \\ \begin{cases} \tilde{\rho}\tilde{c}\ \dot{\vartheta} = -\nabla \overline{\mathbf{q}} + \overline{D}_{mech} + \overline{F}(\vartheta, \bar{\varepsilon}) + r & for \quad \mathbf{x} \in \Omega_{\mathbf{x}} / \Gamma_{\mathbf{x}} \\ \|\mathbf{q}\|_{\Gamma_{\mathbf{x}}} \cdot \mathbf{n} = \overline{\overline{D}}_{mech} & for \quad \mathbf{x} \in \Gamma_{\mathbf{x}} \end{cases} \end{cases} \tag{3-70}$$

We note that this equation is time dependent (in particular, the thermal transfer process is non-stationary), so the problem should be solved by time linearization method. In particular, the whole process is divided into many time steps (Δt), and the problem turns into identifying the mechanical and thermal variables at the next time step (n+1) by assuming that the mechanical and thermal variables at the current time step (n) are already known. This linearization method will be discussed in detail in the following.

3.3.3.1 For mechanical balance equation

For mechanical balance equation $(70)_1$, by applying incompatible mode method (see [17], [18], [25]), we can establish the following form of the discretized equation:

$$\begin{cases} \underset{e=1}{\overset{N_{elem}}{\mathbf{A}}}\left[\int_{\Omega_x}\mathbf{f}_{int}^{e}(t)-\mathbf{f}_{ext}^{e}(t)\right]=0 & for\ \mathbf{x}\in\Omega_{\mathbf{x}}/\Gamma_{\mathbf{x}} \\ \mathbf{h}^{e}(t)=\int_{\Omega_e}\overline{\mathbf{G}}_v^{T}\boldsymbol{\sigma}(\boldsymbol{\varepsilon},\vartheta)d\Omega^{e}+\int_{\Gamma_{\bar{\bar{x}}}}\overline{\overline{\mathbf{G}}}_v^{T}\mathbf{t}(\overline{\overline{\mathbf{u}}},\vartheta_{\Gamma_x})d\Gamma=0 & for\ \mathbf{x}\in\Gamma_{\mathbf{x}} \end{cases} \tag{3-71}$$

where $\mathbf{G}_{1v}(\mathbf{x})=\mathbf{G}_{1r}(x)-\frac{1}{A_e}\int_{\Omega_e}\mathbf{G}_{1r}(\mathbf{x})d\Omega_e=\overline{\mathbf{G}}_{1v}(\mathbf{x})+\overline{\overline{\mathbf{G}}}_{1v}(\mathbf{x})\delta_{\Gamma_x}$ is the "modified" interpolation function of "virtual" strain, which is chosen different from the interpolation function of "real" strain $\mathbf{G}_{1r}(\mathbf{x})$ in order to satisfy the "patch test" (see [18]) and $f_{\text{int}}^{e}(t)=\int_{\Omega_e/\Gamma_x}\mathbf{B}^{T}\sigma(\boldsymbol{\varepsilon},\vartheta)d\Omega_e$.

By taking into account the interpolation function of strain and temperature: $\boldsymbol{\varepsilon}=\mathbf{B}\mathbf{d}(t)+\mathbf{G}_{1r}\overline{\overline{\mathbf{u}}}(t)$, $\vartheta=\mathbf{N}_a^{\vartheta}\mathbf{d}^{\vartheta}(t)+M_2^{\vartheta}\lambda$, $\vartheta_{\Gamma_x}=\mathbf{N}_a^{\vartheta}(\overline{\overline{\mathbf{x}}})\mathbf{d}_a^{\vartheta}+\underbrace{M_2^{\vartheta}(\overline{\overline{\mathbf{x}}})}_{1}\lambda$, equation (72) can be brought to the linearized form:

Given $\mathbf{d}_n,\overline{\overline{u}}_n,\mathbf{d}_n^{\vartheta},\lambda_n$*find* $\Delta\mathbf{d}_{n+1}^{(i)},\Delta\overline{\overline{\mathbf{u}}}_{n+1}^{(i)},\Delta\mathbf{d}_{n+1}^{\vartheta(i)},\Delta\lambda_{n+1}^{\vartheta(i)}$

$$\begin{cases} \left(\int_{\Omega_e}\mathbf{B}^{\mathbf{t}}\frac{\partial\boldsymbol{\sigma}}{\partial\mathbf{d}}\Big|_{n+1}^{(i)}d\Omega_e\right)\Delta\mathbf{d}_{n+1}^{(i)}+\left(\int_{\Omega_e}\mathbf{B}^{\mathbf{t}}\frac{\partial\boldsymbol{\sigma}}{\partial\overline{\overline{\mathbf{u}}}}\Big|_{n+1}^{(i)}d\Omega_e\right)\Delta\overline{\overline{\mathbf{u}}}_{n+1}^{(i)} \\ +\left(\int_{\Omega_e}\mathbf{B}^{\mathbf{t}}\frac{\partial\boldsymbol{\sigma}}{\partial\mathbf{d}^{\vartheta}}\Big|_{n+1}^{(i)}d\Omega_e\right)\Delta\mathbf{d}_{n+1}^{\vartheta,(i)}+\left(\int_{\Omega_e}\mathbf{B}^{\mathbf{t}}\frac{\partial\boldsymbol{\sigma}}{\partial\lambda}\Big|_{n+1}^{(i)}d\Omega_e\right)\Delta\lambda_{n+1}^{\vartheta,(i)}=\mathbf{f}_{n+1}^{ext(i)}(t)-\mathbf{f}_{n+1}^{\text{int}(i)}(t) \\ -\mathbf{h}_{n+1}^{e(i)}=\left(\int_{\Omega_e}\overline{\mathbf{G}}_v^{T}\frac{\partial\boldsymbol{\sigma}}{\partial\mathbf{d}}\Big|_{n+1}^{(i)}d\Omega^{e}\right)\Delta\mathbf{d}_{n+1}^{(i)}+\left(\int_{\Omega_e}\overline{\mathbf{G}}_v^{T}\frac{\partial\boldsymbol{\sigma}}{\partial\overline{\overline{\mathbf{u}}}}\Big|_{n+1}^{(i)}d\Omega^{e}\right)\Delta\overline{\overline{\mathbf{u}}}_{n+1}^{(i)}+\left(\int_{\Omega_e}\overline{\mathbf{G}}_v^{T}\frac{\partial\boldsymbol{\sigma}}{\partial\mathbf{d}^{\vartheta}}\Big|_{n+1}^{(i)}d\Omega^{e}\right)\Delta\mathbf{d}_{n+1}^{\vartheta,(i)}\left(\int_{\Omega_e}\overline{\mathbf{G}}_v^{T}\frac{\partial\boldsymbol{\sigma}}{\partial\lambda^{\vartheta}}\Big|_{n+1}^{(i)}d\Omega^{e}\right)\Delta\lambda_{n+1}^{\vartheta,(i)} \\ +\left(\int_{\Gamma_x}\overline{\overline{\mathbf{G}}}_v^{T}\frac{\partial\mathbf{t}}{\partial\mathbf{d}}\Big|_{n+1}^{(i)}d\Gamma_x\right)\Delta\mathbf{d}_{n+1}^{(i)}+\left(\int_{\Gamma_x}\overline{\overline{\mathbf{G}}}_v^{T}\frac{\partial\mathbf{t}}{\partial\overline{\overline{\mathbf{u}}}}\Big|_{n+1}^{(i)}d\Gamma_x\right)\Delta\overline{\overline{\mathbf{u}}}_{n+1}^{(i)}+\left(\int_{\Gamma_x}\overline{\overline{\mathbf{G}}}_v^{T}\frac{\partial\boldsymbol{\sigma}}{\partial\mathbf{d}^{\vartheta}}\Big|_{n+1}^{(i)}d\Omega^{e}\right)\Delta\mathbf{d}_{n+1}^{\vartheta,(i)}+\left(\int_{\Gamma_x}\overline{\overline{\mathbf{G}}}_v^{T}\frac{\partial\mathbf{t}}{\partial\lambda}\Big|_{n+1}^{(i)}d\Gamma_x\right)\Delta\lambda_{n+1}^{\vartheta,(i)} \end{cases} \tag{3-72}$$

3.3.3.2 For thermal balance equation

The thermal balance equation is taken from equation $(3\text{-}70)_2$:

$$\begin{cases} \tilde{\rho}\tilde{c}\,\dot{\vartheta}=-\nabla\overline{\mathbf{q}}+\overline{D}_{mech}+\overline{F}(\overline{\boldsymbol{\varepsilon}},\overline{\mathbf{D}},\vartheta)+r & for\quad \mathbf{x}\in\Omega_{\mathbf{x}}/\Gamma_{\mathbf{x}} \\ \|\mathbf{q}\|_{\Gamma_{\mathbf{x}}}\cdot\mathbf{n}=\overline{\overline{D}}_{mech} & for\quad \mathbf{x}\in\Gamma_{\mathbf{x}} \end{cases} \tag{3-73}$$

By applying the Fourier laws $\mathbf{q}=-k\nabla\cdot\vartheta$ for this problem, we have:

at continuum domain: $\mathbf{x}\in\Omega_x/\Gamma_x$:

$$\overline{\mathbf{q}}=-k\nabla\vartheta\rightarrow\nabla\overline{\mathbf{q}}=-k\nabla^{2}\vartheta \tag{3-74}$$

at the crack surface Γ_x:

$$\left\|\mathbf{q}\right\|_{\Gamma_x}\cdot\mathbf{n}\delta_{\Gamma_x}=-k_{\Gamma_x}\nabla^2\vartheta\Big|_{\Gamma_x}=-k_{\Gamma_x}(\nabla^2N_a^{\vartheta}d_a+\underbrace{\nabla^2M_a^{\vartheta}}_{\delta_{\Gamma_x}}\lambda)=-k_{\Gamma_x}\lambda\delta_{\Gamma_x} \tag{3-75}$$

where k is the heat conductivity coefficient of the material at continuum domain and k_{Γ_x} is the heat conductivity coefficient at the localized failure zone.

By combining equation (75) and equation $(73)_b$, we obtain the equation to determine λ:

$$\lambda=-\frac{\overline{\overline{D}}_{mech}}{k_{\Gamma_x}} \tag{3-76}$$

If we introduce $w_{\vartheta}(\mathbf{x})$ the virtual temperature field and using the Fourier equation for heat flux $\overline{\mathbf{q}}=-k\nabla\vartheta$ then the weak form of equation $(74)_a$ becomes:

$$\underset{e=1}{\overset{N_{el}}{A}}\left(\int_{\Omega^e/\Gamma_x}w_{\vartheta}\tilde{\rho}\tilde{c}\,\dot{\vartheta}d\Omega+\int_{\Omega^e/\Gamma_x}\nabla w_{\vartheta}k\nabla\vartheta d\Omega+\int_{\Gamma_{eq}}w_{\vartheta}q_n d\Gamma_{eq}-\int_{\Omega^e/\Gamma_x}w_{\vartheta}\left(\underbrace{\overline{D}_{mech}+\overline{F}(\vartheta,\bar{\boldsymbol{\varepsilon}})+r}_{R_{add}}\right)d\Omega\right)=0 \tag{3-77}$$

If the iso-parametric interpolation function is used for the virtual temperature $w_{\vartheta}(\mathbf{x})=N_a^{\vartheta}w_a^{\vartheta}=\mathbf{N}^{\vartheta}\mathbf{w}^{\vartheta}$ then we can establish discrete version of this equation as follows:

$$\begin{aligned}&\underset{e=1}{\overset{N_{el}}{A}}\left(\int_{\Omega^e/\Gamma_x}\mathbf{N}^{\vartheta,T}\mathbf{w}^{\vartheta}\tilde{\rho}\tilde{c}\left(\mathbf{N}^{\vartheta}\dot{\mathbf{d}}^{\vartheta}+M_2\dot{\lambda}\right)d\Omega+\int_{\Omega^e/\Gamma_x}\mathbf{B}^{\vartheta,T}\mathbf{w}^{\vartheta}\cdot k\cdot\left(\mathbf{B}^{\vartheta}\mathbf{d}^{\vartheta}+\mathbf{G}_2\lambda\right)d\Omega\right)\\&=\underset{e=1}{\overset{N_{el}}{A}}\left(-\int_{\Gamma_{eq}}\mathbf{N}^{\vartheta,T}\mathbf{w}^{\vartheta}q_n d\Gamma_{eq}+\int_{\Omega^e/\Gamma_x}\mathbf{N}^{\vartheta,T}\mathbf{w}^{\vartheta}R_{add}d\Omega\right)\end{aligned} \tag{3-78}$$

Note that this equation should be valid for any value of virtual temperature, thus we have:

$$\underset{e=1}{\overset{N_{el}}{A}}\left(\mathbf{M}_{\vartheta}^e\dot{\mathbf{d}}^{\vartheta}+\mathbf{P}_{\vartheta}^e\dot{\lambda}+\mathbf{K}_{\vartheta}^e\mathbf{d}^{\vartheta}+\mathbf{F}_{\vartheta}^e\lambda\right)=\underset{e=1}{\overset{N_{el}}{A}}\left(\mathbf{Q}_{\vartheta}^1\right) \tag{3-79}$$

where

$$\mathbf{M}_{\vartheta}^{e} = \tilde{\rho}\tilde{c}\int_{\Omega_e/\Gamma_x} \mathbf{N}^{\vartheta,T}(x)\mathbf{N}^{\vartheta}(x)d\Omega \tag{3-80}$$

$$\mathbf{P}_{\vartheta}^{e} = \tilde{\rho}\tilde{c}\int_{\Omega_e/\Gamma_x} \mathbf{N}^{\vartheta,T}(x)M_2(x)d\Omega \tag{3-81}$$

$$\mathbf{K}_{\vartheta}^{e} = k\int_{\Omega_e/\Gamma_x}\left(\frac{\partial\mathbf{N}^{\vartheta}}{\partial x}\frac{\partial\mathbf{N}^{\vartheta}}{\partial x}+\frac{\partial\mathbf{N}^{\vartheta}}{\partial y}\frac{\partial\mathbf{N}^{\vartheta}}{\partial y}\right)d\Omega \tag{3-82}$$

$$\mathbf{F}_{\vartheta}^{e} = k\int_{\Omega_e/\Gamma_x}\left(\frac{\partial\mathbf{N}^{\vartheta}}{\partial x}\frac{\partial M_2}{\partial x}+\frac{\partial\mathbf{N}^{\vartheta}}{\partial y}\frac{\partial M_2}{\partial y}\right)d\Omega \tag{3-83}$$

$$\mathbf{Q}_{\vartheta}^{1} = \int_{\Omega_e/\Gamma_x}\mathbf{N}^{\vartheta}(\mathbf{x})R_{add}d\Omega - \int_{\Gamma_{eq}}\mathbf{N}^{\vartheta}(\mathbf{x})\bar{q}_n d\Gamma \tag{3-84}$$

By applying the Euler backward integration for time-dependent equation and by linearization, equation (3-79) becomes:

$$\overset{N_{el}}{\underset{e=1}{A}}\left(\frac{\gamma}{\beta\Delta t}\mathbf{M}_{\vartheta}^{e}+\mathbf{K}_{\vartheta}^{e}\right)\Delta\mathbf{d}_{n+1}^{\vartheta} = \overset{N_{el}}{\underset{e=1}{A}}\left(\mathbf{R}_{n,\vartheta}^{1}\right) \tag{3-85}$$

where γ, β are the Newmark coefficients (see [17]) and

$$\mathbf{R}_{n,\vartheta}^{1} = \mathbf{Q}_{\vartheta,n}^{1} - \mathbf{M}_{\vartheta}^{e}\dot{\mathbf{d}}_{a,n}^{\vartheta} - \mathbf{P}_{\vartheta}^{e}\dot{\lambda}_n - \mathbf{K}_{\vartheta}^{e}\mathbf{d}_n^{\vartheta} - \mathbf{F}_{\vartheta}^{e}\lambda_n \tag{3-86}$$

Equation (73) and equation (86) allow us to form a system of four equations for four unknowns $\Delta\mathbf{d}_{n+1}, \Delta\overline{\overline{\mathbf{u}}}_{n+1}, \Delta\mathbf{d}_{n+1}^{\vartheta}, \Delta\lambda_{n+1}$. Several procedures were introduced to solve this system (see [54], [45], [45], [47], [46], [50])]. In this work, we apply an approximation procedure, namely the "adiabatic" splitting procedure, in order to solve the equation faster with guaranty of stability of the numerical scheme (see [46], [50]).

3.4 Operator split solution procedure

In this procedure, the total process is split into "mechanical" process and "thermal" process. Particularly, in the "mechanical" process, the force balance equation is solved while considering that the temperature rising is due to the structural heating only (or adiabatic condition). On the other hand, for the "thermal" process, we compute the "remaining" evolution of the temperature due to the internal heat supply r and mechanical dissipation D_{mech}. The jump in heat flow due to the localized mechanical dissipation is also considered in this process. This procedure allows us to split equation (3-70) into two separated equations for mechanical process and for thermal process and was proved to provide a stable approximation solution for differential equation system (see [46], [50]).

"Mechanical" process:

$$\begin{cases} \begin{cases} 0 = \nabla \cdot \boldsymbol{\sigma} + \mathbf{b} & for\ \mathbf{x} \in \Omega_{\mathbf{x}} / \Gamma_{\mathbf{x}} \\ (\boldsymbol{\sigma} \cdot \mathbf{n})\big|_{\Gamma_x} = \mathbf{t}\big|_{\Gamma_x} & for\ \mathbf{x} \in \Gamma_{\mathbf{x}} \end{cases} \\ \dot{\eta}^e = 0 \rightarrow \tilde{\rho}\tilde{c}\,\dot{\vartheta} = -\vartheta(\overline{\mathbf{D}}^{-1} \cdot \boldsymbol{\alpha}) \cdot \dot{\bar{\boldsymbol{\varepsilon}}} + \vartheta((\overline{\mathbf{D}}^{-1} \cdot \dot{\overline{\mathbf{D}}} \cdot \overline{\mathbf{D}}^{-1}) \cdot \boldsymbol{\alpha})\left[\bar{\boldsymbol{\varepsilon}} - \boldsymbol{\alpha}(\vartheta - \vartheta_0)\right] = \overline{F}(\bar{\boldsymbol{\varepsilon}}, \overline{\mathbf{D}}, \vartheta) \end{cases} \tag{3-87}$$

"Thermal" process:

$$\begin{cases} \tilde{\rho}\tilde{c}\,\dot{\vartheta} = -\nabla\overline{\mathbf{q}} + \overline{D}_{mech} + r & for\ \mathbf{x} \in \Omega_{\mathbf{x}} / \Gamma_{\mathbf{x}} \\ \|\mathbf{q}\|_{\Gamma_{\mathbf{x}}} \mathbf{n} = \overline{\overline{D}}_{mech} & for\ \mathbf{x} \in \Gamma_x \end{cases} \tag{3-88}$$

The overall scheme of adiabatic splitting operation is described in Figure 3-4.

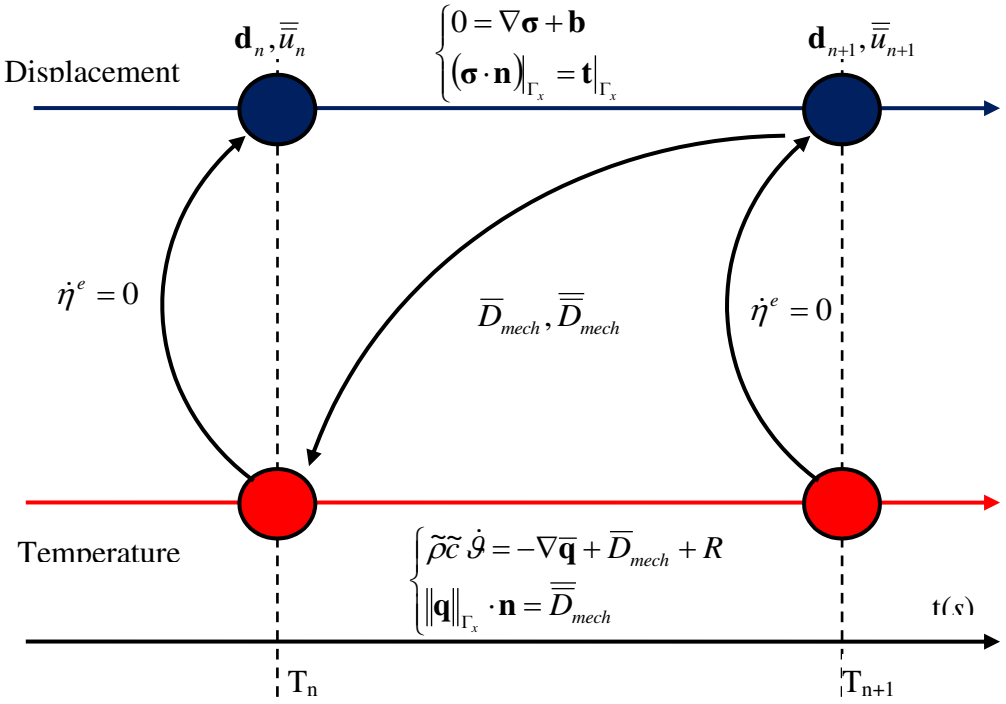

Figure 3-4. *"Adiabatic" splitting procedure.*

We present in the following the different steps of the adiabatic scheme in detail beginning by the "mechanical process".

3.4.1 Mechanical process

3.4.1.1 Mechanical process in continuum damage

In this part, we go back to the theoretical formulation to highlight the modification induced by the adiabatic condition considered in our numerical scheme. The evolution of the temperature due to structural heating (equation $(3\text{-}87)_b$) is established for adiabatic condition by the equation:

$$\dot{\eta}^e = 0 \rightarrow \tilde{\rho}\tilde{c}\,\dot{\vartheta} = -\vartheta(\overline{\mathbf{D}}^{-1}\cdot\boldsymbol{\alpha})\cdot\dot{\bar{\boldsymbol{\varepsilon}}} + \vartheta((\overline{\mathbf{D}}^{-1}\cdot\dot{\overline{\mathbf{D}}}\cdot\overline{\mathbf{D}}^{-1})\cdot\boldsymbol{\alpha})\left[\bar{\boldsymbol{\varepsilon}} - \boldsymbol{\alpha}\left(\vartheta - \vartheta_0\right)\right]$$

$$\rightarrow \tilde{\rho}\tilde{c}\,\dot{\vartheta} = -\vartheta\underbrace{(\overline{\mathbf{D}}^{-1}\cdot\boldsymbol{\alpha})}_{\boldsymbol{\beta}}\cdot\dot{\bar{\boldsymbol{\varepsilon}}} + \vartheta(\underbrace{(\overline{\mathbf{D}}^{-1}\cdot\boldsymbol{\alpha})}_{\boldsymbol{\beta}}\cdot\dot{\overline{\mathbf{D}}}\cdot\underbrace{(\overline{\mathbf{D}}^{-1}\cdot\left[\bar{\boldsymbol{\varepsilon}} - \boldsymbol{\alpha}\left(\vartheta - \vartheta_0\right)\right])}_{\boldsymbol{\sigma}} \tag{3-89}$$

From equation (3-26), we have $\bar{\gamma}\dfrac{\partial\overline{\Phi}}{\partial\boldsymbol{\sigma}} = \dfrac{\partial\overline{D}_{\text{int}}}{\partial\boldsymbol{\sigma}} = \dot{\overline{\mathbf{D}}}\cdot\boldsymbol{\sigma}$, therefore, the time evolution of temperature due to 'adiabatic' condition can be written:

$$\dot{\vartheta} = -\frac{\vartheta\boldsymbol{\beta}}{\tilde{\rho}\tilde{c}}\left[\dot{\bar{\boldsymbol{\varepsilon}}} - \bar{\gamma}\frac{\partial\overline{\Phi}}{\partial\boldsymbol{\sigma}}\right] \tag{3-90}$$

From the constitutive equation (18) we can estimate the stress evolution:

$$\boldsymbol{\sigma} = \frac{\partial\psi}{\partial\boldsymbol{\varepsilon}} = \overline{\mathbf{D}}^{-1}\cdot[\bar{\boldsymbol{\varepsilon}} - \boldsymbol{\alpha}(\vartheta - \vartheta_0)] \rightarrow \dot{\boldsymbol{\sigma}} = \overline{\mathbf{D}}^{-1}\cdot(\dot{\bar{\boldsymbol{\varepsilon}}} - \boldsymbol{\alpha}\dot{\vartheta}) - (\overline{\mathbf{D}}^{-1}\cdot\dot{\overline{\mathbf{D}}}\cdot\overline{\mathbf{D}}^{-1})\cdot[\boldsymbol{\varepsilon} - \alpha(\vartheta - \vartheta_0)]$$

$$\rightarrow \dot{\boldsymbol{\sigma}} = \overline{\mathbf{D}}^{-1}\cdot\left(\dot{\bar{\boldsymbol{\varepsilon}}} - \gamma\frac{\partial\overline{\Phi}}{\partial\boldsymbol{\sigma}}\right) - \boldsymbol{\beta}\dot{\vartheta}$$

$$\rightarrow \dot{\boldsymbol{\sigma}} = \left[\overline{\mathbf{D}}^{-1} + \frac{\vartheta}{\tilde{\rho}\tilde{c}}\overline{\boldsymbol{\beta}}\otimes\overline{\boldsymbol{\beta}}\right]\cdot\left(\dot{\bar{\boldsymbol{\varepsilon}}} - \gamma\frac{\partial\overline{\Phi}}{\partial\boldsymbol{\sigma}}\right) \tag{3-91}$$

If a damage loading is considered, the consistency condition $\dot{\overline{\Phi}} = 0$ gives:

$$\dot{\overline{\Phi}} = \frac{\partial\overline{\Phi}}{\partial\boldsymbol{\sigma}}\cdot\dot{\boldsymbol{\sigma}} + \frac{\partial\overline{\Phi}}{\partial\overline{q}}\dot{\bar{q}} + \frac{\partial\overline{\Phi}}{\partial\vartheta}\dot{\vartheta} = 0 \tag{3-92}$$

If we assume that the damage threshold is temperature independent and given that $\dot{\bar{q}} = -\dfrac{\partial^2\overline{\Xi}}{\partial\bar{\xi}^2}\dot{\bar{\xi}}$

then this equation further leads to:

$$\dot{\overline{\Phi}} = \frac{\partial\overline{\Phi}}{\partial\boldsymbol{\sigma}}\cdot\left[\overline{\mathbf{D}}^{-1} + \frac{\vartheta}{\tilde{\rho}\tilde{c}}\overline{\boldsymbol{\beta}}\otimes\overline{\boldsymbol{\beta}}\right]\cdot\left(\dot{\bar{\boldsymbol{\varepsilon}}} - \gamma\frac{\partial\overline{\Phi}}{\partial\boldsymbol{\sigma}}\right) - \frac{\partial\overline{\Phi}}{\partial\overline{q}}\frac{\partial^2\overline{\Xi}}{\partial\bar{\xi}^2}\dot{\bar{\xi}} = 0 \tag{3-93}$$

By applying the time evolution of hardening variable (3-23): $\dot{\bar{\xi}} = \bar{\gamma}\dfrac{\partial\overline{\Phi}}{\partial\overline{q}}$, we have:

$$\dot{\overline{\Phi}} = \frac{\partial\dot{\overline{\Phi}}}{\partial\boldsymbol{\sigma}}\cdot\left[\overline{\mathbf{D}}^{-1} + \frac{\vartheta}{\tilde{\rho}\tilde{c}}\overline{\boldsymbol{\beta}}\otimes\overline{\boldsymbol{\beta}}\right]\cdot\left(\dot{\bar{\boldsymbol{\varepsilon}}} - \gamma\frac{\partial\overline{\Phi}}{\partial\boldsymbol{\sigma}}\right) - \frac{\partial\overline{\Phi}}{\partial\overline{q}}\frac{\partial^2\overline{\Xi}}{\partial\bar{\xi}^2}\gamma\frac{\partial\overline{\Phi}}{\partial\overline{q}} = 0 \tag{3-94}$$

We can thus deduce the corresponding value of the Lagrange multiplier for adiabatic condition:

$$\bar{\gamma} = \frac{\dfrac{\partial \overline{\Phi}}{\partial \boldsymbol{\sigma}} \cdot \left(\overline{\mathbf{D}}^{-1} + \dfrac{\vartheta}{\widetilde{\rho c}} \overline{\boldsymbol{\beta}} \otimes \overline{\boldsymbol{\beta}} \right)}{\dfrac{\partial \overline{\Phi}}{\partial \boldsymbol{\sigma}} \cdot \left(\overline{\mathbf{D}}^{-1} + \dfrac{\vartheta}{\widetilde{\rho c}} \overline{\boldsymbol{\beta}} \otimes \overline{\boldsymbol{\beta}} \right) \cdot \dfrac{\partial \overline{\Phi}}{\partial \boldsymbol{\sigma}} + \dfrac{\partial^2 \overline{\Xi}}{\partial \bar{\xi}^2} \left(\dfrac{\partial \overline{\Phi}}{\partial \bar{q}} \right)^2} \cdot \dot{\boldsymbol{\varepsilon}} \tag{3-95}$$

The rate form of the constitutive equation which can be used to compute the evolution of each internal variable is finally given for mechanical part as:

$$\begin{cases} \dot{\boldsymbol{\sigma}} = (\overline{\mathbf{D}}^{-1} + \dfrac{\vartheta}{\widetilde{\rho c}} \overline{\boldsymbol{\beta}} \otimes \overline{\boldsymbol{\beta}}) \cdot \dot{\bar{\boldsymbol{\varepsilon}}} & \text{if } \bar{\gamma} = 0 \\ \dot{\boldsymbol{\sigma}} = \left[\overline{\mathbf{D}}^{-1} + \dfrac{\vartheta}{\widetilde{\rho c}} \overline{\boldsymbol{\beta}} \otimes \overline{\boldsymbol{\beta}} - \dfrac{\dfrac{\partial \overline{\Phi}}{\partial \boldsymbol{\sigma}} \cdot \left(\overline{\mathbf{D}}^{-1} + \dfrac{\vartheta}{\widetilde{\rho c}} \overline{\boldsymbol{\beta}} \otimes \overline{\boldsymbol{\beta}} \right) \dfrac{\partial \overline{\Phi}}{\partial \boldsymbol{\sigma}}}{\dfrac{\partial \overline{\Phi}}{\partial \boldsymbol{\sigma}} \cdot \left(\overline{\mathbf{D}}^{-1} + \dfrac{\vartheta}{\widetilde{\rho c}} \overline{\boldsymbol{\beta}} \otimes \overline{\boldsymbol{\beta}} \right) \cdot \dfrac{\partial \overline{\Phi}}{\partial \boldsymbol{\sigma}} + \dfrac{\partial^2 \overline{\Xi}}{\partial \bar{\xi}^2} \left(\dfrac{\partial \overline{\Phi}}{\partial \bar{q}} \right)^2} \right] \cdot \dot{\bar{\boldsymbol{\varepsilon}}} & \text{if } \bar{\gamma} > 0 \end{cases} \tag{3-96}$$

Or in short:

$$\dot{\boldsymbol{\sigma}} = \overline{\mathbf{C}}^{\mathbf{ad}} \cdot \dot{\bar{\boldsymbol{\varepsilon}}} \tag{3-97}$$

Before carrying out the global computation, we have to estimate some ingredients including: mechanical internal variables, 'adiabatic' tangent modulus ($\mathbf{C_{ad}}$) and updated stress. These computations should be performed at the element level, or in other word, at the local level. An algorithm to calculate these variables by using 'return-mapping' algorithm (see [51])is introduced in Figure 3-5.

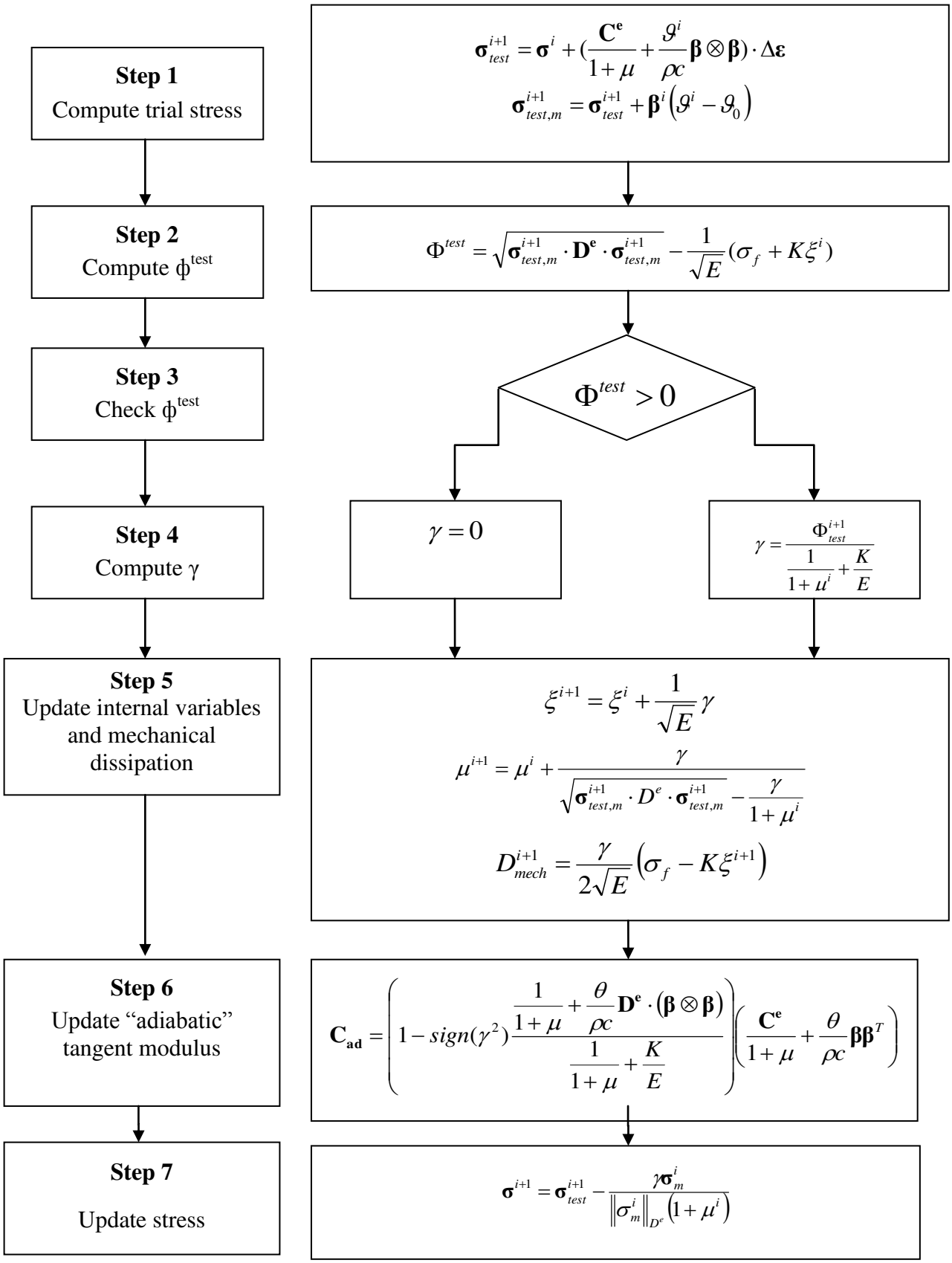

Figure 3-5. *Local computation for mechanical part*

3.4.1.2 Mechanical process at localized failure

The localized failure in this case happens due to mechanical loading only. The irregular part of the Lagrange multiplier is determined from the consistency condition: $\dot{\overline{\overline{\Phi}}}_1 = 0$ and/or $\dot{\overline{\overline{\Phi}}}_2 = 0$ which leads to:

Strong failure due to normal stress: $\dot{\overline{\overline{\Phi}}}_1 = 0 \rightarrow \frac{\partial \overline{\overline{\Phi}}_1}{\partial \mathbf{t}} \cdot \dot{\mathbf{t}} + \frac{\partial \overline{\overline{\Phi}}_1}{\partial \overline{\overline{q}}} \cdot \dot{\overline{\overline{q}}} = 0$ (3-98)

Strong failure due to shear stress: $\dot{\overline{\overline{\Phi}}}_2 = 0 \rightarrow \frac{\partial \overline{\overline{\Phi}}_2}{\partial \mathbf{t}} \cdot \dot{\mathbf{t}} + \frac{\partial \overline{\overline{\Phi}}_2}{\partial \overline{\overline{q}}} \cdot \dot{\overline{\overline{q}}} = 0$ (3-99)

Where $\overline{\overline{q}} = -\overline{\overline{K}}\,\overline{\overline{\xi}} \rightarrow \dot{\overline{\overline{q}}} = -\overline{\overline{K}}\,\dot{\overline{\overline{\xi}}}$ (for linear isotropic softening)

The evolution of traction can be established from the state equation (3-45):

$$\mathbf{t} = \overline{\overline{\mathbf{Q}}}^{-1} \cdot \overline{\overline{\mathbf{u}}} \rightarrow \dot{\mathbf{t}} = \overline{\overline{\mathbf{Q}}}^{-1} \cdot \dot{\overline{\overline{\mathbf{u}}}} + \overline{\overline{\mathbf{Q}}}^{-1} \dot{\overline{\overline{\mathbf{Q}}}} \underbrace{\overline{\overline{\mathbf{Q}}}^{-1} \overline{\overline{\mathbf{u}}}}_{\mathbf{t}} \rightarrow \dot{\mathbf{t}} = \overline{\overline{\mathbf{Q}}}^{-1} \cdot \dot{\overline{\overline{\mathbf{u}}}} - \overline{\overline{\mathbf{Q}}}^{-1} \sum_{k=1}^{2} \left(\dot{\overline{\overline{\gamma}}}_k \frac{\partial \overline{\overline{\Phi}}_k}{\partial \mathbf{t}} \right) \tag{3-100}$$

These equations finally lead to the following expressions for Lagrange multipliers:

$$\dot{\overline{\overline{\gamma}}}_k = \frac{\dfrac{\partial \overline{\overline{\Phi}}_k}{\partial \mathbf{t}} \cdot \overline{\overline{\mathbf{Q}}}^{-1}}{\dfrac{\partial \overline{\overline{\Phi}}_k}{\partial \mathbf{t}} \cdot \overline{\overline{\mathbf{Q}}}^{-1} \dfrac{\partial \overline{\overline{\Phi}}_k}{\partial \mathbf{t}} + \dfrac{\partial \overline{\overline{\Phi}}_k}{\partial \overline{\overline{q}}} \cdot \overline{\overline{K}} \dfrac{\partial \overline{\overline{\Phi}}_k}{\partial \overline{\overline{q}}}} \cdot \dot{\overline{\overline{\mathbf{u}}}}; \qquad k = 1,2 \tag{3-101}$$

And the rate constitutive equation between traction and "jump" in displacement can be established:

$$\begin{cases} \dot{\mathbf{t}} = \overline{\overline{\mathbf{Q}}}^{-1} \cdot \dot{\overline{\overline{\mathbf{u}}}} & \text{if } \dot{\overline{\overline{\gamma}}}_k > 0 \\ \dot{\mathbf{t}} = \left[\overline{\overline{\mathbf{Q}}}^{-1} - \dfrac{\left(\dfrac{\partial \overline{\overline{\Phi}}_k}{\partial \mathbf{t}} \cdot \overline{\overline{\mathbf{Q}}}^{-1} \right) \otimes \left(\overline{\overline{\mathbf{Q}}}^{-1} \cdot \dfrac{\partial \overline{\overline{\Phi}}_k}{\partial \mathbf{t}_n} \right)}{\dfrac{\partial \overline{\overline{\Phi}}_k}{\partial \mathbf{t}} \cdot \overline{\overline{\mathbf{Q}}}^{-1} \dfrac{\partial \overline{\overline{\Phi}}_k}{\partial \mathbf{t}} + \dfrac{\partial \overline{\overline{\Phi}}_k}{\partial \overline{\overline{q}}} \cdot \overline{\overline{K}} \dfrac{\partial \overline{\overline{\Phi}}_k}{\partial \overline{\overline{q}}}} \right] \cdot \dot{\overline{\overline{\mathbf{u}}}} & \text{if } \dot{\overline{\overline{\gamma}}}_k > 0 \end{cases} \tag{3-102}$$

$$\dot{\mathbf{t}} = \overline{\overline{\mathbf{C}}}_{ad} \cdot \dot{\overline{\overline{\mathbf{u}}}} \tag{3-103}$$

3.4.1.3 Finite element method for "mechanical" process

By applying the "adiabatic" spitting procedure, we can establish the evolution of stress and traction due to the evolution of strain and displacement "jump" with "adiabatic" tangent modulus

(equation (3-97) and (3-104)). This allows us to write the linearization form of equation (3-72) without the temperature evolution:

$$\begin{cases} \mathbf{K}_{n+1}^{e,(i)}\Delta\mathbf{d}_{n+1}^{(i)} + \mathbf{F}_{r,n+1}^{e,(i)}\Delta\overline{\overline{\mathbf{u}}}_{n+1}^{(i)} = \mathbf{f}_{n+1}^{ext(i)}(t) - \mathbf{f}_{n+1}^{\text{int}(i)}(t) \\ -\mathbf{h}_{n+1}^{e(i)} = \mathbf{F}_{v,n+1}^{e,(i),T}\Delta\mathbf{d}_{n+1}^{(i)} + \left(\mathbf{H}_{v,n+1}^{e,(i)} + \mathbf{K}_{\alpha,n+1}^{(i)}\right)\Delta\overline{\overline{\mathbf{u}}}_{n+1}^{(i)} \end{cases} \tag{3-104}$$

where

$$\mathbf{K}_{n+1}^{e,(i)} = \int_{\Omega_e} \mathbf{B}^T \left.\frac{\partial\boldsymbol{\sigma}}{\partial\mathbf{d}}\right|_{n+1}^{(i)} d\Omega_e = \int_{\Omega_e} \mathbf{B}^T \overline{\mathbf{C}}_{n+1}^{ad,(i)}\mathbf{B}d\Omega_e \tag{3-105}$$

$$\mathbf{F}_{v,n+1}^{e,(i),T} = \int_{\Omega_e} \overline{\mathbf{G}}_v^T \left.\frac{\partial\boldsymbol{\sigma}}{\partial\mathbf{d}}\right|_{n+1}^{(i)} d\Omega^e = \int_{\Omega_e} \overline{\mathbf{G}}_v^T \overline{\mathbf{C}}_{n+1}^{ad,(i)}\mathbf{B}d\Omega^e \tag{3-106}$$

$$\mathbf{H}_{n+1}^{e,(i)} = \int_{\Omega_e} \overline{\mathbf{G}}_v^T \left.\frac{\partial\boldsymbol{\sigma}}{\partial\overline{\overline{\mathbf{u}}}}\right|_{n+1}^{(i)} d\Omega^e = \int_{\Omega_e} \overline{\mathbf{G}}_v^T \overline{\mathbf{C}}_{n+1}^{ad,(i)}\overline{\mathbf{G}}_r d\Omega^e \tag{3-107}$$

$$\mathbf{K}_{\alpha,n+1}^{(i)} = \int_{\Gamma_x} \overline{\overline{\mathbf{G}}}_v^T \left.\frac{\partial\mathbf{t}}{\partial\overline{\overline{\mathbf{u}}}}\right|_{n+1}^{(i)} d\Gamma_x = l_{\Gamma_x}^e \overline{\overline{\mathbf{C}}}_{n+1}^{an,(i)} \tag{3-108}$$

where $l_{\Gamma_x}^e$ is the length of the crack for the consider element.

Equation (3-104) can be solved by an operator split, where $\Delta\overline{\overline{\mathbf{u}}}_{n+1}$ is solved at the element level and $\Delta\mathbf{d}_{n+1}$ is solved at the global level (see [25]). By that way, from equation (3-104)$_2$ we can compute:

$$\Delta\overline{\overline{\mathbf{u}}}_{n+1}^{(i)} = -\left(\mathbf{H}_{v,n+1}^{e,(i)} + \mathbf{K}_{\alpha,n+1}^{(i)}\right)^{-1}\mathbf{F}_{v,n+1}^{e,(i),T}\Delta\mathbf{d}_{n+1}^{(i)} \tag{3-109}$$

By using static condensation at the element level, the system (3-104) is reduced to:

$$\overset{N_{el}}{\underset{e=1}{A}}\left(\hat{\mathbf{K}}_{n+1}^{e,(i)}\Delta\mathbf{d}_{n+1}^{(i)}\right) = \overset{N_{el}}{\underset{e=1}{A}}\left(\mathbf{f}_{n+1}^{ext(i)}(t) - \mathbf{f}_{n+1}^{\text{int}(i)}(t)\right) \tag{3-110}$$

where

$$\hat{\mathbf{K}}_{n+1}^{e,(i)} = \mathbf{K}_{n+1}^{e,(i)} - \mathbf{F}_{r,n+1}^{e,(i)}\left(\mathbf{H}_{v,n+1}^{e,(i)} + \mathbf{K}_{\alpha,n+1}^{(i)}\right)^{-1}\mathbf{F}_{v,n+1}^{e,(i),T} \tag{3-111}$$

is the modified element tangent stiffness.

3.4.2 Thermal process

Once the "mechanical" process is solved, the mechanical dissipation and the evolution of the displacement "jump" are known. We can introduce these values to the equation (3-83) to solve the "remaining" evolution of temperature and also the "jump" in the heat flow through the crack

surface. Note that the evolution of temperature in this process is due to mechanical dissipation, internal heat supply and external heat source (and does not include the structural heating, which was computed before in the "mechanical" process). We obtain then the following form for equation (3-85)

$$\left(\frac{\gamma}{\beta\Delta t}\mathbf{M}^{e}_{\vartheta}+\mathbf{K}^{e}_{\vartheta}\right)\Delta\tilde{\mathbf{d}}^{\vartheta}_{n+1}=\tilde{\mathbf{R}}^{1}_{n,\vartheta} \tag{3-112}$$

where

$$\tilde{\mathbf{R}}^{1}_{n,\vartheta}=\tilde{\mathbf{Q}}^{1}_{\vartheta}-\mathbf{M}^{e}_{\vartheta}\dot{\mathbf{d}}^{\vartheta}_{a,n}-\mathbf{P}^{e}_{\vartheta}\dot{\lambda}_{n}-\mathbf{K}^{e}_{\vartheta}\mathbf{d}^{\vartheta}_{n}-\mathbf{F}^{e}_{\vartheta}\lambda_{n} \tag{3-113}$$

$$\tilde{\mathbf{Q}}^{1}_{\vartheta,3x1}=\int_{\Omega_e}\mathbf{N}^{\vartheta}_{a}(\mathbf{x})\tilde{R}^{n}_{add}d\Omega-\int_{\Gamma_{eq}}\mathbf{N}^{\vartheta}_{a}(\mathbf{x})\bar{q}_{n}d\Gamma \tag{3-114}$$

$$\lambda_{n}=-\frac{\overline{\overline{D}}^{n}_{mech}}{k_{\Gamma_x}} \tag{3-115}$$

$$\tilde{R}^{n}_{add}=\overline{D}^{n}_{mech}+r \tag{3-116}$$

Where $\overline{D}^{n}_{mech}$ and $\overline{\overline{D}}^{n}_{mech}$ denote the regular part and the singular part of the mechanical dissipation at time step 'n'.

3.5 Numerical Examples

In this section, several illustrative numerical examples are presented in order to show the capability of the proposed model. In these examples, the material properties of concrete are temperature dependent with the relations taken from Nielsen et al. (see [55]) and Eurocode 1992 (see [7]). In particular, the following equations are used:

For Young modulus:

$$E\left(\vartheta\right)=E_{20^0C}\left(1-\left(\frac{\vartheta-20}{10000}\right)\right)^2 \tag{3-117}$$

For hardening modulus:

$$K\left(\vartheta\right)=K_{20^0C}\left(1-\left(\frac{\vartheta-20}{10000}\right)\right)^2 \tag{3-118}$$

For facture stress:

$$\begin{cases}\bar{\sigma}_f\left(\vartheta\right)=\bar{\sigma}_{f,20^0C} & for \quad 20^0C\le\vartheta\le100^0C\\ \bar{\sigma}_f\left(\vartheta\right)=\left(1-\frac{\vartheta-100}{500}\right)\bar{\sigma}_{f,20^0C} & for \quad 100^0C\le\vartheta\le600^0C\end{cases} \tag{3-119}$$

The same relation is used for tensile stress:

$$\begin{cases}\bar{\bar{\sigma}}_f\left(\vartheta\right)=\bar{\bar{\sigma}}_{f,20^0C} & for \quad 20^0C\le\vartheta\le100^0C\\ \bar{\bar{\sigma}}_f\left(\vartheta\right)=\left(1-\frac{\vartheta-100}{500}\right)\bar{\bar{\sigma}}_{f,20^0C} & for \quad 100^0C\le\vartheta\le600^0C\end{cases} \tag{3-120}$$

For specific heat

$$\begin{cases}c_p\left(\vartheta\right)=0.9\times10^6 \quad \left(\frac{Nmm}{kgK}\right) & for \quad 20^0C\le\vartheta\le100^0C\\ c_p\left(\vartheta\right)=0.9\times10^6+\frac{\left(\vartheta-100\right)}{1000}\times10^6 \quad \left(\frac{Nmm}{kgK}\right) & for \quad 100^0C\le\vartheta\le200^0C\\ c_p\left(\vartheta\right)=1\times10^6+\frac{\vartheta-200}{2000}\times10^6 \quad \left(\frac{Nmm}{kgK}\right) & for \quad 200^0C\le\vartheta\le400^0C\\ c_p\left(\vartheta\right)=1.1\times10^6 \quad \left(\frac{Nmm}{kgK}\right) & for \quad 400^0C\le\vartheta\le1200^0C\end{cases} \tag{3-121}$$

For mass density

$$\begin{cases} \rho(\vartheta) = \rho_{20^0C} & for \quad 20^0C \le \vartheta \le 115^0C \\ \rho(\vartheta) = \rho_{20^0C}\left(1 - \dfrac{0.02(\vartheta - 115)}{85}\right) & for \quad 115^0C \le \vartheta \le 200^0C \\ \rho(\vartheta) = \rho_{20^0C}\left(0.98 - \dfrac{0.03(\vartheta - 200)}{200}\right) & for \quad 200^0C \le \vartheta \le 400^0C \\ \rho(\vartheta) = \rho_{20^0C}\left(0.95 - \dfrac{0.07(\vartheta - 400)}{800}\right) & for \quad 400^0C \le \vartheta \le 1200^0C \end{cases} \tag{3-122}$$

and for thermal conductivity (upper limit)

$$k = 2 - 0.2451\frac{\vartheta}{100} + 0.0107\left(\frac{\vartheta}{100}\right)^2 \quad for \quad 20^0C \le \vartheta \le 1200^0C \tag{3-123}$$

All computations are performed by a research version of the finite element analysis program FEAP (see [56], [57]).

3.5.1 Tension Test and Mesh independency

We consider here a concrete plate (300mm – 200mm) fixed in its left edge. Material properties at the reference temperature (20^0C) are given in Table 3-1.

Table 3-1. Material Properties

Material Properties	**Values**	**Units**
Young modulus (E_{20^0C})	38000	MPa (N/mm^2)
Fracture stress ($\bar{\sigma}_{f,20^0C}$)	2.00	MPa (N/mm^2)
Isotropic hardening modulus (K_{20^0C})	4000	MPa (N/mm^2)
Tensile stress $\bar{\bar{\sigma}}_{f,20^0C}$	3.00	MPa (N/mm^2)
Mass density (ρ_{20^0C})	2.5×10^{-6}	kg.mm^{-3}

3.5.1.1 Mesh independency

We start by studying the mesh independency of the proposed strategy. To that end, the problem is solved with two different meshes: a coarse mesh (15x5x2 elements) and a fine mesh (24x10x2 elements) in order to show the mesh independency of the method. The concrete plate is subjected to an increasing imposed displacement at the right edge, which increases from 0 mm to 0.2 mm in 100s and then decreases back to 0 mm also in 100 s. In order to drive the localization (the test performed is homogeneous), a material defect at the middle of the bottom edge (by reducing

from 3.0 MPa to 2.9 MPa the ultimate strength). Received results are showed in Figure 3-6, Figure 3-7, Figure 3-8 and Figure 3-9.

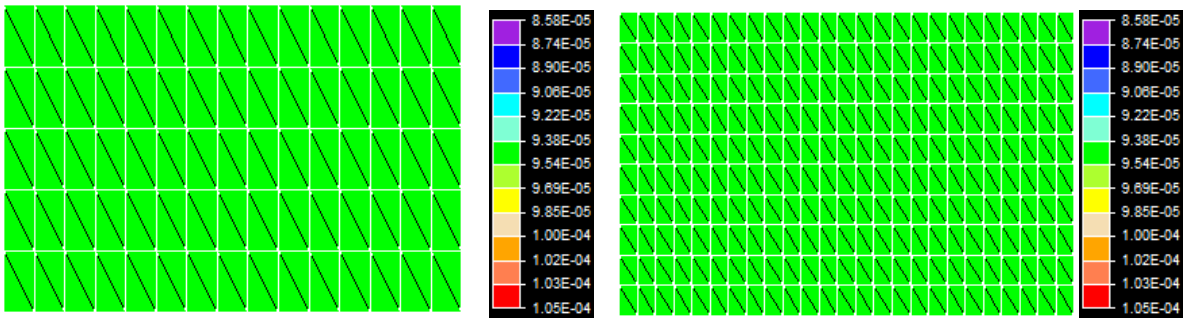

Coarse mesh Fine Mesh

Figure 3-6. *Temperature distribution in the plate at t = 20s*

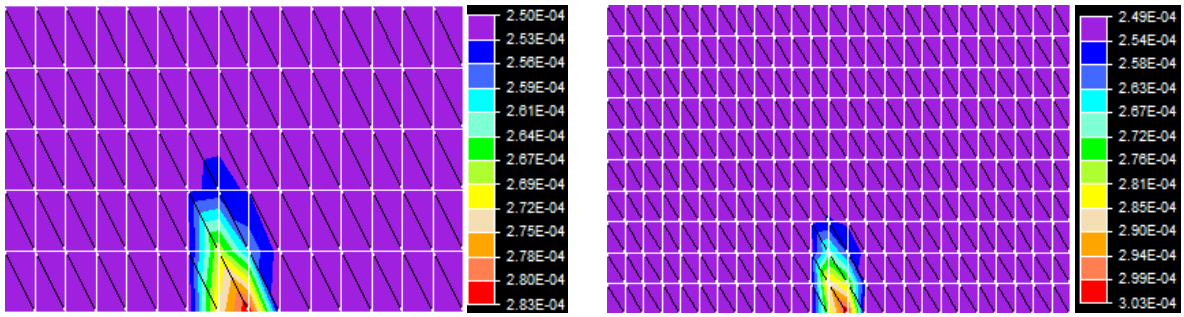

Coarse mesh Fine Mesh

Figure 3-7. *Temperature distribution in the plate at t = 52.4s*

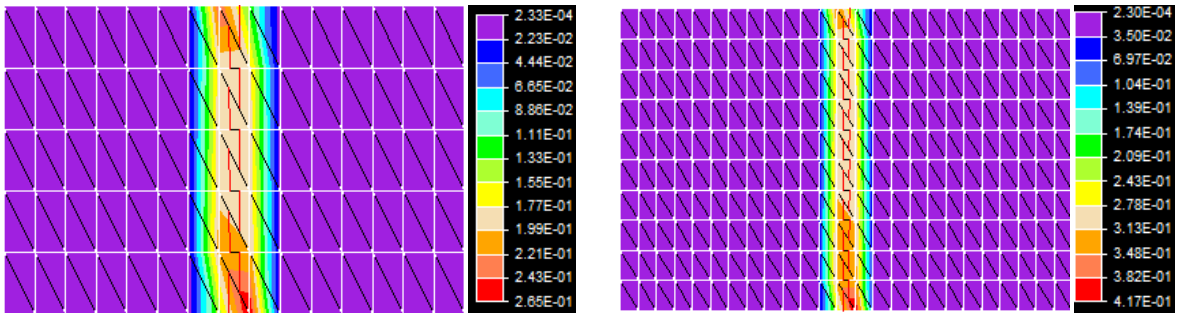

Coarse mesh Fine Mesh

Figure 3-8. *Temperature distribution in the plate at t = 100s*

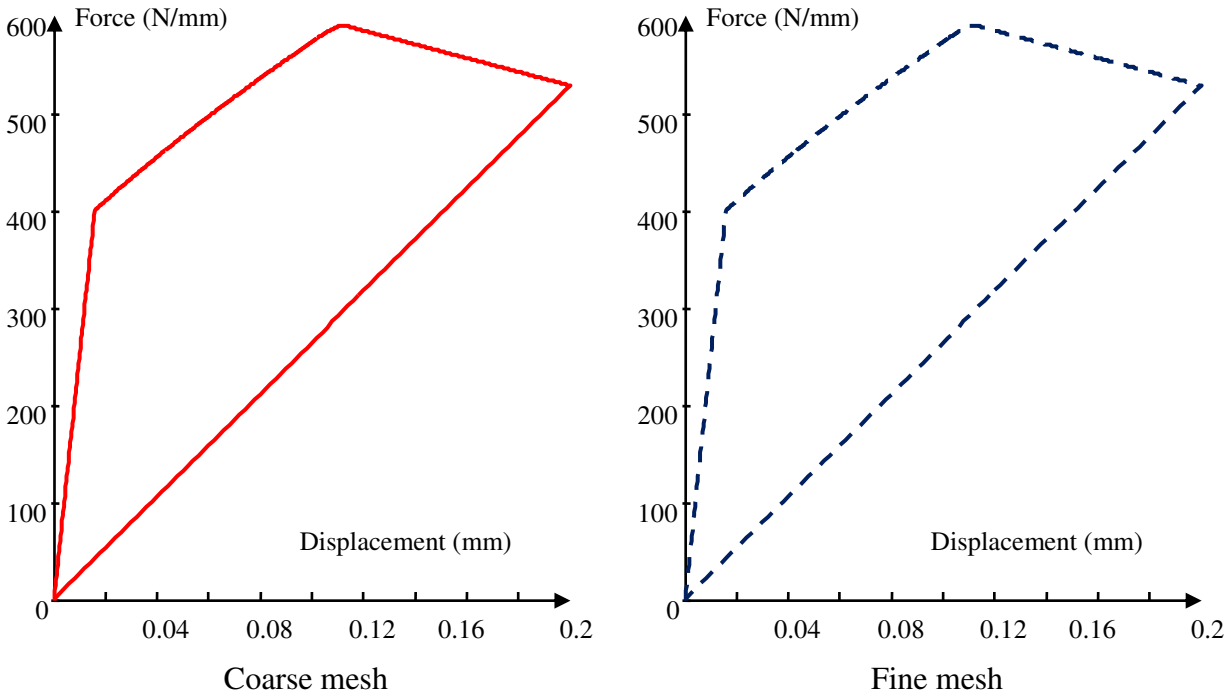

Figure 3-9. *Load/Displacement Curve for the coarse and the fine mesh*

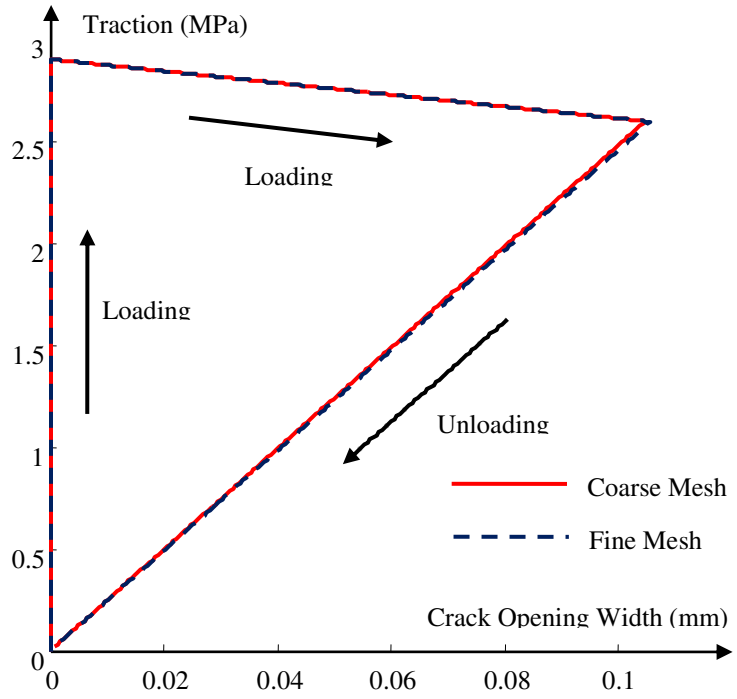

Figure 3-10. *Traction - Crack Opening relation at the localized failure*

Figure 3-6, Figure 3-7 and Figure 3-8 describe the evolution of temperature during the loading process at the plate, while the load/displacement curve of the plate is plotted in Figure 3-9 and the relationship between the traction and the crack opening in the localization failure at the

middle of the bottom edge is shown in Figure 3-10.

We can find out in Figure 3-6 that: for the loading state corresponding to t = 20s, the plate works in continuum damage threshold, the damage is uniformly distributed in all the material which leads to the uniform distribution of temperature; after that at t = 52.4s, the localization failure happens on the defect (at the middle of the bottom edge) and the localized mechanical dissipation becomes a heat source which helps raising the temperature at this position; the localization failure then propagates from the defect to the top edge of the plate and the temperature continues to rise and transfer from the localization zone to the neighbor zone (Figure 3-7). At the final loading state (t = 100s) (see Figure 3-8), the final crack line exists through the height of the plate with the direction perpendicular to the principal stress, the temperature raising due localization is largest at the defect ($\Delta\vartheta = 0.35^0 C$) and smaller at the middle of the plate ($\Delta\vartheta = 0.25^0 C$). These values are relative small but much larger than the temperature raising due to "continuum" mechanical dissipation, which is $\vartheta = 2.3\times10^{-4\ 0} C$ (see Figure 3-6 and Figure 3-7)

Figure 3-9 and Figure 3-9 show the perfect 'match' of the load/displacement curve and the between traction/crack opening curve taken for the two meshes. It is clear from these figures that the mechanical behavior of the concrete plate does not depend on the mesh. These results prove the mesh-independency of the method.

3.5.1.2 Concrete plate subjected to coupling thermo-mechanical loadings

In this test, we consider the behavior of the concrete under two others thermo-mechanical loading cases. For the first loading case, the plate is simultaneously subjected to an imposed displacement at the right edge (increasing with the velocity 0.002 mm/s) and an imposed temperature applied at the bottom edge (increasing with the velocity 5^0C/s). For the second loading case, the plate is firstly heated at its bottom until 500^0C and then submitted to an imposed displacement at the right edge (with the velocity = 0.002 mm/s). Figure 3-11 shows the load/displacement curves of these two thermo-mechanical loading cases in comparison to the mechanical loading case introduced in section 3.5.1.

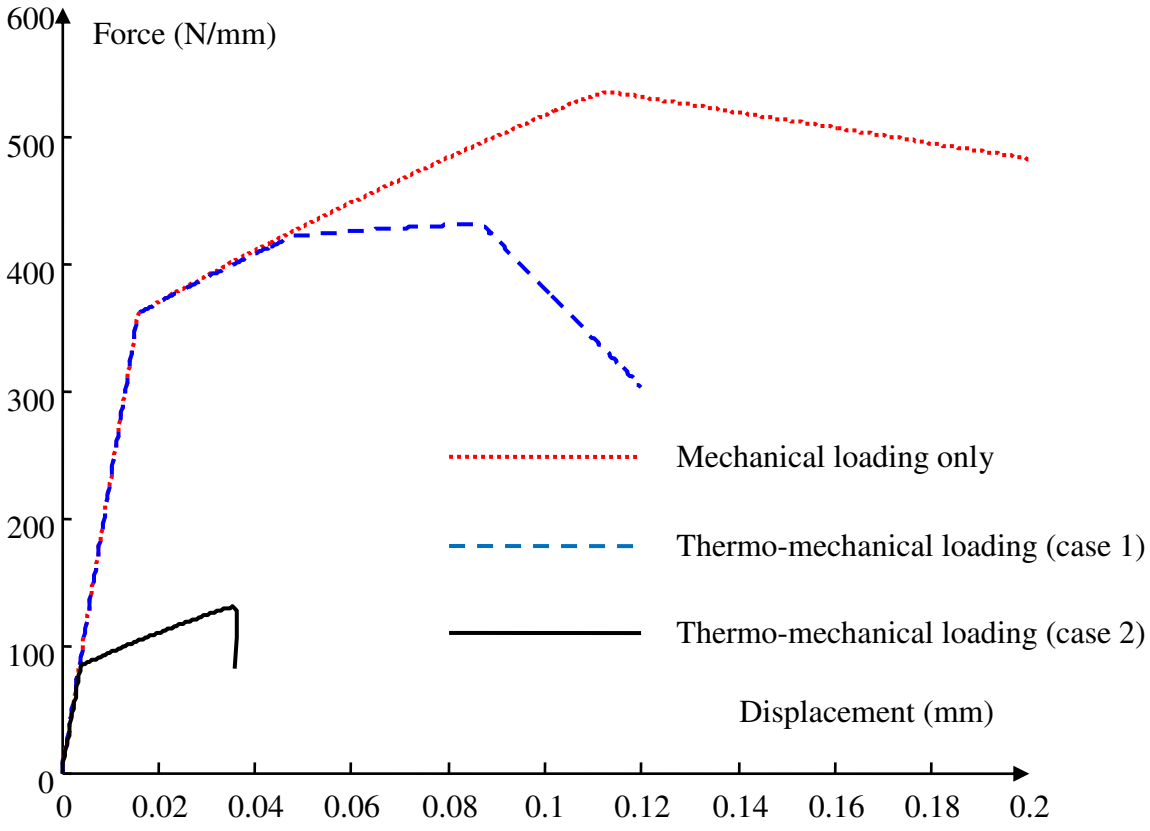

Figure 3-11. *Load/ Displacement Curve of the plate in thermo-mechanical loadings*

Figure 3-11 clearly illustrates the effect of temperature loading on the mechanical behavior of the concrete plate. The 'mechanical' bearing resistance of the concrete plate significantly reduces for the two thermo-mechanical loading cases in comparison to the mechanical loading case. In particular, the imposed displacement which leads to localized failure in the plate reduce from 0.115 mm in the mechanical loading case to 0.086 mm in the first thermo-mechanical loading case and then to 0.038 mm in the second thermo-mechanical loading case. This is the consequence of the reduction of material properties of concrete in high temperature as well as the effect of thermal stress in the plate.

3.5.2 Simple bending test

We consider a short beam (h =200mm, l=200mm) fixed at its left edge. The material properties are the same as for the first example (see Table 1). Two loading cases are considered for this example: (1) the beam is submitted to mechanical loading only, in which the right edge is submitted to vertical imposed displacement (increasing from 0mm to 0.16mm in 100s and then reduces to 0mm in also 100s); (2) the beam is submitted to mechanical loading as in the first loading case and also an imposed temperature at its fixed edge (which increasing from 0^0C to

500^0C in 100s and then decreasing to 0^0C in another 100s).

Figure 3-12 shows the temperature evolution for the first loading case, in which we can figure out the evolution of temperature due to continuum damage (at t =10s) and due to localization failure (at t =89.5s and t = 100s). We note that the temperature is mainly distributed in the fixed edge of the beam (where the stress is large). The value of temperature is very small when the beam is working in the continuum damage behavior but significantly increases when localized failure happens (from $\vartheta_{\max} = 1.75 \times 10^{-6^0} C$ at t = 10s to $\vartheta_{\max} = 0.157^0 C$ at t = 89.5s then to $\vartheta_{\max} = 0.22^0 C$ at t = 100s). It is also interesting to note that the temperature continue to rising in the beam in the unloading state (see Figure 3-12). The remaining temperature will further lead to the existing of the remaining stress in the beam after unloading (as showed in Figure 3-14).

The temperature evolution in the beam for the second loading case is presented in Figure 3-13. The temperature remaining in the beam in this case is different to the temperature remaining in the first loading case and is mainly due to the temperature propagation from the external heat source.

In both two cases, the initial cracks are detected in the bottom-left zone of the beam, where the maximum principle stress is greatest (see Figure 3-14 and Figure 3-15). The crack then propagates into the middle fiber of the beam in the vertical direction. This phenomena is really suitable to the expected behavior of the beam in bending.

The load-displacement curves for both loading cases are plotted in Figure 3-16. We can again identify the contribution of temperature loading in the mechanical response of the beam in the elastic state, the continuum damage state and also the localized failure state. In particular, this figure clearly shows that the bending resistance of concrete beam significantly reduces when submitted to thermal loading.

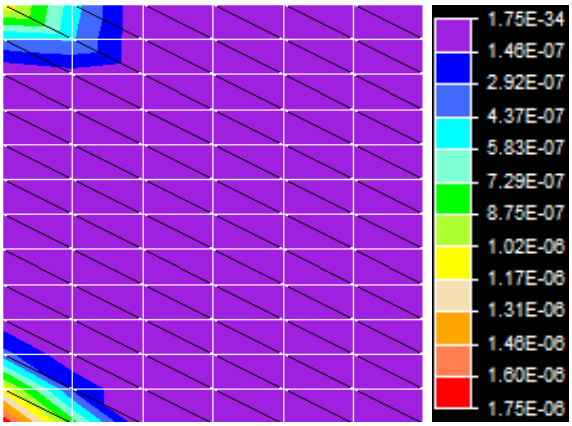

t= 10s (loading state)

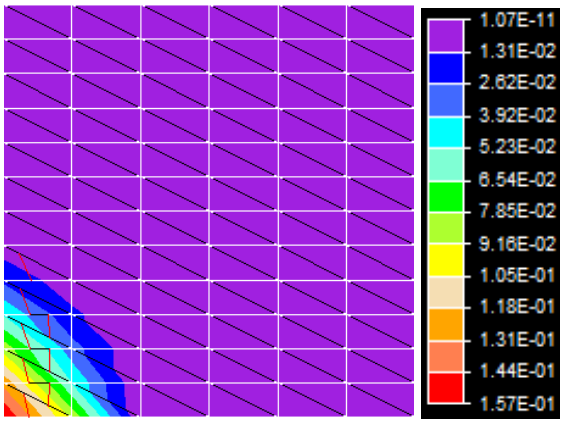

t =89.5s (loading state)

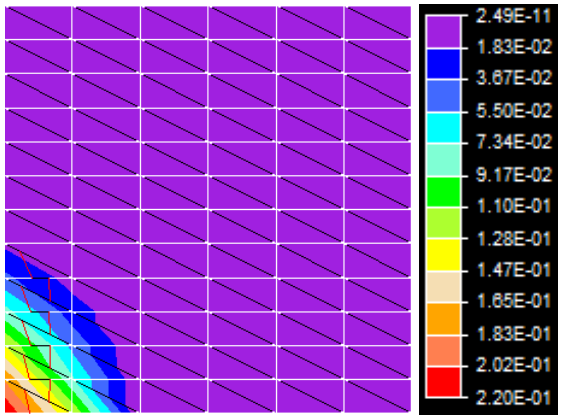

t =100s (final loading state)

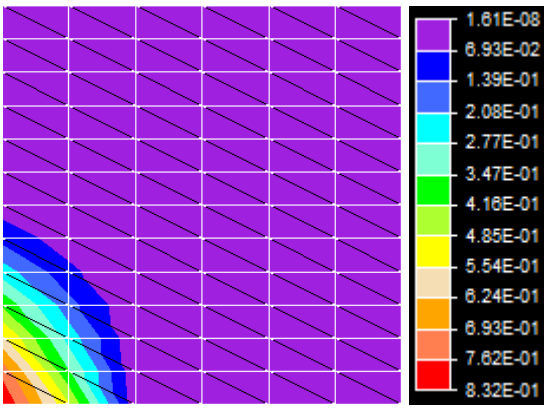

t = 200s (final unloading state)

Figure 3-12. *Temperature evolution in the plate for the first loading case (0C)*

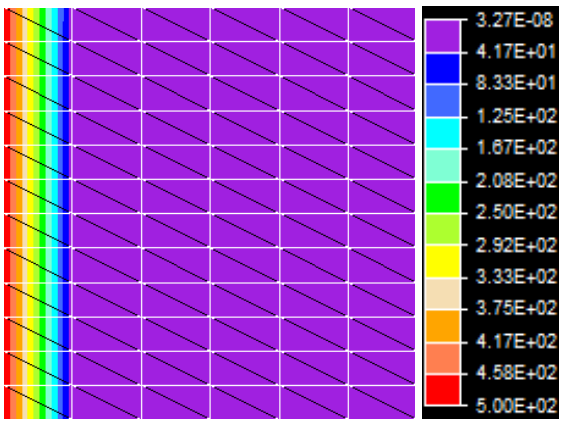

t = 100 s (final loading state)

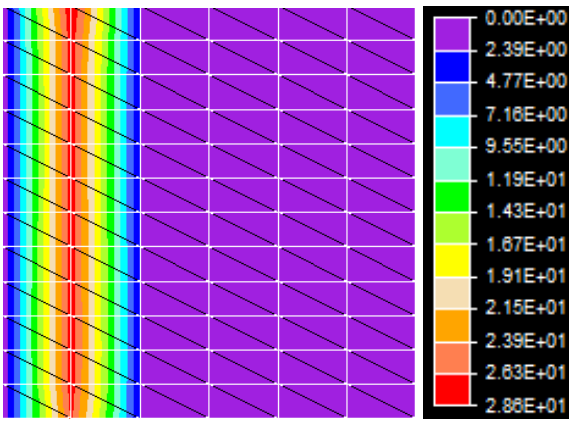

t = 200 s (final unloading state)

Figure 3-13. *Temperature evolution in the plate for the second loading case (^0C)*

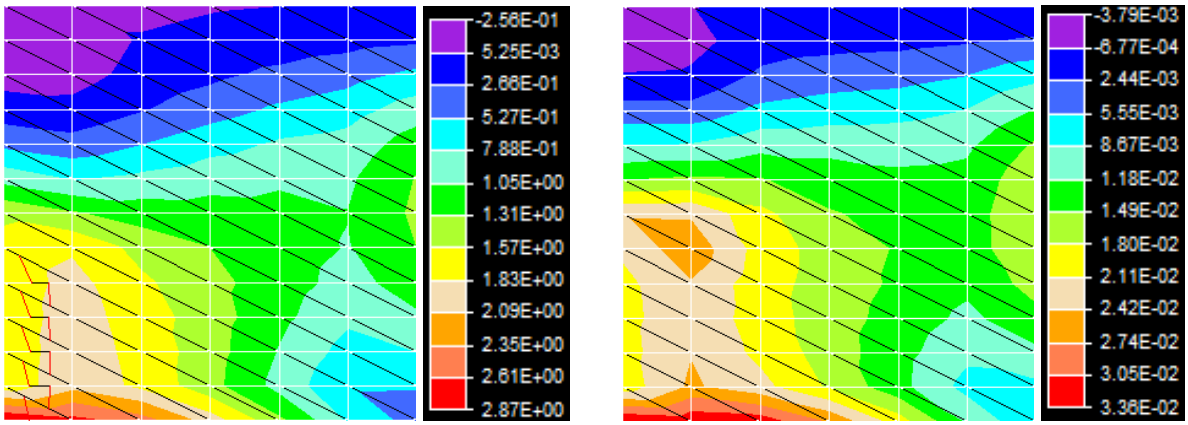

t = 10s (final loading state) t = 20s (final unloading state)

Figure 3-14. *Evolution of maximum principal stress for the first loading case (MPa)*

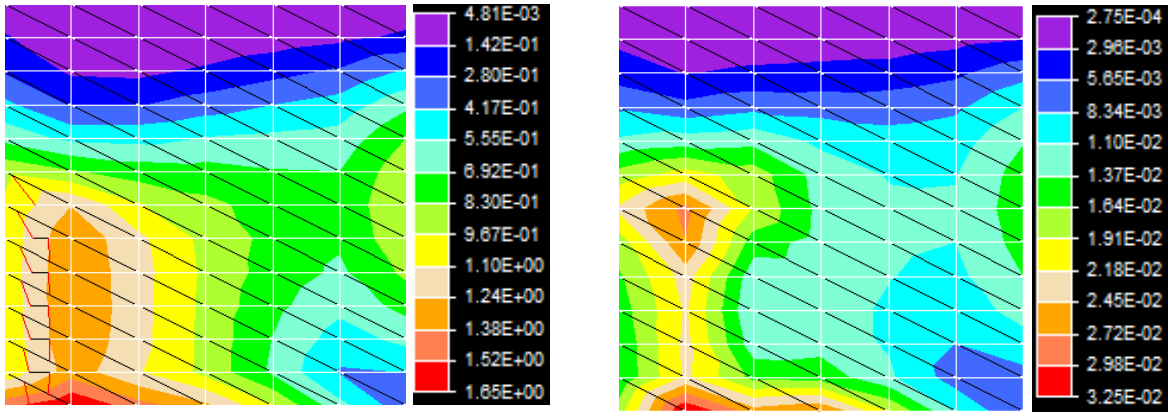

t = 10s (final loading state) t = 20s (final unloading state)

Figure 3-15. *Evolution of maximum principal stress for the second loading case (MPa)*

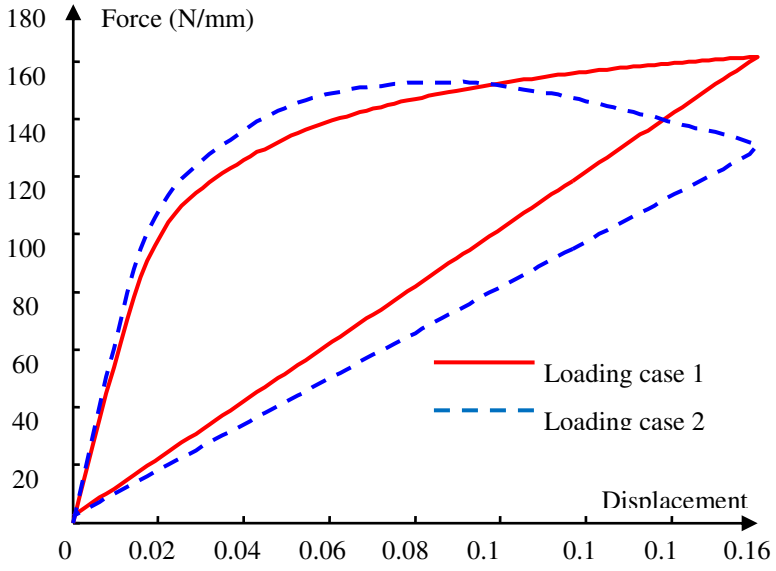

Figure 3-16. *Load/ Displacement curve for 2 loading cases*

3.5.3 Concrete beam subjected to thermo-mechanical loads

In this example, we study a concrete plate (500 x 250 mm) submitted to a jack load and fire loading. The material properties of the plate are given in Table 3-1 and the configuration of the test is described in Figure 3-17. In terms of mechanical loading, the plate is subjected to an imposed vertical displacement (increasing by -0.003 mm per second in 20s and then decreasing by -0.003 in also 20s) at the top edge. At the same time, the plate is also submitted to a fire loading, which leads to an imposed temperature at the middle zone of the bottom edge (increasing by 4^0C per second in 20s and then decreasing by 4^0C per second in also 20s).

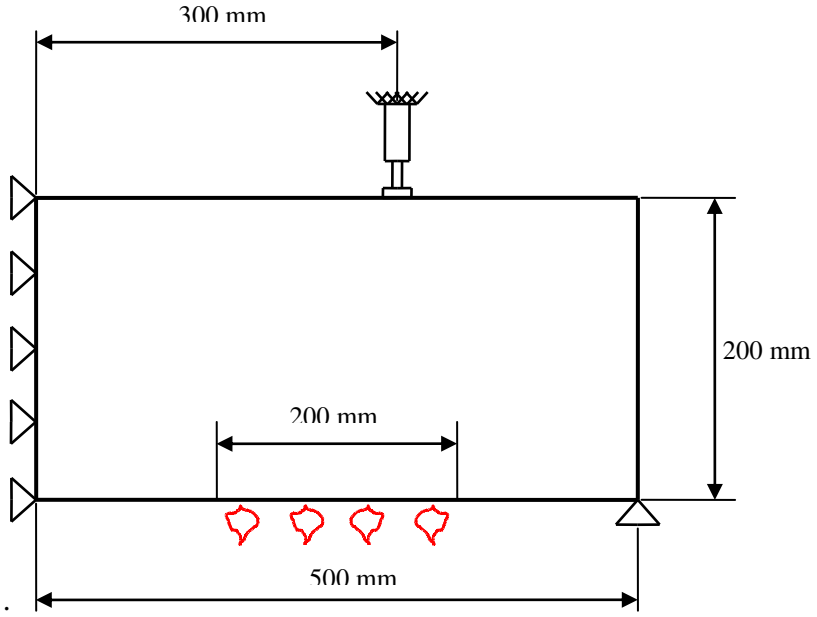

Figure 3-17. *Example configuration*

The evolution of maximum principal stress and temperature in the plate due to time are described in Figure 3-18. From Figure 3-18, we note that the initial crack appears in the top-left point of the plate where the maximum principal stress is largest (t =10s) and then propagates downward (see t =12s, t = 20s). The second crack is detected near the bottom edge of the plate (about 275 mm from the left edge) about 8 seconds later than the initial crack (t=18s). Due to time, the second crack becomes bigger and propagates upward to the middle of the plate (see Figure 3-19). The mechanical and thermal state of the plate at the final loading stage (t=20s) and after unloading (t=40s) are plotted in Figure 3-19 and Figure 3-20. We note that after unloading, the cracks are completely closed but the temperature and the 'thermal' stress is still exist in the plate.

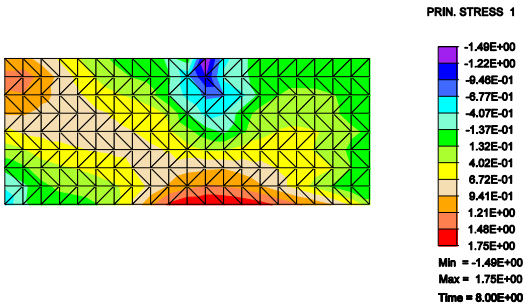

Maximum principal stress at t = 8 s

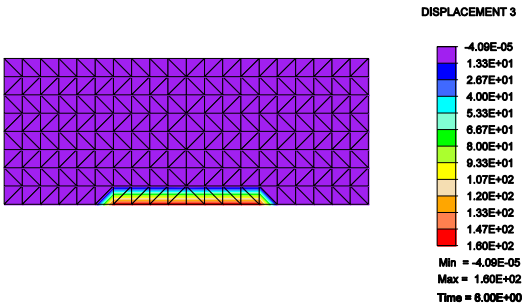

Temperature distribution at t = 8s

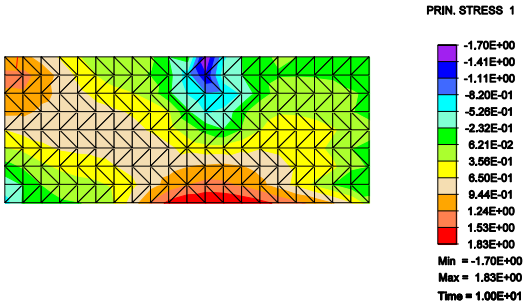

Maximum principal stress at t = 10 s

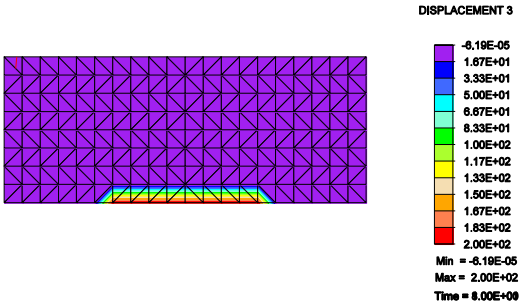

Temperature distribution at t = 10s

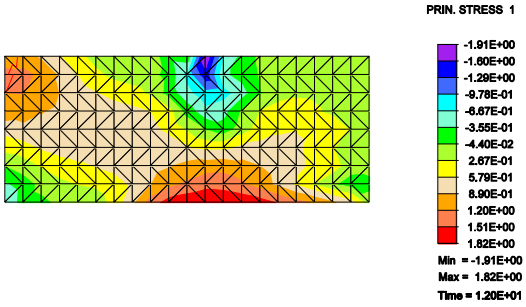

Maximum principal stress at t = 12 s

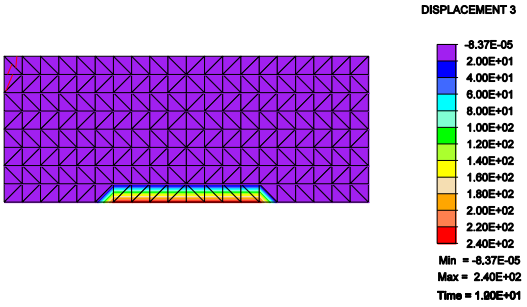

Temperature distribution at t = 12s

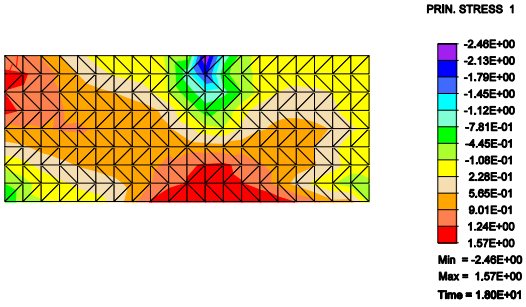

Maximum principal stress at t = 18 s

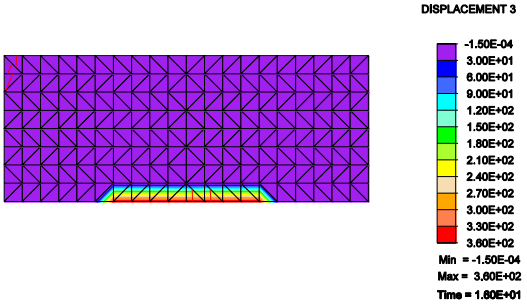

Temperature distribution at t = 18s

Figure 3-18. *Evolution of maximum principal stress and temperature due to time*

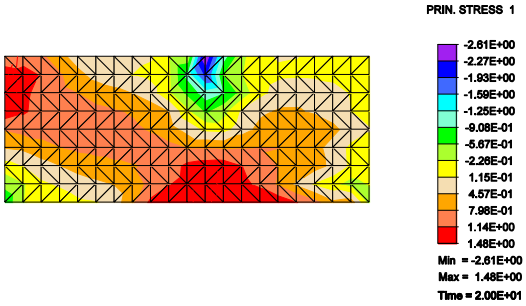

Maximum principal stress

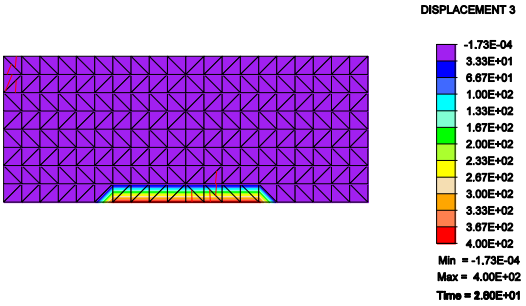

Temperature distribution

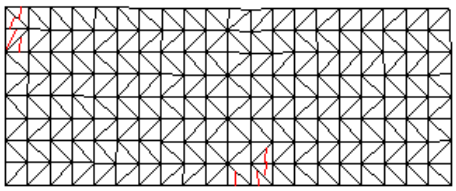

Deformed shape and crack pattern

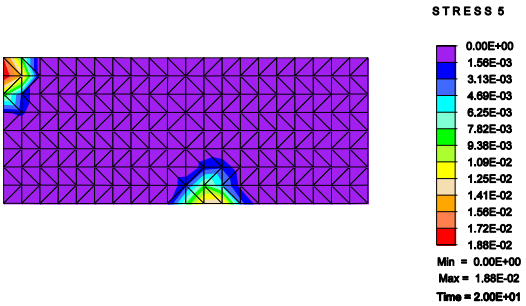

Crack Opening Width

Figure 3-19. *State of the plate at the final loading stage (t = 20s)*

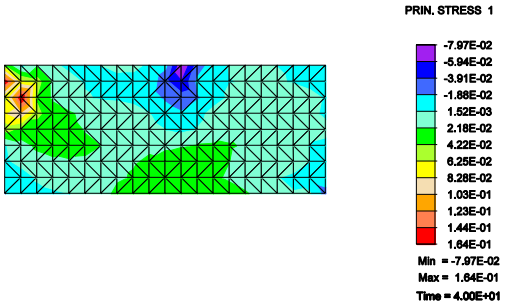

Maximum principal stress

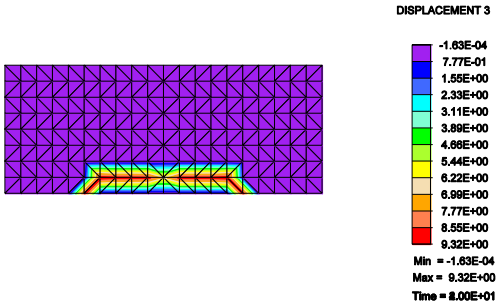

Temperature distribution

Figure 3-20. *Mechanical and Thermal state of the plate after unloading (t=40s)*

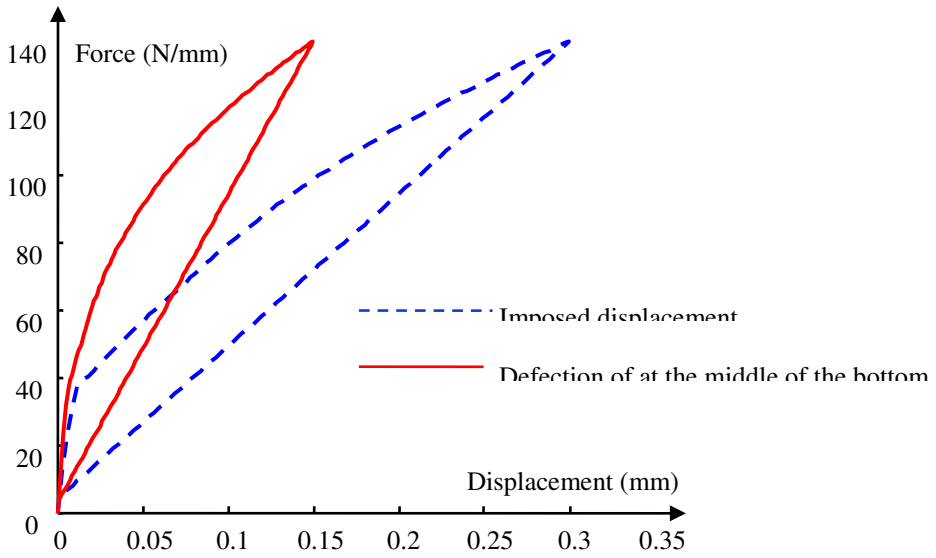

Figure 3-21. *Reaction/ Deflection curve*

Figure 3-21 shows the relation between the vertical reaction at the right support with the deflection of the plate at the middle of the bottom and with the imposed displacement. It is interesting to note that the curve does not return to the origin after unloading, it means that the vertical reaction of the support still exist after unloading. This vertical reaction corresponds to the remaining 'thermal' stress in the plate. This figure clearly shows the contribution of temperature loading into the mechanical behavior of the structure.

3.6 Conclusion

We have introduced in this chapter a new localized failure model with themo-damage coupling for concrete material. The main contribution consists in the ability of the model to describe the softening behavior of the material at localization failure zone, which is necessary to estimate the load limitation of the structure under the fully thermo-mechanical loading. Both theoretical formulation and solution procedure for the problem were carefully considered in order to make a successful development. The theoretical formulation proved that there is a "jump" in heat flux through the cracking surface when localized failure happens due to mechanical loading, which is represented by a "jump" in displacement field. These "discontinuity" values of displacement and heat flux were modeled in the framework of the embeded-discontinuity finite element method. The solution procedure for the problem exploits the adiabatic operator split. This implies that the problem is first solved for mechanical part (with adiabatic condition), and then for thermal part (or heat transfer problem). The theoretical development and the numerical solution were carried out for general two-dimensional problems. Three most general examples concerning the traction test and the bending test were performed and discussed to illustrate the capabilities of the proposed approach.

The received results illustrate the considerable effect of temperature loading on the mechanical response of concrete structure. In particular, one can infer that the mechanical resistance of the structure significantly reduces when it is subjected to thermal loading at the same time. On the constrary, the mechanical loading also leads to the thermal response of the structure. Whereas, the temperature of the concrete at damage and/or localized failure zone increases due to the appearance of mechanical dissipation and structural heating.

4 Thermomechanics failure of reinforced concrete frames

4.1 Introduction

In this chapter we present a new model for computing the nonlinear response of reinforced concrete frames subjected to coupled thermomechanical loads. The first major novelty of the model is its ability to account for both bending and shear failure of the reinforced concrete frames. The second novelty concerns the model capability to represent the total degradation of the material properties due to high temperature and the thermal deformations. These nouvelties will be introduced in this chapter by the following sequence. In section 4.2, we studied the degradation of mechanical resistance of the reinforced concrete cross-section under bending moment, shear force and axial loading due to temperature increase. These degradations was studied based on the 'layer' method in the framework of Modified Compression Theory proposed by Vecchio and Collins (see [41],[58],[59]) but was extended to include the temperature dependence of material properties and the stress-strain condition due to thermal loading. In this method, the cross-section is divided into layers, which are small enough to assume uniform stress and strain condition and constant temperature in all over the layer. By that way, the reduction of material properties due to temperature at each layer isconsidered and accumulated into the degradation of overall resistance of the cross-section. The thermal strain due to temperature gradient at each layer is also taken into account to estimate the total deformation of the cross-section and to compute the total stress at each layer. The latter contributes in total response of the section, especially for high temperature typical of fire loading. In section 4.3, we introduce the finite element method to provide an efficient computational frameworkusing the stress-resultant constitutive model of reinforced concrete beam element. The latteris then used for limit load computations of the reinforced concrete frame structures subjected to combined mechanical loading and fire. Several numerical examples will be introduced and discussed in section 4.4 to prove the capablity of the proposed method.

4.2 Stress-resultant model of a reinforced concrete beam element subjected to mechanical and thermal loads.

4.2.1 Stress and strain condition at a position in reinforced concrete beam element under mechanical and temperature loading.

Table 4-1. *List of symbols for thermomechanical model*

Symbol	Meaning
θ	Angle of principal direction (for both deformation and stress condition)
σ_x	Normal stress in x direction (longitudinal direction)
σ_y	Normal stress in y direction (tranverse direction)
τ	Shear stress
σ_1	1st (maximum) principal stress
σ_2	2nd (minimum) principal stress
ε_{xm}	Mechanical normal strain in x direction (longitudinal direction)
ε_{ym}	Mechanical normal strain in y direction (tranverse direction)
γ	Shear strain
ε_1	1st (maximum) principal strain
ε_2	2nd (minimum) principal strain
σ_{xt}	Thermal stress in x direction (longitudinal direction)
σ_{yth}	Thermal stress in y direction (tranverse direction)
ε_{xth}	Thermal strain in x direction (longitudinal direction)

Consider a reinforce concrete beam element subjected to mechanical loading and thermal loading (see Figure 4-1)

Figure 4-1. *Mechanical loading and fire acting on reinforced concrete element*

In this element, beside the mechanical deformation, a thermal strain is also acting. The total strain is then the sum of mechanical strain and thermal strain:

$$\varepsilon = \varepsilon_m + \varepsilon_{th} \tag{4-1}$$

Figure 4-2 represents the thermal stress and strain condition at a given point in the element.

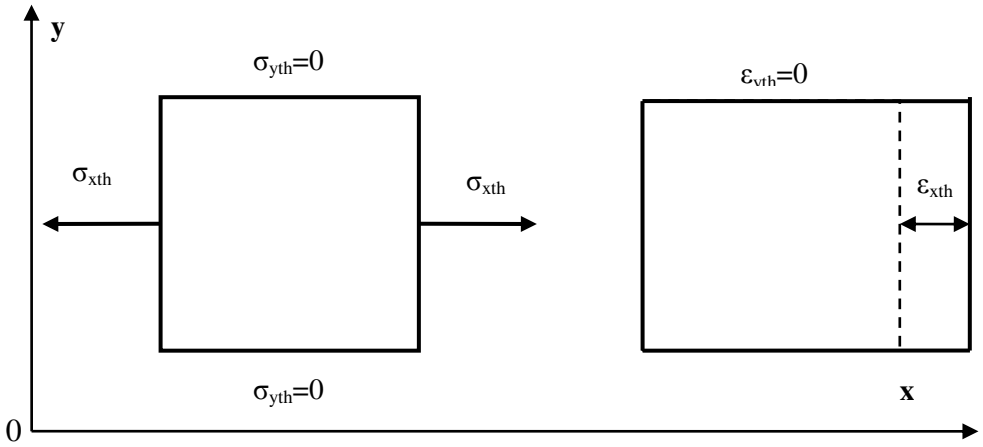

Figure 4-2. *Thermal stress and thermal strain condition*

The thermal strain of concrete depends on the temperature and the kind of aggregates [7], such that we have for calcareous aggregates

$$\varepsilon_{cth}(T) = \begin{cases} -1.2\times10^{-4} + 6\times10^{-6}T + 1.4\times10^{-11}T^3 & for \quad 20^0C \le T \le 805^0C \\ 12\times10^{-3} & for \quad T > 805^0C \end{cases} \tag{4-2}$$

for siliceous aggregates:

$$\varepsilon_{cth}(T) = \begin{cases} -1.8\times10^{-4} + 9\times10^{-6}T + 2.3\times10^{-11}T^3 & for \quad 20^0C \le T \le 700^0C \\ 14\times10^{-3} & for \quad 700^0C \le T \le 1200^0C \end{cases} \tag{4-3}$$

The thermal strain of steel also depends on the temperature [7]:

$$\varepsilon_{stm} = \begin{cases} -2.416\times10^{-4} + 1.2\times10^{-5}T + 0.4\times10^{-8}T^2 & for \quad 20^0C \le T \le 750^0C \\ 11\times10^{-3} & for \quad 750^0C < T \le 860^0C \\ -6.2\times10^{-3} + 2\times10^{-5}T & for \quad 860^0C < T \le 1200^0C \end{cases} \tag{4-4}$$

Noted that we have assumed that the normal part of the thermal strain and thermal stress in the transverse direction of the element is equal to zero (ε_{yth}=0 and σ_{yth}=0, see Figure 4-2). A similar assumption also applies to mechanical stress and strain; in particular, the normal part of mechanical stress and mechanical strain are also ignored ($\varepsilon_y = 0, \sigma_y = 0$). This assumption is sometimes declared by 'no interactive compression between longitudinal layers of the element' or 'the depth of the cross-section is constant after loading', which is a well-known and widely accepted hypothesis in beam analysis. Due to this assumption, only the longitudinal strain (ε_x) and the shear strain (γ) are considered as non-zero strain components of the beam element (see Figure 4-3).

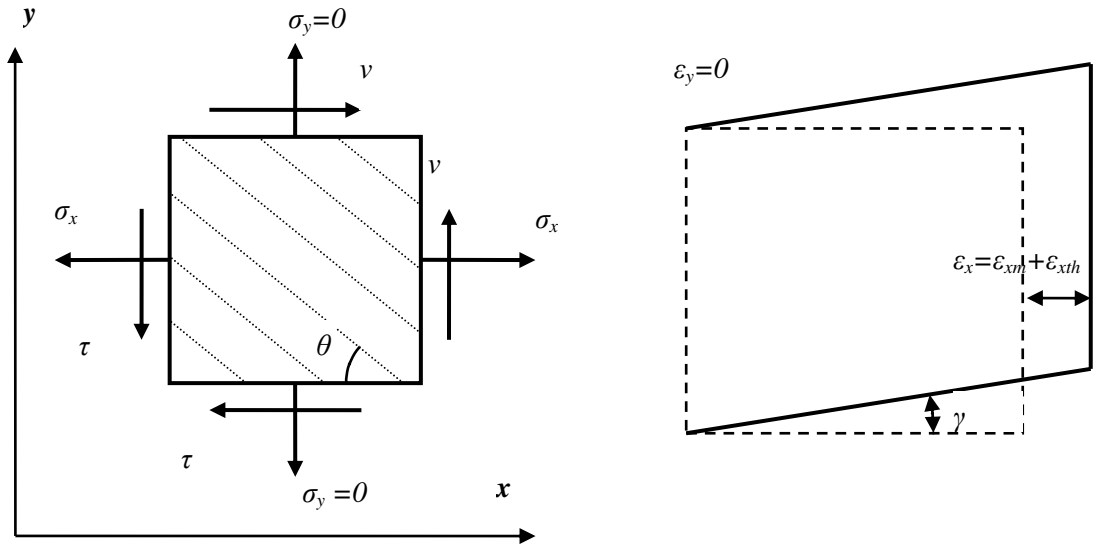

Figure 4-3. *Total stress and strain condition at a position in beam element (ε_y=0 and σ_y=0)*

The total stress and strain condition at a point in reinforced concrete beam element can be represented by a Mohr circle (see Figure 4-4).

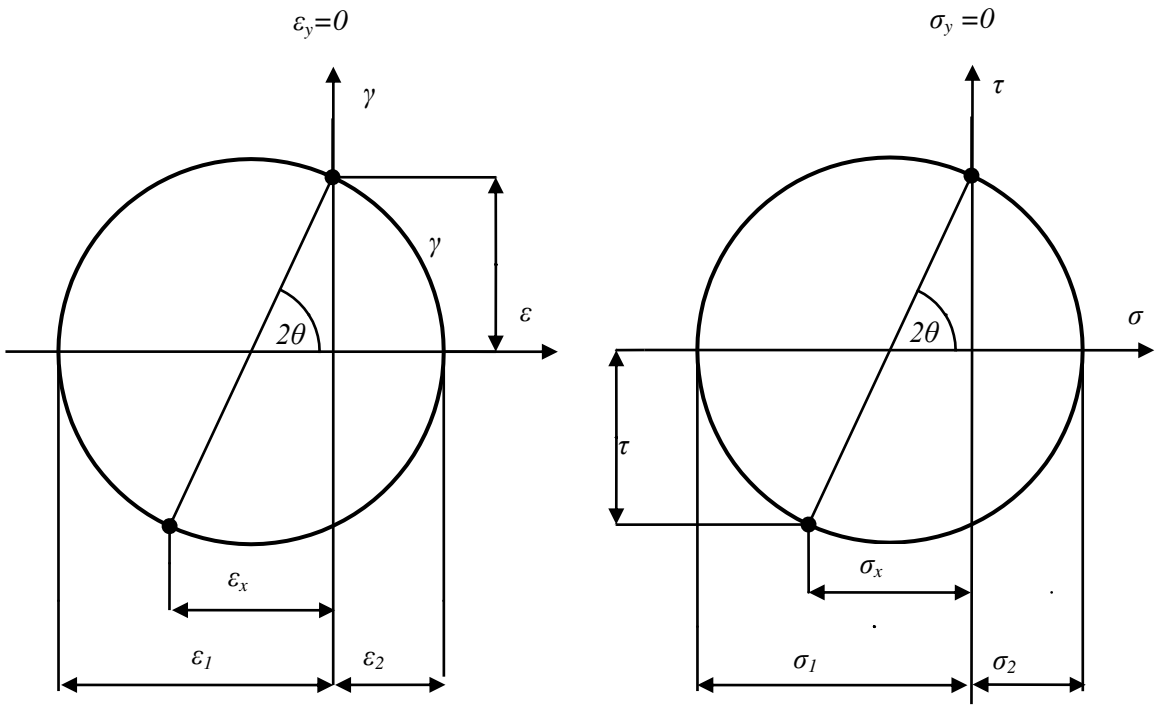

Figure 4-4. *Mohr circle representation for strain and stress condition at a point in beam element*

The angle giving the orientation of the principal directions can then be defined according to:

$$\tan 2\theta = -\frac{2\gamma}{\varepsilon_x} \rightarrow \theta \tag{4-5}$$

The maximum value of principal strain is:

$$\varepsilon_1 = \sqrt{\left(\frac{\varepsilon_x}{2}\right)^2 + (\gamma)^2} + \frac{\varepsilon_x}{2} \tag{4-6}$$

The mimimum value of principal strain is:

$$\varepsilon_2 = -\sqrt{\left(\frac{\varepsilon_x}{2}\right)^2 + (\gamma)^2} + \frac{\varepsilon_x}{2} \tag{4-7}$$

We note that in this case, the maximum strain is always positive and the minimum strain is always negative.

Once the strain components are known, we can compute the corresponding stress components by using the constitutive equation between principal stress and principal strain (assuming that the

principal directionsfor strain and stress are the same). The constitutive equation between principal stress and principal strain of concrete and rebaris dependent on the temperature; it canbe approximated by a number of mathematical equations (see [59],[7] ,[9],[11],[60], [61], [55]). In the following, some typical relationships are introduced:

Concrete

The mechanical stress-strain constitutive equation for concrete in compression can be computed by the following equation (see [10]) (see Figure 4-5):

$$\sigma_{c2}=\begin{cases} f_c^{'}(T)\left[1-\left(\dfrac{\varepsilon_{c2}-\varepsilon_{\max}(T)}{\varepsilon_{\max}(T)}\right)^2\right] & for \quad \varepsilon_c \le \varepsilon_{\max}(T) \\ f_c^{'}(T)\left[1-\left(\dfrac{\varepsilon_{\max}(T)-\varepsilon_c}{3\varepsilon_{\max}(T)}\right)^2\right] & for \quad \varepsilon_c > \varepsilon_{mex}(T) \end{cases} \tag{4-8}$$

where $\varepsilon_{\max}(T)=0.025+\left(6T+0.04T^2\right)\times 10^{-6}$

The compressive strength of concrete is dependent on temperature [7]:

$$f_c^{'}(T)=\begin{cases} f_c^{'} & for \quad T \le 100^0 C \\ f_c^{'}\left[1.067-0.00067T\right] & for \quad 100^0 C < T \le 400^0 C \\ f_c^{'}\left[1.44-0.0016T\right] & for \quad 400^0 C < T \le 900^0 C \\ 0 & for \quad 900^0 C < T \end{cases} \tag{4-9}$$

where $f_c^{'}$ is the compressive strength of concrete at room temperature (20^0C)

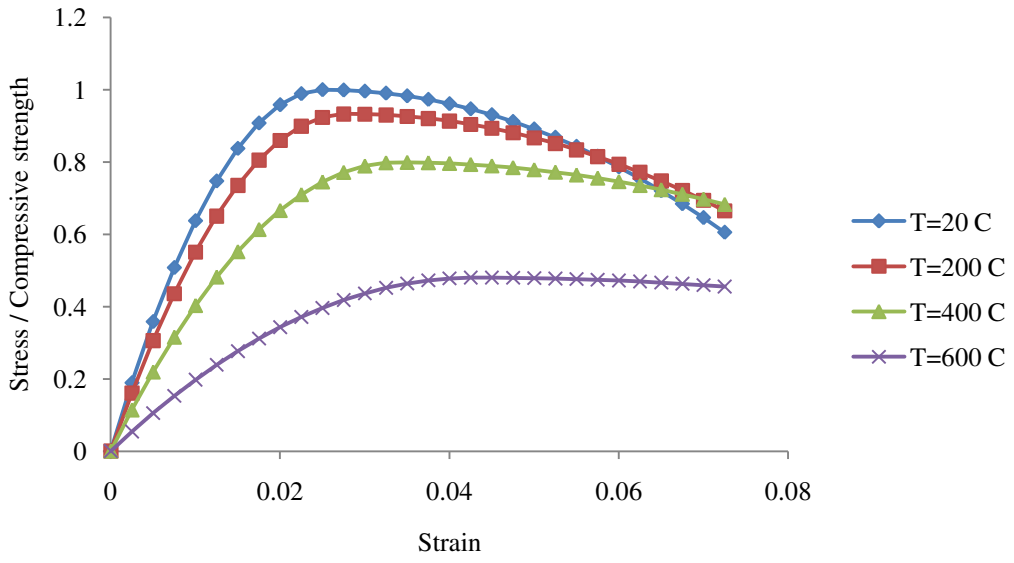

Figure 4-5. *Relation between compressive stress and strain of concrete due to tempeture***[10]**

The negative principal stress of concrete can also be computed from the negative principal strain by the equations of Vecchio and Collins (see [61]), which are widely used in American building codes (see[9], [12]). In which, the minimum principal stress is computed by the equation:

$$\sigma_{c2} = \sigma_{c2_{\max}} \left(2\frac{\varepsilon_{c2}}{\varepsilon_c^{'}} - \left(\frac{\varepsilon_{c2}}{\varepsilon_c^{'}} \right)^2 \right) \tag{4-10}$$

where

$$\sigma_{c2_{\max}} = \left(\frac{1}{0.8 - 0.34\frac{\varepsilon_{c1}}{\varepsilon_c^{'}}} \right) f_c^{'} \le f_c^{'} \tag{4-11}$$

The principal stress-strain relation of concrete in tension can be computed by following the suggestion of Vecchio and Collins (see [61]):

$$\sigma_{c1} = \begin{cases} E_c(T)\varepsilon_{c1} & if \quad \varepsilon_c \le \dfrac{f_{cr}(T)}{E_c(T)} \\ \dfrac{f_{cr}(T)}{1+\sqrt{200\varepsilon_{c1}}} & if \quad \varepsilon_c > \dfrac{f_{cr}(T)}{E_c(T)} \end{cases} \tag{4-12}$$

The Young modulus of concrete ($E_c(T)$) also depends on the temperature (see[55]):

$$E_c^{'}(T) = E_c\left(1-\left(\frac{T-20}{10000}\right)\right)^2 \tag{4-13}$$

where E_c is the Young modulus of concrete at room temperature.

The crack limit of concrete in tension $f_{cr}(T)$ also depends on the temperature [7]:

$$f_{cr}(T) = \begin{cases} f_{cr} & if \quad T \le 50^0 C \\ f_{cr}\left(1-0.001356(T-20)\right) & if \quad 50 < T \le 640^0 C \\ 0.2 f_{cr} & if \quad 640 < T \le 800^0 C \\ 0 & if \quad T > 800^0 C \end{cases} \tag{4-14}$$

where f_{cr} is the crack limit of concrete at room temperature and, if there is no experiment value, can be compute from the compressive strength of concrete (see [9]): $f_{cr} = 0.62\sqrt{f_c^{'}}$

Steel rebar

For reinforcement bar, a bi-linear mathematical model is usually used for both compression and tension condition (see Figure 4-6):

$$f_s(T) = \begin{cases} E_s(T)\varepsilon_s & for \quad \varepsilon_s \le 0.02 \\ f_y(T) & for \quad 0.02 < \varepsilon_s \end{cases} \tag{4-15}$$

The yield stress $f_y(T)$ of rebar is a function of the temperature [7]:

$$f_y(T)=\begin{cases} f_y & if \quad 0^0C \le T \le 350^0C \\ f_y\left[1.8848-2.528\times10^{-3}T\right] & if \quad 350^0C < T \le 706^0C \\ f_y\left[0.242992764-2.02494\times10^{-4}T\right] & if \quad 706^0C < T \le 1200^0C \end{cases} \tag{4-16}$$

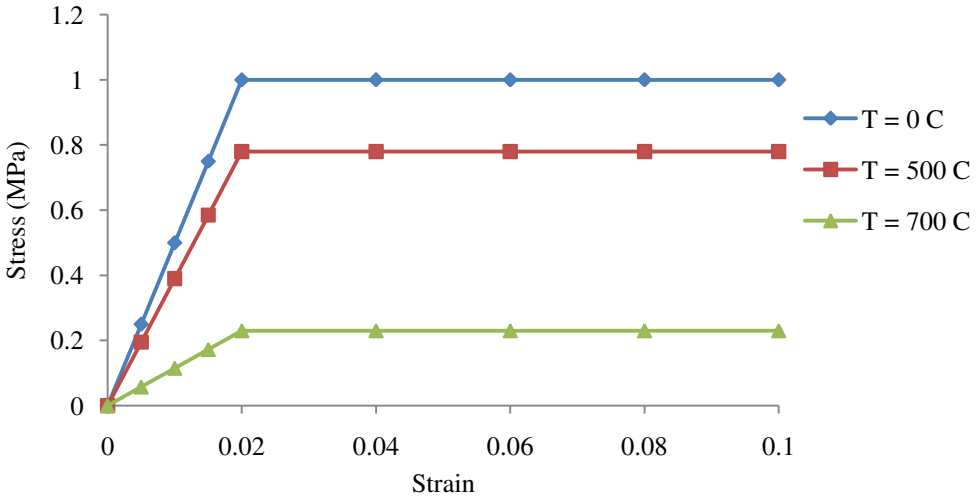

Figure 4-6. *Stress- strain relationship of rebar in different temperature*

By using the constitutive equation for concrete and steel rebar described above, we can obtain the principal stresses due to the principal strain, at a given considered position. Assuming that the angle of the principal stress axis is the same as to the angle of the principal strain, we can estimate the longitudinal normal stress (σ_x) and the shear stress (v) by using the Mohr circle for stress condition (see Figure 4-4):

The shear stress:

$$\tau=\sqrt{(\sigma_1-\sigma_2)^2}\sin(2\theta) \tag{4-17}$$

The longitudinal stress:

$$\sigma_x=-\tau\tan(2\theta) \tag{4-18}$$

4.2.2 Response of a reinforced concrete element under external loading and fire loading.

The mechanical response at the cross-section level is defined with respect to the generalized deformations (in th e given section) represented by the curvature κ, the longitudinal strain ε_x at the middle of the section and the sectional shear deformation γ. We can further apply the 'layer' method (see[41], [15], [13]), where the cross-section is divided into a number of layers across the

beam depth. Each layer is assumed to be thin enough to allow for uniform distributions of stress, strain and temperature (see Figure 4-7).

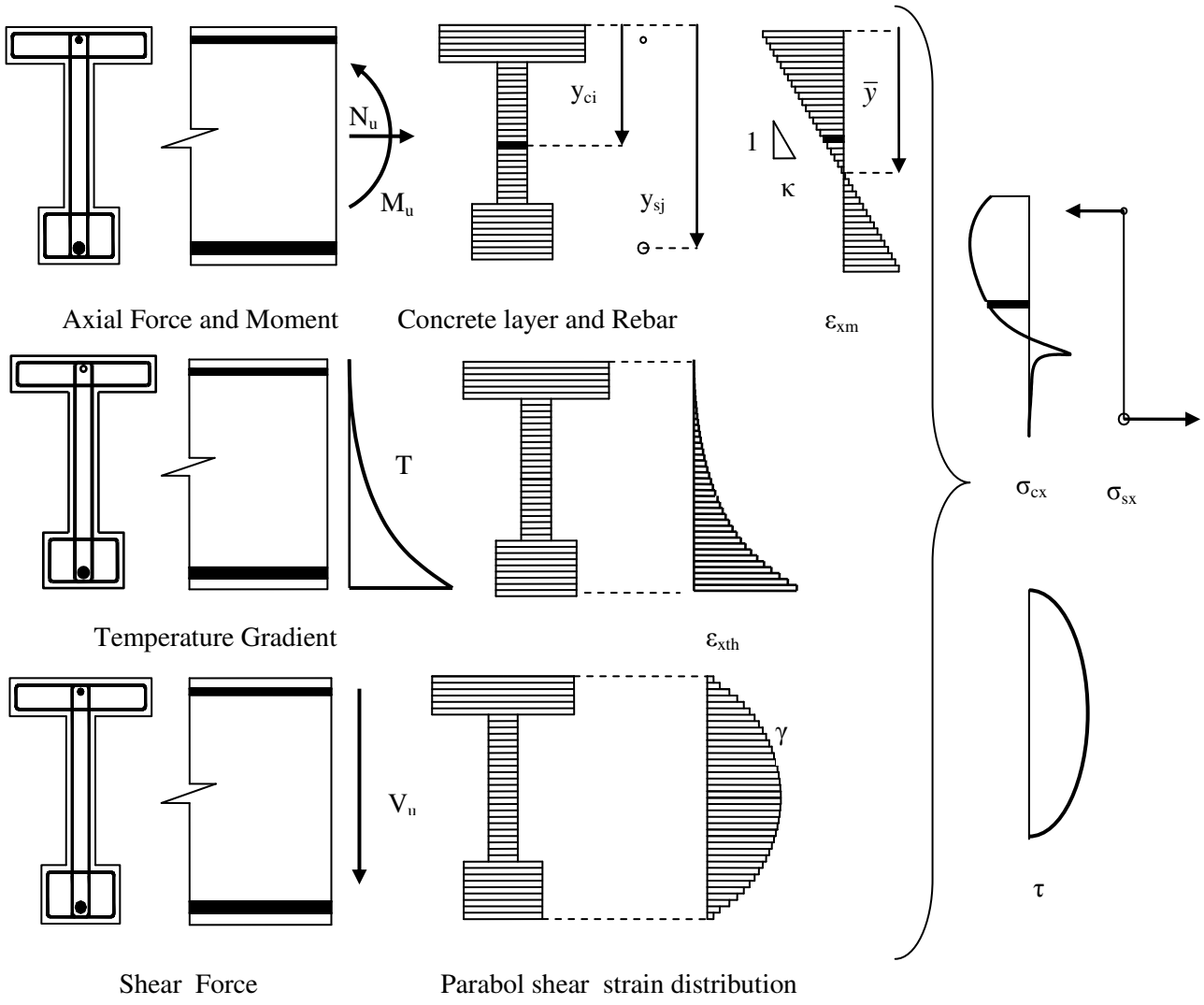

Figure 4-7. *Response of reinforced concrete element under mechanical and thermal loads*

We denote the layer width and height as b_{ci} and h_{ci}, the longitudinal stress as σ_{cxi} and the distance from the middle of the layer to the top of the cross-section of concrete layer 'i^{th}' as y_{ci}; furthermore, we denote the steel bar area a_{sxj}, the longitudinal stress σ_{sxj} and the distance from the middle of the rebar element to the top of the cross section of the rebar element 'j^{th}' as y_{sj}, we can establish the following set of equilibrium equations:

$$\begin{cases} \sum_{i=1}^{N_c} \sigma_{cxi} b_{ci} h_{ci} + \sum_{j=1}^{Ns} \sigma_{sxj} a_{sxj} = N \\ \sum_{i=1}^{N_c} \sigma_{cxi} b_{ci} h_{ci} \left(y_{ci} - \bar{y} \right) + \sum_{j=1}^{N_s} \sigma_{sxj} a_{sxj} \left(y_{sj} - \bar{y} \right) = M \\ \sum_{i=1}^{N_c} \tau_i b_i h_i = V \end{cases} \tag{4-19}$$

where $\bar{y}$ is the distance from the neutral axis (where $\varepsilon_x = 0$) to the top of the cross-section.

This system allows us to compute the response of the cross-section, and in particular curvature, longitudinal strain and shear deformation, at a given force and temperature loads; the following procedure is used (see Figure 4-8):

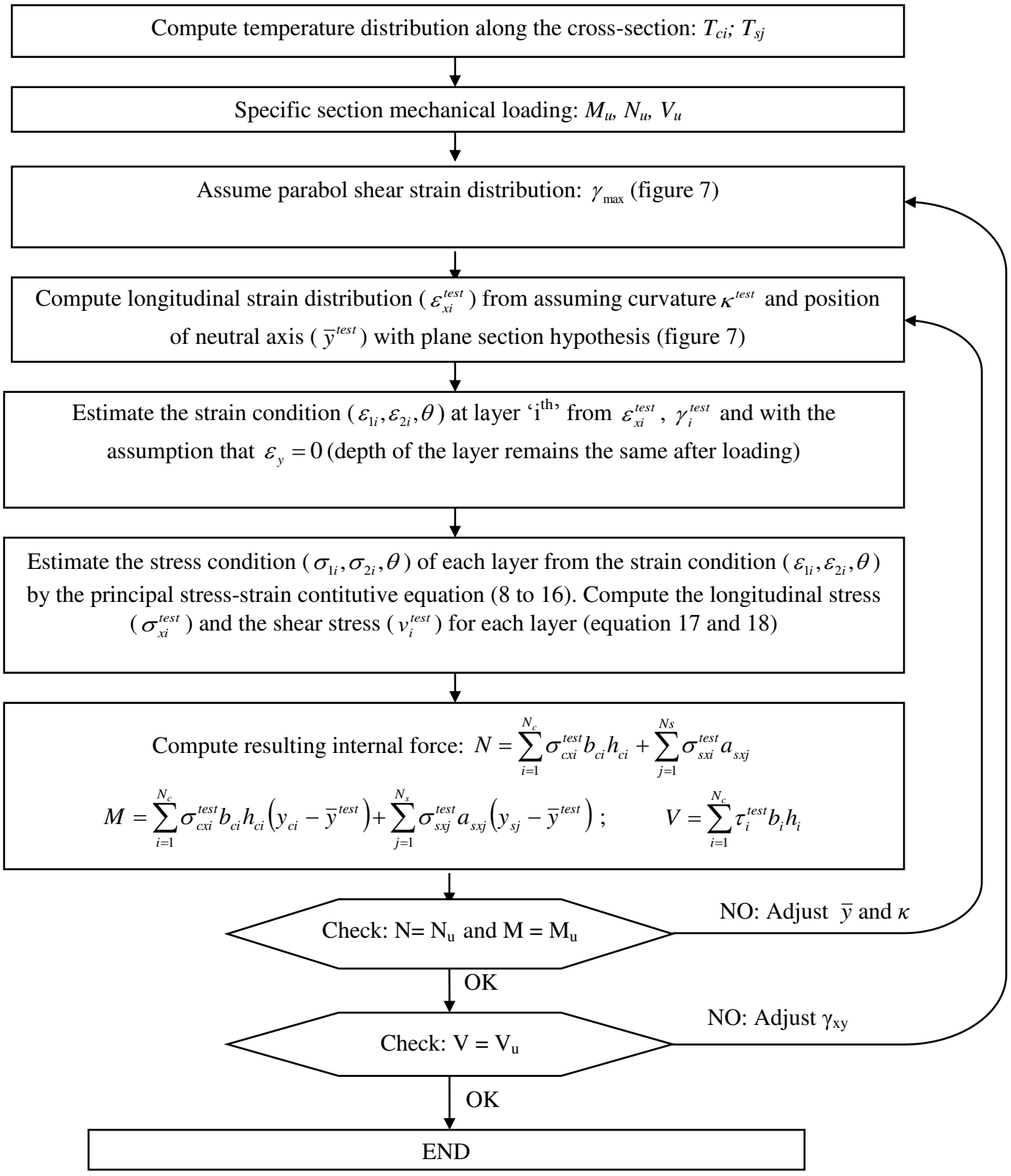

Figure 4-8. *Procedure to determine the mechanical response of RC beam element*

4.2.3 Effect of temperature loading, axial force and shear load on mechanical moment-curvature response of reinforced concrete beam element.

By applying the procedure illustrated inFigure 4-8, we can establish the moment-curvature relation for a reinforced concrete beam element, by fixing the temperature loading, the shear loading, the axial force and tracking the increase of the internal moment (M) proportional to the increase of the curvature (κ).

Figure 4-11shows the degradation of the moment-curvature response of a rectangular reinforced concrete beam exposed to ASTM 119 fire acting on the bottom (see Figure 4-9) in case external axial force and shear force equals to zero (pure bending test) (N_u = 0, V_u =0). The temperature profile of the RC beam subjected to fire loading increases due to time (Figure 4-10-[11]).When temperature increases, the strength of materials (concrete and rebar) decreases and leads to the degradation of moment-curvature resistance of the element.

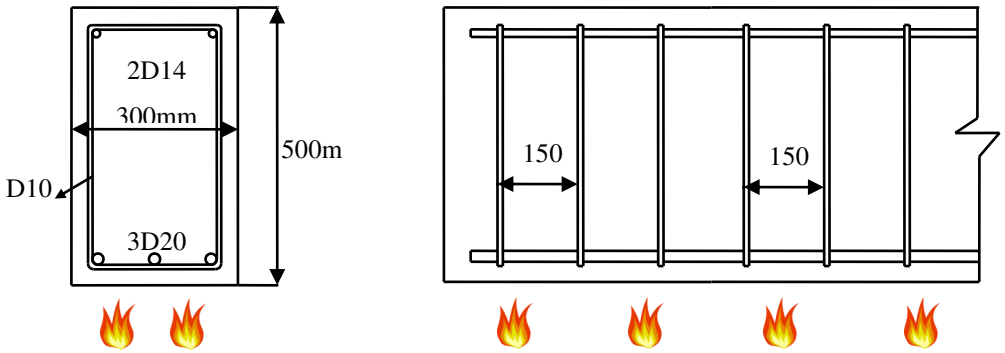

Figure 4-9. *Cross-section and Dimensioning of the consider reinforced concrete element*

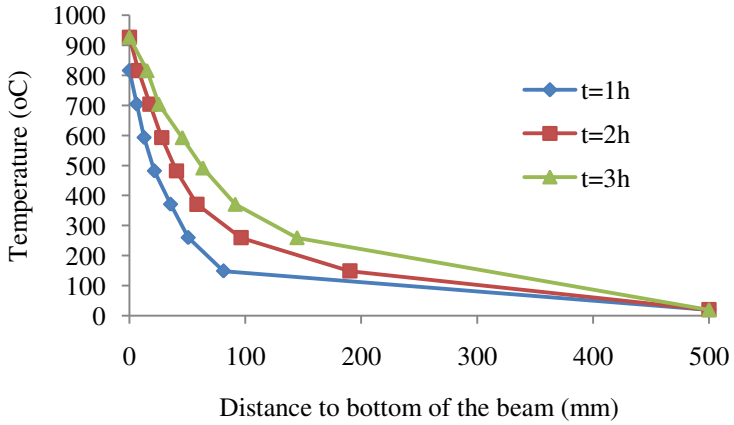

Figure 4-10. *Evolution of temperature profile due to time***[11]**

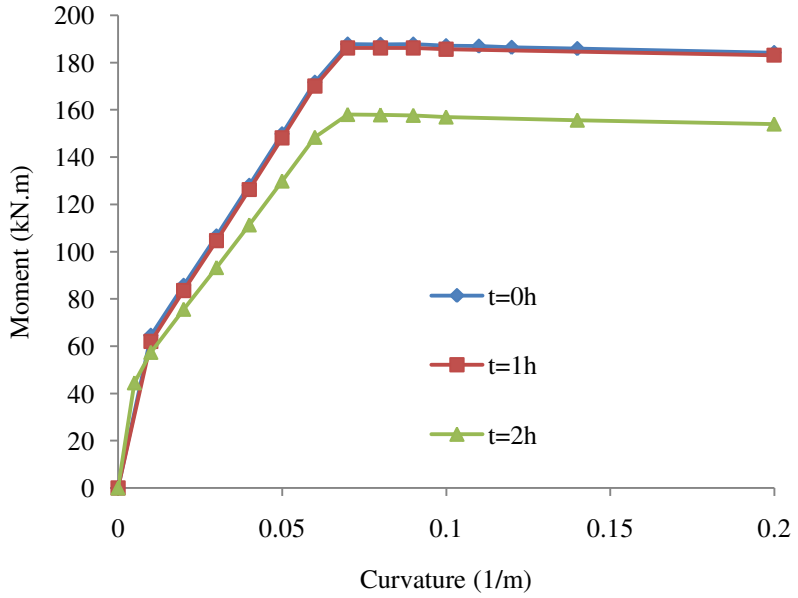

Figure 4-11. *Dependence of moment-curvature with time exposure to fire ASTM119*

Figure 4-12 illustrates the evolution of bending resistance of the frame with an increase of the axial compression.

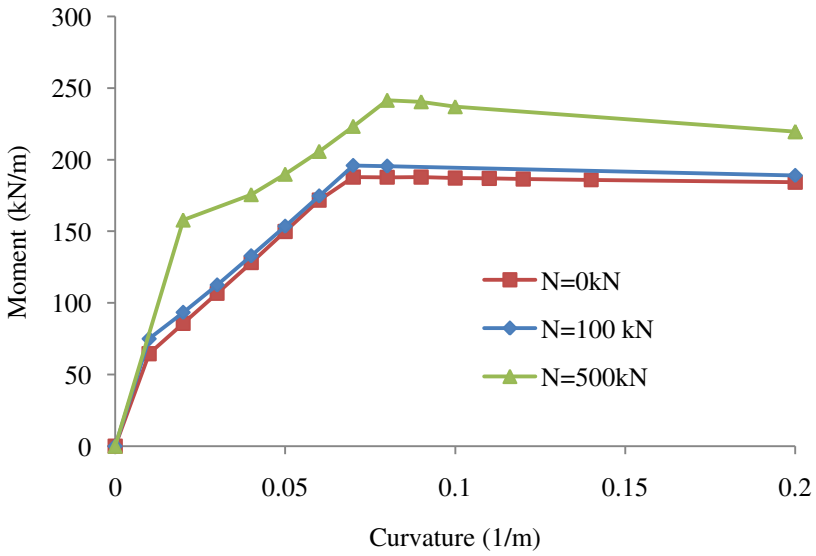

Figure 4-12. *Dependence of moment-curvature on axial compression*

Figure 4-13 expresses the reduction of the bending resistance when shear load increases at four instants: t =0h, t=1h, t=2h and t=3h.

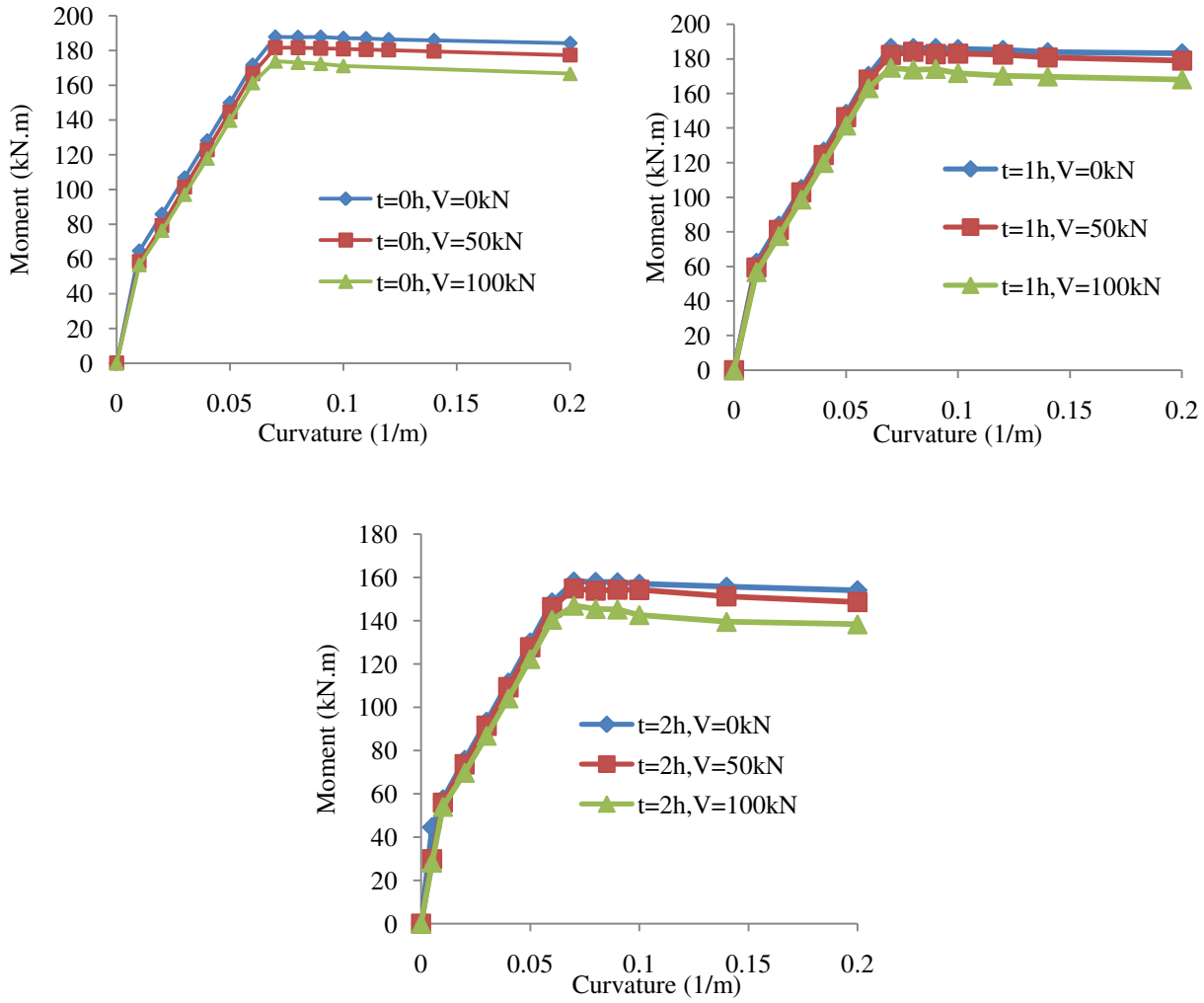

Figure 4-13. *Dependence of moment-curvature response on shear loading*

From Figure 4-11 to Figure 4-13, we have indicated that the moment-curvature curve can approximately be represented by a multi-linear curve (see [62]) with the 'crack' moment M_c, the 'yield' moment M_y, the 'ultimate' moment M_u and the corresponding values of curvature: κ_c, κ_y, κ_u. The 'crack' moment is obtained at the state where the tensile fiber of concrete starts to crack. The 'yield' moment is the moment acting on the cross section to make the tensile rebar starts to yield. The peak resistance of the beam is reached when both the tensile rebar yields and the concrete the compressive fiber collapses to make the 'ultimate' bearing state of the beam. From this state on, the 'bending hinge' occurs at the cross-section and the bending resistance of the cross-section starts to decrease with further curvature increase (see Figure 4-14).

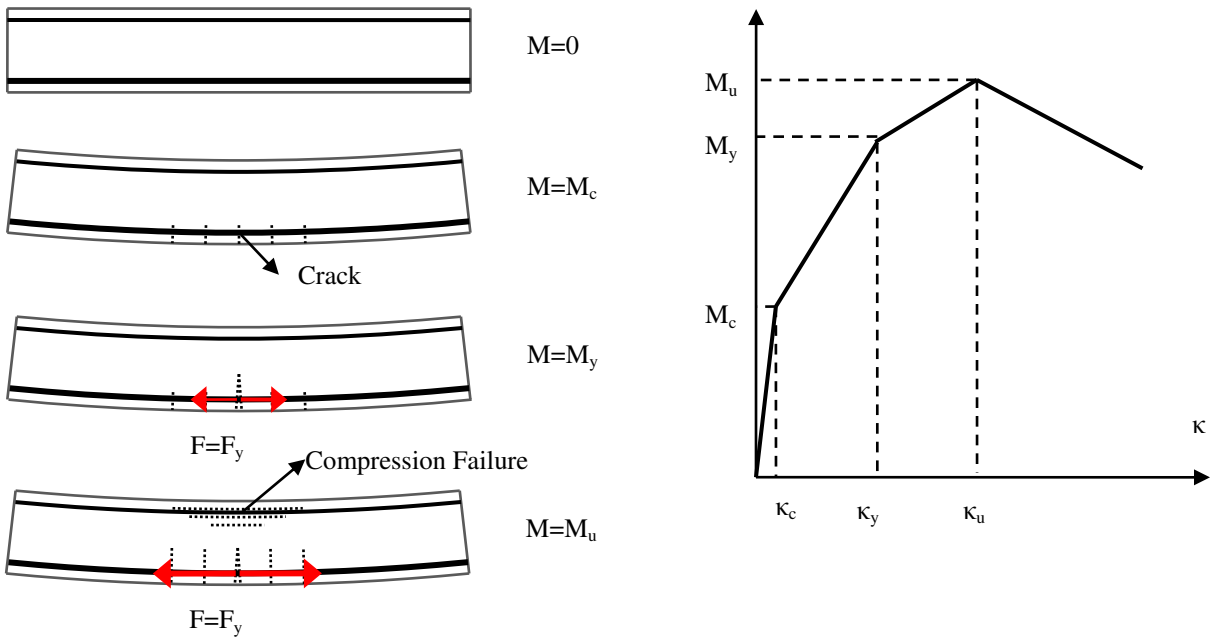

Figure 4-14. *Multi-linear moment-curvature model of the reinforced concrete beam in bending*

4.2.4 Compute the mechanical shear load – shear strain response of a reinforced concrete element subjected to pure shear loading under elevated temperature

There can be several positions in frame structure where moment and axial force are small enough in comparison to shear force (for example, at the place on the top of the pin support), at such a position, the failure of the frame is due to shear force rather than bending moment. The shear strength of reinforced concrete element is normally assumed to be the total of the concrete component and stirrups component; it can be computed by the proposed general algorithm shown in Figure 4-8or by applying the compression field theory. In this theory, the shear resistance of the beam is considered by assuming that the longitudinal strain of the cross-section is equal to zero. This model implies that the angle of the principal stress and strain is equal to 45^0C:

$$\tan 2\theta = -\frac{2\gamma}{\varepsilon_x = 0} \rightarrow \tan 2\theta = \infty \rightarrow \theta = 45^0 \tag{4-20}$$

The maximum and the minimum strains are opposite in sign and equal in magnitude:

$$\varepsilon_1 = \sqrt{\left(\frac{\varepsilon_x = 0}{2}\right)^2 + (\gamma)^2} + \frac{\varepsilon_x = 0}{2} \rightarrow \varepsilon_1 = \gamma \tag{4-21}$$

$$\varepsilon_2 = -\sqrt{\left(\frac{\varepsilon_x = 0}{2}\right)^2 + (\gamma)^2} + \frac{\varepsilon_x = 0}{2} \rightarrow \varepsilon_2 = -\gamma \tag{4-22}$$

The principal stress can be computed from principal strain for concrete and steel bar by applying equations from equation (4-8) to equation (4-16). The shear stress therefore can be computed from the shear strain and the temperature at each concrete layer and/or rebar element:

$$v_i = \sigma_{1mi} = f(\varepsilon_{1mi}, T_i) = f(\gamma_i, T_i) \tag{4-23}$$

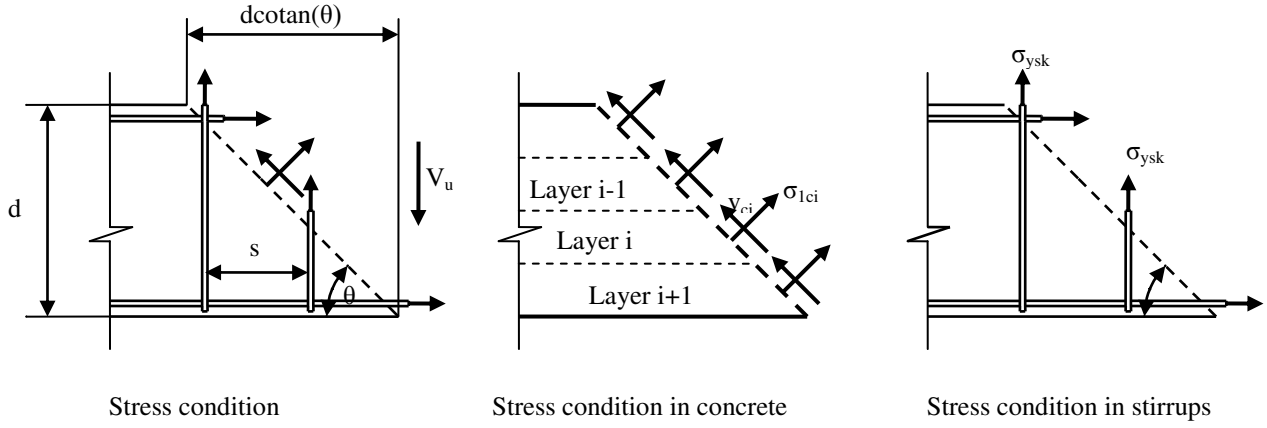

Stress condition | Stress condition in concrete | Stress condition in stirrups

Figure 4-15. *Stress components of reinforced concrete subjected to pure shear loading*

The equilibrium equation for shear force:

$$V_u = V_c + V_s = \sum_{i=1}^{N_c} v_{ci} b_{ci} h_{ci} + \frac{d\cot an(\theta)}{s} A_{sv} \sigma_{sv} \tag{4-24}$$

Where d is the 'effective' depth of reinforced concrete cross section subjected to shear load, *s* is the stirrups' spacing, A_{sv} is the area of stirrup and σ_{sv} is the stress in the stirrups corresponding to the considered shear strain. For pure shear test ($\theta = 45^0$), equation (4-24) becomes:

$$V_u = V_c + V_s = \sum_{i=1}^{N_c} \tau_{ci} b_{ci} h_{ci} + \frac{d}{s} A_{sv} \sigma_{sv} \tag{4-25}$$

From the equation (4-23) to (4-25), we can estimate the corresponding shear force (V_u) of a given shear deformation (γ), which allows us to draw the shear force–shear strain diagram in a given cross-section.

Figure 4-16 shows the reduction of shear resistance of the RC element given in Figure 4-9when subjected to fire ASTM119.

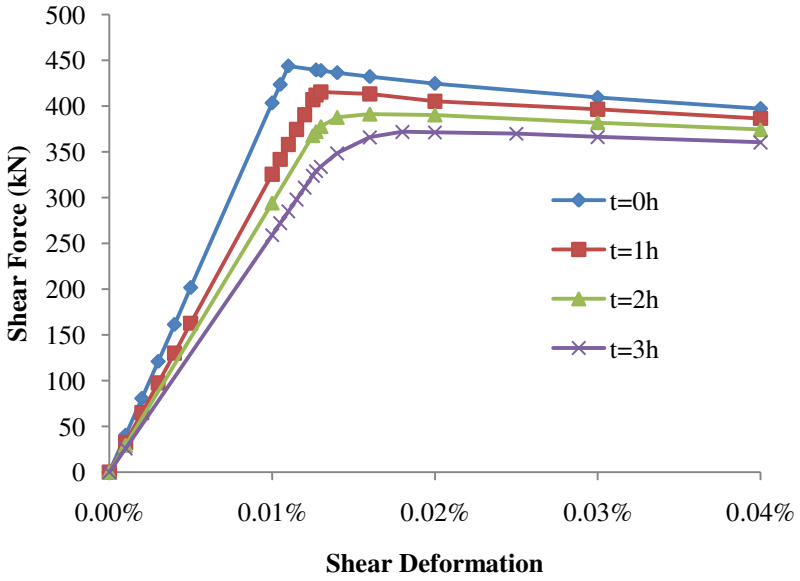

Figure 4-16. *Mechanical shear force- shear deformation diagram*

With a similar approximation already usedfor the moment-curvature curve, we also introduce a multi-linearresponse forthe shear resistance of a reinforced concrete element (see Figure 3-16 for illustration). In the next section, we show how to apply these stress-resultant models inthe finite element analysis of reinforced concrete frame structure subjected to combined mechanical and thermal loads, by using the Timoshenko beam element.

4.3 Finite element analysis of reinforced concrete frame

4.3.1 Timoshenko beam with strong discontinuities

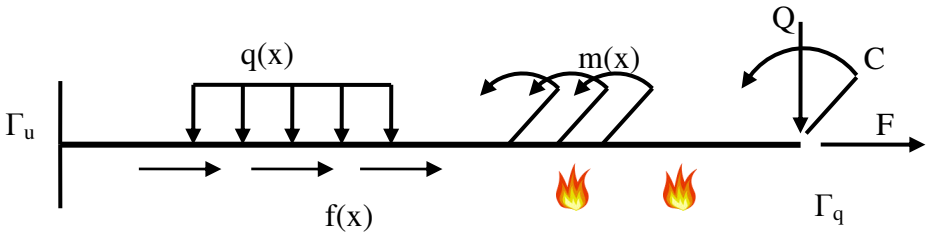

Figure 4-17. *Beam under external loading and fire*

We consider a straight Timoshenko beam of length *l*and cross-section A. The beam is submitted to distributed axial load f(x), transverse load q(x), bending moment m(x), the concentrated forces F, Q and C. The beam is also exposed to fire loading. We denote as Γ_u and Γ_q the set of points in (0,l) where displacements and forces are prescribed, respectively (seeFigure 4-17). We consider a point $x, x \in [0,l]$, on the beam neutral axis, and denote as $\mathbf{u}(x) = (u(x), v(x), \varphi(x))$ the generalized displacements (namely the longitudinal displacement, transverse displacement and rotation) at that point. With such a notation, the generalized strains at point *x*are obtained by taking into account the standard Timoshenko beam formulations:

$$\boldsymbol{\varepsilon}(x) = \begin{pmatrix} \varepsilon(x) = \dfrac{\partial u}{\partial x} \\ \gamma(x) = \dfrac{\partial v}{\partial x} - \varphi(x) \\ \kappa(x) = \dfrac{\partial \varphi}{\partial x} \end{pmatrix} \tag{4-26}$$

Denoting as N, V and M respectively the axial force, transverse shear force and bending moment, the strong form of the local equilibrium can be written as:

$$\begin{cases} \dfrac{\partial N}{\partial x} + f(x) = 0 \\ \dfrac{\partial V}{\partial x} + q(x) = 0 \\ \dfrac{\partial M}{\partial x} + T(x) + m(x) = 0 \end{cases} \tag{4-27}$$

The corresponding weak form for the standard Timoshenko beam model can then be written as:

$$\int_0^l \boldsymbol{\sigma}^T \varepsilon(\mathbf{w}) dx = \int_0^l f^T B dx + F^T \mathbf{w} \tag{4-28}$$

Where $\boldsymbol{\sigma}$ is the stress-resultant vector ($\boldsymbol{\sigma} = [N \quad V \quad M]^T$), $\mathbf{w}$ is a virtual generalized displacement ($\mathbf{w} \in V_0$ where $V_0 = \left\{ \mathbf{w} : [0,l] \to R^3 \middle| \mathbf{w} \in H^1([0,l]) and\ \mathbf{w} = 0 on\ \Gamma_u \right\}$), $\mathbf{f} = (f, q, m)^T$ is the vector of distributed load $\mathbf{F} = (F, Q, C)^T$ the vector of concentrated forces.

In order to represent the development of localized failure mechanism or 'plastic hinge' in a reinforced concrete beam, we consider discontinuity in the generalized displacement field at a particular point x_c of the neutral-axis. Indeed, a plastic hinge that is no more than a narrow zone where plastic behavior concentrates leading to a very localized dissipation, at the scale of the beam, can simply be interpreted as a discontinuity of the generalized displacement field. In that case, the generalized displacement *u* is now decomposed into a regular part and a discontinuous part as:

$$\mathbf{u}(x) = \overline{\mathbf{u}}(x) + \boldsymbol{\alpha} \mathrm{H}_{x_c} = \begin{bmatrix} \overline{u}(x) \\ \overline{v}(x) \\ \overline{\varphi}(x) \end{bmatrix} + \begin{bmatrix} \alpha_u \\ \alpha_v \\ \alpha_\varphi \end{bmatrix} \mathrm{H}_{x_c} \tag{4-29}$$

where $\boldsymbol{\alpha} = (\alpha_u, \alpha_v, \alpha_\varphi)$ is the displacement jump at point x_c and H_{x_c} is the Heaviside function defined by $\mathrm{H}_{x_c}(x) = 0$ for $x \le x_c$ and $\mathrm{H}_{x_c}(x) = 1$ for $x > x_c$. A graphic illustration of the beam kinematics is presented inFigure 4-18.

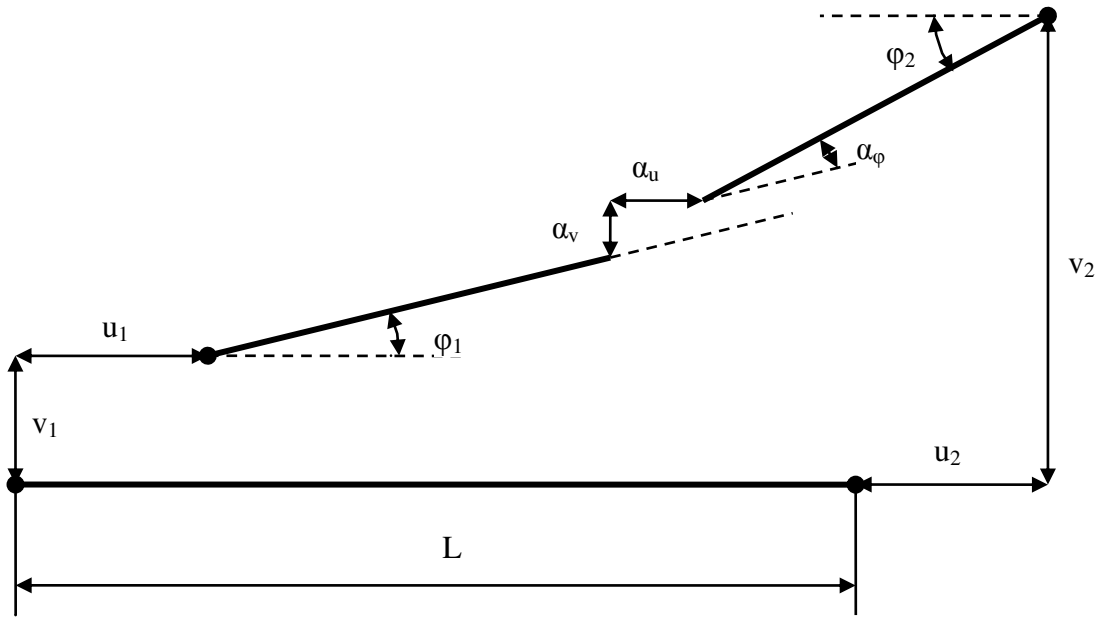

Figure 4-18. *Kinematic of beam element*

With such a representation, taking into account the essential boundary conditions on Γ_u involves the use of both $\bar{\mathbf{u}}$ and $\boldsymbol{\alpha}$. We introduce a regular differentiable function $\phi(x)$ being 0 at x = 0 and 1 at x = l. The generalized displacement field can then be rewritten as:

$$\mathbf{u}(x) = \tilde{\mathbf{u}}(x) + \boldsymbol{\alpha}\left(\mathrm{H}_{x_c}(x) - \phi(x)\right) \tag{4-30}$$

where $\tilde{\mathbf{u}}(x)$ is given in terms of $\bar{\mathbf{u}}(x)$ and $\boldsymbol{\alpha}$ as:

$$\tilde{\mathbf{u}}(x) = \bar{\mathbf{u}}(x) + \boldsymbol{\alpha}\phi(x) \tag{4-31}$$

It has to be noticed that, with this decomposition, taking into account the essential boundary conditions only involves the regular displacement field $\tilde{\mathbf{u}}(x)$. This is of great importance for the finite element implementation of such a model.

Due to the discontinuous feature of the displacement field, the generalized strain field is singular and given as:

$$\boldsymbol{\varepsilon}(x) = \boldsymbol{\varepsilon}(\bar{\mathbf{u}})(x) + \boldsymbol{\alpha}\delta_{x_c}(x) \tag{4-32}$$

where $\delta_{x_c}(x)$ is the Dirac delta function. We can write this result in an equivalent form:

$$\boldsymbol{\varepsilon}(x)=\boldsymbol{\varepsilon}(\tilde{\mathbf{u}})(x)+\boldsymbol{\alpha}\mathbf{G}(x)+\boldsymbol{\alpha}\delta_{x_c}(x) \tag{4-33}$$

where $\mathbf{G}$ is equal to $\mathbf{L}(-\phi)(x)$, $\mathbf{L}$ being the displacement-to-strain operator.

Practically, there is no need to define precisely the function $\phi(x)$, only its derivative is needed. Indeed, in the finite element implementation, the interpolation of displacement is considered in its standard form whereas the strain field is locally enriched in each finite element to take into account the influence of a displacement discontinuity. This point is discussed in the next section.

4.3.2 Stress-resultant constitutive model for reinforced concrete element

In this article, the stress-resultant models are used to describe the behavior of reinforced concrete beam element. Two different failure modes are considered here: one is related to bending failure giving rise to a rotation discontinuity (or bending 'hinge') and the other one is related to shear failure accompanied by a vertical displacement discontinuity (or shear 'hinge') (see[20],[19]). For both models, a plasticity-type formulation is chosen.

4.3.2.1 Model for bending failure

Relaying upon the generalized procedure for the classical plasticity (see [17]), we consider the following main modeling gradients:

• additive decomposition of the curvature:

$$\kappa=\kappa^e+\kappa^p \tag{4-34}$$

where κ^e denotes the elastic part of the curvature and κ^p denotes the plastic part of the curvature.

• Helmholtz free energy:

$$\psi(\kappa^e,\xi)=\frac{1}{2}\kappa^e EI\kappa^e+\Xi(\xi) \tag{4-35}$$

where E is the homogenized Young modulus of the reinforced concrete beam, I is the cross-section inertia and Ξ is the hardening potential written in terms of the hardening variable ξ.

• yield function:

$$\Phi(M,q)=|M|-(M_y-q) \tag{4-36}$$

where M_y demotes the elastic limit moment, $q$is the stress-like variable associated to the hardening variable ξ.

The use of the second principle of thermodynamics for elastic case provides constitutive equations:

$$M = EI(\kappa-\kappa^p)=EI\kappa^e \;\; ; \;\; q=-KI\xi \tag{4-37}$$

where we have considered a linear hardening law with *KI* the hardening parameter. Moreover, by considering the principle of maximum plastic dissipation, the evolution law and constitutive equations are obtained as:

$$\dot{\kappa}^p=\dot{\lambda}\frac{\partial\Phi}{\partial M}=\dot{\lambda}sign(M) \qquad ; \; \dot{\xi}=\dot{\lambda}\frac{\partial\Phi}{\partial q}=\dot{\lambda} \tag{4-38}$$

and

$$\dot{M}=\begin{cases} EI\dot{\kappa} & \dot{\lambda}=0 \\ \dfrac{EIKI}{EI+KI}\dot{\kappa} & \dot{\lambda}=0 \end{cases} \tag{4-39}$$

along with the loading/unloading conditions $\dot{\lambda}\Phi=0,\dot{\lambda}\geq 0,\Phi\leq 0$ and consistency condition $\dot{\lambda}\Phi=0$.

Due to the activation of different dissipative (irreversible) mechanisms in the materials that constitute the reinforced concrete, different stages of the bulk behavior have to be reproduced. To that end, we consider two different subsequent yield functions of the type presented in equation (4-36) to describe the bulk hardening part for bending response (see Figure 4-19). Those two functions are characterized by different limit values and hardening parameters:

• the first yield function is used to describe the behavior when the first cracks occur in concrete, with nonlinearities and dissipation appearing in the beam:

$$\Phi_c(M, q_c) = |M| - (M_c - q_c) \tag{4-40}$$

where M_c corresponds to the elastic limit of the beam (when first concrete crack appears) and $q_c = -K_1 I\xi$ is the stress-like variable associated to hardening with $K_1 I$ the hardening parameter;

• the second phase is characterized by the yielding of steel rebars. The corresponding yield function is given by:

$$\Phi_y(M, q_y) = |M| - (M_y - q_y) \tag{4-41}$$

where M_y denotes the bending moment corresponding to the yielding of steel rebar and $q_y = -K_y I\xi$ with $K_2 I$the hardening parameter.

The softening part of the behavior is controlled by the following yield condition:

$$\overline{\overline{\Phi}}(M_{x_c}, \overline{\overline{q}}) = |M_{x_c}| - (M_u - \overline{\overline{q}}) \leq 0 \tag{4-42}$$

where M_{xc} denotes the bending moment on the discontinuity at x_c, M_u is the ultimate bending moment value and $\overline{\overline{q}}$ is the stress-like variable associated to softening. Here again, as for the bulk, we consider a linear softening, so that we have: $\overline{\overline{q}} = -\overline{\overline{K}} I \overline{\overline{\xi}}$ with $\overline{\overline{K}} < 0$.

It has to be noticed here that, due to the rigid behavior of the plastic hinge at x_c, the equivalent total strain α_θ and the plastic strain are equal. $\alpha_\theta$is then interpreted as a plastic strain and its evolution is given by:

$$\dot{\alpha}_\theta = \dot{\overline{\overline{\lambda}}} \frac{\partial \overline{\overline{\Phi}}}{\partial M} = \dot{\overline{\overline{\lambda}}}\, sign(M) \qquad and \qquad \dot{\overline{\overline{\xi}}} = \dot{\overline{\overline{\lambda}}} \frac{\partial \overline{\overline{\Phi}}}{\partial \overline{\overline{q}}} = \dot{\overline{\overline{\lambda}}} \tag{4-43}$$

where $\dot{\overline{\overline{\lambda}}}$ is the plastic multiplier associated to the plastic hinge behavior. The constitutive equation is then given by:

$$\dot{M}_{x_c} = \overline{\overline{K}} I \dot{\alpha}_\theta \tag{4-44}$$

A representation of the bulk and discontinuity behavior is given inFigure 4-19, which is similar to what had been explained inFigure 4-14, expect the fact that the softening behavior of the

model is represented by a moment-rotation curve instead of the moment-curvature curve. All the parameter of the model can be identified by the layer method as already explained in Section 4.2.

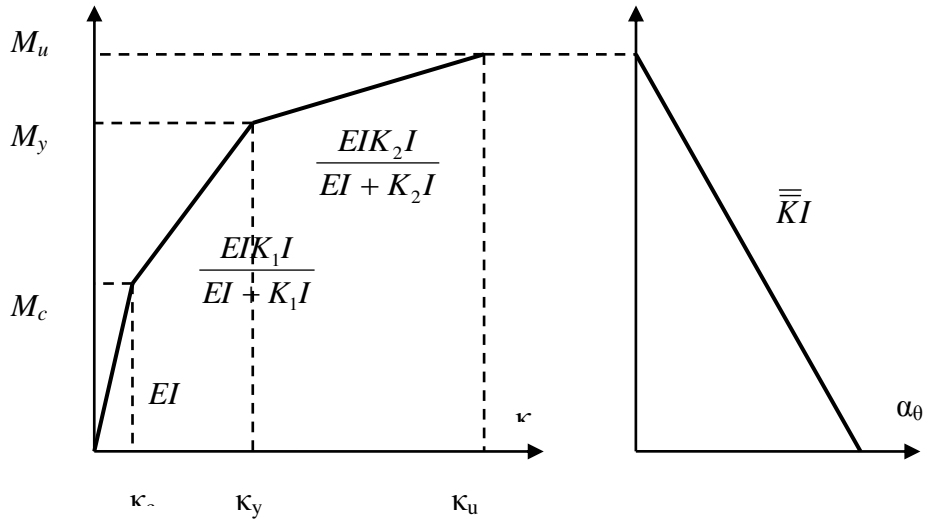

Figure 4-19. *Moment-curvature relation for bending stress-resultant model*

4.3.2.2 Model for shear failure

The model for shear failure, similar to the bending failure model, is also based upon the classical plasticity formulation. Thus, the shear strain is assumed to be the composition of elastic part and plastic part:

$$\gamma = \gamma^e + \gamma^p \tag{4-45}$$

The Helmholtz free energy is now given by:

$$\psi_v\left(\gamma^e, \xi_v\right) = \frac{1}{2}\gamma^e GA\gamma^e + \Xi_v\left(\xi_v\right) \tag{4-46}$$

where G is the equivalent shear modulus and A is the area of the beam cross-section. We consider, for the case of shear failure, two different regimes for the bulk behavior. The first regime corresponds to the elastic response and the second to the hardening regime. Those regimes are separated by the yield function:

$$\Phi_v(V,q_v)=V-(V_y-q_v)\le 0 \tag{4-47}$$

where V_y denotes the elastic limit, q_v denotes the stress-like variable which controls the yield limit: $q_v=-K_vA\xi_v$

The state equations, evolution equations and constitutive equations are now of the following form:

$$V=GA(\gamma-\gamma^p)=GA\gamma^e \tag{4-48}$$

and

$$\dot{\gamma}^p=\dot{\lambda}_v\frac{\partial\Phi_v}{\partial V}=\dot{\lambda}_v sign(V) \qquad and \qquad \dot{\xi}_v=\dot{\lambda}_v\frac{\partial\Phi_v}{\partial q_v}=\dot{\lambda}_v \tag{4-49}$$

$$\dot{V}=\begin{cases} GA\dot{\gamma} & \dot{\lambda}_v=0 \\ \dfrac{GAK_vA}{GA+K_vA}\dot{\gamma} & \dot{\lambda}_v>0 \end{cases} \tag{4-50}$$

As regards to the plastic hinge in shear, the same kind of modification as the one already presented for the bending failure is introduced but with respect to vertical displacement discontinuity. The corresponding yield function is now given by:

$$\overline{\overline{\Phi}}(V_{x_c},\overline{\overline{q}}_v)=|V_{x_c}|-(V_u-\overline{\overline{q}}_v)\le 0 \tag{4-51}$$

where V_{x_c} denotes the shear load at the discontinuity point x_c, $V_u$is the ultimate shear load value and finally $\overline{\overline{q}}_v$ denotes the stress-like variable thermodynamically conjugate to the softening variable $\overline{\overline{\xi}}_v$: $\overline{\overline{q}}_v=-\overline{\overline{K}}_vA\overline{\overline{\xi}}_v$ (if we consider linear softening). The shear hinge model is also rigid-plastic, and the displacement discontinuity α_v is interpreted as an equivalent plastic strain. Hence, the corresponding constitutive equation for softening response in shear failure can be written as:

$$\dot{V}_{x_c}=\overline{\overline{K}}_vA\dot{\alpha}_v \tag{4-52}$$

A representation of the shear behavior (bulk and discontinuity) is given inFigure 4-20.

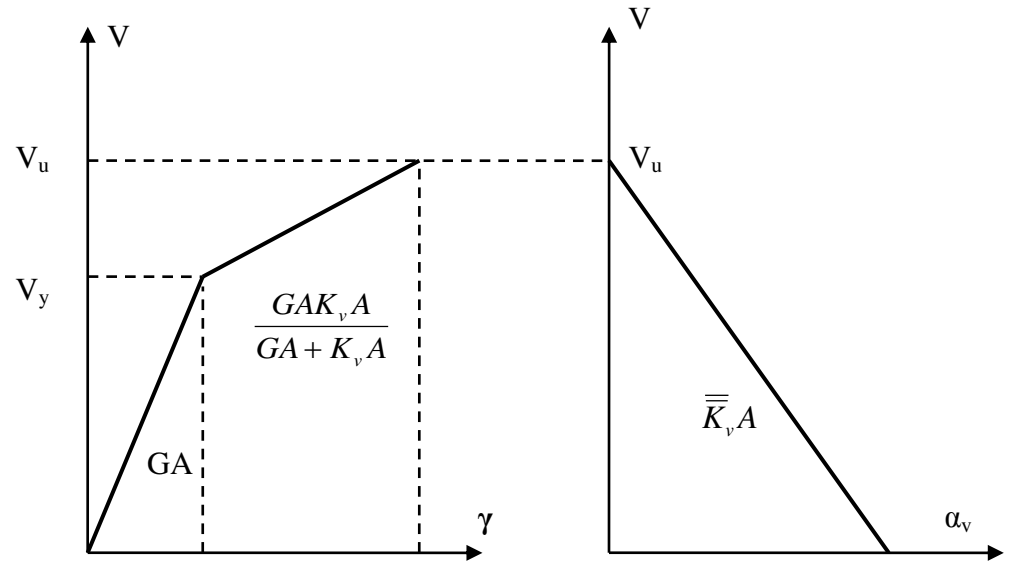

Figure 4-20. *Shear load-shear strain relation for shear stress-resultant model*

4.3.3 Finite element formulation

4.3.3.1 Finite Element interpolations and global resolution

The finite element implementation of the model presented herein is based upon the incompatible mode method (see [18]). The use of such a technique ensures that the enrichment with a generalized displacement jump remains local, and that no additional degrees of freedom are required at the global level of the solution the procedure. We present subsequently the key points of the finite element implementation and the added interpolation shape functions used in our case.

We consider a standard two-node Timoshenko beam finite element. The classical interpolation for such an element is then given by:

$$\mathbf{u}^h(x) = \begin{bmatrix} u^h(x) = N_1(x)u_1 + N_2(x)u_2 \\ v^h(x) = N_1(x)v_1 + N_2(x)v_2 \\ \varphi^h(x) = N_1(x)\varphi_1 + N_2(x)\varphi_2 \end{bmatrix} = \mathbf{Nd} \tag{4-53}$$

where

$$\mathbf{N}=\begin{bmatrix} N_1 & & & N_2 & & \\ & N_1 & & & N_2 & \\ & & N_1 & & & N_2 \end{bmatrix} \quad with \quad N_1(x)=1-\frac{x}{l^e};\ N_2(x)=\frac{x}{l^e} \tag{4-54}$$

and **d** is the vector of generalized displacement defined as:

$$\mathbf{d}=\begin{bmatrix} u_1 & v_1 & \varphi_1 & u_2 & v_2 & \varphi_2 \end{bmatrix}^T \tag{4-55}$$

The standard interpolation of the generalized strain is then given by:

$$\boldsymbol{\varepsilon}^h(x)=\begin{bmatrix} \varepsilon^h(x)=B_1(x)u_1+B_2(x)u_2 \\ \gamma^h(x)= B_1(x)v_1+B_2(x)v_2-N_1(x)\varphi_1-N_2(x)\varphi_2 \\ \kappa^h(x)= B_1(x)\varphi_1+B_2(x)\varphi_2 \end{bmatrix}=\mathbf{Bd} \tag{4-56}$$

with

$$\mathbf{B}=\begin{bmatrix} B_1 & 0 & 0 & B_2 & 0 & 0 \\ 0 & B_1 & -N_1 & 0 & B_2 & -N_2 \\ 0 & 0 & B_1 & 0 & 0 & B_2 \end{bmatrix} \tag{4-57}$$

In order to take into account the generalized displacement discontinuity, we consider the incompatible mode method to enhance the strain field. To that end, the displacement interpolation is considered in its standard form whereas the strain field is locally enriched in each finite element to take into account the influence of the discontinuity. We thus obtain the following result for discretized strain measure:

$$\boldsymbol{\varepsilon}^h(x)=\mathbf{B}(x)\mathbf{d}+\mathbf{G}_r\boldsymbol{\alpha}=B(x)d+\overline{\mathbf{G}}_r(x)\boldsymbol{\alpha}+\boldsymbol{\alpha}\delta_{x_c} \tag{4-58}$$

Where $\overline{\mathbf{G}}_r$ is a discrete representation of the function **G** introduced in equation(3-41). A possibility to choose the interpolation function $\overline{\mathbf{G}}_r$ is to consider the discrete displacement from which the strain derives. In that case, considering equation (3-29) and the fact that the regular part $\overline{\mathbf{u}}$ can be interpolated with standard shape functions, we obtain:

$$\mathbf{u}^h(x)=N_1(x)\overline{\mathbf{d}}_1+N_2(x)\overline{\mathbf{d}}_2+\boldsymbol{\alpha}H_{x_c} \tag{4-59}$$

Where $\overline{\mathbf{d}}_i$ is the vector of nodal regular part of generalized displacement for node *i*. Due to the properties of the interpolation functions and of the Heaviside function H_{x_c}, we obtain for the total nodal displacements at node 1 in position x_1 and at node 2 in position x_2:

$$\mathbf{u}^h(x_1)=\mathbf{d}_1=\overline{\mathbf{d}}_1 \qquad \text{and} \qquad \mathbf{u}^h(x_2)=\mathbf{d}_2=\overline{\mathbf{d}}_2+\boldsymbol{\alpha} \tag{4-60}$$

so that the expression in (4-59) can be rewritten as:

$$\mathbf{u}^h(x)=N_1(x)\mathbf{d}_1+N_2(x)(\mathbf{d}_2-\boldsymbol{\alpha})+\boldsymbol{\alpha}\mathrm{H}_{x_c}(x) \tag{4-61}$$

$$\mathbf{u}^h(x)=N_1(x)\mathbf{d}_1+N_2(x)\mathbf{d}_2+\boldsymbol{\alpha}\left(\mathrm{H}_{x_c}(x)-N_2(x)\right) \tag{4-62}$$

We choose then for function $\phi(x)$ in (4-30), the function $N_2(x)$ being C^1 and equal to 0 at x_1 and to 1 at x_2. With such a choice, the function $\overline{\mathbf{G}}_r$ is given by:

$$\overline{\mathbf{G}}_r(x)=\begin{bmatrix} -B_2 & 0 & 0 \\ 0 & -B_2 & 0 \\ 0 & 0 & -B_2 \end{bmatrix} \tag{4-63}$$

To build the weak form of the equilibrium equation, we consider the Hu-Washizu three-field principle as usually done for incompatible mode method.

To that end, we use the same kind of interpolations for the virtual strain field ε^*:

$$\boldsymbol{\varepsilon}^*(x)=\mathbf{B}(x)\mathbf{d}^*+\mathbf{G}_v(x)\boldsymbol{\beta}^*=\mathbf{B}(x)\mathbf{d}^*+\overline{\mathbf{G}}_v(x)\boldsymbol{\beta}^*+\boldsymbol{\beta}^*\delta_{x_c} \tag{4-64}$$

where $\mathbf{d}^*$ and $\boldsymbol{\beta}^*$ denote the virtual nodal generalized displacement and virtual displacement jump, respectively. With such interpolations, the weak form introduced in (4-28) leads to a set of two equations that can be placed within the framework of incompatible mode method:

$$\forall d^*, \forall \beta \begin{cases} \int_0^l \mathbf{d}^*\mathbf{B}^{\mathrm{T}}\boldsymbol{\sigma}dx=\int_0^l \mathbf{d}^*\mathbf{N}^T\mathbf{f}dx+\mathbf{d}^*\mathbf{F} \\ \int_0^{l_e} \boldsymbol{\beta}^*\overline{\mathbf{G}}_V^T\boldsymbol{\sigma}dx+\sigma\big|_{x_c}=0 \;\forall e\in\left[1,N_{elem}^{\alpha}\right] \end{cases} \tag{4-65}$$

Considering the standard finite element assembly procedure, we obtain:

$$\begin{cases} \underset{e=1}{\overset{N_{elem}}{A}} \left[\mathbf{f}^{e,\text{int}} - \mathbf{f}^{e,ext} \right] = 0 \\ \mathbf{h}^{e} = \int_0^{l_e} \overline{\mathbf{G}}_V^T \boldsymbol{\sigma} dx + \boldsymbol{\sigma}\big|_{x_c} = 0 \qquad \forall e \in \left[1, N_{elem}^{\alpha}\right] \end{cases} \tag{4-66}$$

Where

$$\mathbf{f}^{e,\text{int}} = \int_0^{l_e} \mathbf{B}^{\mathbf{T}} \boldsymbol{\sigma} dx\,, \qquad \mathbf{f}^{e,ext} = \int_0^{l_e} \mathbf{N}^{\mathbf{T}} \mathbf{f} dx + \mathbf{F} \tag{4-67}$$

The first equation is the standard weak form of the equilibrium equation written concerning the whole structure. The second equation, on the contrary, is local and written independently in each element where a discontinuity has been introduced (N_{elem}^{α} denotes the set of elements enriched with a discontinuity). $\boldsymbol{\sigma}\big|_{x_c}$ represents the value of the stress-resultant vector at point x_c where the discontinuity is introduced, this term arises in the equation due to the singularity of virtual strain field ($\int_0^{l_e} \boldsymbol{\sigma} \delta_{x_c} dx = \boldsymbol{\sigma}\big|_{x_c}$). This second equation can be interpreted as the weak form of the stress-resultant continuity across the localized failure point.

Remark: Function G_v is chosen, as suggested in the modified version of incompatible mode method [18], in order to ensure the patch test, namely the verification of the second equation in equation (4-66) for constant stress-resultant $\boldsymbol{\sigma}$. We obtain then:

$$\mathbf{G}_v(x) = \mathbf{G}_r(x) - \frac{1}{l_e} \int_0^{l_e} \mathbf{G}_r(x) dx \tag{4-68}$$

which gives in our case (Timoshenko beam element with only one integration point): $\mathbf{G}_v(x) = \mathbf{G}_r(x)$

4.3.3.2 Local resolution

Denoting as *i*the iteration for time step *n+1* of Newton's iterative procedure, providing the corresponding iterative updates $\Delta\mathbf{d}_{n+1}^{(i)} = \mathbf{d}_{n+1}^{(i+1)} - \mathbf{d}_{n+1}^{i}$ and $\Delta\boldsymbol{\alpha}_{n+1}^{(i)} = \boldsymbol{\alpha}_{n+1}^{(i+1)} - \boldsymbol{\alpha}_{n+1}^{(i)}$, the linearized version of equation (4-66) is given by:

$$\begin{cases} \underset{e=1}{\overset{N_{elm}}{A}} \left[\mathbf{K}_{n+1}^{e,(i)} \Delta\mathbf{d}_{n+1}^{(i)} + \mathbf{F}_{r,n+1}^{e,(i)} \Delta\boldsymbol{\alpha}_{n+1}^{(i)} \right] = \underset{e=1}{\overset{N_{elm}}{A}} \left[\mathbf{f}_{n+1}^{e,ext} - \mathbf{f}_{n+1}^{e,\text{int}(i)} \right] \\ \mathbf{h}_{n+1}^{e,(i)} + \left(\mathbf{F}_{v,n+1}^{e,(i)} + \mathbf{K}_{d,n+1}^{(i)} \right) \Delta\mathbf{d}_{n+1}^{(i)} + \left(\mathbf{H}_{n+1}^{e,(i)} + \mathbf{K}_{\alpha,n+1}^{(i)} \right) \Delta\boldsymbol{\alpha}_{n+1}^{(i)} = 0 \end{cases} \tag{4-69}$$

Here, we have adopted the following notations:

$$\mathbf{K}_{n+1}^{e,(i)} = \int_0^{l_e} \mathbf{B}^T \mathbf{C}_{n+1}^{an,(i)} \mathbf{B} dx\,; \qquad \mathbf{F}_{r,n+1}^{e,(i)} = \int_0^{l_e} \mathbf{B}^T \mathbf{C}_{n+1}^{an,(i)} \overline{\mathbf{G}}_r dx \tag{4-70}$$

$$\mathbf{F}_{n+1}^{e,(i)} = \int_0^{l_e} \overline{\mathbf{G}}_V^T \mathbf{C}_{n+1}^{an,(i)} \mathbf{B} dx\,; \qquad \mathbf{H}_{n+1}^{e,(i)} = \int_0^{l_e} \overline{\mathbf{G}}_V^T \mathbf{C}_{n+1}^{an,(i)} \overline{\mathbf{G}}_r dx \tag{4-71}$$

where $\mathbf{K}_{\mathbf{d},n+1}^{(i)}$ and $\mathbf{K}_{\boldsymbol{\alpha},n+1}^{(i)}$ are the consistent tangent stiffness for the discontinuity:

$$\Delta\boldsymbol{\sigma}\big|_{x_c,n+1}^{(i)} = \mathbf{K}_{d,n+1}^{(i)} \Delta\mathbf{d}_{n+1}^{(i)} + \mathbf{K}_{\alpha,n+1}^{(i)} \Delta\boldsymbol{\alpha}_{n+1}^{(i)} \tag{4-72}$$

and $\mathbf{C}_{n+1}^{an,(i)}$ denotes the consistent tangent modulus for the bulk material obtained as a discretized version of the tangent modulus given in equation (4-39) and equation (4-50):

$$\Delta\boldsymbol{\sigma}_{n+1}^{(i)} = \mathbf{C}_{n+1}^{an,(i)} \Delta\boldsymbol{\varepsilon}_{n+1}^{(i)} \tag{4-73}$$

with $\boldsymbol{\sigma}$ and $\boldsymbol{\varepsilon}$ the generalized stress and strain, respectively.

The solution of the set of two equations in equation system (4-69) is obtained by taking advantage of the local nature of the second equation, and the fact that it can be solved independently in each localized element. For that purpose an operator splitting technique is used. First, for a given nodal displacement increment $\Delta\mathbf{d}_{n+1}^{(i)}$ at iteration *I* of the global Newton procedure, the increment of displacement jump $\Delta\boldsymbol{\alpha}_{n+1}^{(i)}$ is sought by iterating in each localized element upon the local equation $\mathbf{h}_{n+1}^{e,(i)} = 0$ (see equation (4-69)$_b$). At the end of the local solution, we then perform the static condensation at the element level, and carry on to solve the global part of the Finite Element equilibrium equations:

$$\mathop{A}_{e=1}^{N_{elem}} \left[\hat{\mathbf{K}}_{n+1}^{e,(i)} \Delta\mathbf{d}_{n+1}^{(i)} \right] = \mathop{A}_{e=1}^{N_{elem}} \left[\mathbf{f}_{n+1}^{e,ext} - \mathbf{f}_{n+1}^{e,\mathrm{int}(i)} \right] \tag{4-74}$$

where

$$\hat{\mathbf{K}}_{n+1}^{e,(i)} = \left\{ \mathbf{K}_{n+1}^{e,(i)} + \mathbf{F}_{r,n+1}^{e,(i)} \left(\mathbf{H}_{n+1}^{e,(i)} + \mathbf{K}_{\alpha,n+1}^{(i)} \right)^{-1} \left(\mathbf{F}_{v,n+1}^{e,(i)} + \mathbf{K}_{d,n+1}^{(i)} \right) \right\} \tag{4-75}$$

is the element tangent stiffness modified by the static condensation.

We note in passing that the yield functions used in this work are totally uncoupled, so that the vector equation in equation $(4\text{-}66)_b$ can be treated as a collection of corresponding scalar equations. In the following, we present the resolution of such a scalar equation in a general form without specifying the superscript *M* or *V* related to, respectively, bending or shear.

As already mentioned, the behavior on the discontinuity is rigid-plastic. Indeed, the displacement jump is no more than a plastic displacement at discontinuity, with no elastic part contributing to the displacement jump. Dueto this feature, it is not possible to compute trial tractions $\boldsymbol{\sigma}\big|_{x_c}^{tr}$ as usuallydone for return-mapping algorithm ($\boldsymbol{\sigma}\big|_{x_c}$ denotes either M_{x_c} or V_{x_c}).

We have chosen here to use the local equilibrium equation (4-66b) to compute the trial tractions values for a given set of nodal displacements $\mathbf{d}_{n+1}^{(i)}$. For a one point integration Timoshenko beam element, this local equation is very simple and reduces to the strong form of the traction continuity across the localized failure point; that is: $\boldsymbol{\sigma}\big|_{x_c} = \boldsymbol{\sigma}(\mathbf{d},\alpha)$ where $\boldsymbol{\sigma}(\mathbf{d},\alpha)$ is the corresponding generalized stress computed in the bulk. Moreover, we note that the activation of the discontinuity is accompanied with softening, which involves elastic unloading of the bulk so that the bulk and discontinuity internal variables cannot evolve simultaneously.

With this remarks in hand, the sketch of the algorithm can be given as follows:

• first compute the trial traction value by using equation (4-66b) and considering no evolution of the internal variables: $\alpha, \overline{\overline{\xi}}$.

$$\alpha_{n+1} = \alpha_n, \qquad \overline{\overline{\xi}}_{n+1} = \overline{\overline{\xi}}_n \tag{4-76}$$

thus obtain the corresponding trial values of stress resultants:

$$\boldsymbol{\sigma}_{x_c,n+1}^{tr} = \boldsymbol{\sigma}_{n+1}^{tr} = \mathbf{C}^e\left(\mathbf{B}\mathbf{d}_{n+1}^{(i)} + \overline{\mathbf{G}}_r\boldsymbol{\alpha}_{n+1}^{tr} - \boldsymbol{\varepsilon}_n^p\right) \tag{4-77}$$

• then check the value of yield function $\overline{\overline{\Phi}}_{n+1}^{tr} = \overline{\overline{\Phi}}\left(\boldsymbol{\sigma}_{x_c,n+1}^{tr}, \overline{\overline{q}}_{n+1}^{tr}\right)$ at discontinuity.

– if $\overline{\overline{\Phi}}_{n+1}^{tr} \le 0$, the trial state is admissible, no evolution of the internal variables is needed. In that case, the consistent tangent stiffness for the discontinuity (see equation (4-72)) is such that:

$\mathbf{K}^{(i)}_{\mathbf{d},n+1} = -\mathbf{F}^{e,(i)}_{v,n+1}$, the element tangent stiffness is thus, in case of an elastic loading or unloading of the discontinuity not modified.

– if $\overline{\overline{\Phi}}^{tr}_{n+1} > 0$, evolution of internal variables should be computed. To that end, the Newton iterative procedure is used to obtain the value of $\boldsymbol{\alpha}_{n+1}$ and $\overline{\overline{\xi}}_{n+1}$ ensuring $\overline{\overline{\Phi}}\left(\boldsymbol{\sigma}_{x_c,n+1}, \overline{\overline{q}}_{n+1}\right) = 0$ where $\boldsymbol{\sigma}_{x_c,n+1}$ is computed using equation (4-66b). We obtain finally $\boldsymbol{\alpha}_{n+1} = \boldsymbol{\alpha}_n + \lambda_{n+1} sign\left(\boldsymbol{\sigma}^{tr}_{x_c,n+1}\right)$ and $\overline{\overline{\xi}}_{n+1} = \overline{\overline{\xi}}_n + \lambda_{n+1}$ where the Lagrange multiplier λ_{n+1} is obtained as:

$$\lambda_{n+1} = -\frac{\overline{\overline{\Phi}}^{tr}_{n+1}}{C^e \overline{\mathbf{G}}_r + \overline{\overline{K}}} \left(> 0\right) \tag{4-78}$$

The actual value of the traction on the discontinuity is then given by:

$$\boldsymbol{\sigma}_{x_c,n+1} = \boldsymbol{\sigma}^{tr}_{x_c,n+1} + \lambda_{n+1} C^e \overline{\mathbf{G}}_r sign\left(\boldsymbol{\sigma}^{tr}_{x_c,n+1}\right) \tag{4-79}$$

In that case, the tangent stiffness associated to the discontinuity is given by: $\mathbf{K}^{(i)}_{\alpha,n+1} = \overline{\overline{K}}^{(i)}_{n+1}$ and $\mathbf{K}^{(i)}_{\mathbf{d},n+1} = 0$.

4.4 Numerical example

4.4.1 Simple four-point bending test

We consider here a simple reinforced concrete beam subjected to ASTM 119 fire (see[11]) at its bottom and also subjected to external mechanical loads applied in the vertical direction (see Figure 4-21).

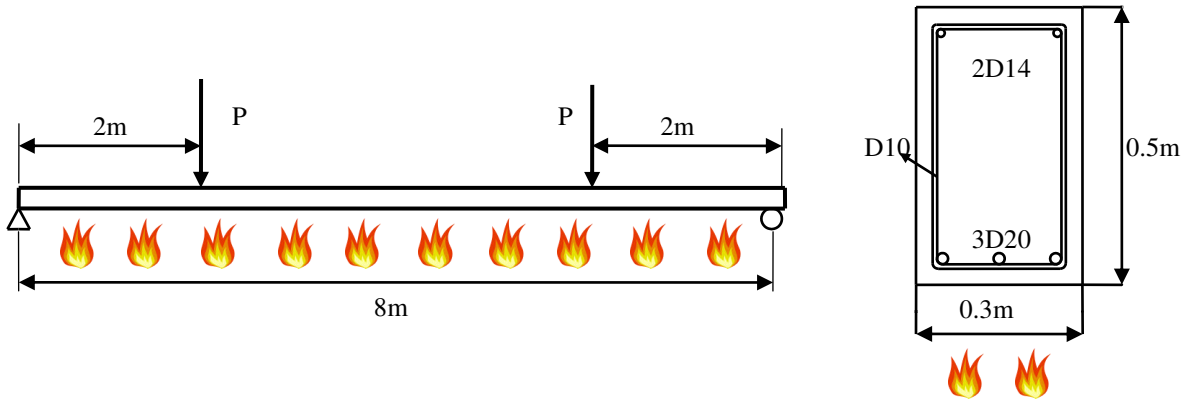

Figure 4-21. *Simple reinforced concrete beam subjected to ASTM 119 fire and vertical forces*

The beam was formed by carbonate concrete with compressive strength $f_c^{'} = 30MPa$, longitudinal reinforced by 2 reinforcement bars D14 on the top and 3bars D20 on the bottom. The concrete cover thickness is 40 mm. The beam is also transverse reinforced by D10 stirrups with the spacing of 125 mm. The yield limit of steel is 400*MPa*.

Using the layer method described in section 3-2, we can identify the stress-resultant models for bending failure and shear failure at different instants of fire loading program (see Figure 4-22 and Figure 4-23).

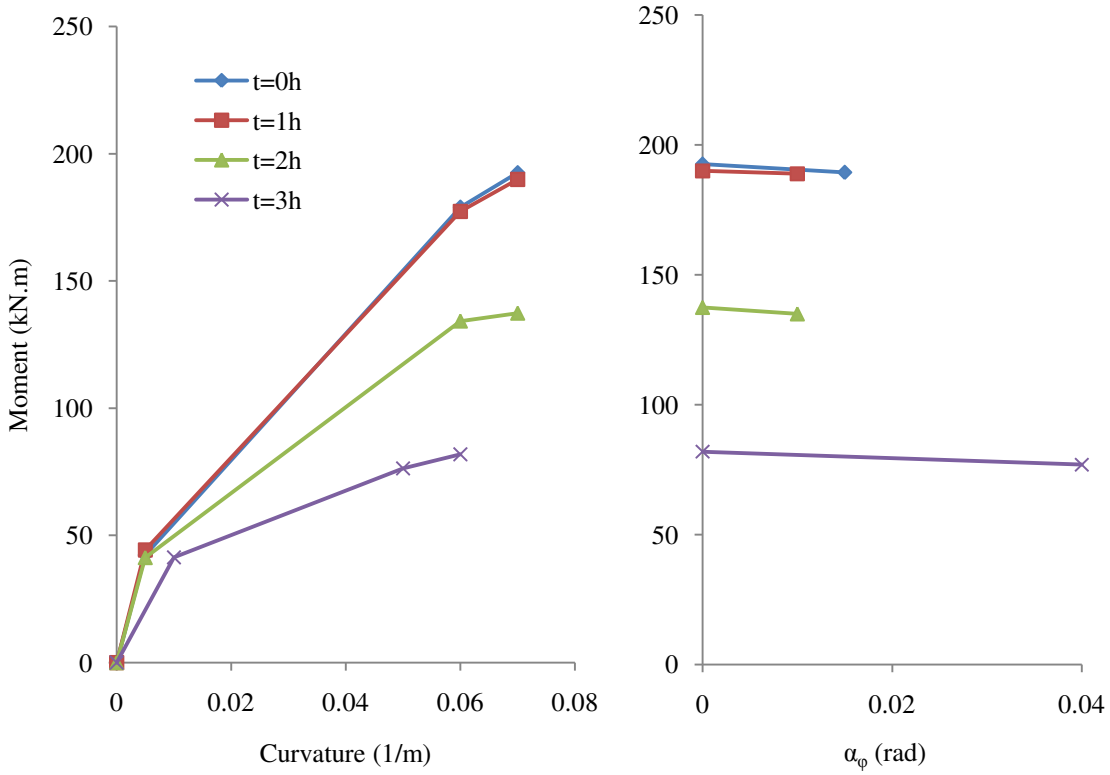

Figure 4-22. *Reduction of bending resistance due to time exposing to fire ASTM 119*

The corresponding values of material parameters for bending model are given inTable 4-2.

Table 4-2. *Bending model parameters for different instants of fire loading program*

Parameters	**t =0h**	**t =1h**	**t =2h**	**t=3h**
Young Modulus (kN/m^2)	2708121	2835722	2644230	1324882
Hardening Modulus K_1 (kN/m^2)	795440.3	773984.9	540969.6	279660.4
Hardening Modulus K_2(kN/m^2)	433372.2	404203.2	99201.84	177893.4
Softening Modulus $\overline{\overline{K}}$ (kN/m)	-66943.8	-34230.2	-79727.8	-40232.5
Crack shear M_c (kN)	42.3144	44.30815	41.3161	41.40257
Yield shear M_y (kN)	87.15347	177.3368	134.2953	76.36012
Ultimate shear M_u (kN)	192.5736	189.9682	137.3953	81.91929

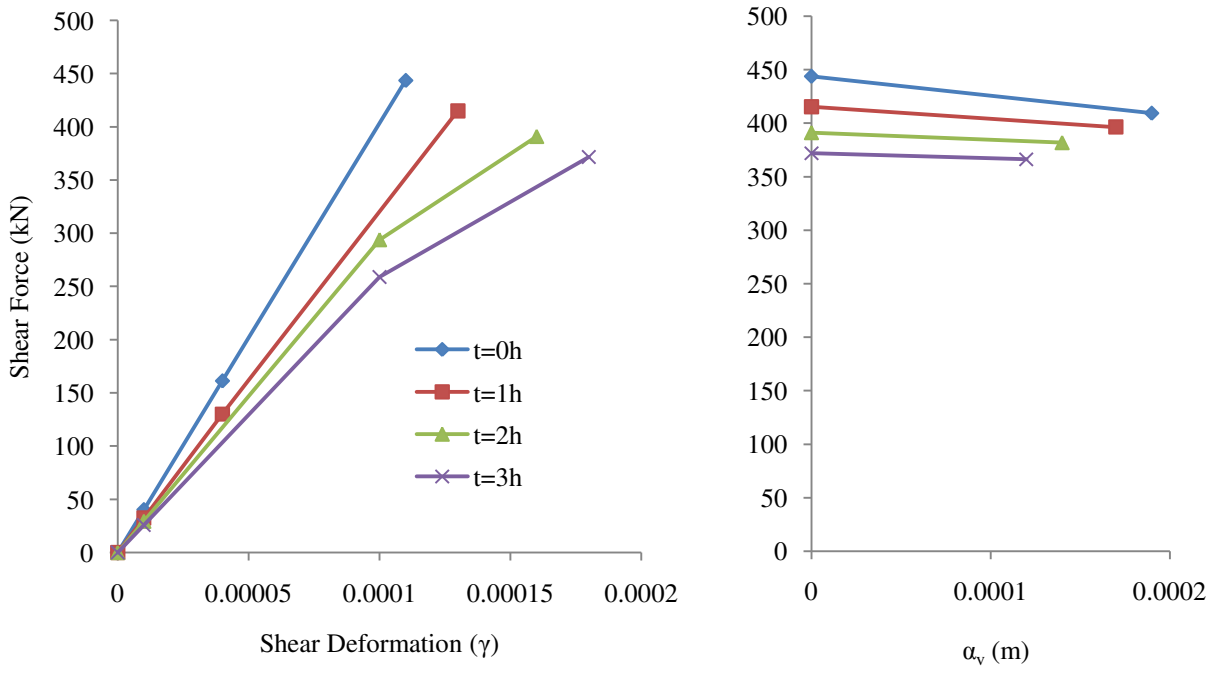

Figure 4-23. *Reduction of shear resistance due to time exposing to fire ASTM 119*

The corresponding parameters for shear failure model are presented in Table 4-3.

Table 4-3. *Parameters of shear model at different instants of fire loading program*

Parameters	**t =0h**	**t =1h**	**t =2h**	**t=3h**
Shear Modulus (kN/m^2)	26892218	21686667	19600983	17267528
Hardening Modulus K_1 (kN/m^2)	26892218	21690899	19520350	17267528
Hardening Modulus K_2(kN/m^2)	26892218	21114573	3850031	8273086
Softening Modulus $\overline{\overline{K}}$ (kN/m^2)	-1208592	-743844	-444255	-310832
Crack shear V_c (kN)	40.33833	32.53	29.40148	25.90129
Yield shear V_y (kN)	161.3533	130.139	371.9836	284.9142
Ultimate shear V_u (kN)	443.7216	415.1858	391.0413	371.7816

Figure 4-24 shows the relation between the load P and the deflection in the middle of the beam exposed to fire loading at times t=0h, t=1h, t=2h and t=3h.

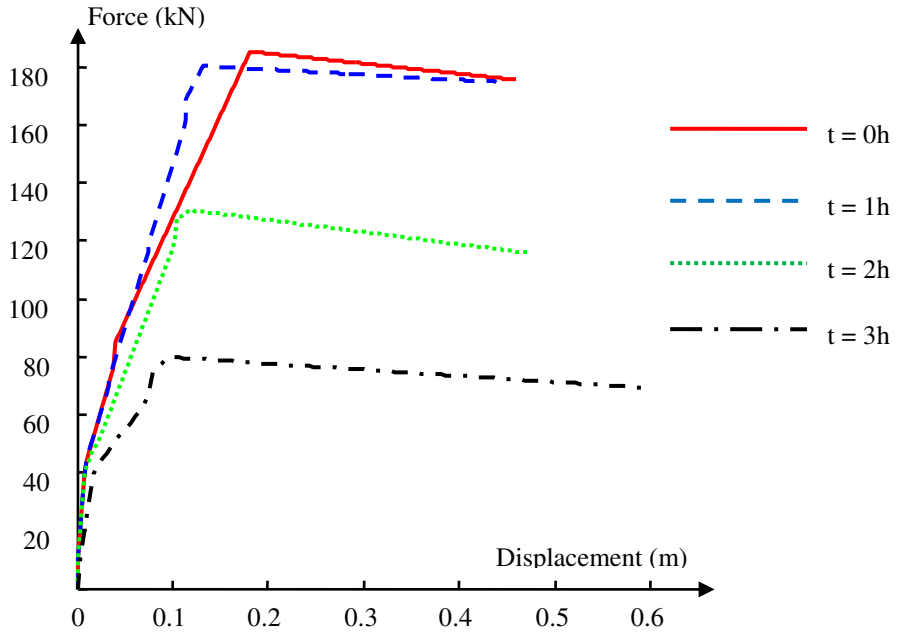

Figure 4-24. *Force/displacement curve of the beam at different instants of fire loading program*

We note that after a long exposure to fire loading, the bearing resistance of the beam is significantly reduced.In particular, after one hour fire exposure, the ultimate load of the beam reduces from 185.27 kN to 180.31 kN; then after two hours, the ultimate load reduces to 130.48 kN and it finally reduces to 79.767 kN after three hours exposure to ASTM 119 fire (seeFigure 4-25).

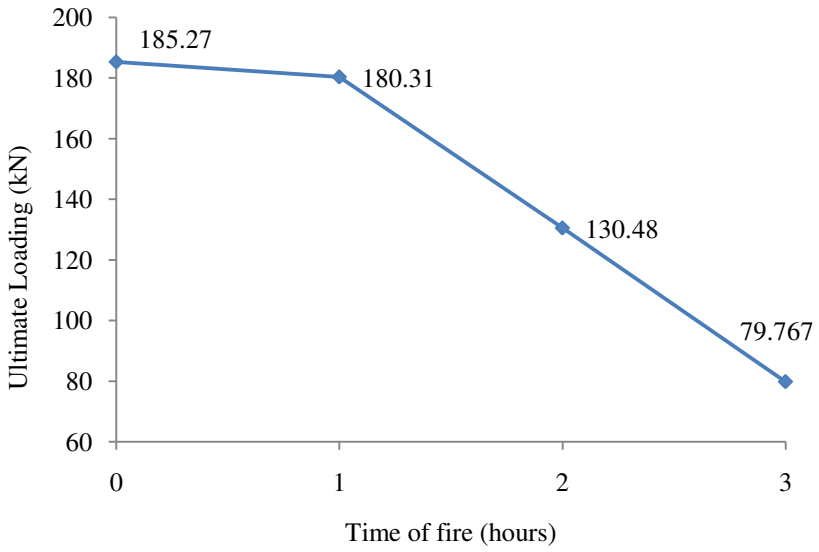

Figure 4-25. *Reduction of ultimate load due to fire exposure*

4.4.2 Reinforced concrete frame subjected to fire

We consider a two- storey frame with geometry given in Figure 4-26. The material properties are listed in Table 4-4. Each of the two columns of the frame is subjected to a compressive load equal to 700kN acting on the top of the column. A horizontal force Q acts on the right edge of the second storey leading to imposing a horizontal displacement of the frame. Two reinforced concrete beams corresponding to the spans of the frame are submitted to ASTM119 standard fire (see[11]) on their bottom. Figure 4-27shows the evolution of temperature of the beam that hasbeen submited to fire for one, two and three hours.

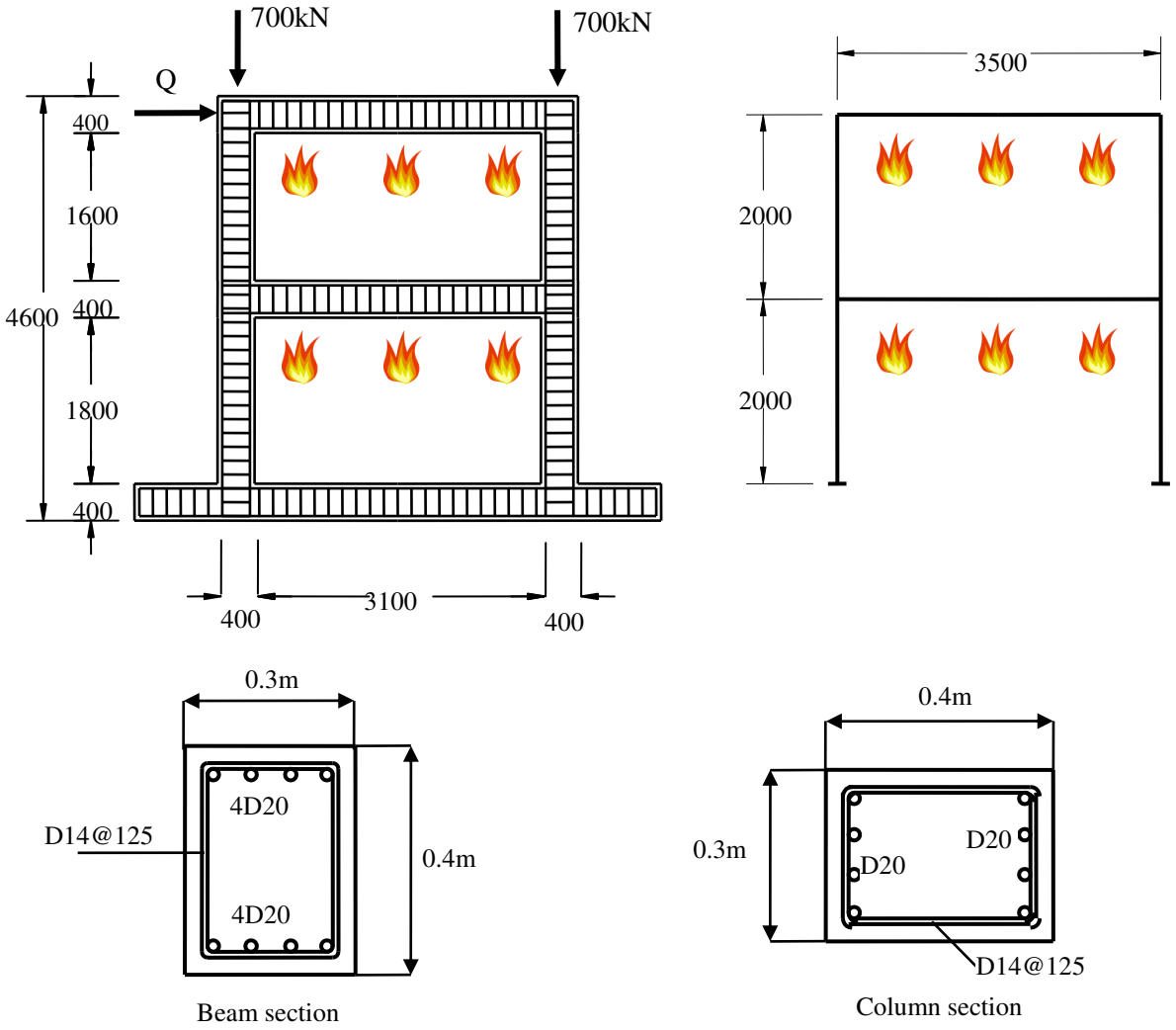

Figure 4-26. *Two-story reinforced concrete frame subjected to loading and fire*

Table 4-4. *Material properties*

Concrete Properties			
Modulus of Elasticity	E_c	26889.6	N/mm^2
Compression Strength	f_{cc}	30	N/mm^2
Steel Properties			
Yield Stress	f_{sy}	400	N/mm^2

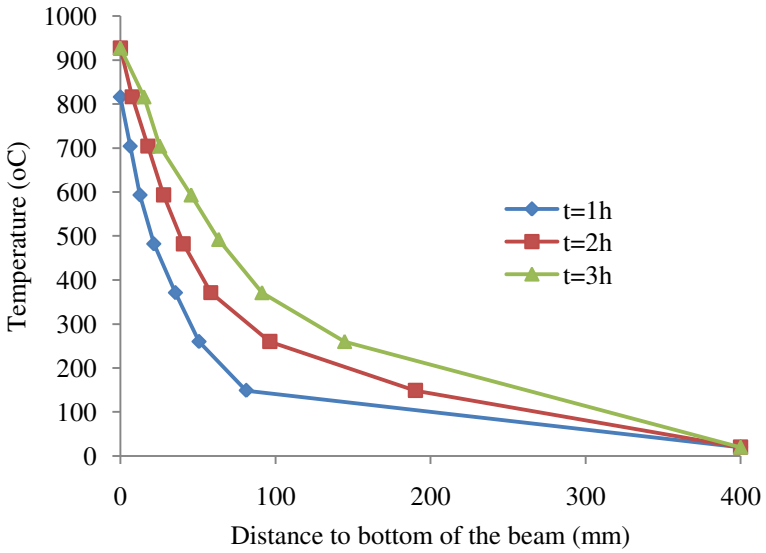

Figure 4-27. *Temperature profile of the reinforced concrete beam due to time of fire*

Since the columns are highly compressed with a 700kN force, their bending resistance is much greater than the bending resistance of the beam. The bending model of the column at room temperature (no fire acting) is given in Figure 4-28.

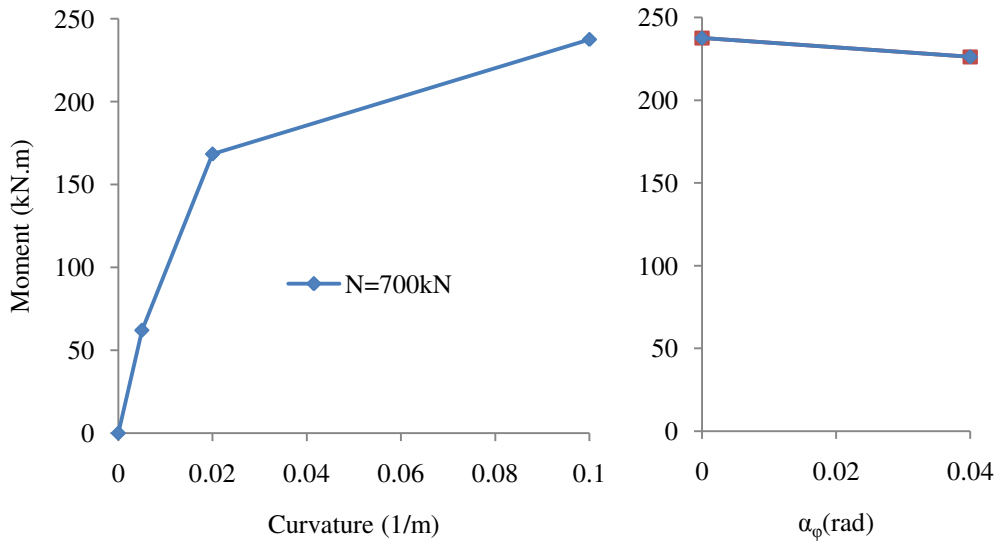

Figure 4-28. ***Moment-curvature model for column***

The shear model of the column is given in Figure 4-29

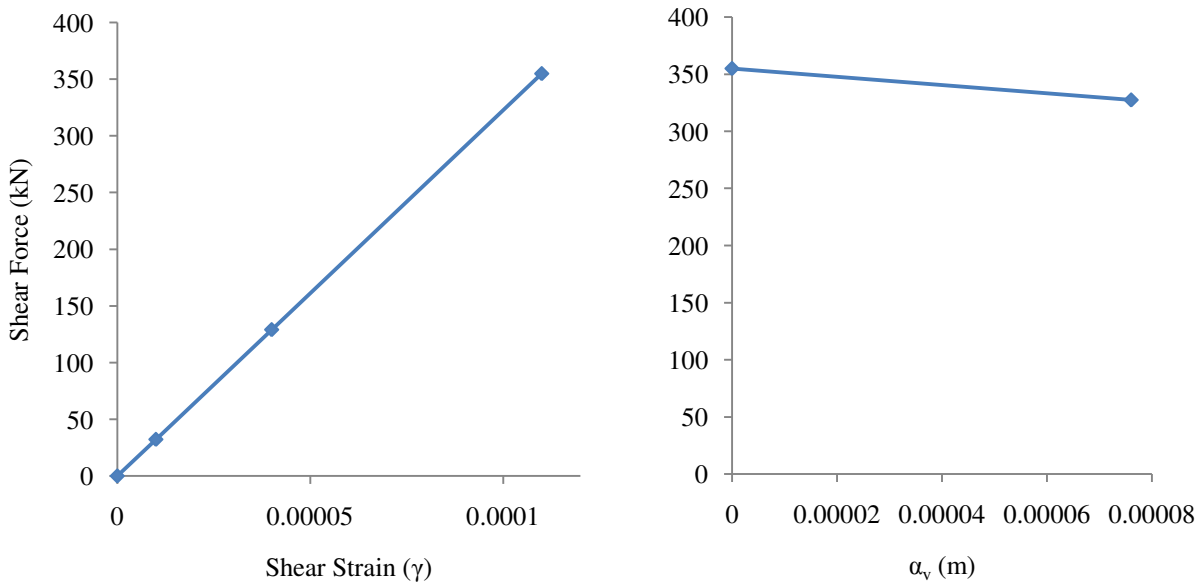

Figure 4-29. *Shear failure model of the column*

Figure 4-30 represents the degradation of moment-curvature curve of the beam after one, two and three hours exposing to fire.

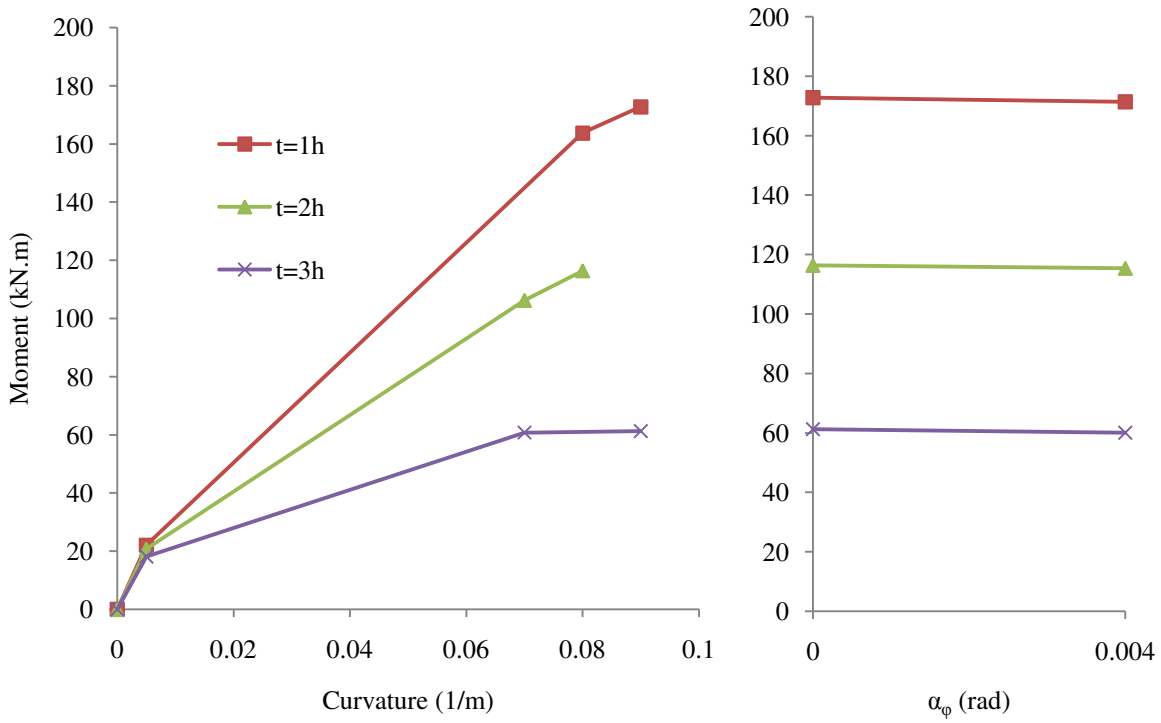

Figure 4-30. *Degradation of bending resistance of reinforced concrete beam versus fire exposure*

Figure 4-31 illustrates the reduction of the overall response of the frame due to fire by plotting the relationship between horizontal force Q with the horizontal displacement of the top beam at different times: t= 1 hour, t = 2 hours and t = 3 hours.

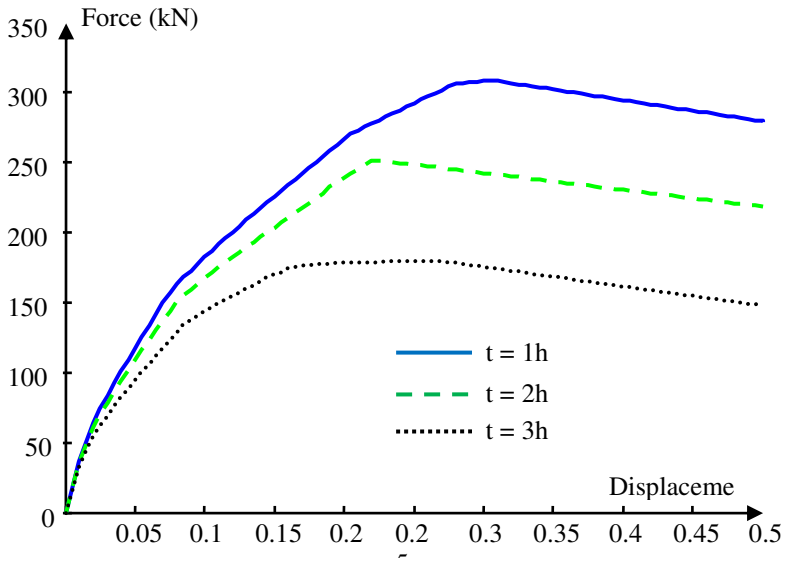

Figure 4-31.*Horizontal force/displacement curve of two-story frame at different instants of fire*

We can note, in particular, that the ultimate horizontal load of the reinforced concrete frame decreases from $308.52kN$ to $251.46kN$ and then to $180.01kN$ after one hour, two hours and three hours submitted to fire. This is the result of the degradation of the material properties due to high temperature and also due to the thermal effect on the beam.

4.5 Conclusion

In this chapter we have developed a method to calculate the behavior of reinforced concrete frame structure subjected to fire, with combined thermal and mechanical loads The main novelty of the proposed method is its capability of taking into account the thermal loading and the degradation of material properties due to the temperature in determining the ultimate load of the reinforced concrete frame. Moreover in the proposed method, we consider not only the bending failure but also the shear failure of the reinforced concrete structure. This is also a new contribution in solving the resistance of reinforced concrete frame exposure to fire and thermal effect. The finite element approach presented for this kind of problem can provide the correct representation of the localized failure of the reinforced concrete structure. Two most frequent failure mechanisms are treated separately in order to provide the most robust computational procedure. The numerical examples we have presented here confirmed a very satisfying results provided by proposed methodology. The introduced method migh also be used to compute the remaining resistance of a damaged structure after being subjected to fire loading, which gives the answer to the question if the damaged consctruction can continue working or not. This proposed strategy is the first important step towards fully coupled thermomechanical problems to achieve reliable description of the structural resistance for different thermal load programs and eventual sudden regime change in the exposure to fire.

5 Conclusions and Perpectives

5.1 Main contributions

In this thesis, we have discussed the general behavior and also the localized failure of steel, concrete and reinforced concrete structures under extreme thermo-mechanical conditions. The main contributions concerns both aspects of model theoretical formulation and its numerical implementation.

In terms of theoretical aspect, new thermo-mechanical models for steel and concrete material were carried out, providing much better understanding of the interaction between mechanical response and thermal response of the structure. First, the mechanical dissipation and structural heating due to inelastic (and/or localized failure) mechanical response will lead to an increase of the temperature and inversly, the thermal loads and tempertaure gradient will result in a considerable amount of stress, strain and/or displacement. We have also proved, based on the local balance equation of energy, that the thermal propagation through a localized failure region will result in a 'jump' in the heat flow, or a change in the temperature gradient, in the localization zone.

In terms of numerical solution, a detailing 'adiabatic'operator split procedure was developed and applied to solve the present multi-physical problem. Here, the coupled thermo-mechanical problem is divided into 'mechanical' process and 'thermal' process with the 'adiabatic' constraint condition. The 'mechanical' process is solved first with the 'adiabatic' tangent modulus (taking into account the evolution of temperature due to structural heating) to compute the mechanical internal variables of the model as well as the mechanical dissipation. Then, the 'thermal' process is solved latter based upon a modified form of the classical heat transfer equation with a corresponding mechanical dissipation acting as an additional heat supply. The 'discontinuity' (or a 'jump') in displacement field and also the 'jump' in the heat flow at the localized failure zone are modeled by additional interpolation functions and are determined at the element level of the operator splitting procedure applying for 'mechanical' process and 'thermal' process, respectively. All the problems were solved in the framework of the embedded-discontinuity finite element method by using the research version of the finite element analysis program FEAP (see [56], [57]).

The thesis also provided a method to estimate the 'ultimate' resistance of a reinforced concrete structure under fire loading. In this method, the structure is considered to be an assembly of many one-dimensional elements such as : frames, beams and columns, which can be modeled by Timoshenko beam element. Main novelties of the method are: 1) capability of taking into account the shear failure (along with the bending failure) into the overal failure of the structure and 2) capability of taking into account the thermal effect on the total response of the structure. Both of these two novelties play important roles in analysing the degradation of the reinforced concrete frame under fire accidents.

5.2 Perpectives

Despite several contributions, one can identify in this thesis a number of deficiencies to be completed and improved. Chief among them is the need of taking into account the thermo-mechanical behavior of bonding interface between steel bar and concrete in the total response of the reinforced concrete structure. How does the bonding interface response under the thermal loading? How does this response influence the total response of the reinforced concrete structure? These challenge questions might be studied in the future based on the previous works of Tran & Sab (see [37]), Davenne et al.(see [63]), Boulkestous et al. (see [64], [26], [65]). Another development can be expected from this study is to widen the models to accumulate other behaviors such as the creep and shrinkage of concrete due to age and humidity, as well as the fatigue and/or buckling behavior of the steel (see [66]). Last but not least, the idea of extending the proposed theoretical model and the numerical solution to compute the dynamic response of the structure is also a good direction to go.

6 Bibliography

[1] John L. Gross and Therese P. McAllister,". Structural Fire Response and Probable Collapse Sequence of the World Trade Center Towers," The United States, 2005.

[2] T. W. Eagar and C. Musso, "Why Did the World Trade Center Collapse? Science, Engineering, and Speculation," *JOM*, no. December 2001, 2001.

[3] T. Foecke, W.E.Luecke, J.D. McColskey, C.N. McCowan, T.A. Siewert, F.W. Gayle S.W. Banovic, "The Role of Metallurgy in the NIST Investigation of the World Trade Center Towers Collapse," *JOM*, no. December 2007, December 2007.

[4] Society of Fire Protection Engineers, "Guidelines for Designing Fire Safety in Very Tall Buildings," 2012.

[5] A. J. C. B. Saint-Venant, "Memoire sur la Torsion des Prismes," *Mémoires présentés par divers savants*, vol. 14, pp. 233-560, 1855.

[6] EN 1993-1-2, "Eurocode 3. Design of steel structures. Part 1.2 : General rules. Structure fire design," 2005.

[7] EN-1992-1-2, *Eurocode 2: Design of Concrete Structure - Part 1-2: General rules-Structural Fire Design.*: Eurocode, 2004.

[8] ACI-216, *Standard Method for Determining Fire Resistance of Concrete and Mansonry Construction Assemblies*.: American Concrete Institute, 1997.

[9] ACI-318, *Building Code Requirements for Structural Concrete and Commentary*.: American Concrete Institute , 2008.

[10] ASCE-1992, *Structural Fire Protection*. New York: ASCE Manual and Reports on Engineering Practice, 1992.

[11] ASTM-E119, *Standard Test Methods for Fire Tests of Building Construction and Material*.: American Society for Testing and Materials, 2000.

[12] AASHTO-LRFD-2012, "AASHTO LRFD Bridge Design Specifications," 2012, 2011.

[13] V.K.P Kodur and M. Dwaikat, "A Numerical Model for Predicting the Fire Resistance of Reinforced Concrete Beams.," *Cement & Concrete Composites*, pp. 431-443, 2008.

[14] M. Dwaikat and V.K.P Kodur, "A Numerical Approach for Modeling the Fire Induced Restraint Effects in Reinforced Concrete Beams.," *Fire Safety Journal. Volume 43*, pp. 291-307, 2008.

[15] J.H Hsu and C.S. Lin, "Residual Bearing Capabilities of Fire-Exposed Reinforced Concrete Beams.," *International Journal of Applied Science and Engineering. Volume 4*, pp. 151-163, 2006.

[16] D. Di Capua and A.R Mari, "Nonlinear Analysis of Reinforced Concrete Cross-Section Exposed to Fire," *Fire Safety Journal*, vol. 103, no. 4, pp. 139-149, 2007.

[17] A. Ibrahimbegovic, *Nonlinear Solid Mechanics: Theoretical Formulation and Finite Element Solution Methods*.: Springer, 2009.

[18] A. Ibrahimbegovic and E.L Wilson, "A Modified Method of Incompatible Modes.," *Communications in Applied Mechanics Methods*, pp. 187-194, 1991.

[19] B.H. Pham, "Stress-Resultant Models for Optimal Design of Reinforced Concrete Frames.," Cachan. France, 2009.

[20] B.H. Pham, L. Davenne, D. Brancherie, and A. Ibrahimbegovic, "Stress Resultant Model for Ultimate Load Design of Reinforced Concrete Frames: Combined Axial Force and Bending Moment.," *Computers and Concrete*, pp. 303-315, 2010.

[21] N.N Bui, V.M Ngo, D. Brancherie, and A. Ibrahimbegovic, "Enriched Timoshenko beam finite element for modelling bending and shear failure of reinforced concrete frames," *Computer and Structures*, vol. submitted.

[22] A. Ibrahimbegovic and S. Melnyk, "Embedded discontinuity finite element method for modeling of localized failure in heterogeneous materials with structured mesh: an alternative to extended finite element method," *Computational Mechanics*, vol. 40, pp. 149-155, 2007.

[23] A. Ibrahimbegovic and D. Brancherie, "Combined hardening and softening constitutive model of plasticity: precursor to shear slip line failure," *Computational Mechanics*, pp. 88-100, 2003.

[24] D. Brancherie, "Modeles continus et “discrets” pour les problemes de localisation et de rupture fragile et/ou ductile," Cachan, 2003.

[25] D. Brancherie and A. Ibrahimbegovic, "Novel anisotropic continuum-discrete damage model capable of representing localized failure of massive structures. Part I: theoretical formulation and numerical," *International Journal for Computer-Aided Engineering and Software*, vol. 26, pp. 100-127, 2009.

[26] A. Ibrahimbegovic, A. Boulkertous, L. Davenne, and D. Brancherie, "Modeling of Reinforced Concrete Structures Providing Crack-Spacing based on X-FEM, ED-FEM and novel operator split solution procedure," *International Journal for Numerical Methods in Engineering*, vol. 83, pp. 452-481, 2010.

[27] M. Ortiz, Y. Leroy, and A. Needleman, "A finite element method for localized failure analysis," *Computer Methods in Applied Mechanics and Engineering*, vol. 61, no. 2, pp. 189-214, March 1987.

[28] J. Oliver, F. Armero J. C. Simo, "An analysis of strong discontinuities induced by strain-softening in rate-independent inelastic solids," *Computational Mechanics*, vol. 12, no. 5, pp. 277-296, 1993.

[29] F. Armero, "Localized anisotropic damage of brittle materials," in *5th, Computational plasticity: fundamentals and applications*, 1997, pp. 635-640.

[30] F. Armero and K. Garikipati, "Recent advances in the analysis and numerical simulation of strain localization in inelastic solids," in *4th Computational Plasticity: Fundamentals and Applications.*, Barcelona, 1995, pp. 547–561.

[31] F. Armero, "Large-scale modeling of localized dissipative mechanisms in a local continuum: applications to the numerical simulation of strain localization in rate-dependent inelastic solids," *Mechanics of Cohesive-frictional Materials*, vol. 4, no. 2, pp. 101-131,

March 1999.

[32] J. Oliver, "Modelling strong discontinuities in solid mechanics via strain softening constitutive equations. Part I& Part II," *International Journal for Numerical Methods in Engineering*, vol. 39, pp. 3575-3623, 1996.

[33] F. Armero and J.C. Simo, "A priori stability estimates and unconditionally stable product formula algorithms for nonlinear coupled thermoplasticity," *International Journal of Plasticity*, vol. 9, no. 6, 1993.

[34] A. Ibrahimbegovic and L. Chorfi, "Covariant principal axis formulation of associated coupled thermoplasticity at finite strains and its numerical implementation," *International Journal of Solids and Structures*, vol. 39, pp. 499-528, 2002.

[35] A. Ibrahimbegovic, L.Chorfi, and F. Gharzeddine, "Thermomechanical Coupling at Finite Elastic Strain: Covariant Formulation and Numerical Implementation," *Communications in Numerical Methods in Engineering*, vol. 17, pp. 275-289, 2001.

[36] G. Baker and R. de Borst, "An anisotropic thermomechanical damage model for concrete at transient elevated temperatures," *Philosophical transactions. Mathematical physical and engineering*, vol. 363, no. 1836, pp. 2603-2628, 2005.

[37] N.C Tran, "Développement d'un modèle d'interface béton-acier à haute température. Modélisation des structures en béton exposées au feu.," École des Ponts ParisTech, Université Paris-Est, Ph.D Thesis 2011.

[38] K. Runession, P. Steinmann, and R. Larsson, "On localization in thermo-elastoplastic solids subjected to adiabatic conditions," *European Journal of Mechanics- A/Solids*, vol. 18, pp. 557-579, 1999.

[39] F. Armero and J. Park, "An analysis of strain localisation in a shear layer under thermally coupled dynamic conditions. Part 2: Localized thermoplastic model," *International Journal for Numerical Methods in Engineering*, vol. 56, no. 14: Computational Failure Mechanics, pp. 2101-2133, April 2003.

[40] K. William, I. Rhee, and B. Shing, "Interface Damage Model for Thermomechanical

Degradation of Heterogeneous Materials," *Computer Methods in Applied Mechanics and Engineering*, vol. 1993, no. 30-32: Computational Failure Mechanics, pp. 3327-3350, July 2004.

[41] F.J Vecchio and M.P. Collins, "Predicting the Response of Reinforced Concrete Beams Subjected to Shear Using Compression Field Theory," *ACI Structural Journal*, pp. 258-268, 1988.

[42] J.C. Simo and C. Miehe, "Associative coupled thermoplasticity at finite strains: Formulation, numerical analysis and implementation," *Computer Methods in Applied Mechanis and Engineering*, vol. 98, no. 1, pp. 41-104, 1992.

[43] J.B. Colliat, A. Ibrahimbegovic, and L. Davenne, "Modeling thermomechanical behaviour of cellular structure made of brittle material," 2003.

[44] V.M. Ngo, A. Ibrahimbegovic, and D. Brancherie, "Continuum damage model for thermo-mechanical coupling in quasi-brittle materials," *Engineering Structure*, vol. 50, pp. 170-178, 2013.

[45] D. Gawin, C.E. Majorana, F. Pesavento, and B.A. Schrefle, "A fully compled multiphase FE model of hygro-thermo-mechanical behavior of concrete at high temperature," in *Computational Mechanics: New Trends and Application*, Barcelona, 1998.

[46] C. Kassiotis, J.B. Colliat, and A. Ibrahimbegovic, "Multiscale in time and stability analysis of operator split solution procedures applied to thermomechanical problems," *International Journal for Computer-Aided Engineering and Software*, vol. 26, 2009.

[47] M. Gross and P. Betsch, "Galerkin-based energy-momentum consistent time-stepping algorithms for classical nonlinear thermo-elastodynamics," vol. 82, no. 4, pp. 718-770, December 2001.

[48] T. Belytschko and T. Black, "Elastic crack growth in finite elements with minimal remeshing," *International Journal for Numerical Methods in Engineering*, vol. 45, pp. 601-620, 1999.

[49] A. Ibrahimbegovic and D. Brancherie, "Combined hardening and softening constitutive

model of plasticity: precursor to shear slip line failure," *Computational Mechanics*, vol. 31, pp. 88-100, 2003.

[50] C. Kassiotis, J.B. Colliat, A. Ibrahimbegovic, and H. Matthies, "Multiscale in time and stability analysis of operator split solution procedure," *International Journal of Engineering Computations*, vol. 26, pp. 205-223, 2009.

[51] M. Ortiz and E.P. Popov, "Accuracy and stability of integration algorithms for elastoplastic constitutive relations," *International Journal for Numerical Methods in Engineering*, vol. 21, no. 9, pp. 1561-1576, 1985.

[52] F. Armero and C. Linder, "New finite elements with embedded strong discontinuities in the finite deformation range," *Computer Methods in Applied Mechanics and Engineering*, pp. 3138-3170, 2008.

[53] V.M. Ngo, A. Ibrahimbegovic, and D. Brancherie, "Model for localized failure with thermo-plastic coupling. Theoretical formulation and ED-FEM implementation," *Computers and Structures*, vol. 127, pp. 2-18, 2013.

[54] C. Farhat, K.C. Park, and Y. Dubois-Pelerin, "An unconditionally stable staggered algorithm for transient finite element analysis of coupled thermoelastic problems," vol. 85, pp. 349-365, 1991.

[55] Claus V. Nielsen, Chris J. Pearce, and Nenad Bicanic, "Improved phonomenological modelling of transient thermal strains for concrete at high temperatures," *Computers and Concrete. Volume 1*, pp. 189-209, 2004.

[56] R. Taylor, "FEAP - A Finite Element Analysis Program. Version 7.5 User Manual," 2004.

[57] R. Taylor, "FEAP - A Finite Element Analysis Program. Version 7.5. Programmer Manual," 2004.

[58] F.J Vecchio and Emara, "Shear Deformation in Reinforced Concrete Frames," *ACI Structural Journal*, pp. 46-56, 1992.

[59] D. Bentz, F.J. Vecchio, and M.P. Collins, "Simplifed Modified Compression Field Theory

for Calculating Shear Strength of Reinforced Concrete Elements," *ACI Structural Journal*, no. 103-S65, pp. 614-624, 2006.

[60] T.T.H Le, "Etude multi-échelles du comportement Thermo-Hydro-Mécanique des matériaux cimentaires. Approche morphologique pour la prise en compte de la mésostructure," France, 2011.

[61] F.J. Vecchio and M.P. Collins, "Predicting the Response of Reinforced Concrete Beams Subjected to Shear Using Compression Field Theory," *ACI Structural Journal.*, pp. 258-268, 1988.

[62] A. Ibrahimbegovic and F. Frey, "Stress Resultant Finite Element Analysis of Reinforced Concrete Plates," *Engineering Computations*, vol. 10, no. 1, pp. 15-30, 1993.

[63] L. Davenne and A. Ibrahimbegovic A. Boulkestous, "Influence of the steel-concrete bond-slip on the behavior of RC structures under severe conditions," in *CONSEC10*, 2010.

[64] 17. A. Ibrahimbegovic, A. Boulkertous, M. Muhasilovic L. Davenne, J. Duhovnik, and A. Pokrklic, "Fire Induced Damage in Structures and Infrastructure: Analysis, Testing and Modeling," *Damage Assesment and Reconstruction after War or Natural Disaster*, pp. 321-342, 2009.

[65] A. Ibrahimbegovic, A. Boulkertous, L. Davenne, and M., Pokrklic, A. Muhasilovic, "On modeling of fire resistance tests of concrete and reinforced-concrete structures.," *Computers & Concrete*, vol. 7, pp. 285-302, 2010.

[66] J. Besson, G. Cailletaud, JL. Chaboche, and S. Forest, *Mécanique non linéaire des matériaux*, Hermès, Ed.: Lavoisier, 2001.

[67] H.F.B Xavier, "Analysis of Reinforced Concrete Frames Exposed to Fire: Based on Advanced Calculation Methods," Porto, 2009.

[68] A. Ibrahimbegovic, J.B. Colliat, and L. Davenne, "Thermomechanical coupling in folded plates and non-smooth shells," *Computer Methods in Applied Mechanics and Engineering*, vol. 194, pp. 2686-2707, 2005.

[69] I. Romero, "Thermodynamically consistent time-stepping algorithms for non-linear thermomechanical systems," *International Journal for Numerical Methods in Engineering*, pp. 706-732, 2009.

[70] A. Kucerova, D. Brancherie, A. Ibrahimbegovic, J. Zeman, and Z. Bittnar, "Novel anisotropic continuum-discrete damage model capable of representing localized failure of massive structures. Part II: identification from tests under heterogeneous stress field," *Engineering Computations: International Journal for Computer-Aided Engineering and Software*, vol. 26, pp. 128-144, 2009.

[71] N. Mathieu, K. Sab, and S.A. Zaïmi, "An enhanced homogenization approach for masonry structures with compressible joints. Application to hearth thermomechanical computations.," *International Journal for Numerical and Analytical Methods in Geomechanics*, vol. 36, no. 9, pp. 1102-1124, June 2012.